AN INVESTIGATION OF THE EFFECTS OF ANGLE OF ATTACK AND AIRFOIL MODEL SIZE ON THE OCCURRENCE OF SHOCK WAVES IN A TWO DIMENSIONAL WIND TUNNEL

Thesis by

Comdr. L. S. Chambers, USN

Comdr. R. E. Doll, USN

Comdr. D. A. Harrell, USN

In Partial Fulfillment of the Requirements
for the Degree of Aeronautical Engineer

California Institute of Technology
Pasadena, California

June, 1944

ACKNOWLEDGEMENT

The authors are indebted to the staff of the Guggenheim Aeronautical Laboratory, California Institute of Technology.

In particular they wish to express their appreciation to Dr. Th. von Karman for suggesting the investigation, Mr. A. E. Puckett of the supersonic laboratory, and Dr. and Mrs. H. W. Liepmann for valuable help and criticism during the course of the investigation.

Symbols

M - Free stream Mach number

α - Angle of attack

C_L - Lift coefficient

p - Local static pressure

p_o - Atmospheric pressure

q - $\frac{1}{2}\rho V^2$ (free stream values)

TABLE OF CONTENTS

Summary

This paper presents the results of an investigation of the flow in the vicinity of one of the newer symmetrical NACA laminar flow airfoil sections at and above the critical speed of the section, in the form of schlieren photographs and wall pressure distributions. The investigation was carried out in a two dimensional tunnel, designed for this purpose by the authors, at the Guggenheim Aeronautical Laboratory of the California Institute of Technology during the spring of 1944.

The formation and variation of the shock waves with angle of attack and Mach number are presented in a series of high speed photographs. An attempt is made to indicate the effect of model size in a tunnel of fixed cross sectional area by presenting photographic results of the tests on airfoils of 2", 4", and 6" chord lengths.

Curves of C_L versus Mach number at constant angle of attack are presented for the three airfoils.

Introduction

The rapidly increasing flight speeds of modern aircraft, and the promise of even greater increases with new types of propulsive equipment, have forced upon the aerodynamicist the consideration of phenomena of compressible flow at and above the so-called "critical speed" of present day airfoils. It is evident that this speed is being reached even now in certain types of military aircraft. It appears likely that, with the new propulsive systems becoming available, major increases in the speed of flight will be contingent upon the development of suitable lifting surfaces.

Theoretical study of this problem has been hampered by the complications inherent in dealing with the non-linear differential equations describing flow at these speeds, and by the lack of adequate experimental evidence of the exact nature of the phenomena involved. The mass of available data is primarily concerned with the characteristics of airfoils below the critical speed; very little is available on flow conditions above this point.

Also all existing experimental data contain large and unpredictable errors due to the effect of tunnel wall interference. Until very recently all tunnels capable of achieving the desired speeds have been quite small. Data were taken from these tunnels in the form of force measurements or pressure distributions on the airfoils, both of which necessitated the use of relatively large model sizes. As the free stream speed approaches that of sound the flow becomes increasingly sensitive to changes of channel area, thus aggravating the effect of

large model to tunnel size ratios. No wholly satisfactory method of evaluating this effect has as yet been devised.

In reference 1 it was demonstrated that the phenomena occurring at the critical speed are associated with the formation of compression shock waves in the flow in the vicinity of the airfoil. The work described herein was undertaken with a view to furnishing additional information, through the medium of schlieren photographs, as to the occurrence of these shock waves. One of the newer symmetrical NACA laminar flow airfoil sections was used for the tests. The formation, and variation, of the shock waves with angle of attack and Mach number are shown in a series of photographs. In addition an attempt was made to show the effect of model size, for a given tunnel, by repeating the tests for three different sized models. For this purpose schlieren observation has many advantages, since model size is of no particular consequence with respect to sensitivity, and the model may be mounted directly on the tunnel walls, eliminating tip clearance problems or balance strut interferences. It has, of course, very definite limitations in that it provides no force or pressure measurements.

This deficiency was partially overcome by the installation of pressure orifices in the top and bottom walls of the test section to permit the calculation of lift coefficients by integration of wall pressures. Lift coefficients computed by this means are presented for various angles of attack and model sizes as a function of the Mach number.

The tests were conducted in a tunnel designed and built for

the purpose. It is a two dimensional, open return, induction type, having a test section of one by ten inches cross section by twenty inches long. It is capable of giving a Mach number of 0.91 with no model installed.

The tests were made at the Guggenheim Aeronautical Laboratories of the California Institute of Technology in May and June of 1944.

Equipment

The tunnel used is illustrated in Figs. 1 and 2. It is a closed throat, open return, induction type. The jets are located in a rectangular section down stream of the test section, giving a relatively low turbulence flow past the model. The jets are followed by a constant area mixing section which discharges into the diffuser.

The test section is rectangular in section, one inch by ten inches by twenty inches long. The side walls are made of plate glass, gasketed directly to the steel structure with rubber gaskets. The top and bottom walls consist of laminated phenolic resin blocks with 23 flush static orifices each. These were made readily replaceable to facilitate changing the wall shape for various tests. The test section was tapered in the one inch dimension from 0.900 inches at the entrance end to 1.000 inches at the exit end to allow for boundary layer growth.

The model was supported at the center of the glass side walls in trunnion inserted in slots out through the glass. The model was gasketed directly to the glass plates to avoid leakage. This mounting is illustrated in Figs. 3 and 4 which show the two inch chord model mounted in place. Fig. 5 is an "exploded" view of the entire mounting system. The same lugs, through bolt, etc., were used for all models.

Three models were used in the course of the tests. They were all of the same section varying only in chord length. One of the newer symmetrical NACA laminar flow sections was used. They were machined from brass in chord lengths of two inches, four inches, and six

inches respectively. Tolerances were held to 0.001 inches. No pressure orifices were installed in the models for this series of tests since the two inch chord model was too small to accommodate an adequate number of orifices.

The wall block static pressure orifices were connected to a multiple tube, closed system manometer containing butyl alcohol. An orifice showing near maximum pressure in the test section was connected to the reservoir and used as a reference. This gave a very sensitive means of measuring pressure differences along the walls of the test section. A mercury manometer, vented to atmosphere was connected to the reference pressure for use in setting the Mach number of the tests. These manometers are illustrated in Fig. 6.

Conventional schlieren equipment was used for visual and photographic observation. The mirrors used permitted observation of a circular field of about eight inches diameter. The field could be moved to cover the entire test section. An incandescent light source employing a projection type bulb was used for visual observation. A high intensity spark giving an exposure time on the order of 10^{-4} second was used for photographic purposes. The knife edge and light source were capable of being rotated through 360° to observe the density gradient in any direction.

A wet and dry bulb hygrometer supported in the entrance section was used to measure the relative humidity of the air entering the test section.

The tunnel is capable of producing a Mach number of 0.91 with no model, and a Mach number of 0.77 with the four inch chord model installed at six degrees angle of attack. This condition produced the maximum blocking effect encountered.

Static pressures along the wall blocks with no model installed showed a variation, at a Mach number of 0.80, of the order of 1%q. The variation was random, except at the extreme ends of the test section, indicating that it was probably due to slight surface irregularities in the vicinity of the pressure orifices. A slight drop in velocity at the ends of the test section was undoubtedly due to the change in cross-section shape in the vicinity of these points. No positive pressure gradient through the test section could be observed, indicating that the correction for boundary layer growth was very nearly correct.

A static pressure survey across the ten inch dimension of the test section at the model position showed a variation of the order of 0.5%q.

Procedure

The project included the design, construction and assembly of the working section, entrance section, and diffuser, of the wind tunnel used for the tests described. The tunnel was designed around a jet assembly and mixing section of an already proved installation, which resulted in a great saving of time and effort in getting the equipment into operation.

It was at first planned to use the original short diffuser section which was attached to the above mixing section, but early tests indicated the need for a much longer one, which was accordingly designed and installed.

The original upper and lower wall blocks of hard wood, with inset brass tubes for pressure orifices, proved unsatisfactory, since it was practically impossible to maintain the ends of the tubes flush with the block surface, with severe pressure irregularities resulting from imperceptible tube movements. New blocks of a laminated phenolic resin, described under Equipment proved to be a satisfactory solution, both from the standpoint of fabrication and consistent pressure observations.

A number of pressure distributions along the blocks (no model in the tunnel) were taken at varying speeds to investigate the accuracy of the boundary layer correction. Then a vertical survey was made (no model installed), with the investigating static head at the center of the tunnel, in the plane of the model supports.

Runs were made with the two inch chord model installed at various angles to investigate the capabilities of the tunnel and its optical equipment, and to determine the limiting conditions for this report. It became apparent during these runs that some means of filtering oil from the air passing through the tunnel was desirable, since the glass side walls became severely oil-streaked very quickly at high speeds. Large area air filters were designed and installed at the entrance and exit, which partially corrected the condition without appreciable penalty in performance. However, the condition still existed to the extent that it remained necessary to remove and clean the glass side walls between runs.

The spark apparatus for photographic recording was next installed and tested. A convenient system of rapidly shifting from continuous light source to spark source without readjustment was provided in the optical bench, which was a part of the original laboratory equipment.

The procedure for each record run was essentially the same. The first step, after removing and cleaning the glass side walls, was to set the desired angle of attack. This was achieved by means of a reference centerline on the tunnel, set up by measurement, a fairly large scale protractor (four inch radius), and an improvised tool inserted through the entrance end for moving the airfoil about its support pin. The angle was held by friction between the model sides and the support trunnions when the end nuts were set up tight. Additional security was achieved when the side walls were set up firmly, sealing the model ends against the glass.

After replacing the removable filter screen at the entrance, the tunnel was brought up to its maximum speed for the airfoil size and angle of attack. After steady conditions were attained, a schlieren photograph of the shock waves was taken and the wall pressure distribution was recorded. This latter was accomplished by inserting a sheet of paper between the manometer tubes and the backboard and marking the liquid level with pencil. By this means, a distribution could be recorded in less than one minute, for later reduction in quiet and at leisure. Also, by using different color pencils, all of the distributions for a complete run could be recorded on a single sheet.

Three more photographs were taken on each run, with corresponding pressure distributions, at lower speeds, reducing the speed by approximately equal increments. It was attempted to space the speeds so that the photographs covered a range from the maximum to a speed well below that at which the shock wave finally disappeared from the visual screen. It was proved by repeated trial that the speed at which the shock wave appeared with the speed increasing was exactly the same as that at which the shock wave disappeared with speed decreasing. One of the photographs, usually No. 3, was taken at a speed just above this "critical" velocity, and a note was made of the value of M for the disappearance of the shock.

The recorded pressures were measured on the original sheets, and reduced to p/q. Values of q were computed from the relation $\frac{1}{2}\frac{\rho U^2}{p_0} = \frac{\gamma}{2} M^2 \frac{p}{p_0}$. The curves for upper and lower orifice blocks were superimposed, in order to measure the lift on the airfoil by the area enclosed between the curves. The areas were evaluated by

planimeter, and lift coefficients were calculated in the usual way.

Precision

Individual wall pressure measurements should be accurate within 0.1%q for the two inch chord model (measurements made with alcohol manometer) and within 0.5%q for the four and six inch chord models, where measurements were made with the mercury manometer. The effect of any irregularities in the wall blocks has been eliminated by subtracting from each p/q reading recorded for each model condition the value of p/q taken with no model installed at a corresponding Mach number. This subtraction was made orifice by orifice, not from the faired curves. The lack of scatter in the pressure distribution curves tends to justify this procedure.

The Mach number as read should be accurate to within 0.002. However, it was read from the reference pressure for the multiple manometer, which corresponded to a somewhat higher absolute pressure than the free stream. In the case of the two inch chord model the error lies within the above error in reading. With the four and six inch chord models this error may amount to 0.015. In all cases the Mach number as given is less than the true free stream Mach number.

The sensitivity of the schlieren equipment employed is difficult to specify. It is perhaps best estimated by comparing the apparent intensity of the stagnation point on the airfoil at comparable Mach numbers. In all cases the sensitivity was adequate to give a very positive response to the heated air rising from one's hand.

The angles of attack were set within 0.1 degrees. Particular care was taken to achieve zero degrees. Runs were repeated until

the pressure distributions showed a zero lift coefficient. These particular settings are therefore more accurate.

Results and Discussion

The principal results are presented in a series of photographs, Figs. 7 - 25 inclusive. These photographs show the formation and movement of the shock waves at various free stream Mach numbers and various angles of attack for each of the three models.

Figs. 26 - 28a inclusive are plots of lift coefficient versus Mach number at constant angles of attack for each of the models. From a study of the photographs an attempt has been made to determine the first appearance of a shock wave. This point is indicated by a short vertical line across each curve.

The peak value of lift coefficient for each of the above curves was plotted against the Mach number to give Fig. 28b. A study of this figure indicates that a four inch chord model probably represents the practical upper limit in model size for this tunnel, beyond which tunnel wall interference would undoubtedly vitiate any results obtained. The inference is also apparent from a comparison of the photographs of the three airfoils at zero angle of attack (Figs. 7, 14, 21). The two inch chord model apparently offers little blocking effect in a tunnel of this size since the maximum Mach number attained with no model installed was 0.91, while that with the two inch chord model installed was 0.90.

Figs. 29 - 101 inclusive, wall pressure distributions, are included in this report since they represent basic data which may be needed for future analysis of this problem. Lift coefficients were obtained by integration of these curves. It also appears feasible to obtain moment coefficients from these curves by determining the center

of gravity of the enclosed area.

The photographs show several phenomena which run counter to the currently accepted theory for two dimensional flow at sonic speeds. The first and most obvious of these is the triangular based shock waves which appear on the two inch chord airfoil. The phenomenon is most apparent in Figs. 11 - 13 inclusive. It was first considered that the triangular base of these shock waves might be due to a condensation "shock wave". An attempt, therefore, was made to correlate the appearance of waves of this type with the relative humidity of the air entering the tunnel. However, as the tests progressed to models of larger chord, it became apparent that the relative humidity was not the controlling factor. A comparison of Figs. 8, 17, and 22 indicate a steady dimunition of this effect with increase in model size in spite of the fact that the relative humidity was even higher for the two larger sized models. This would tend to indicate that the Reynolds Number may be an important controlling parameter in the occurrence of this type of wave.

The next notable phenomenon brought out by the photographs is the appearance of multiple shock waves. These multiple waves appear in the majority of the photographs. In general, they appear less frequently at the high angles of attack. If it can be assumed that these waves are normal shock waves, their appearance is directly contradictory of existing compressible fluid theory. It would also appear difficult to correlate the appearance of these multiple waves with the current theory of oblique waves.

A further and last peculiarity is particularly evident in Figs. 23 and 24. This is the appearance of some form of shock wave on the upper surface of the airfoil near the leading edge. These waves seem to be completely independent of the main shock waves. They occur most frequently on the larger models at high angles of attack. These waves persist to much lower Mach numbers than the main shock waves. No satisfactory explanation of these waves has been found.

In some of the photographs, lines resembling streamlines are apparent. These lines are caused by a mixture of condensed water vapor and oil collecting on the glass side walls of the tunnel, and do not represent the actual streamlines existing in the free flow since they are in the wall boundary layer. Much difficulty was encountered in keeping the glass walls clear of this effect and frequent dismantling of the test section for cleaning was necessary. The large irregular mass apparently protruding from the surface of the two inch chord airfoil and, to a lesser degree, in the six inch chord airfoil photographs is actually a surface chip in the glass window around the mounting slot. It has no significance as regards flow conditions.

Conclusions

1. Shock waves on airfoils do not conform to the requirements of the existing simple theory of compressible fluid flow. Photographs in this report give visible evidence of many peculiarities which can not be accounted for by the simple theory.

2. The occurrence of the shock wave, particularly in the two smaller models where blocking was not too severe, is not an abrupt phenomenon. The wave first occurs as a small disturbance relatively near the leading edge of the airfoil. As the speed is increased, the disturbance increases in severity and moves back toward the trailing edge. The movement of the wave towards the trailing edge is most apparent at the higher angles of attack. This conclusion is based on a continuous visual observation of the screen as the speed was increased and is difficult to show in still photographs.

3. It is evident that the lift coefficient continues to increase after the first appearance of the shock wave. It is the opinion of the authors that these shock waves, appearing on the upper surface of the airfoil, have the effect of increasing the camber of the airfoil, thereby causing an increase in both the lift and drag coefficients; then, as the wave increases in strength, it disrupts the flow causing a rapid decrease in lift and further increase in drag.

4. It would appear that the maximum allowable blocking effect of a model commensurate with good results is of the order of 5%.

Recommendations

1. It appears both feasible and desirable to conduct some tests with a model containing pressure orifices.

2. Some means of taking a continuous series of pictures of the screen as the tunnel speed is increased would be valuable.

3. Since the theory of compressible fluid flow about an elliptic cylinder has been developed, it would be of interest to make tests on such a body and compare the results directly.

4. It is believed practicable to install a balance system on this tunnel and thus measure forces directly.

References and Bibliography

1. Stack, John; Lindsey, W. F.; and Littell, Robert E.
"The Compressibility Burble and the Effect of Compressibility on Pressures and Forces Acting on an Airfoil".
NACA Report 646, 1939.

2. Taylor, G. I. and Maccoll, J. W.
"The Mechanics of Compressible Fluids".
Vol. III Aerodynamic Theory, W. F. Durand
Durant Reprinting Committee, California Institute of Technology

3. Hood, M. and Anderson, J.
"Tests of an NACA 66, 2-240 Airfoil of Five Foot Chord at High Speed".
Advance Restricted Report NACA, 1942.

4. Geiger, F. W.
"An Approximate Constriction Correction for High Speed Closed Throat Wind Tunnel Data".
Curtiss-Wright Report 5A-23, 1944.

5. Nitzberg, G.
"The Effect of Compressibility on Two Dimensional Tunnel Wall Interference for a Symmetrical Airfoil".
NACA Advance Restricted Report, 1945.

FIG. 1

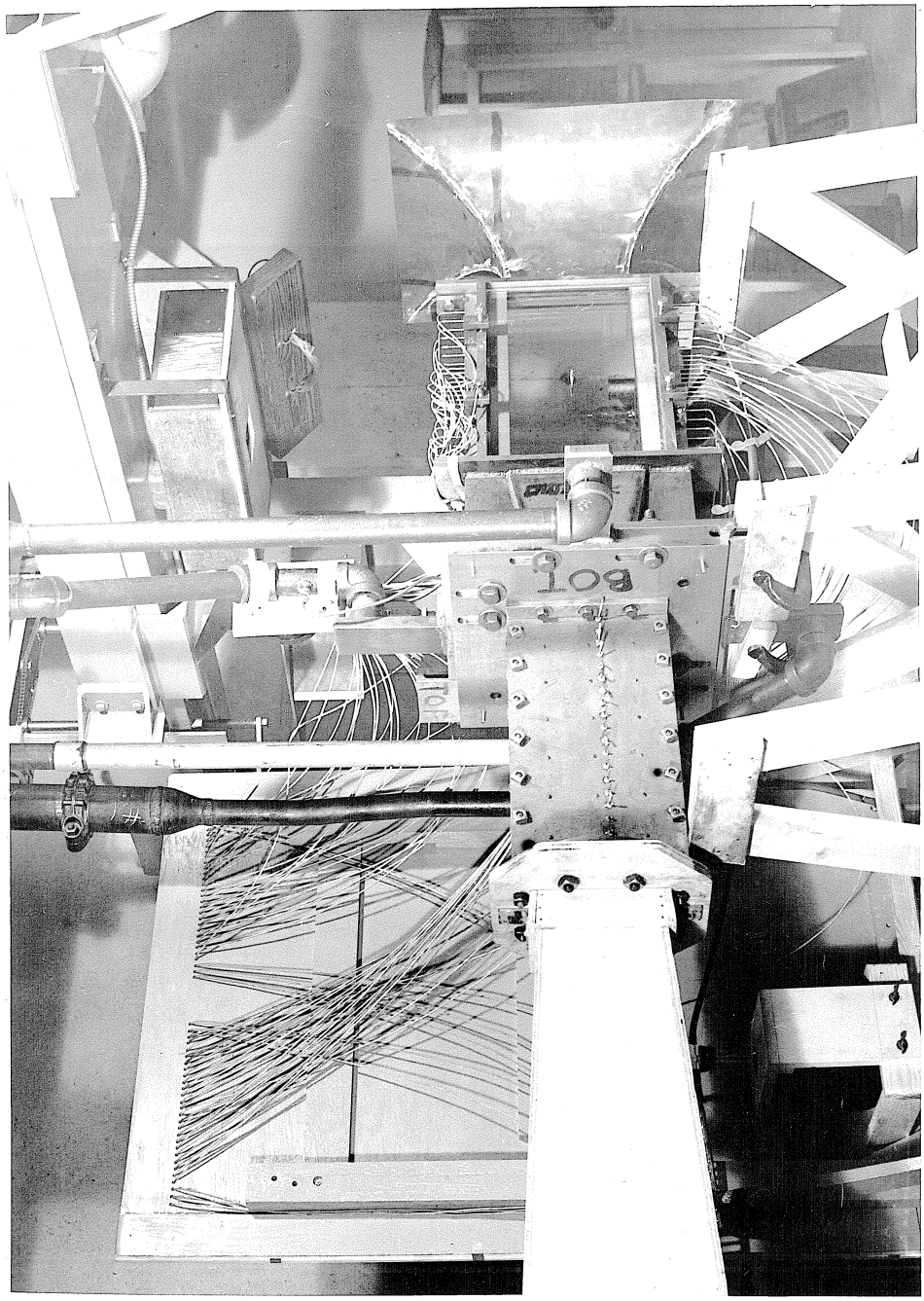

Fig. 2

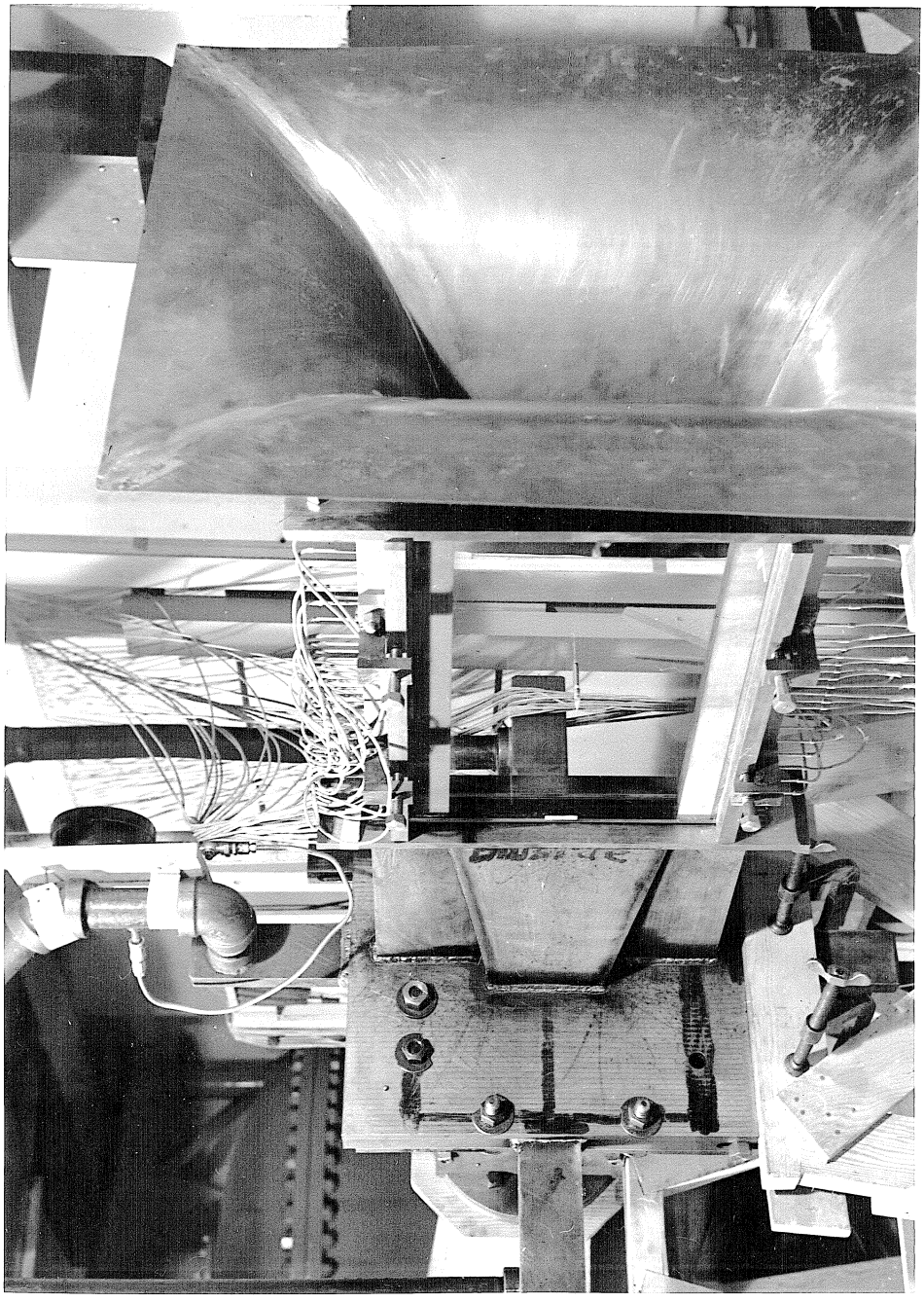

FIG 3

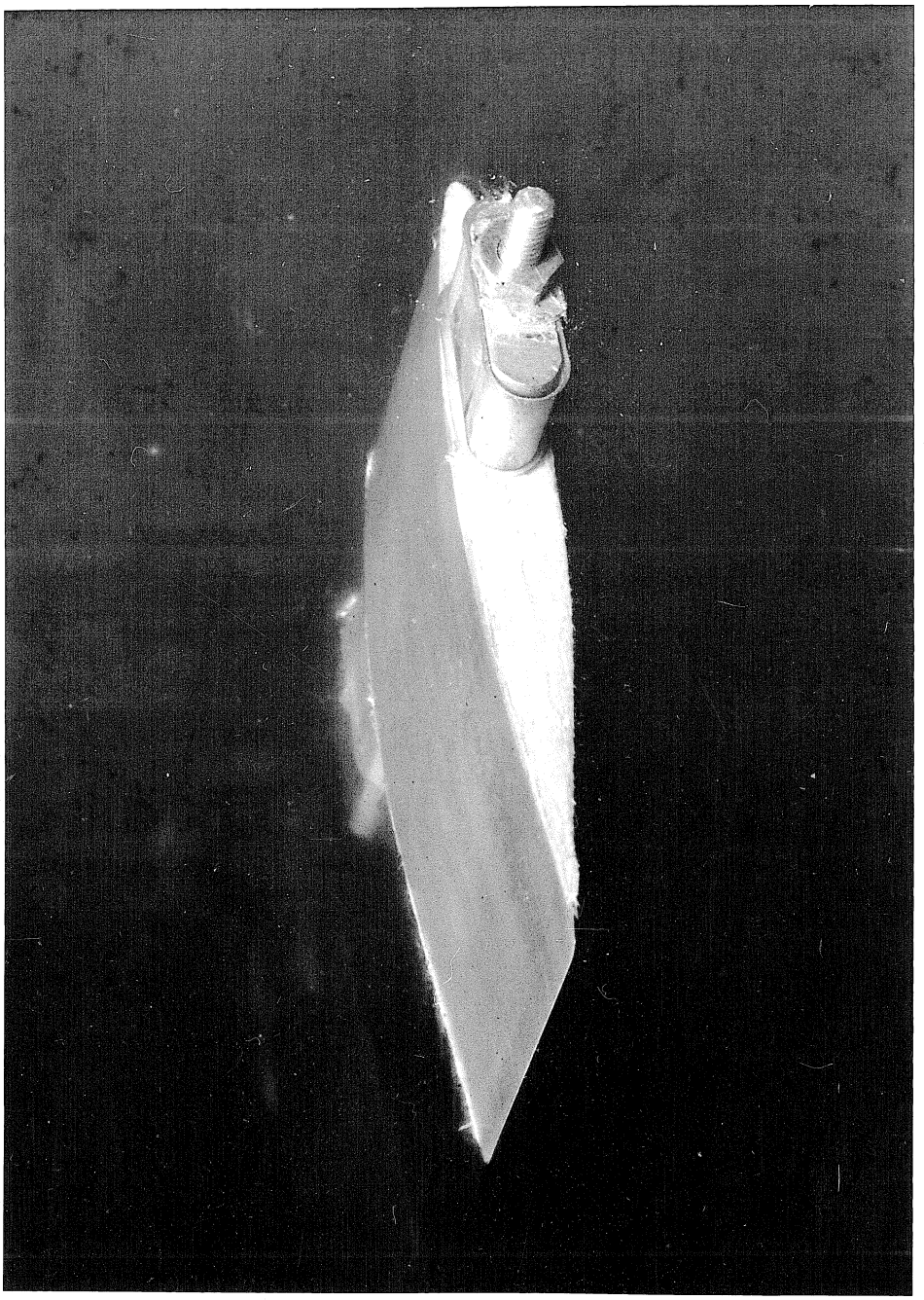

FIG. 4

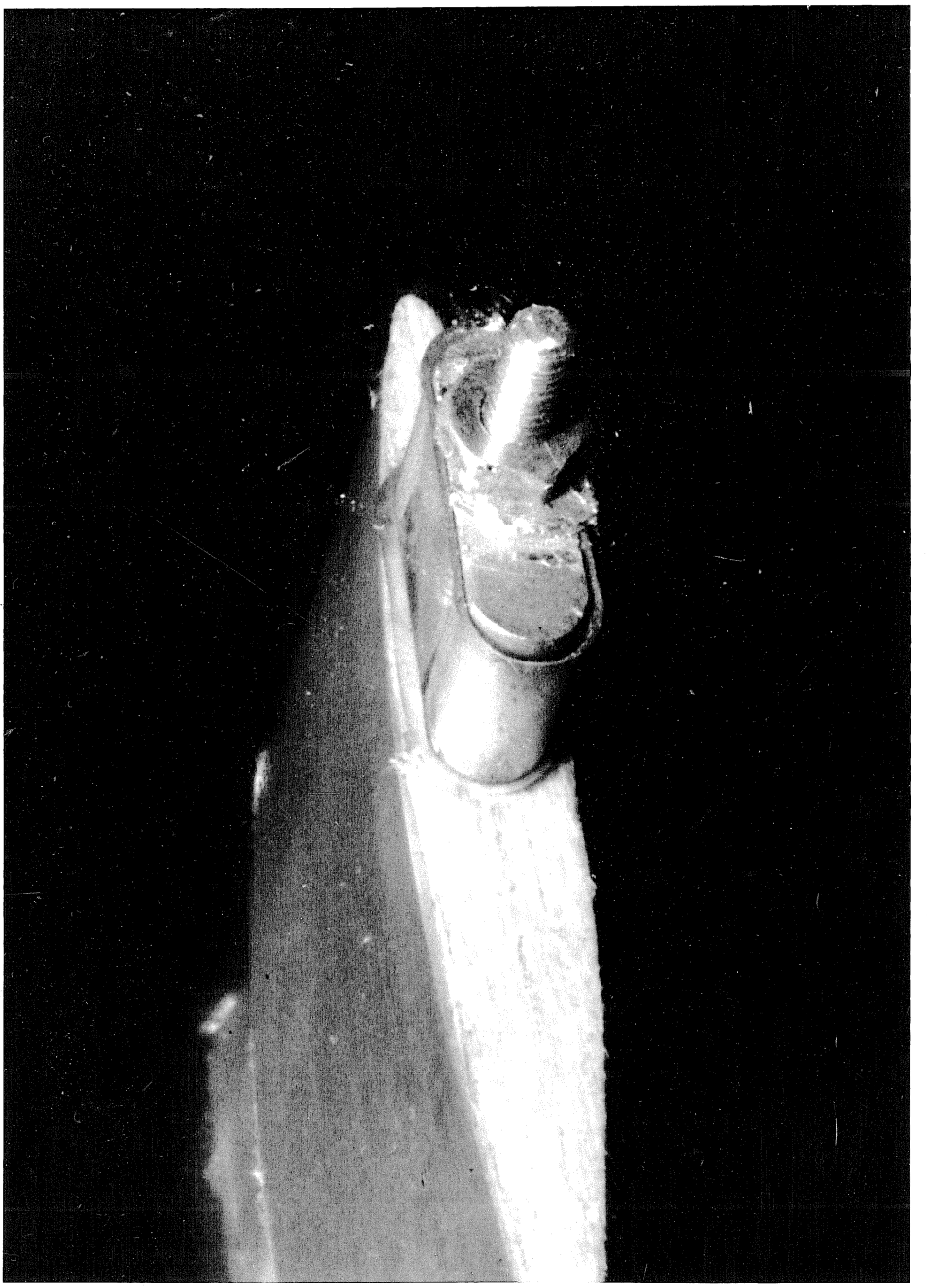

Fig 5

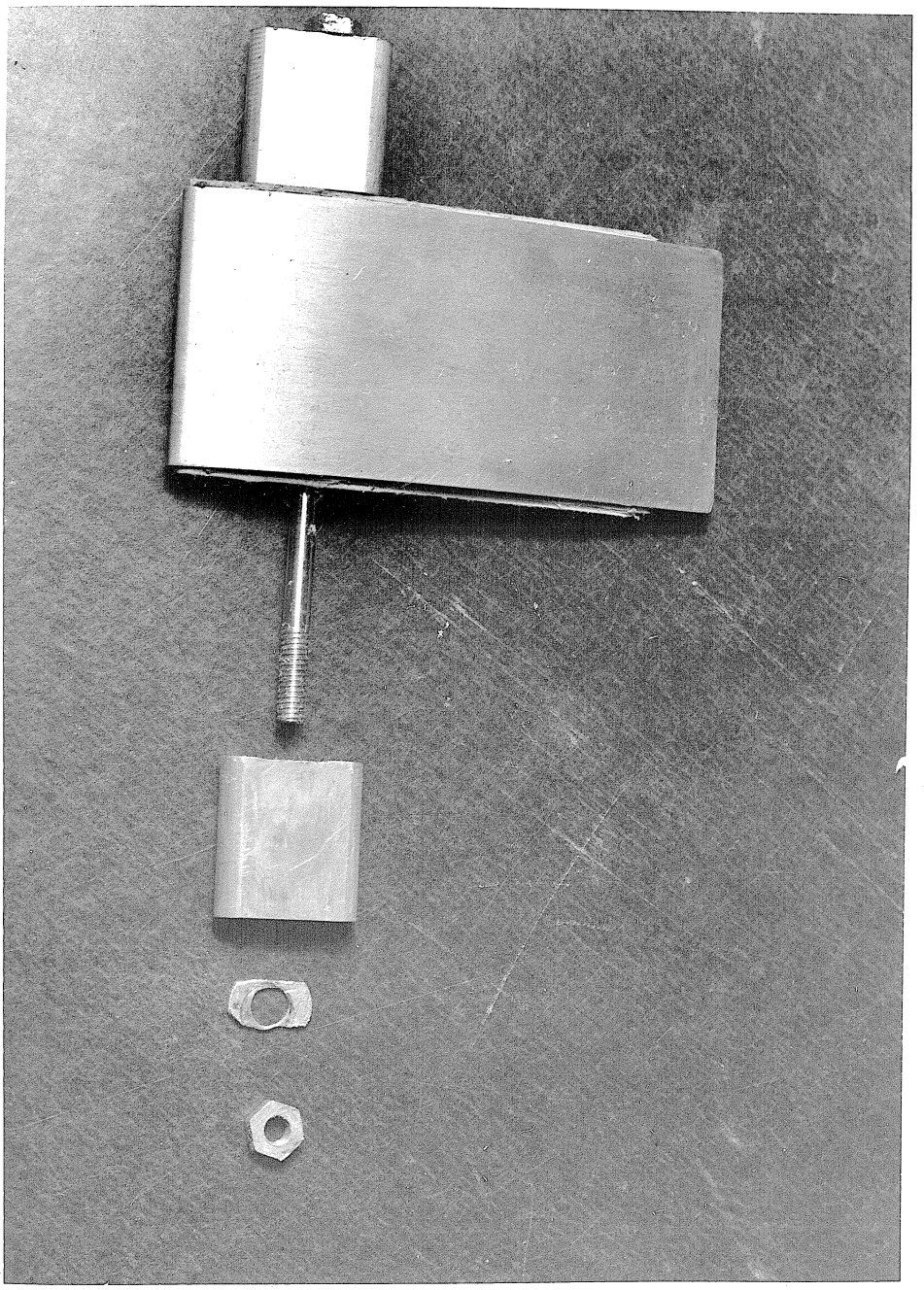

Fig. 6

FIG. 1

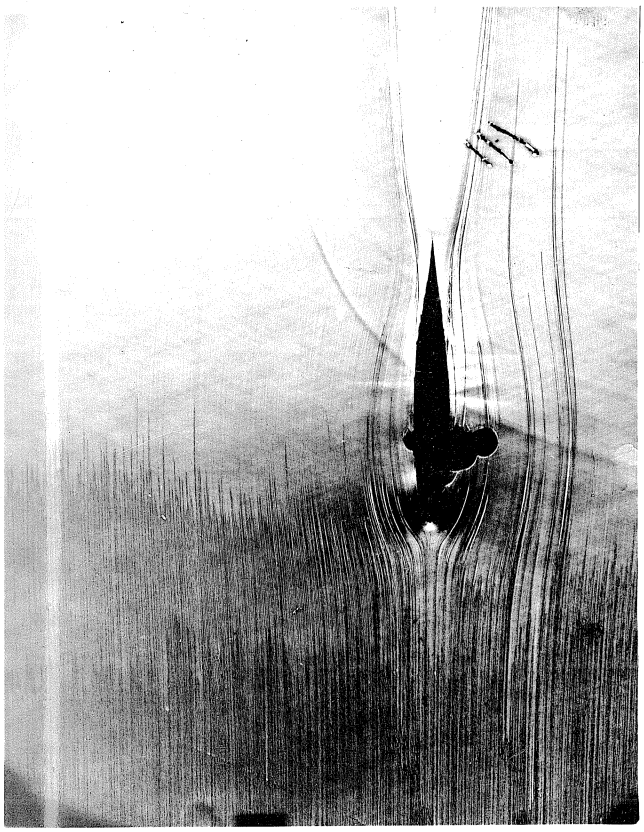

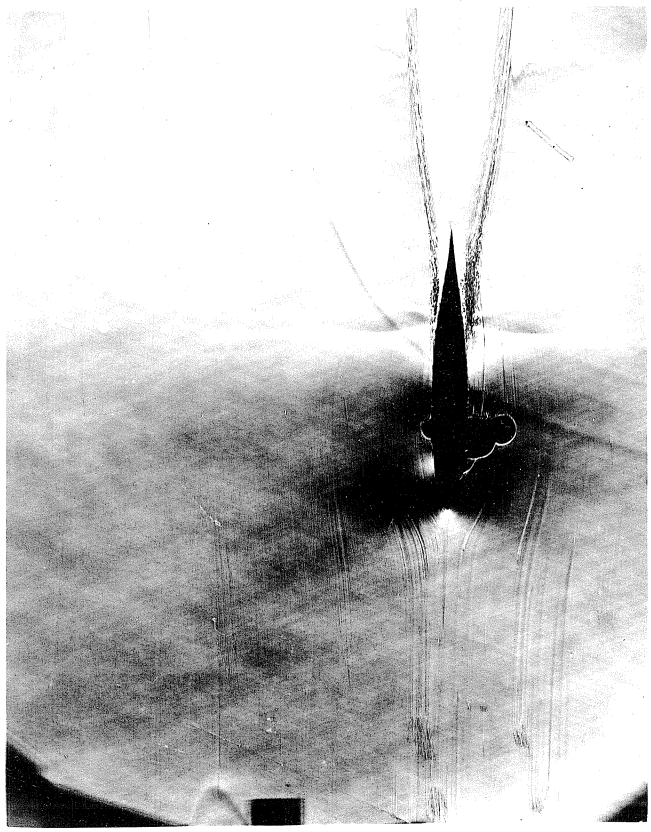

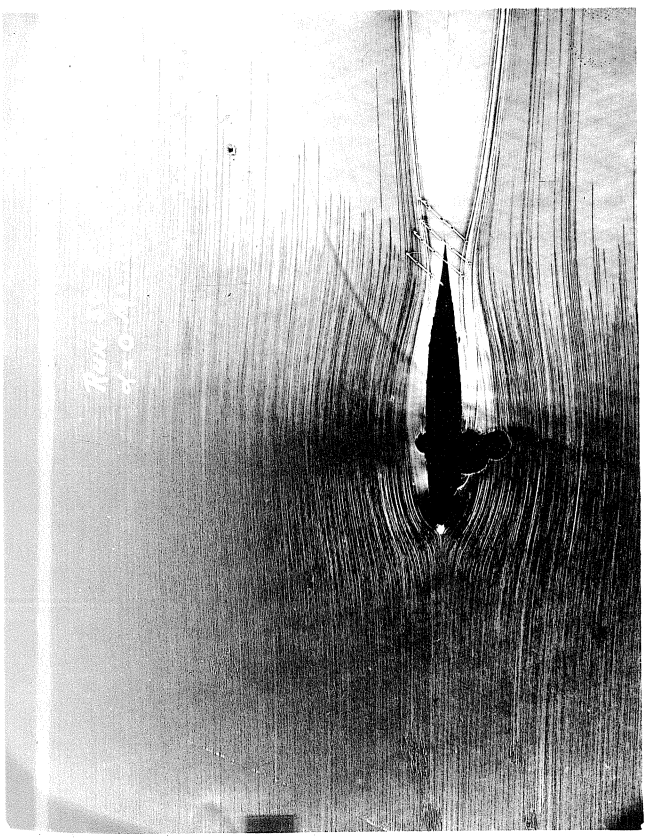

Fig. 8

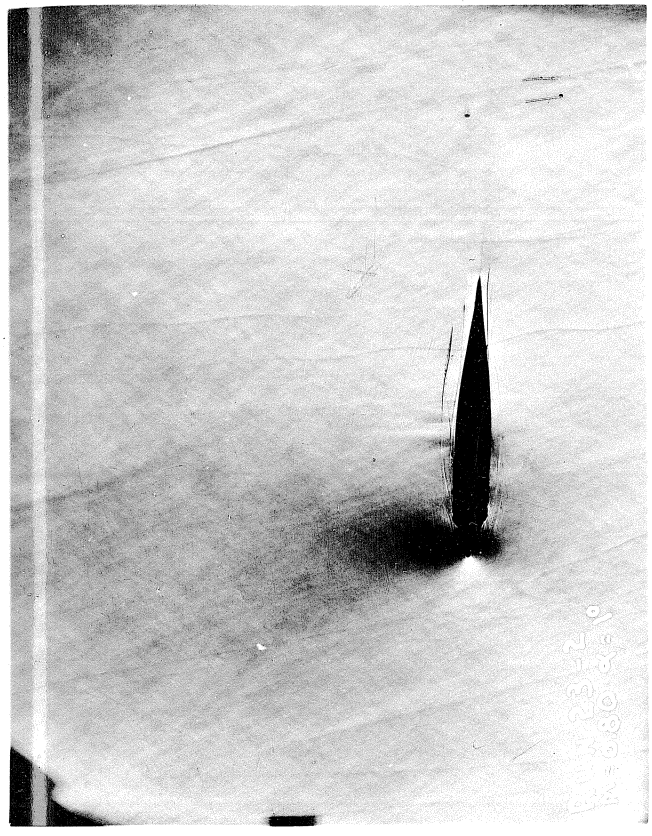

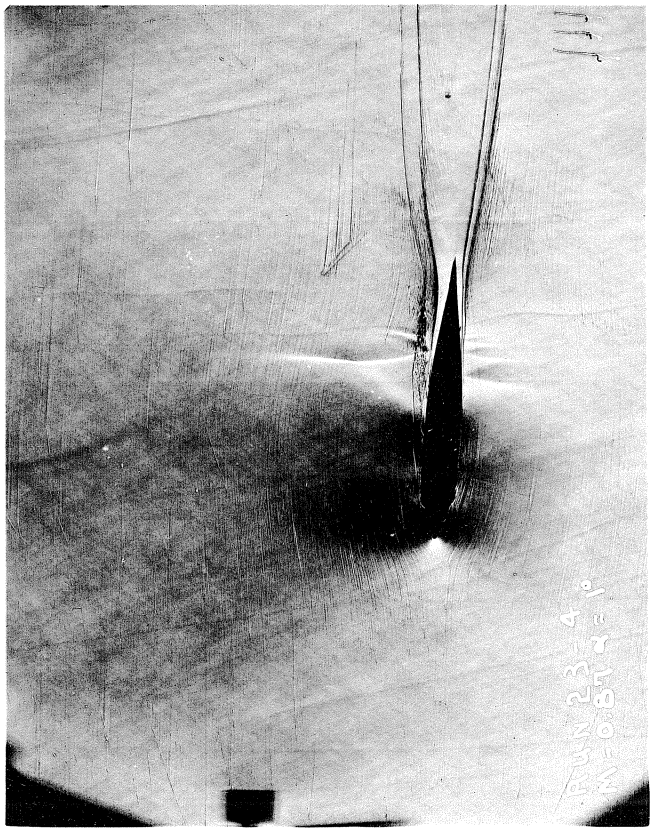

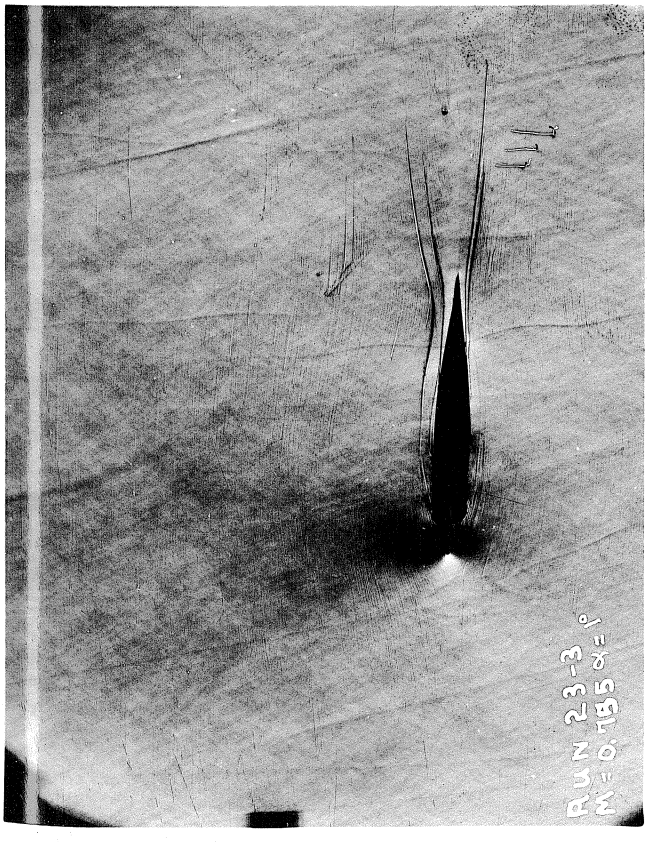

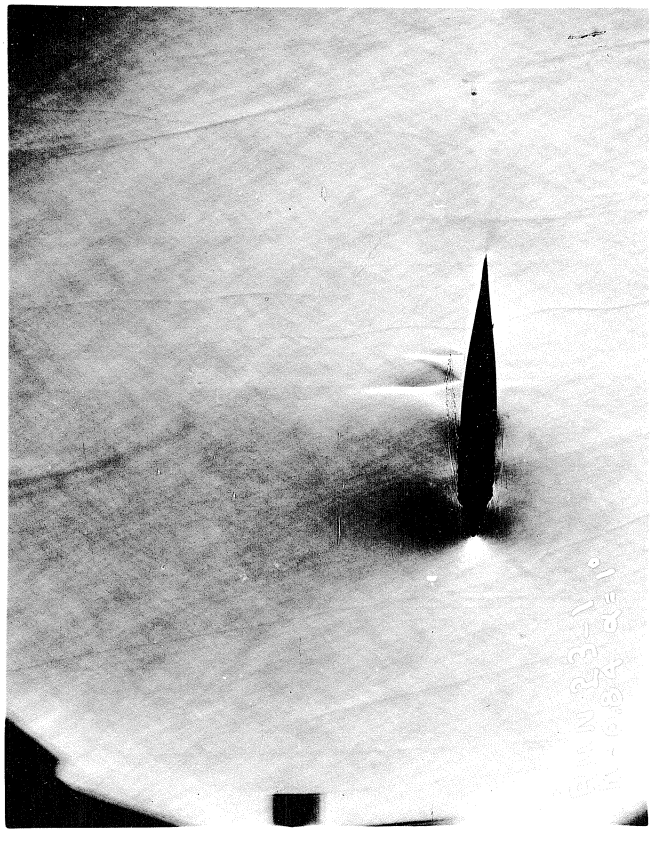

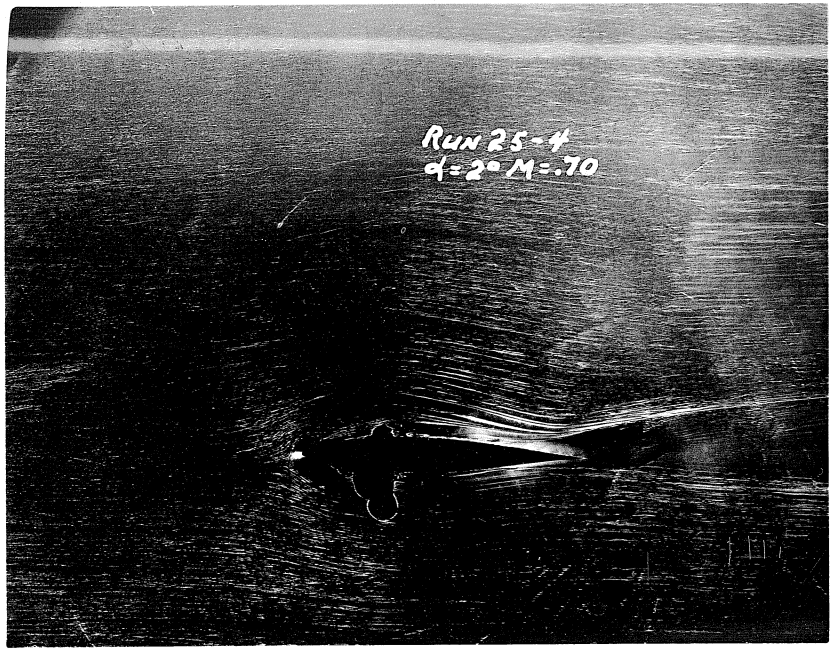
RUN 25-4
α=2° M=.70

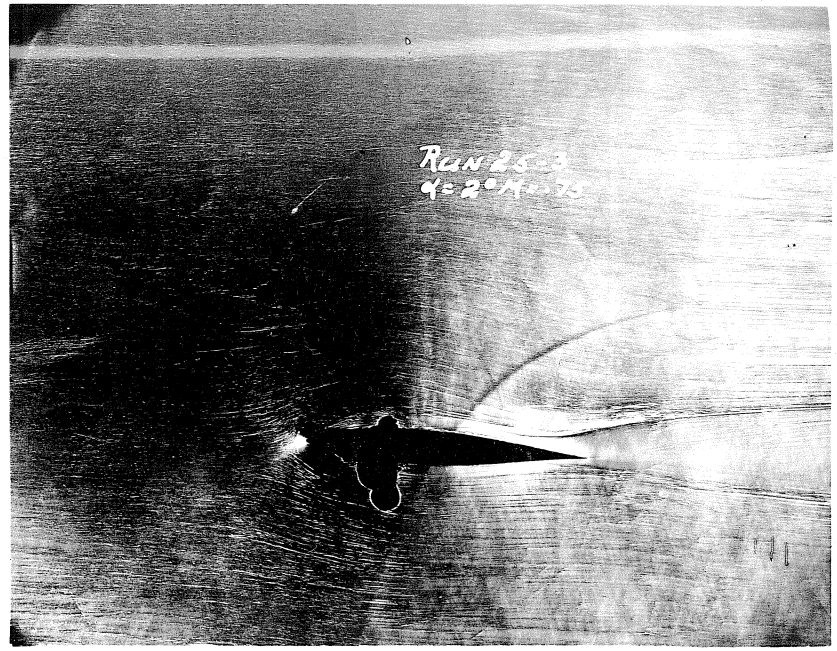
RUN 25-3
α=2° M=.75

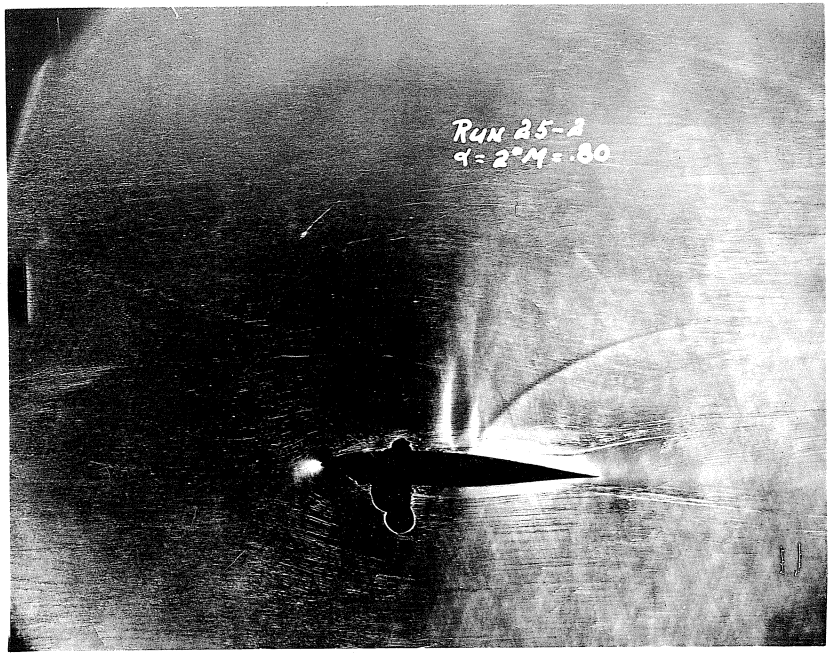
RUN 25-2
α=2° M=.80

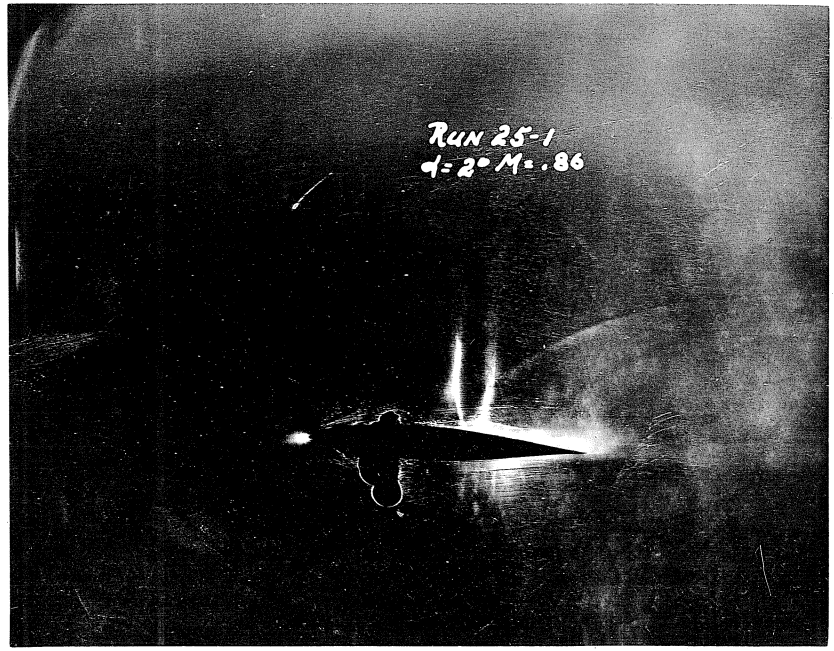
RUN 25-1
α=2° M=.86

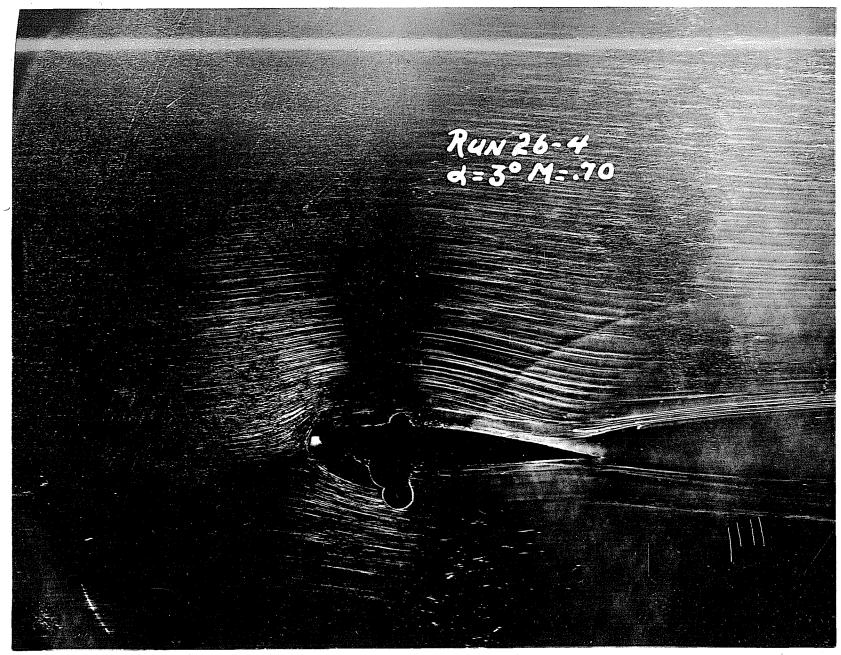

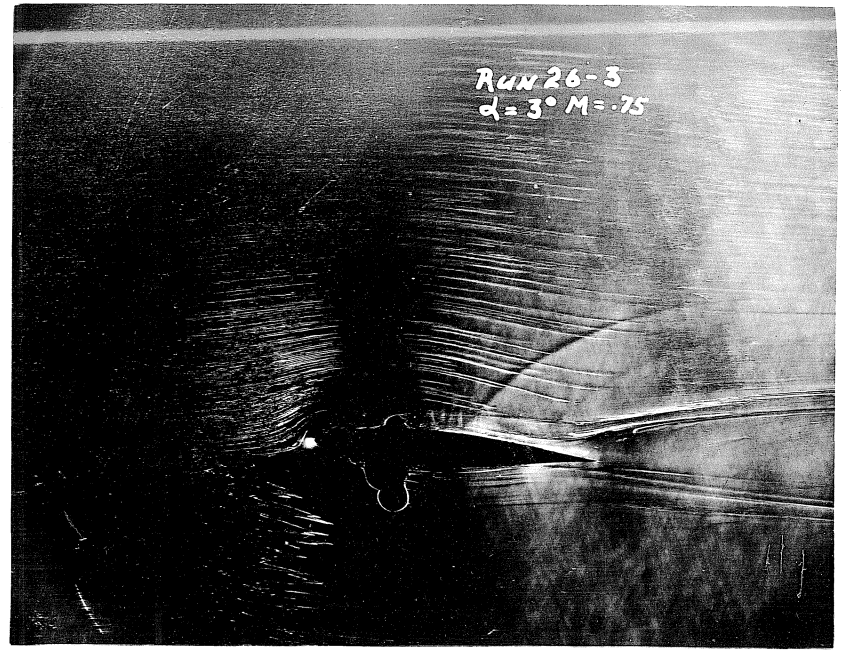

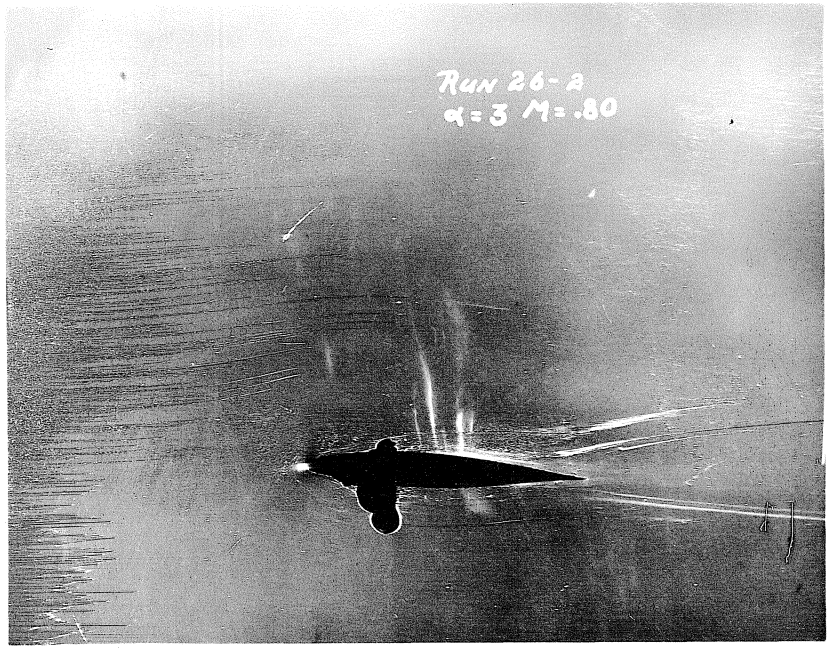

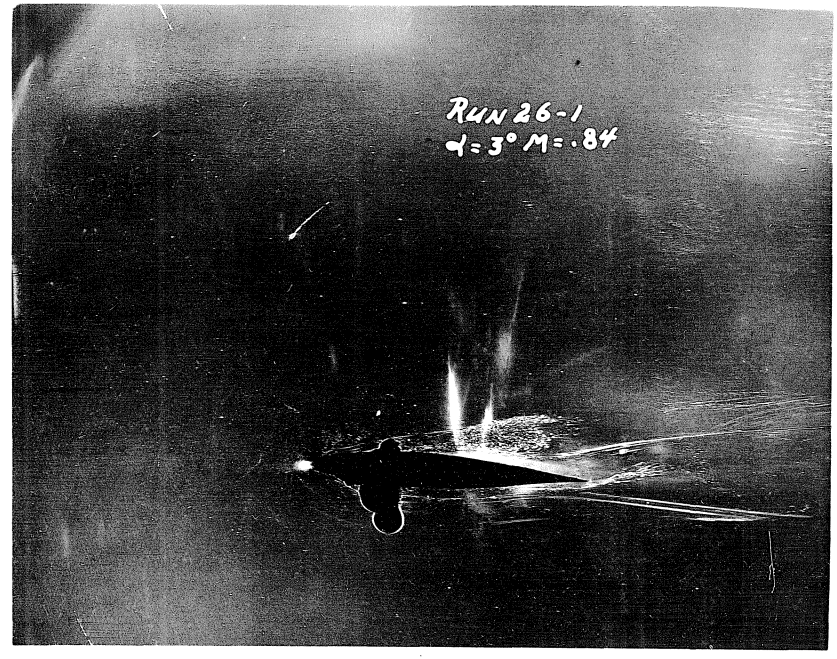

FIG. 10

FIG. 11

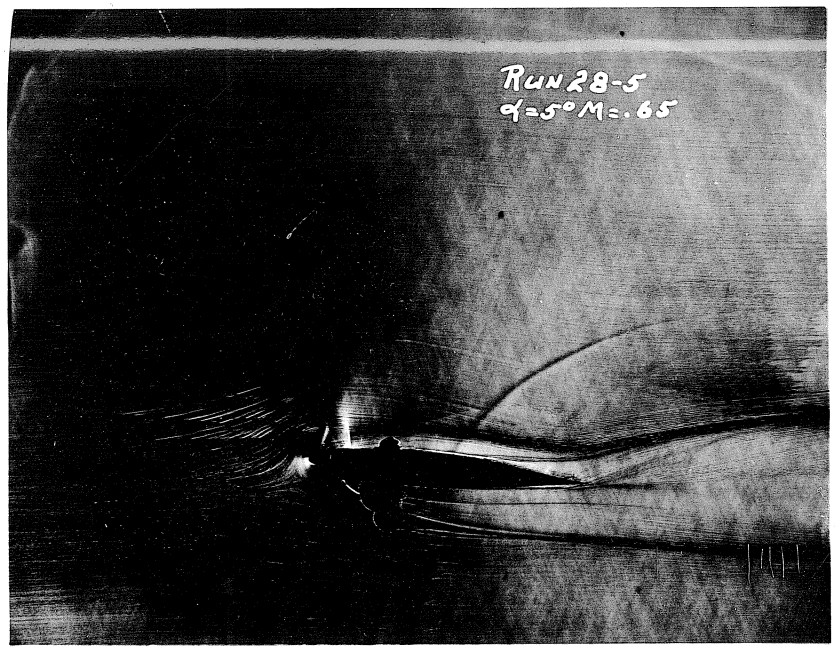

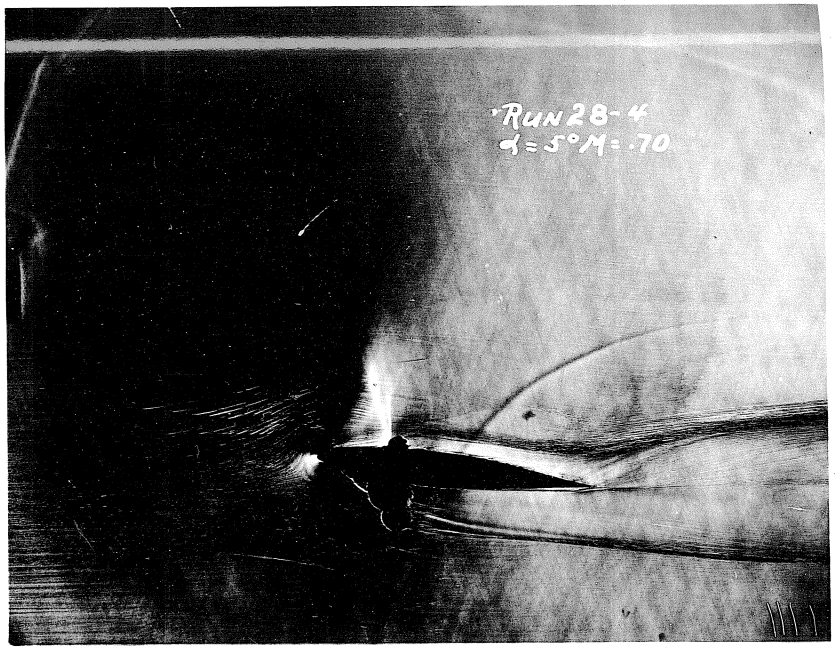

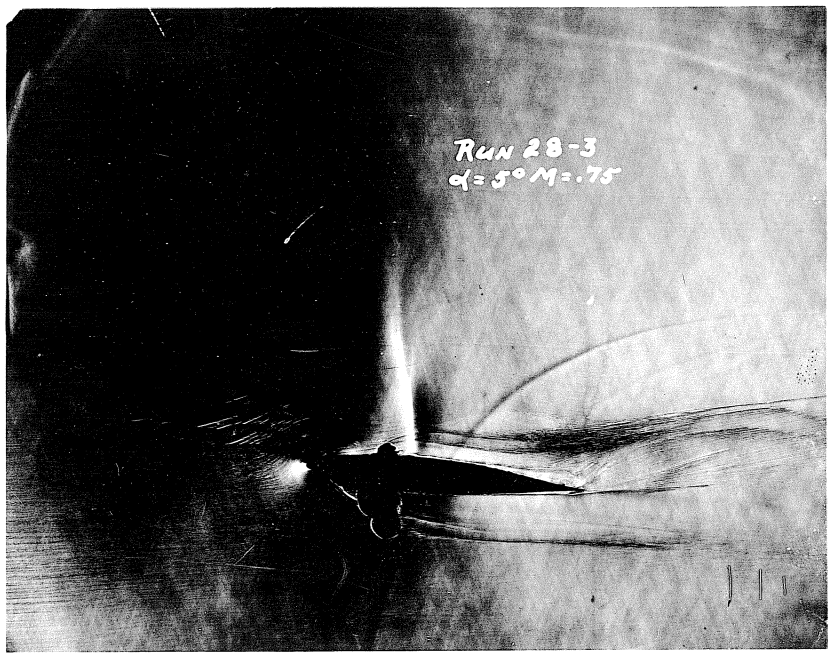

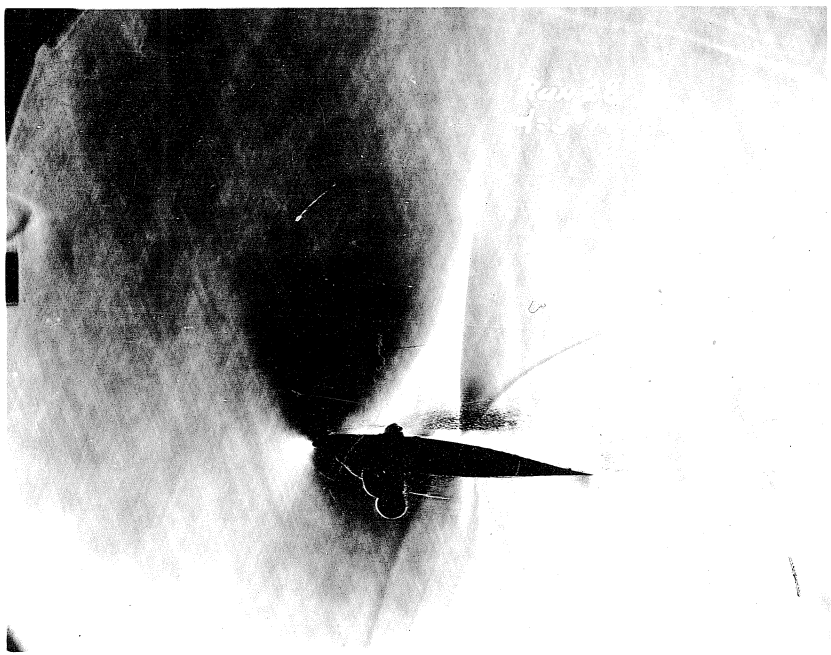

Fig. 12

Fig. 13

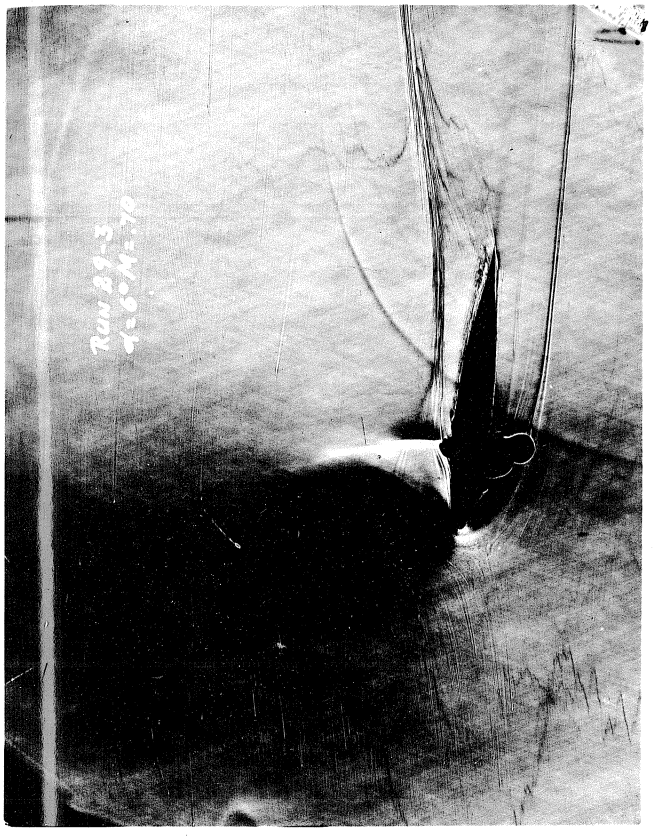

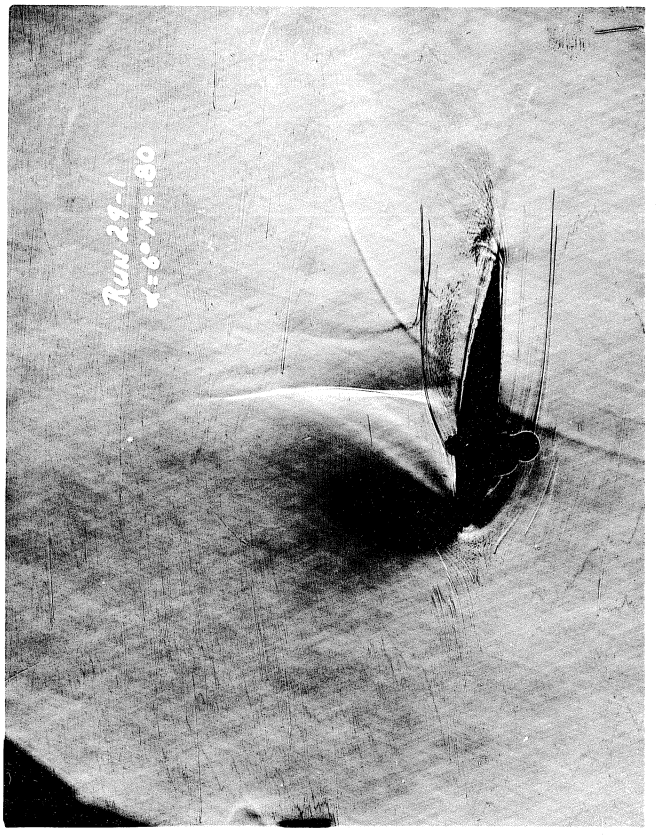

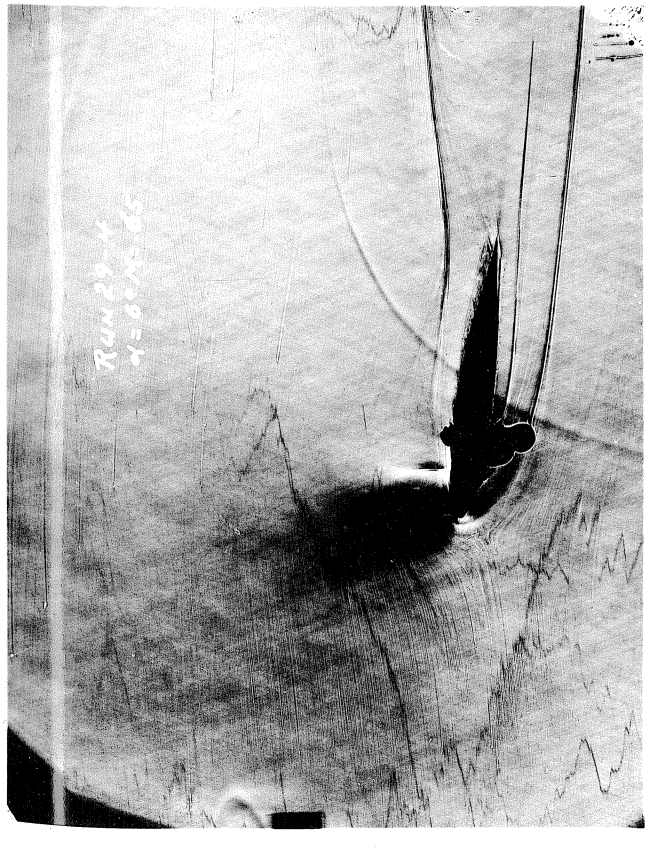

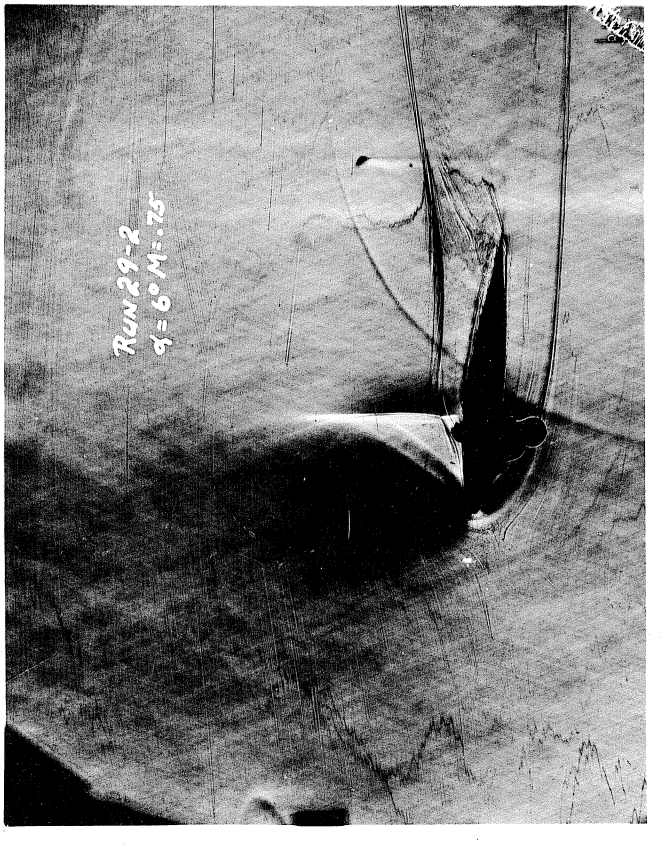

FIG. 14

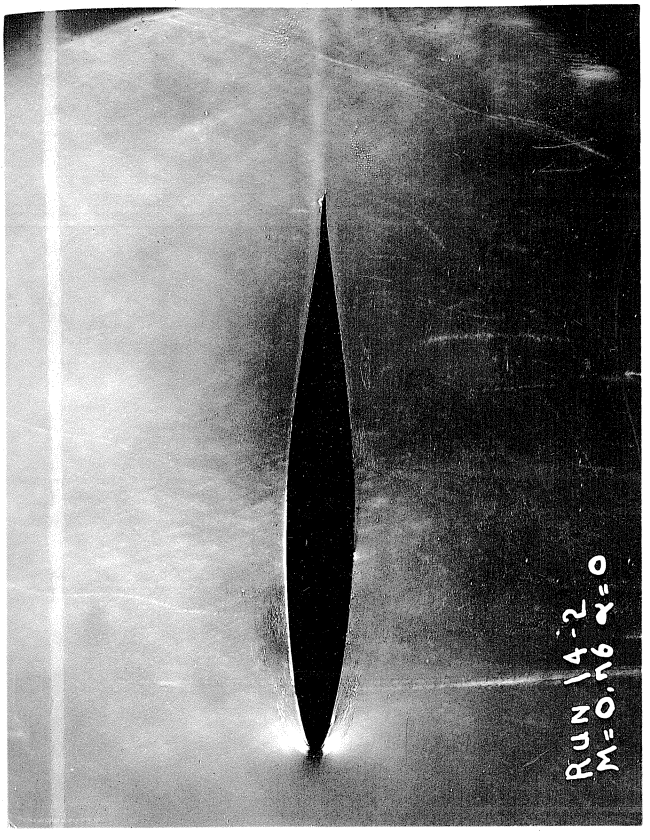

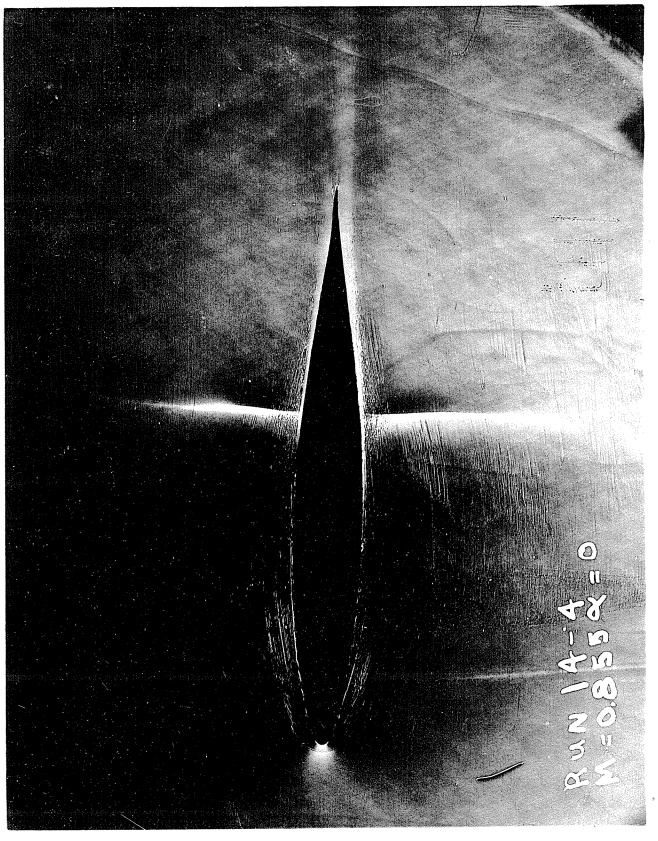

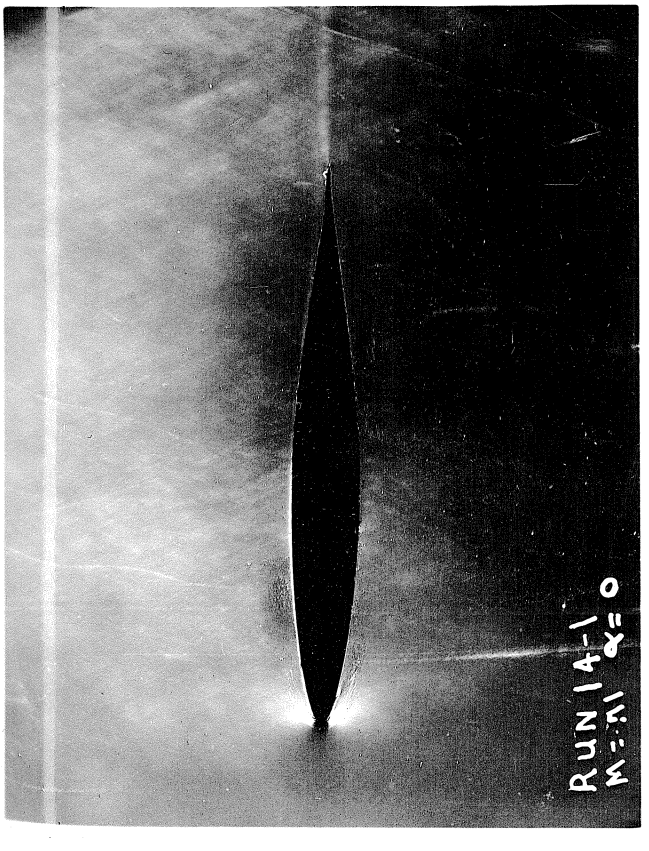

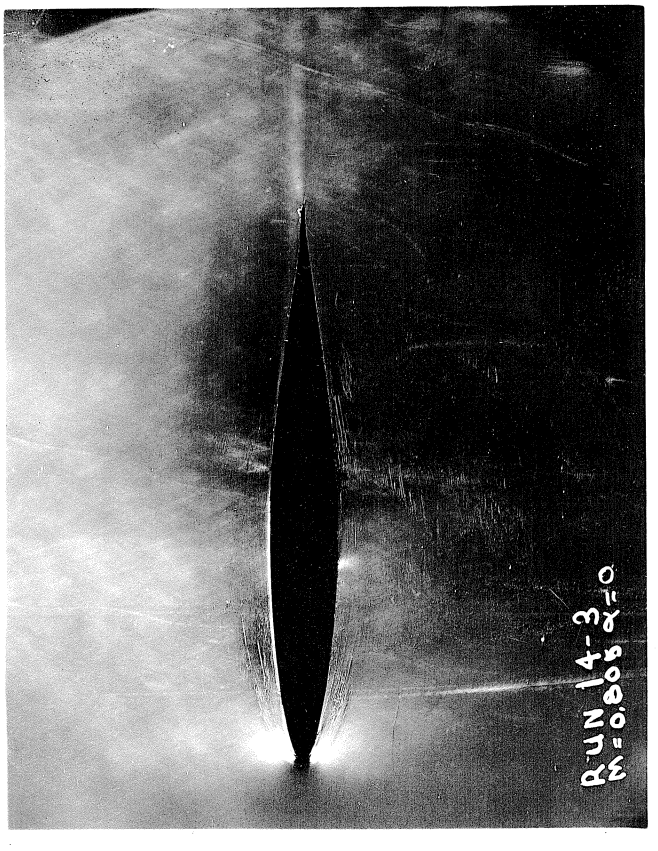

FIG. 15

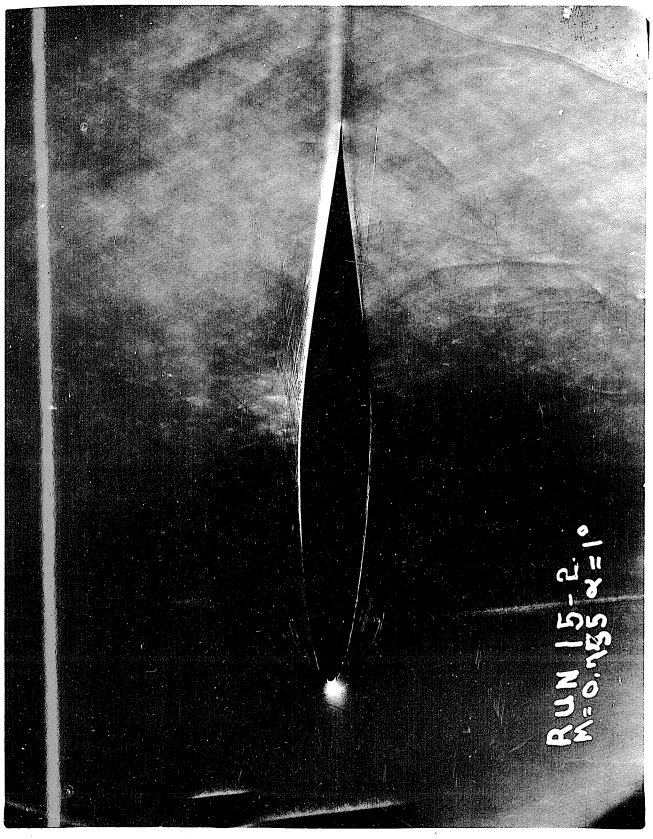

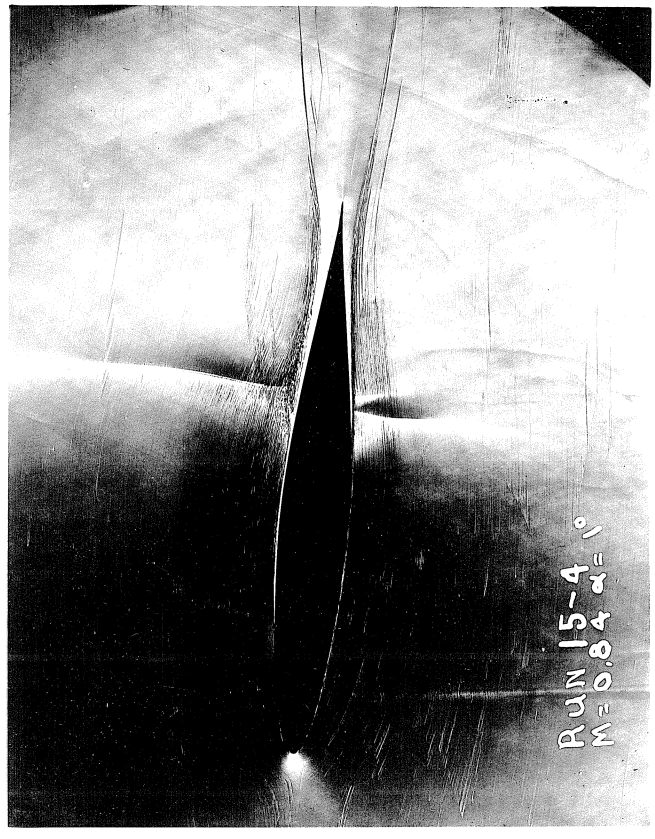

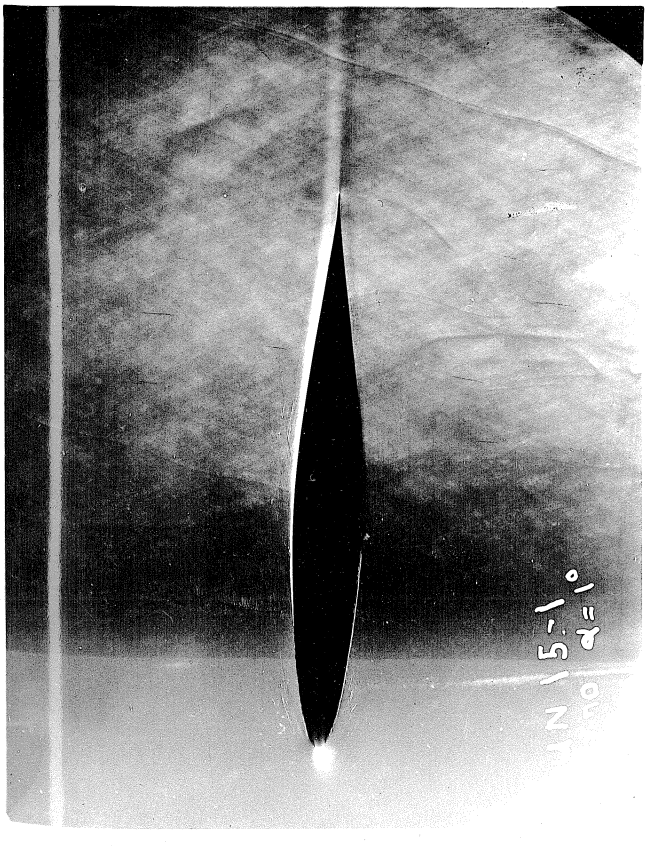

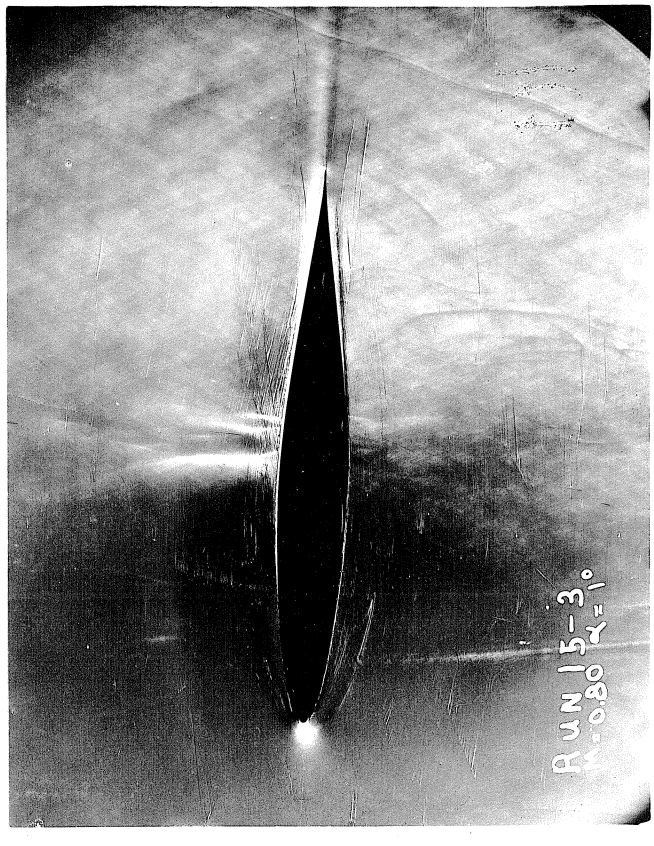

FIG. 16

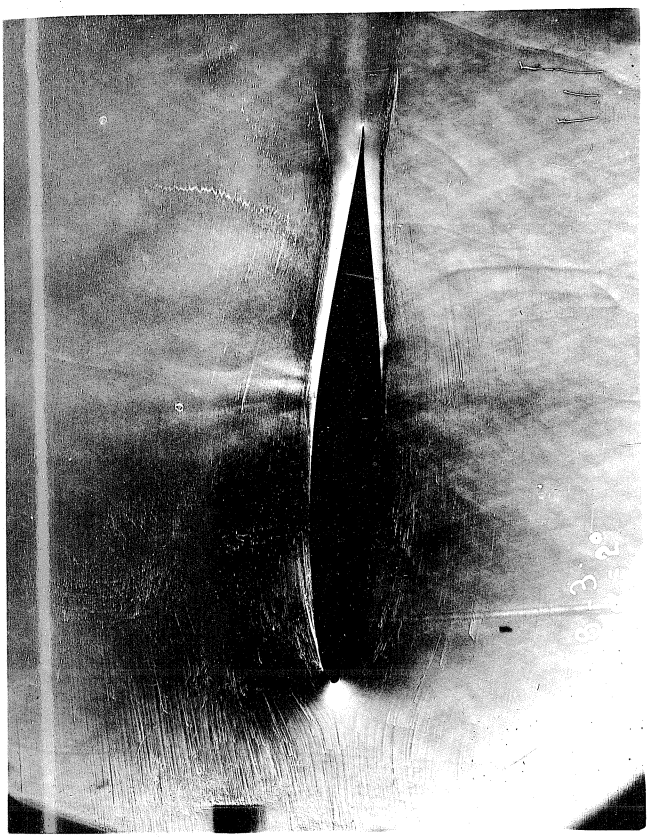

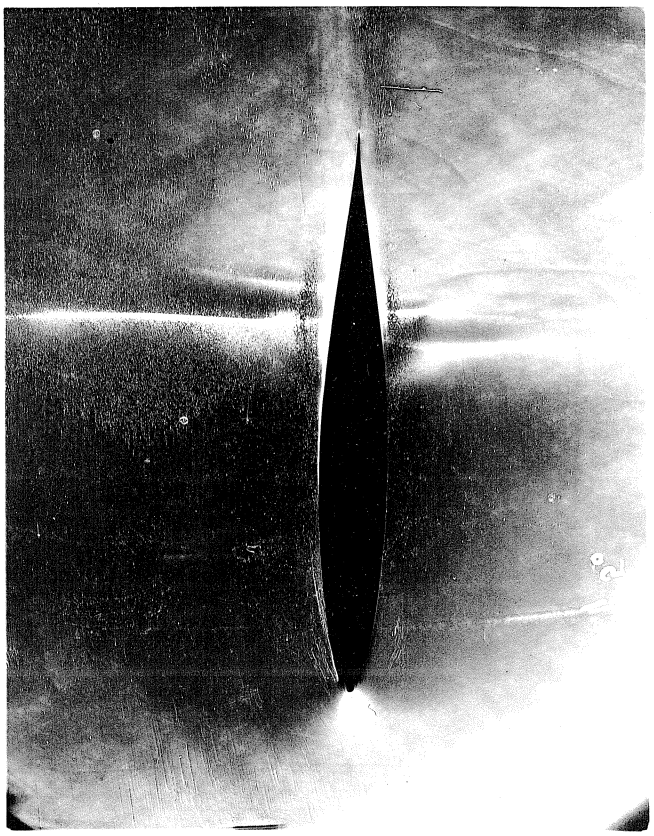

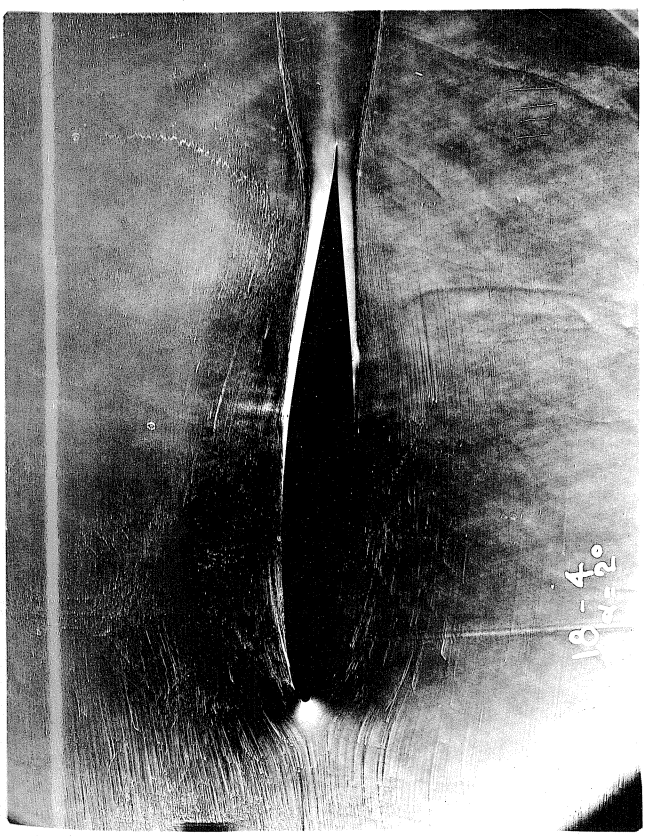

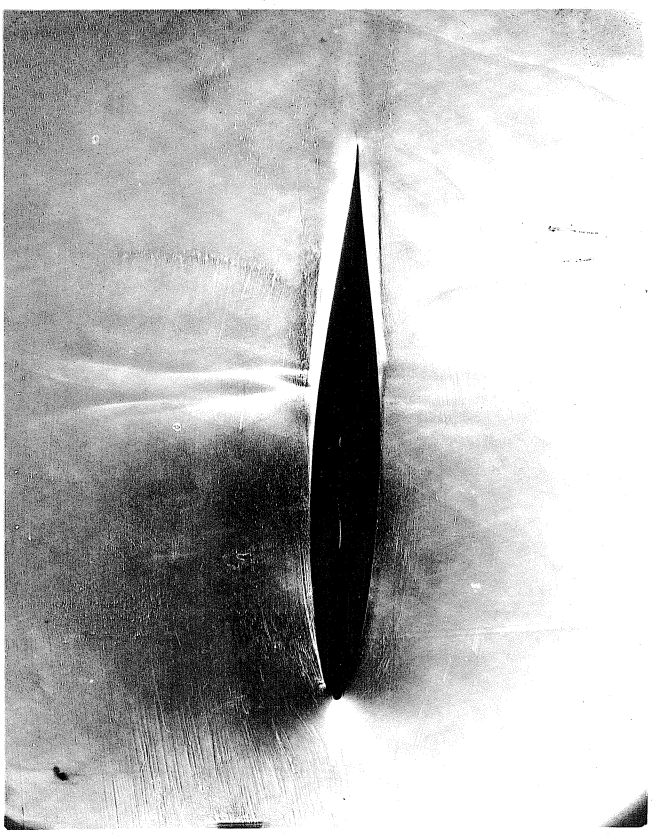

FIG. 17

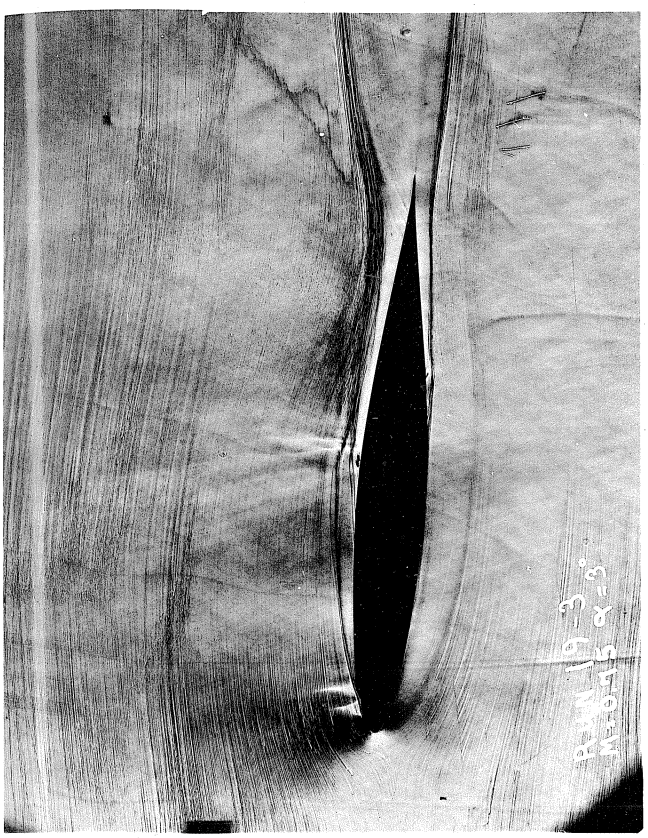

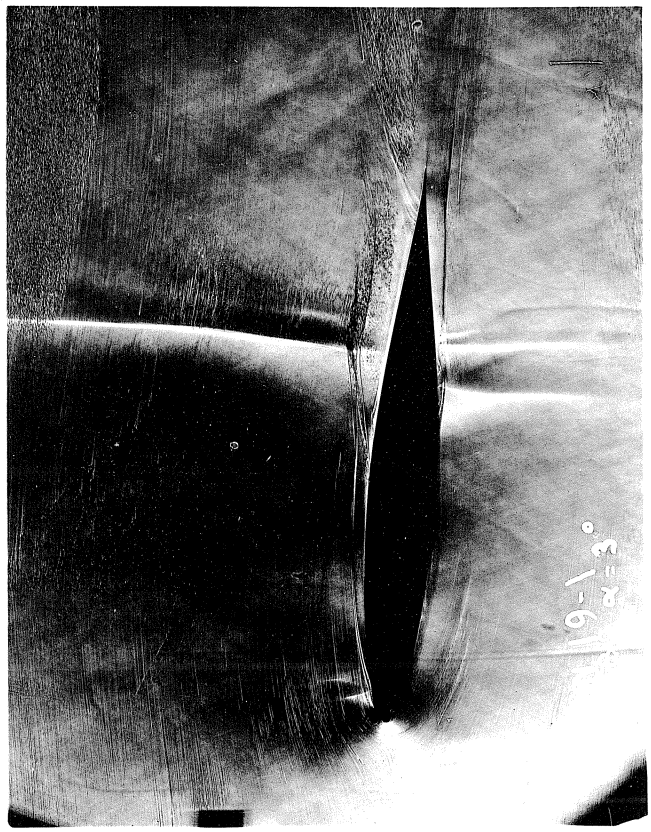

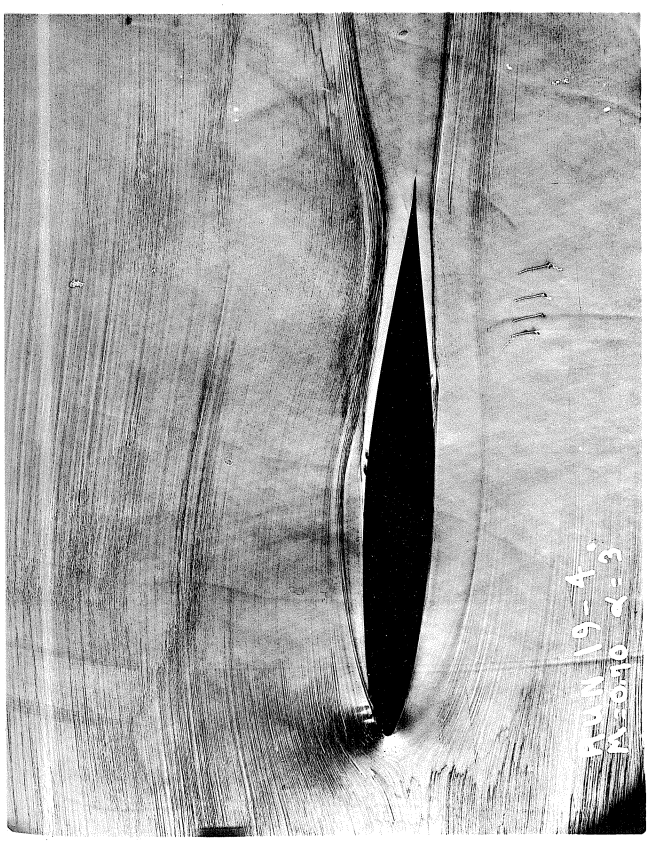

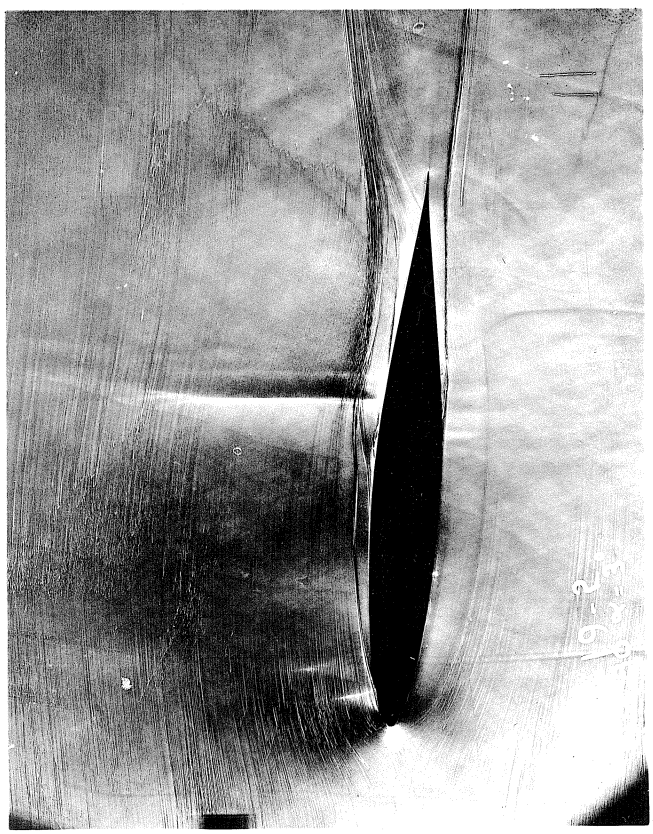

FIG. 18

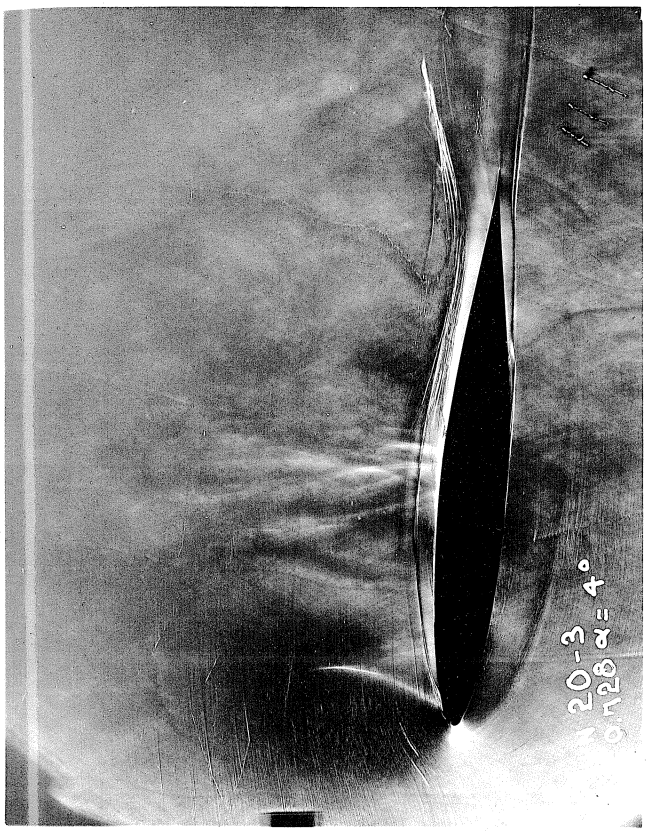

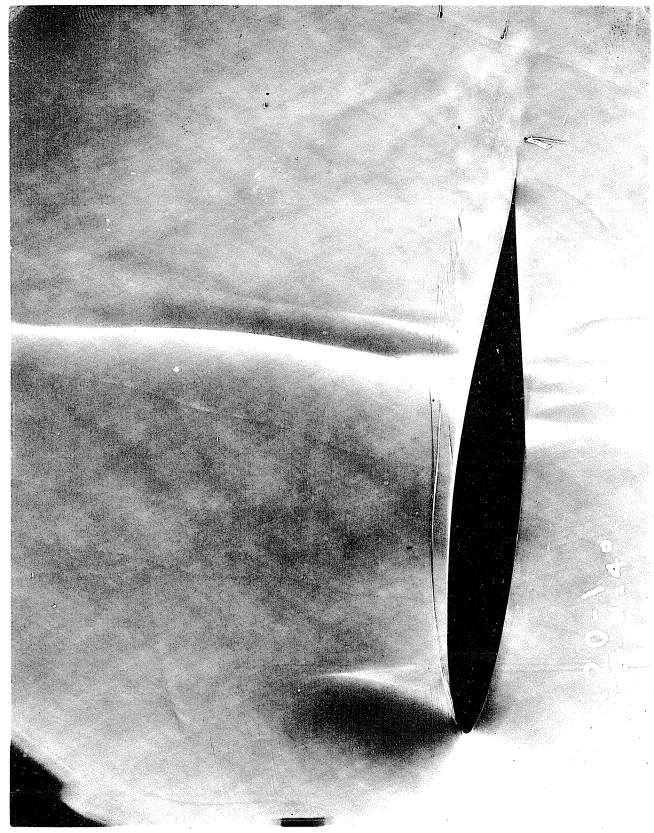

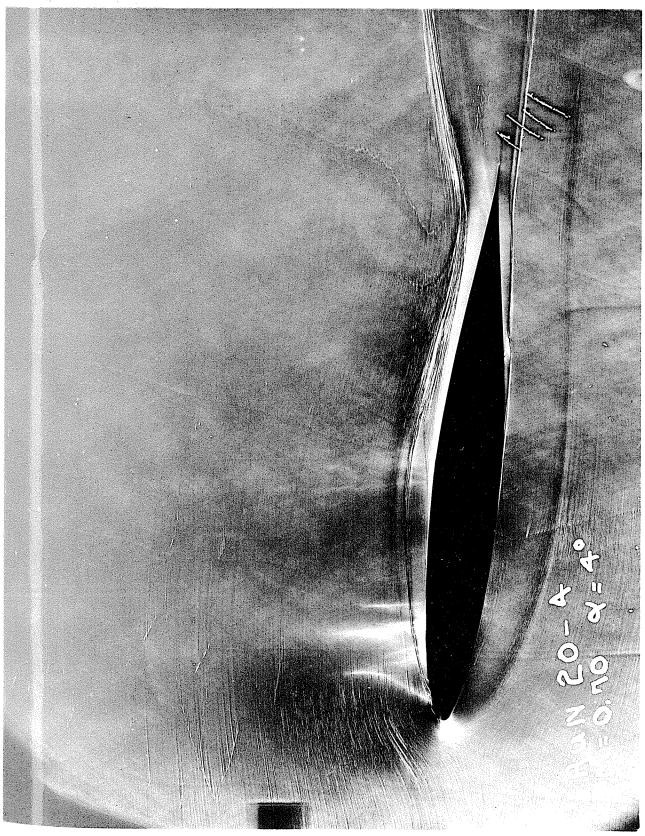

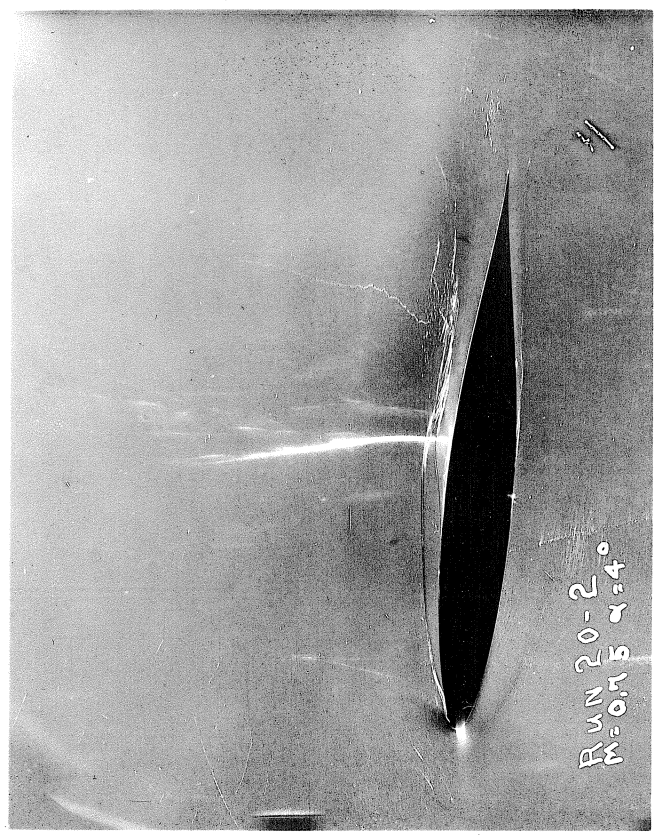

FIG. 19

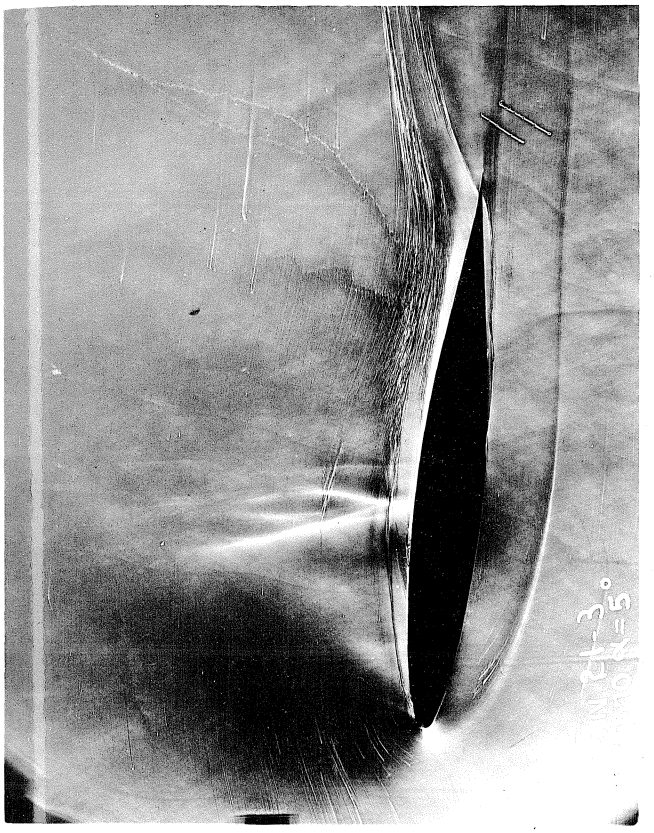

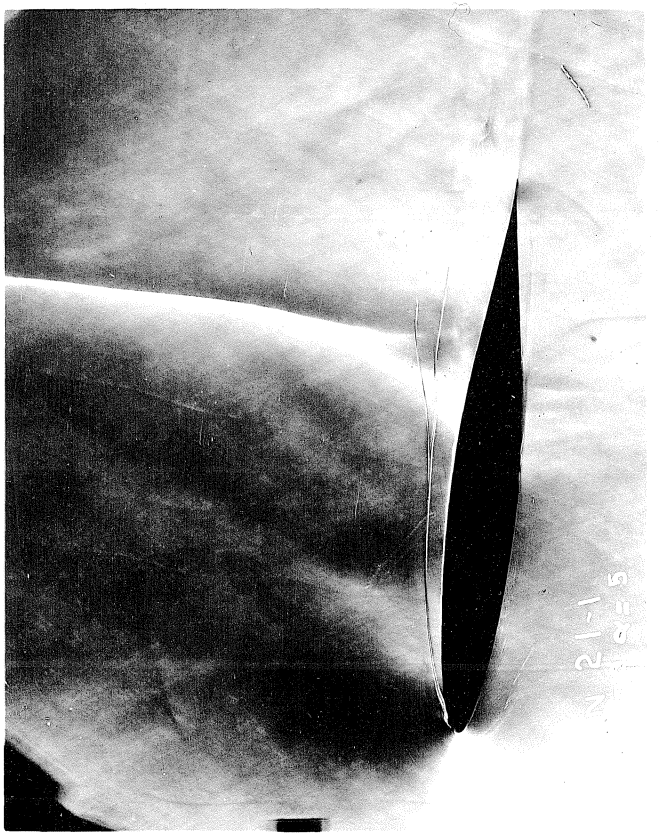

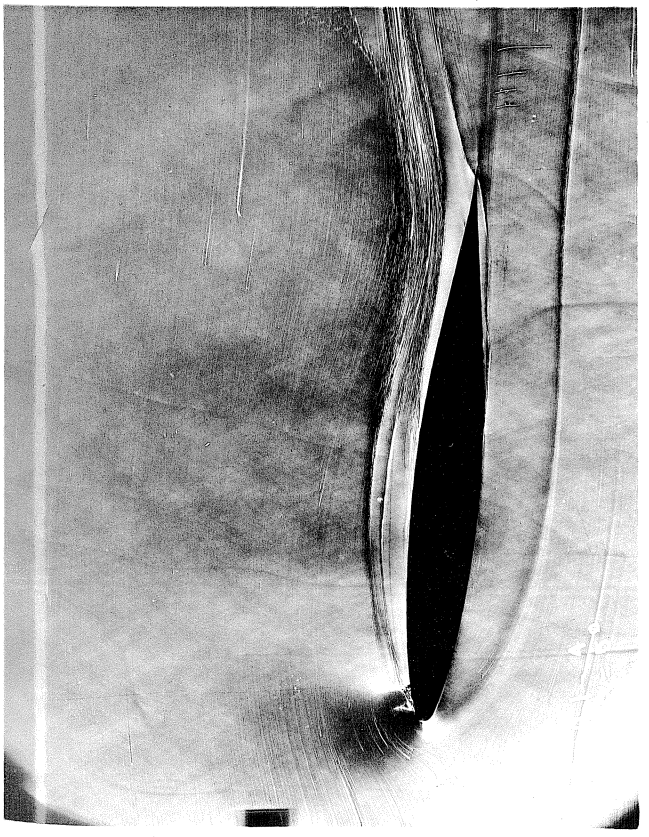

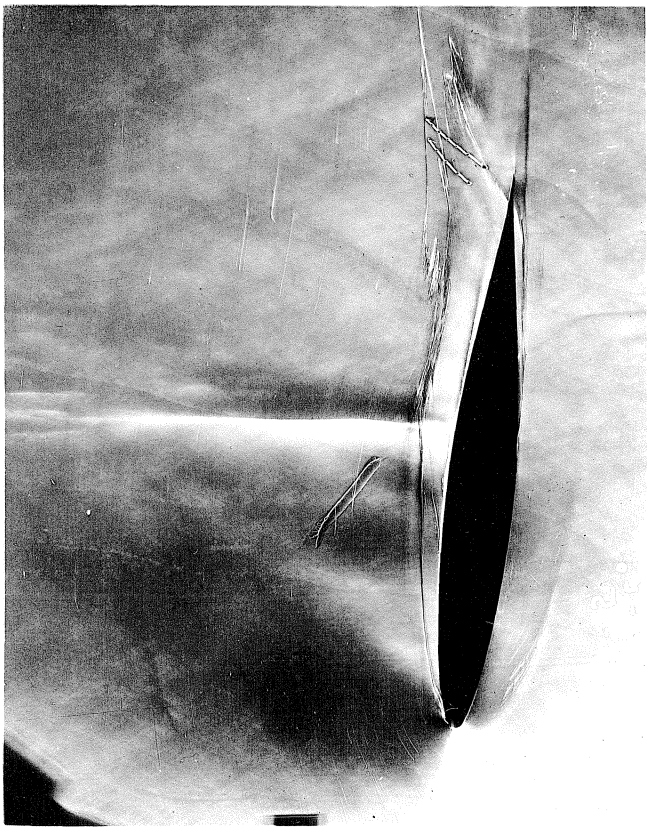

FIG. 20

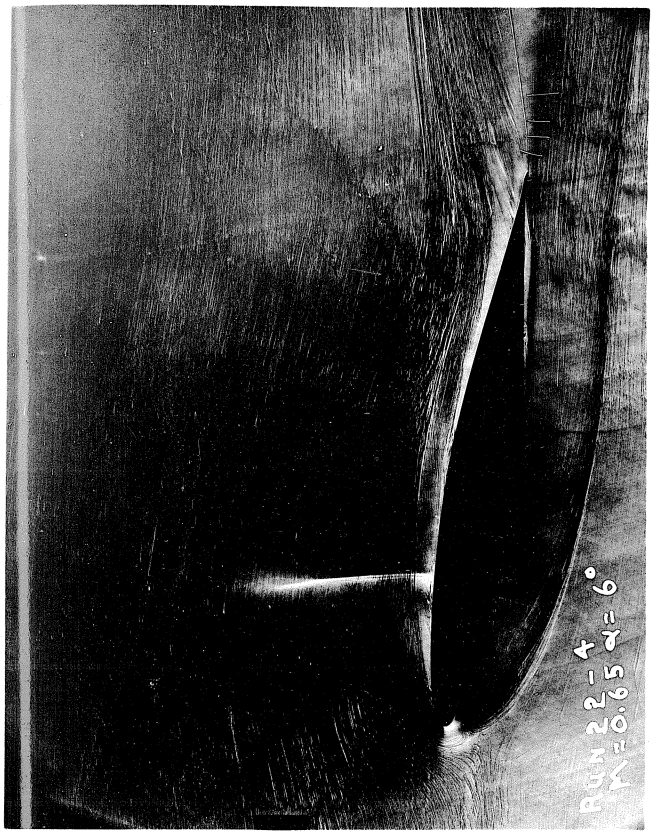

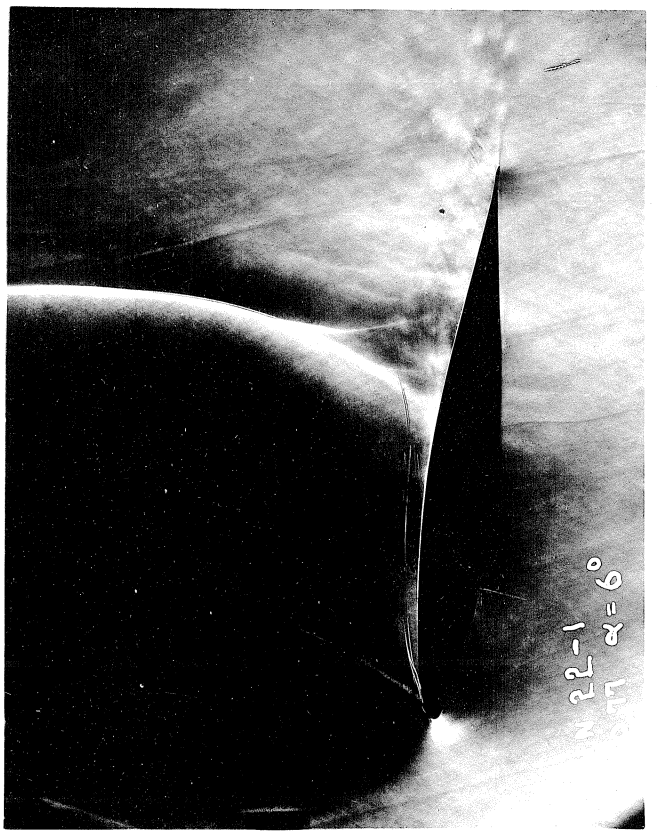

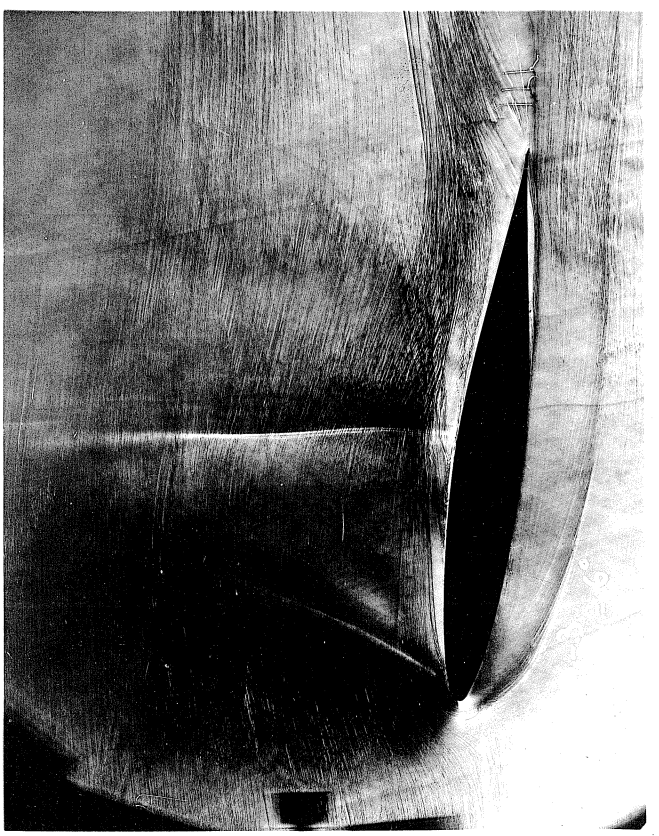

FIG. 21

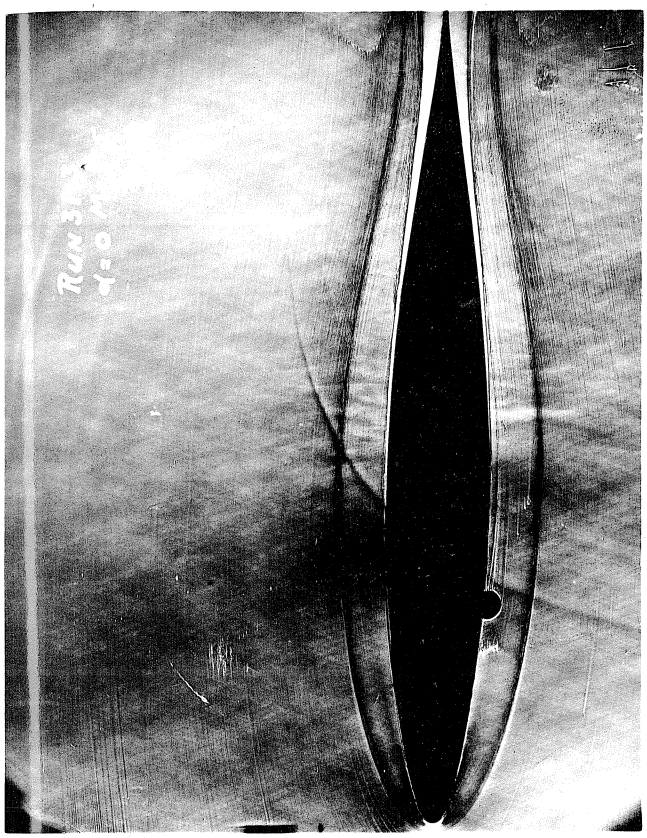

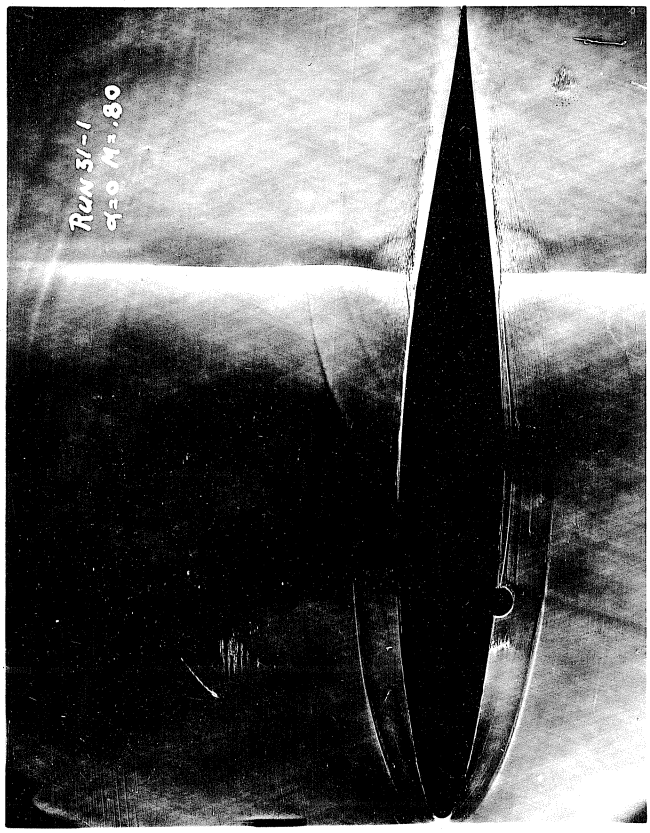

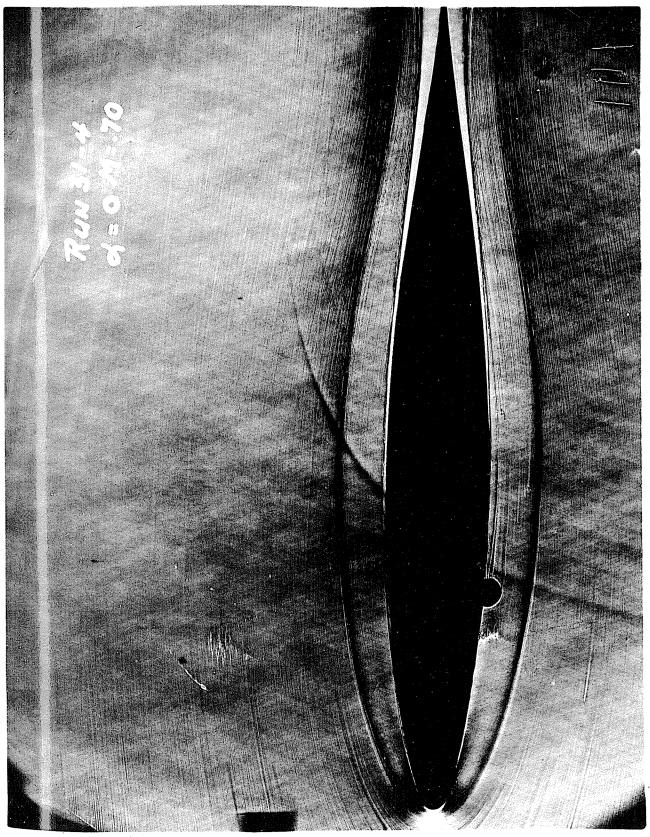

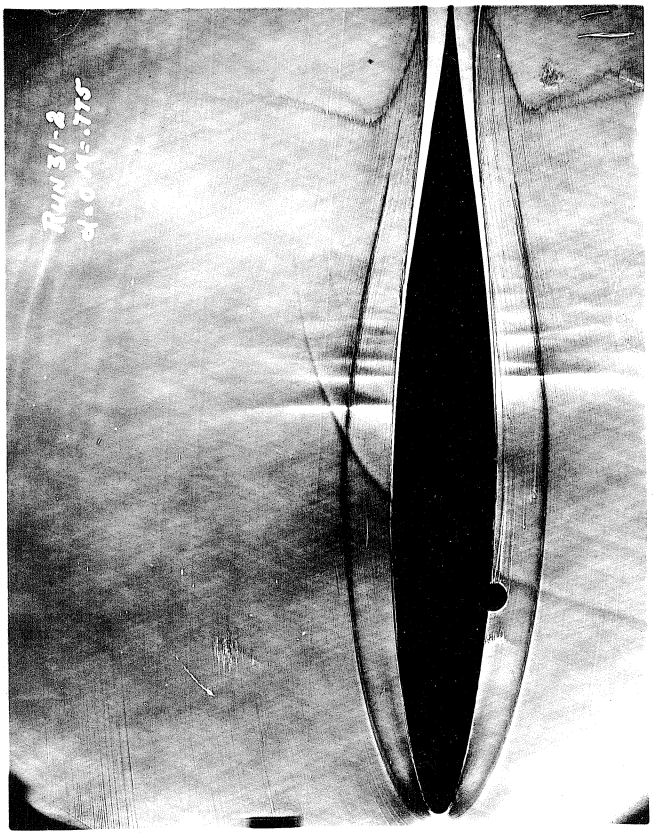

FIG. 22

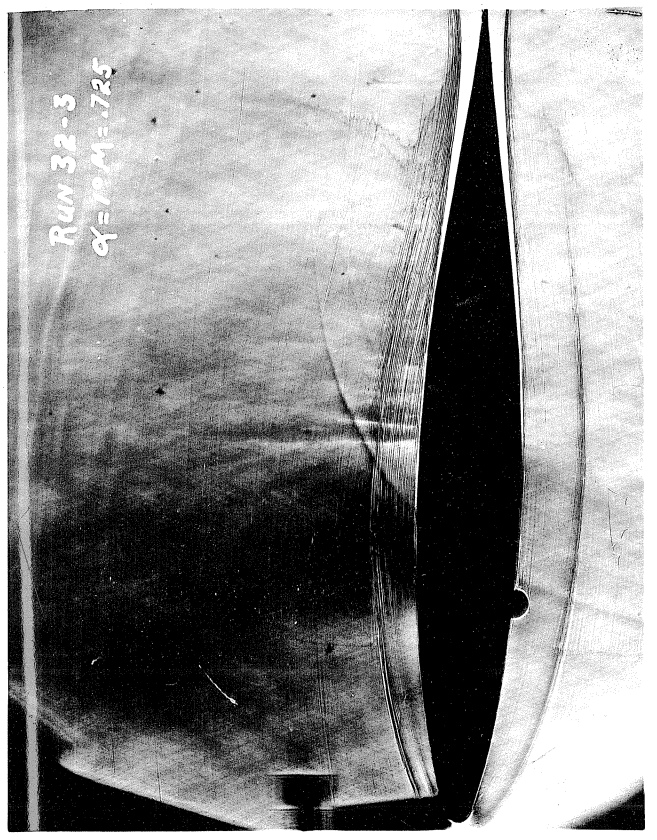
RUN 32-3
q=10 M=.725

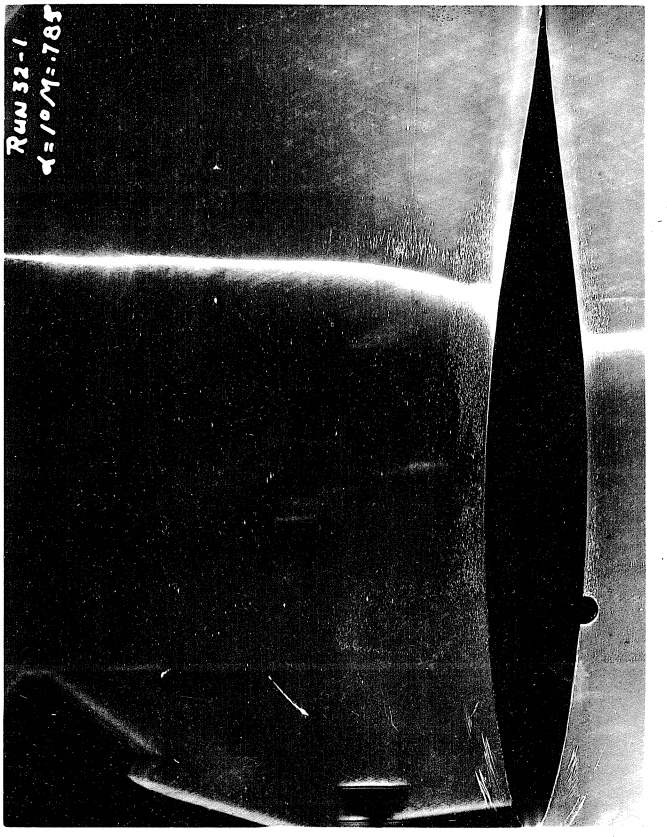
RUN 32-1
q=10 M=.785

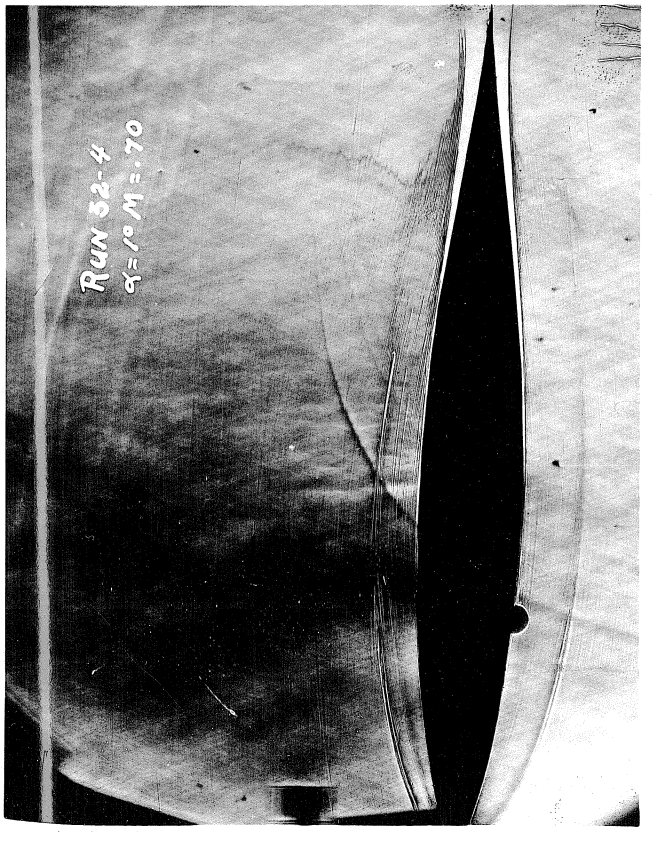
RUN 32-4
q=10 M=.70

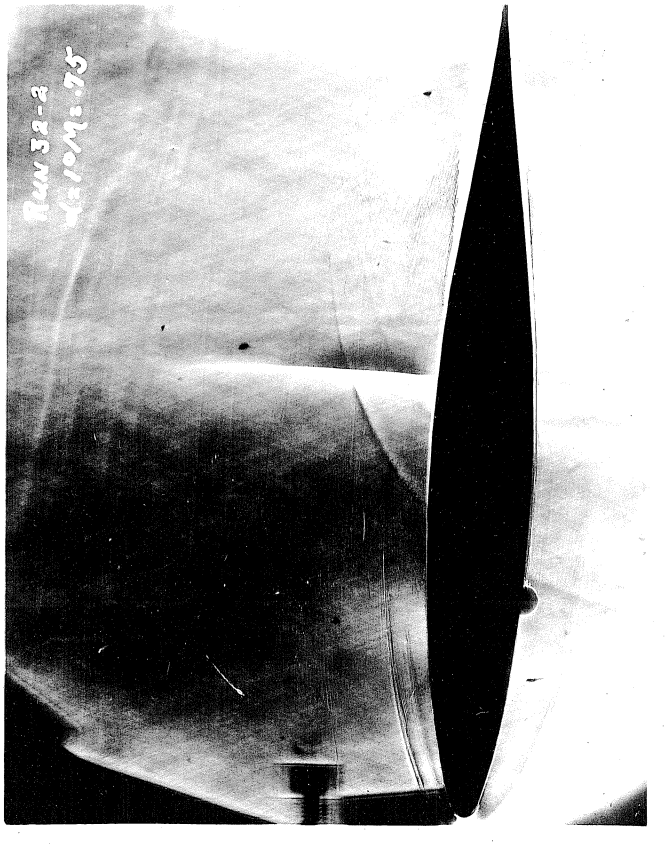
RUN 32-2
q=10 M=.75

FIG. 23

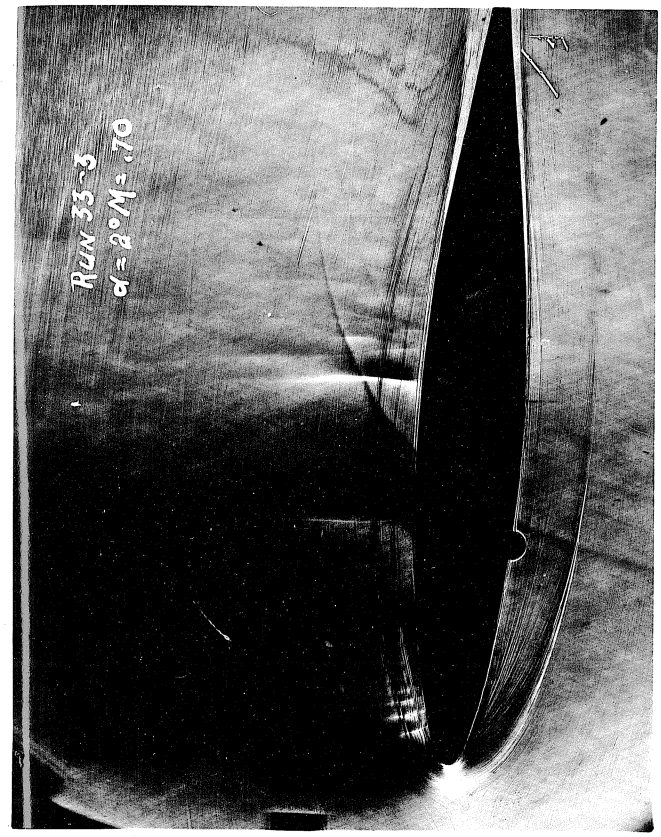

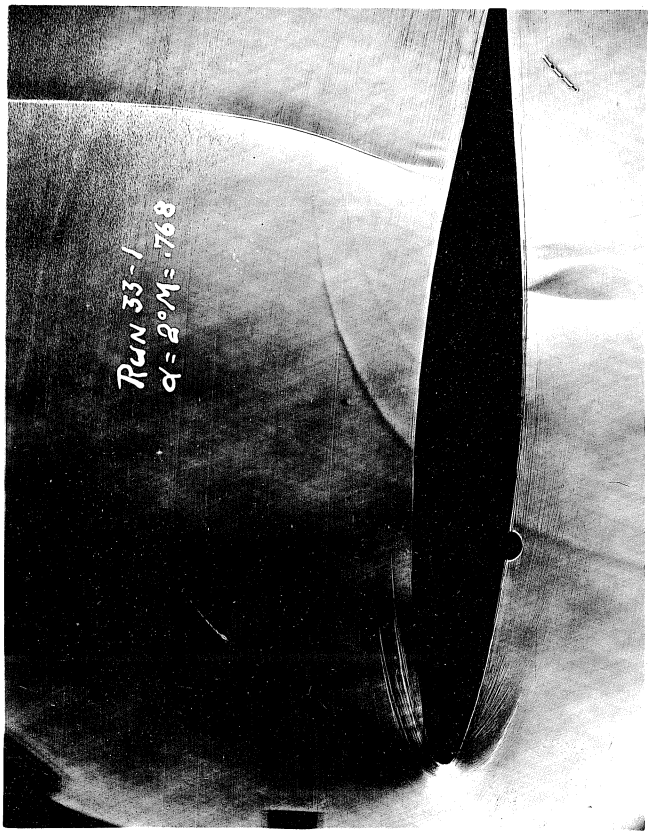

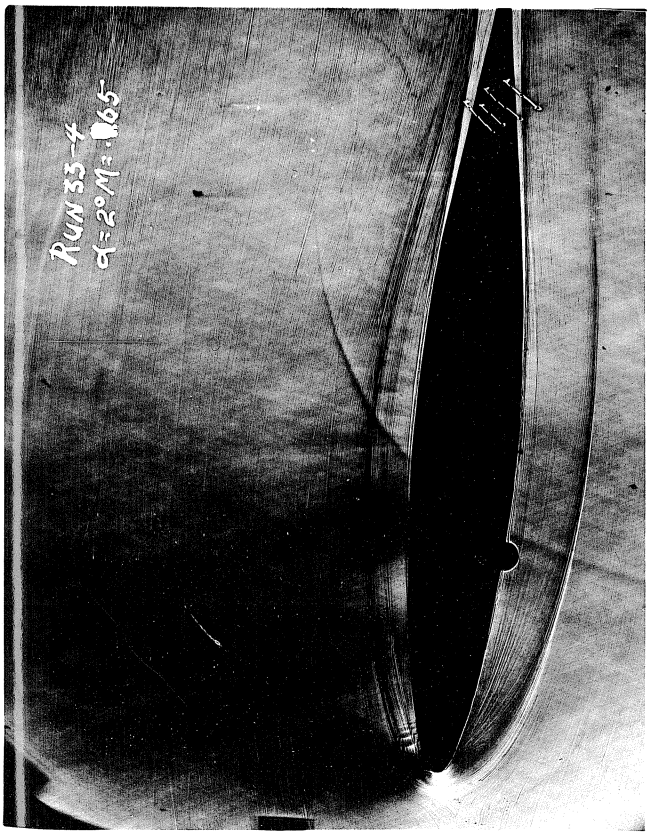

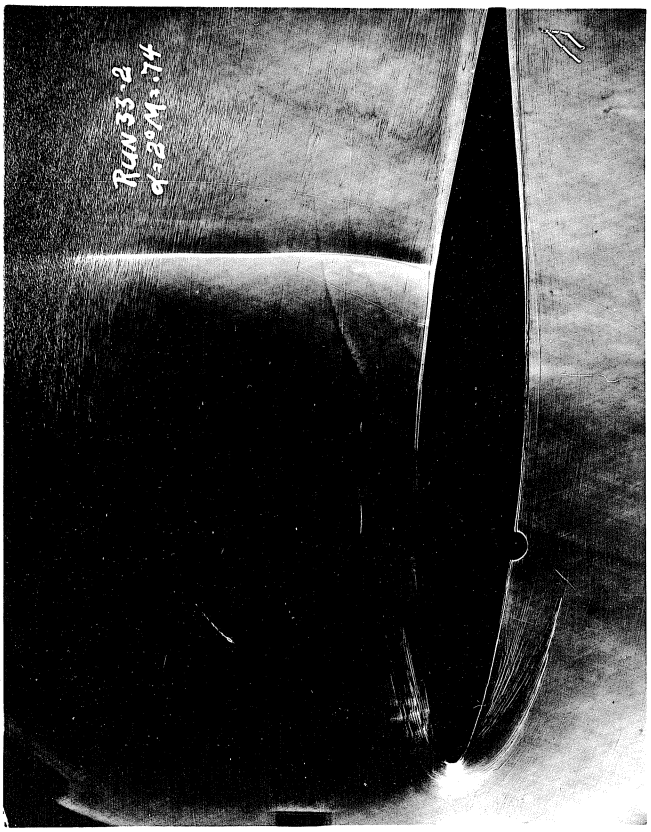

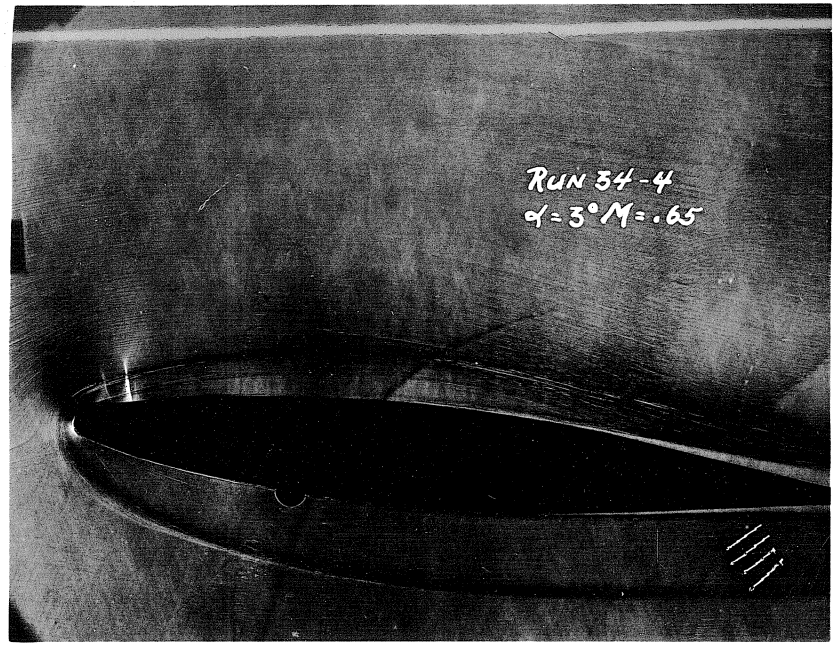

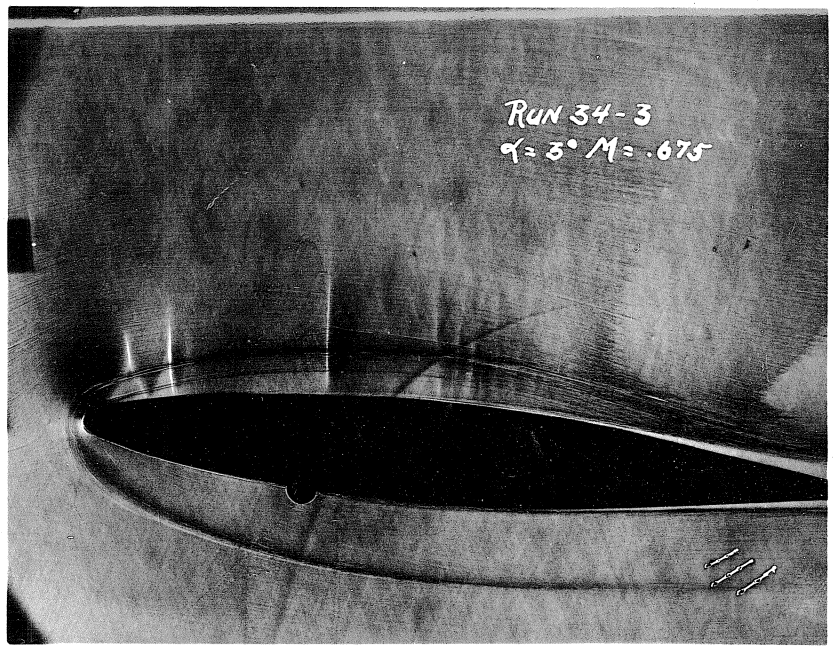

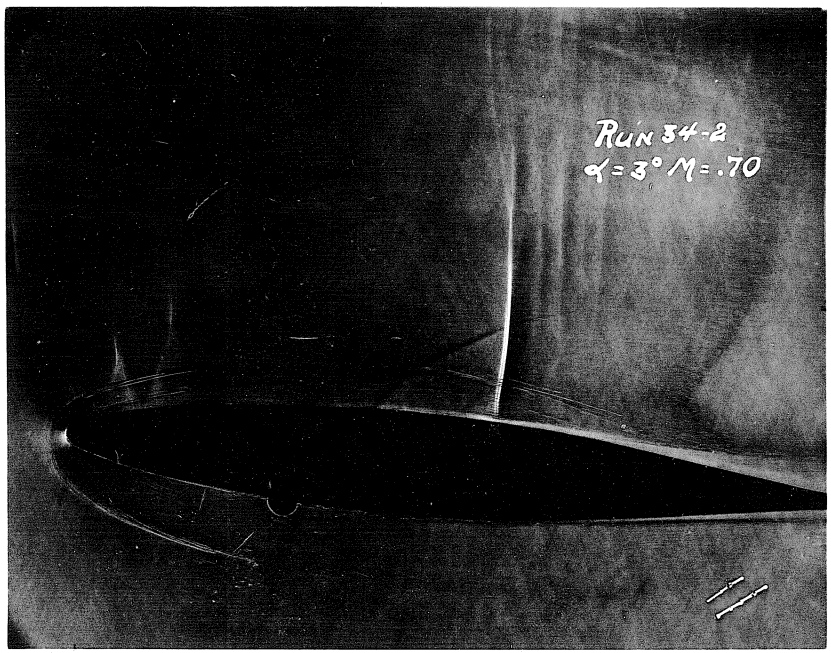

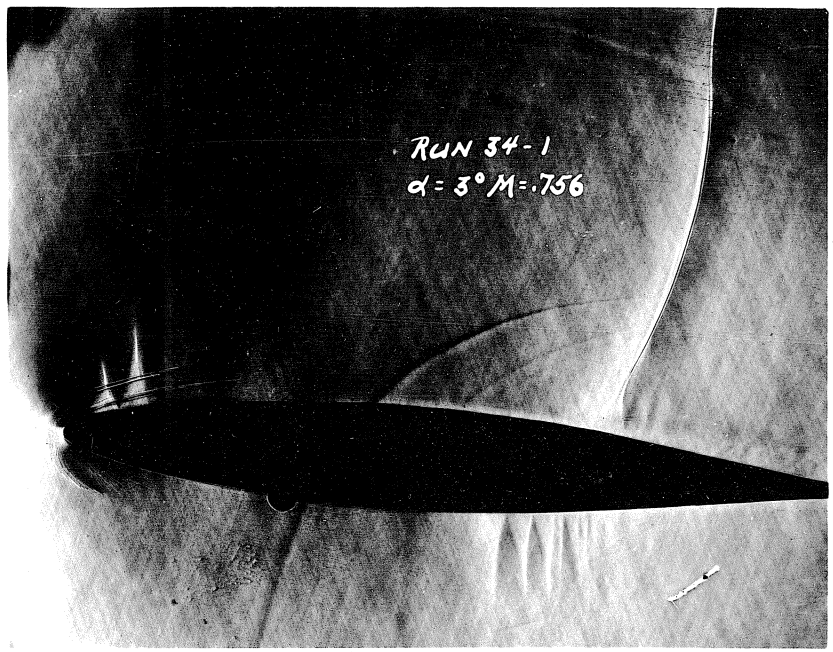

A-18,224

FIG. 25

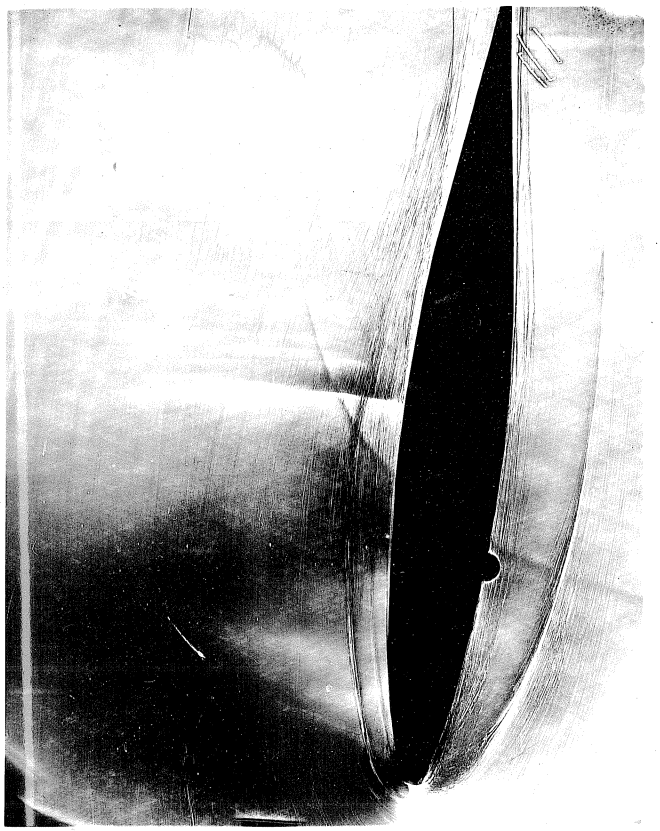

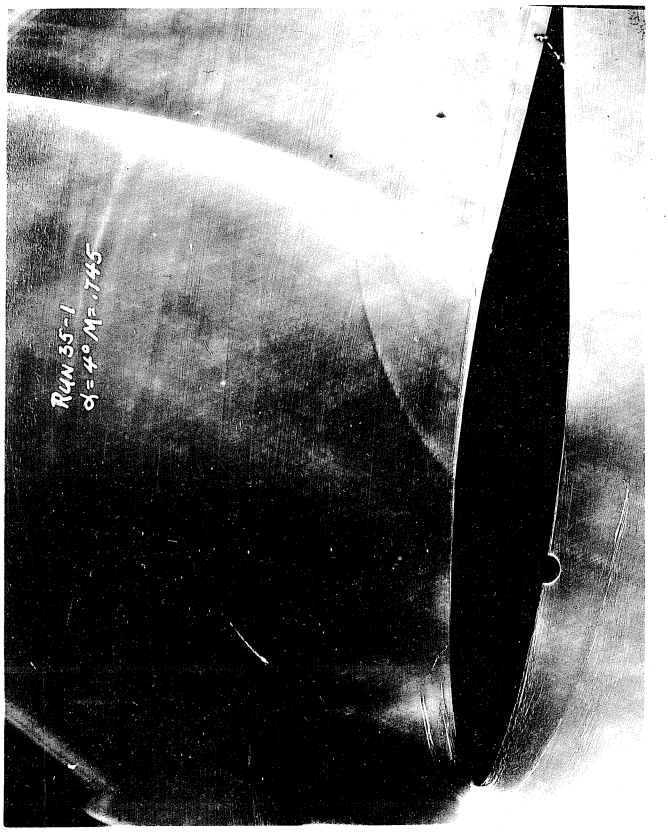

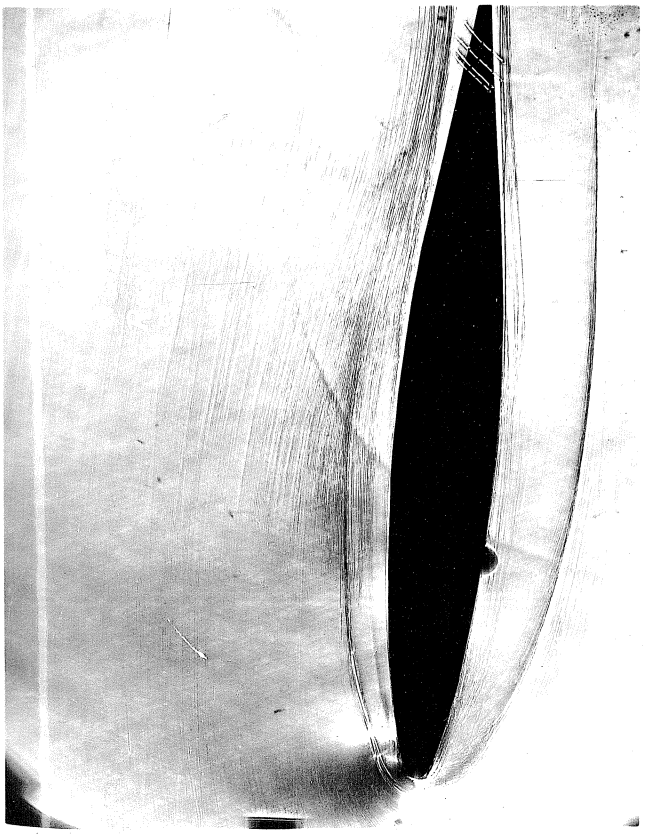

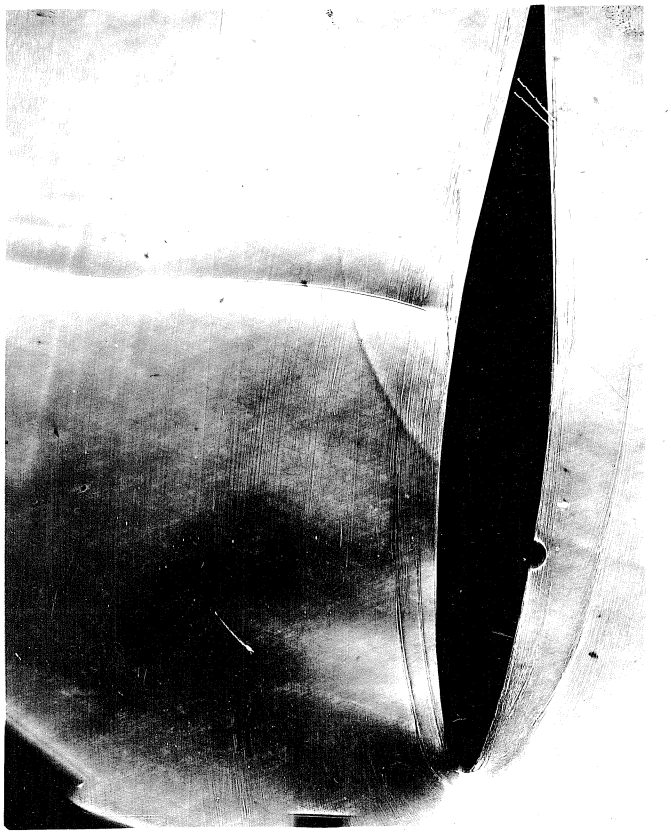

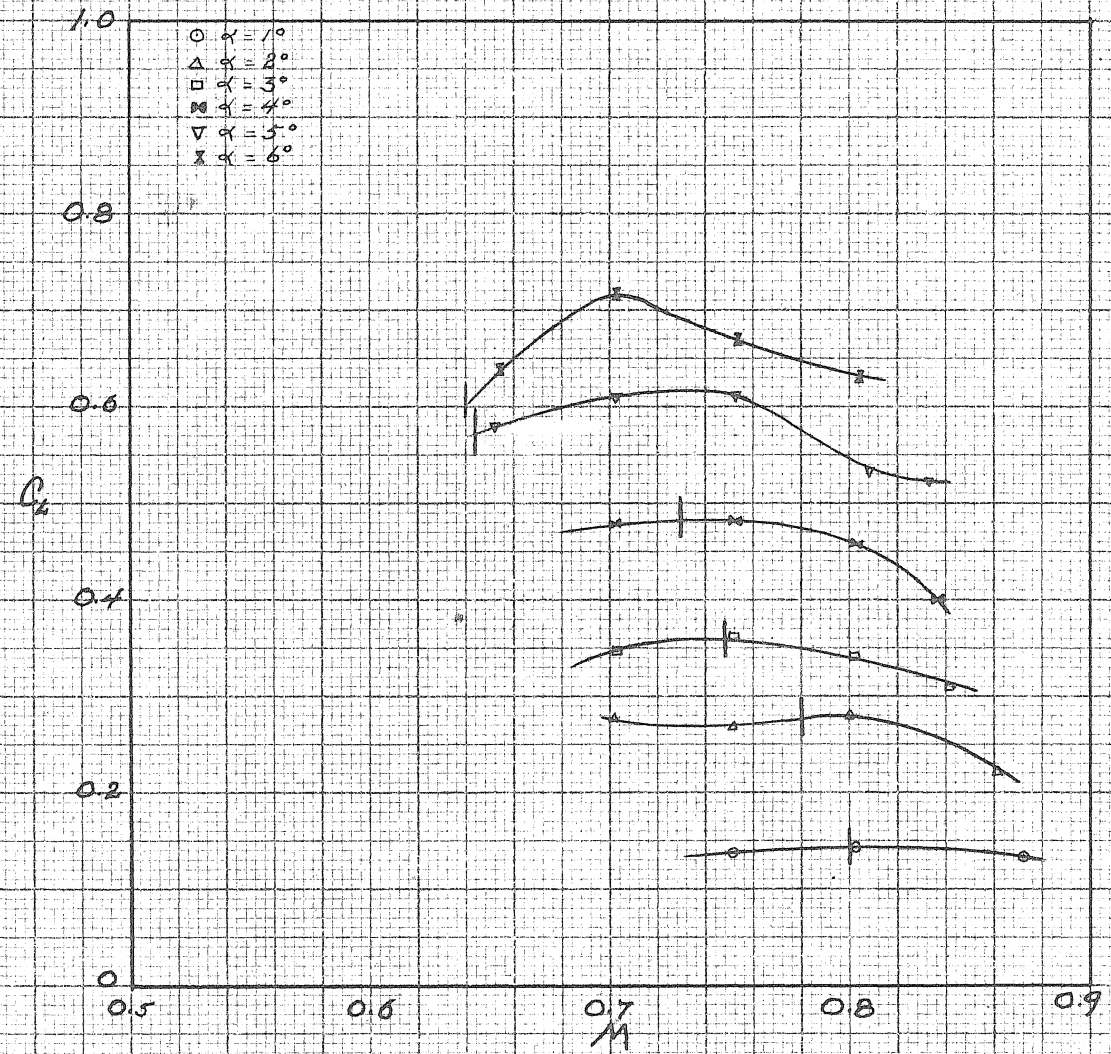

2 Inch Chord Model

C_L vs M

Fig 26

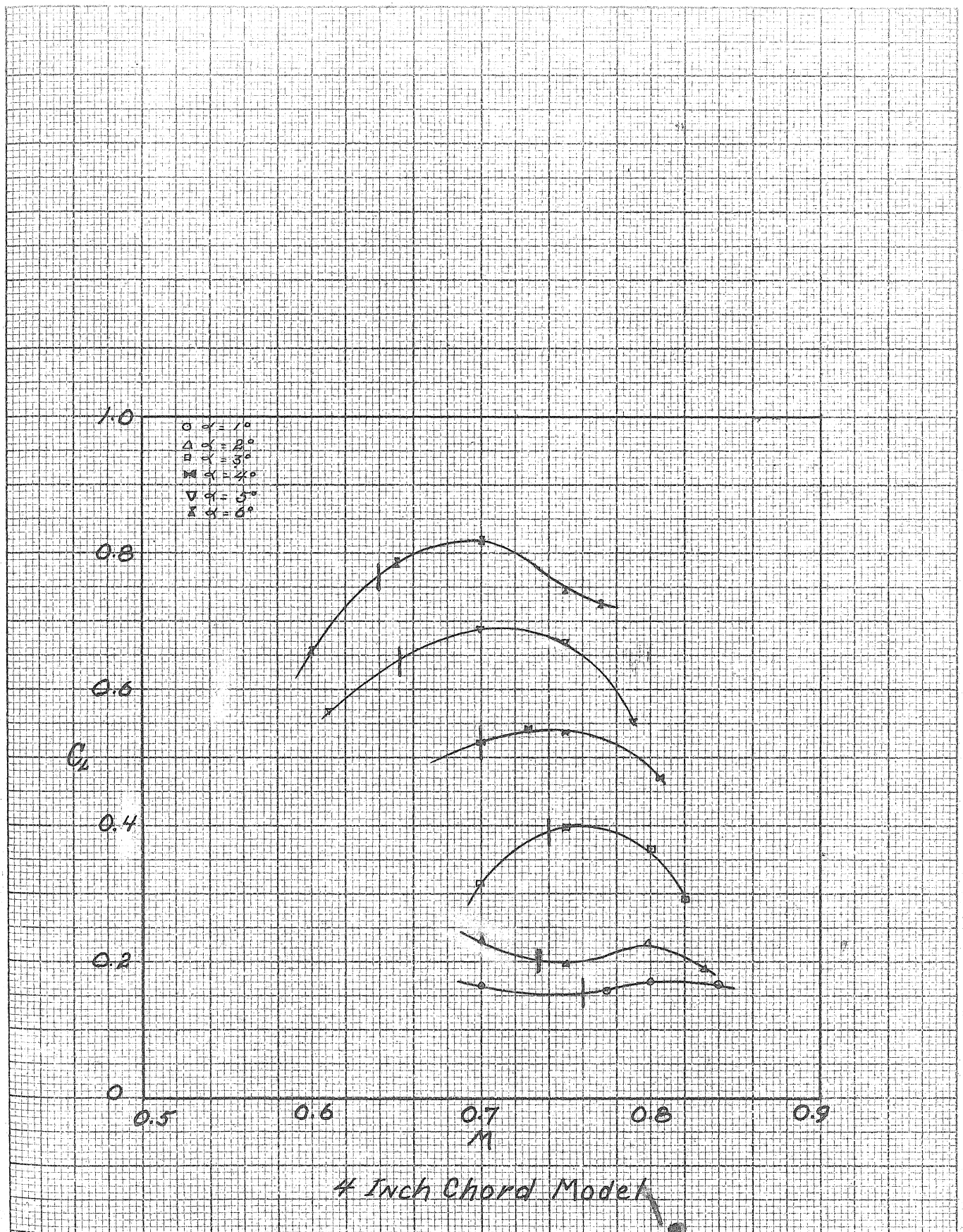
1.0
0.8
0.6
0.4
0.2
0
C_L
○ α = 1°
△ α = 2°
□ α = 3°
▣ α = 4°
▽ α = 5°
⧗ α = 6°
0.5
0.6
0.7
0.8
0.9
M
4 Inch Chord Model

C_L vs M

Fig 28a

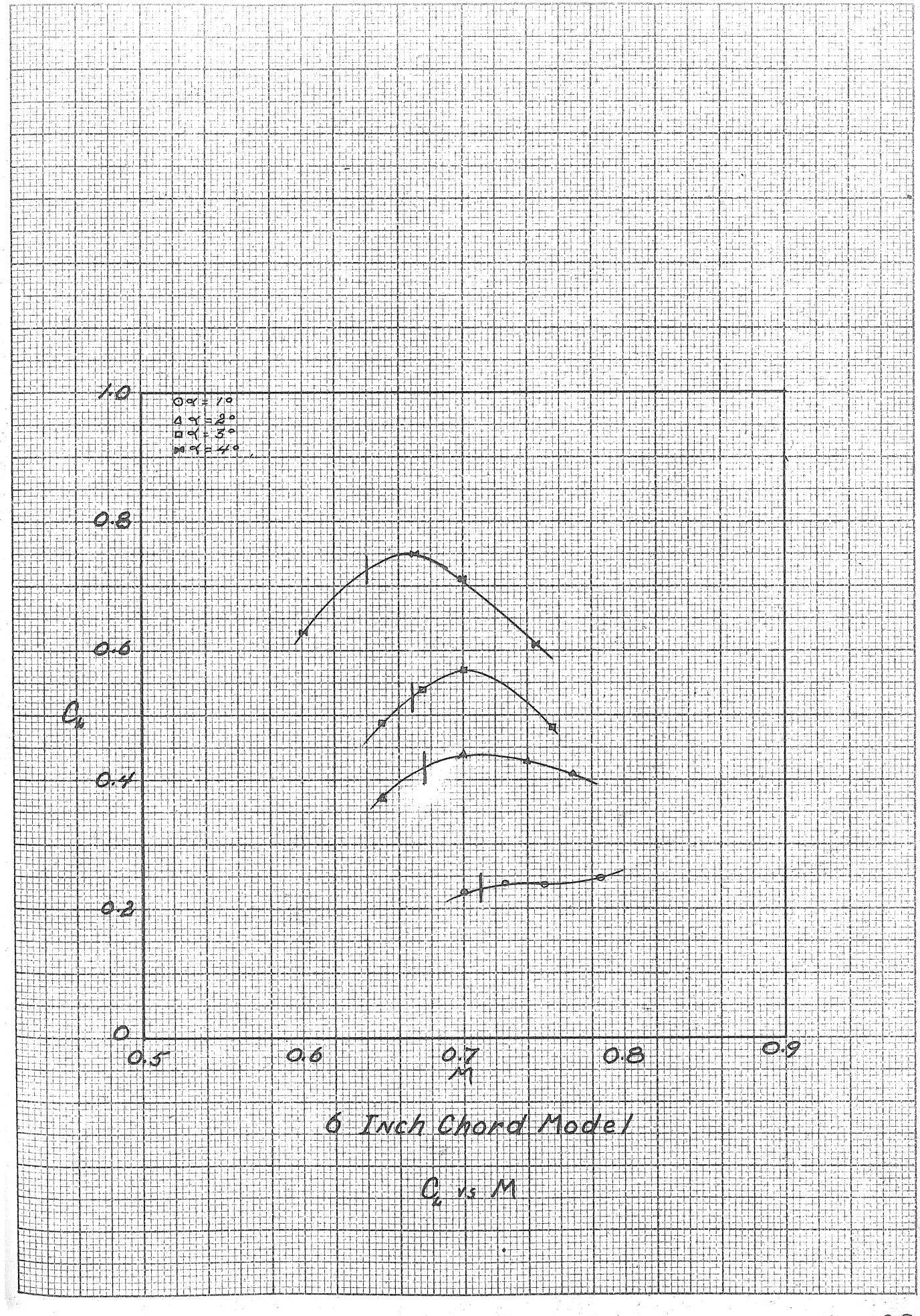

6 Inch Chord Model

C_L vs M

Fig. 28a

Fig. 286

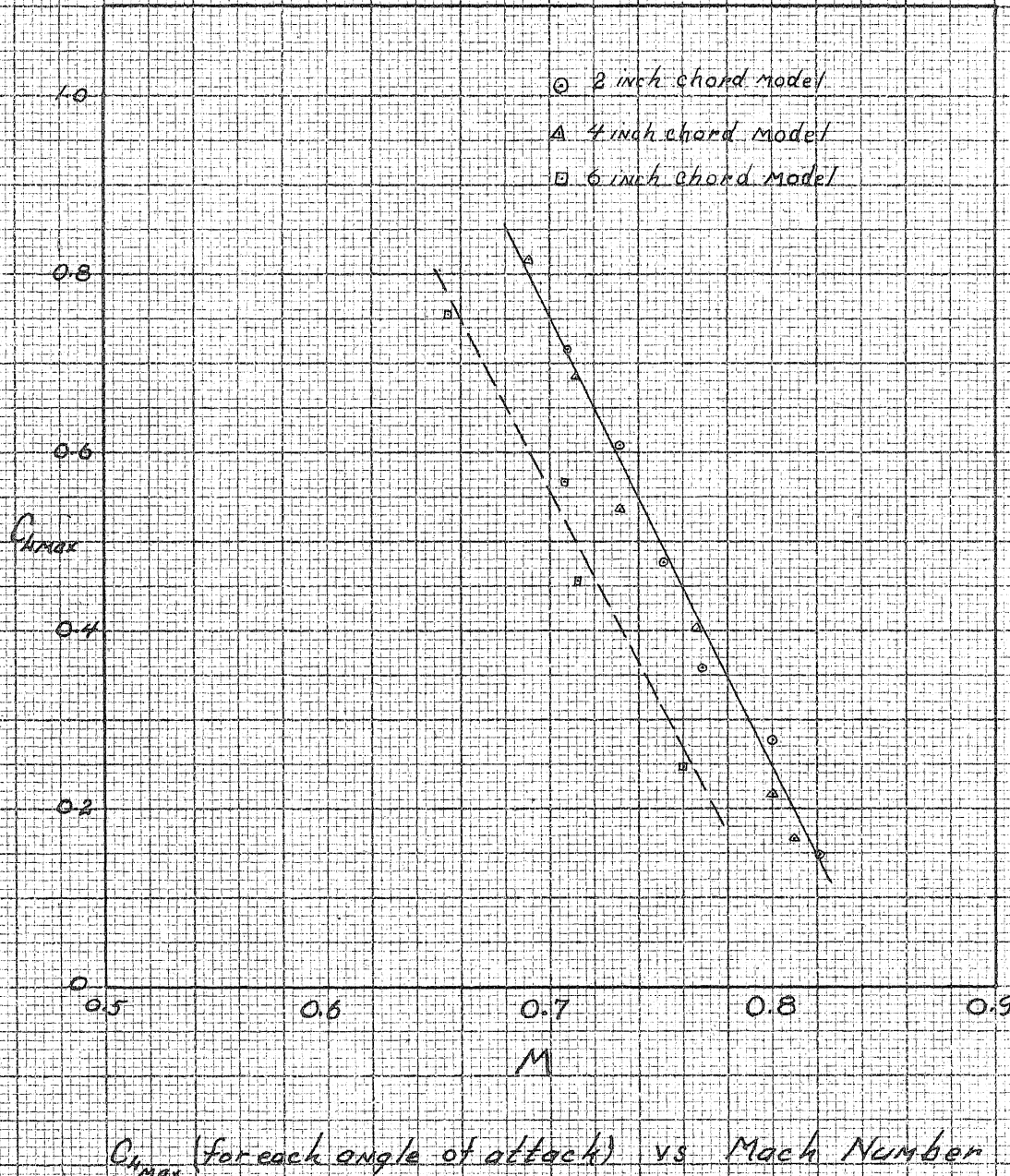

$C_{L_{max}}$ (for each angle of attack) vs Mach Number

Fig. 286

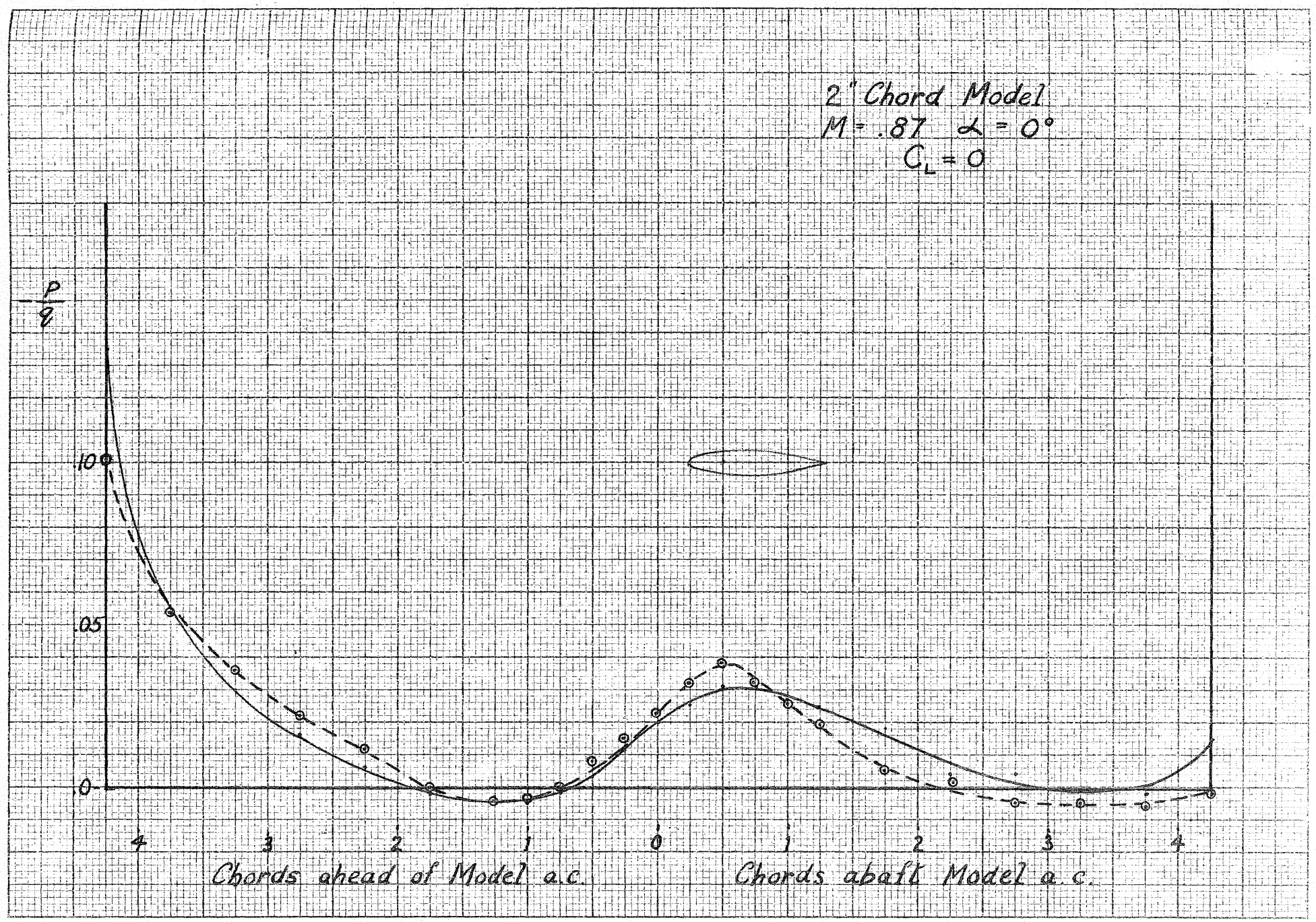
2" Chord Model
M = .87 α = 0°
C_L = 0
-P/q
.10
.05
0
4
3
2
1
0
1
2
3
4
Chords ahead of Model a.c.
Chords abaft Model a.c.

FIG. 29

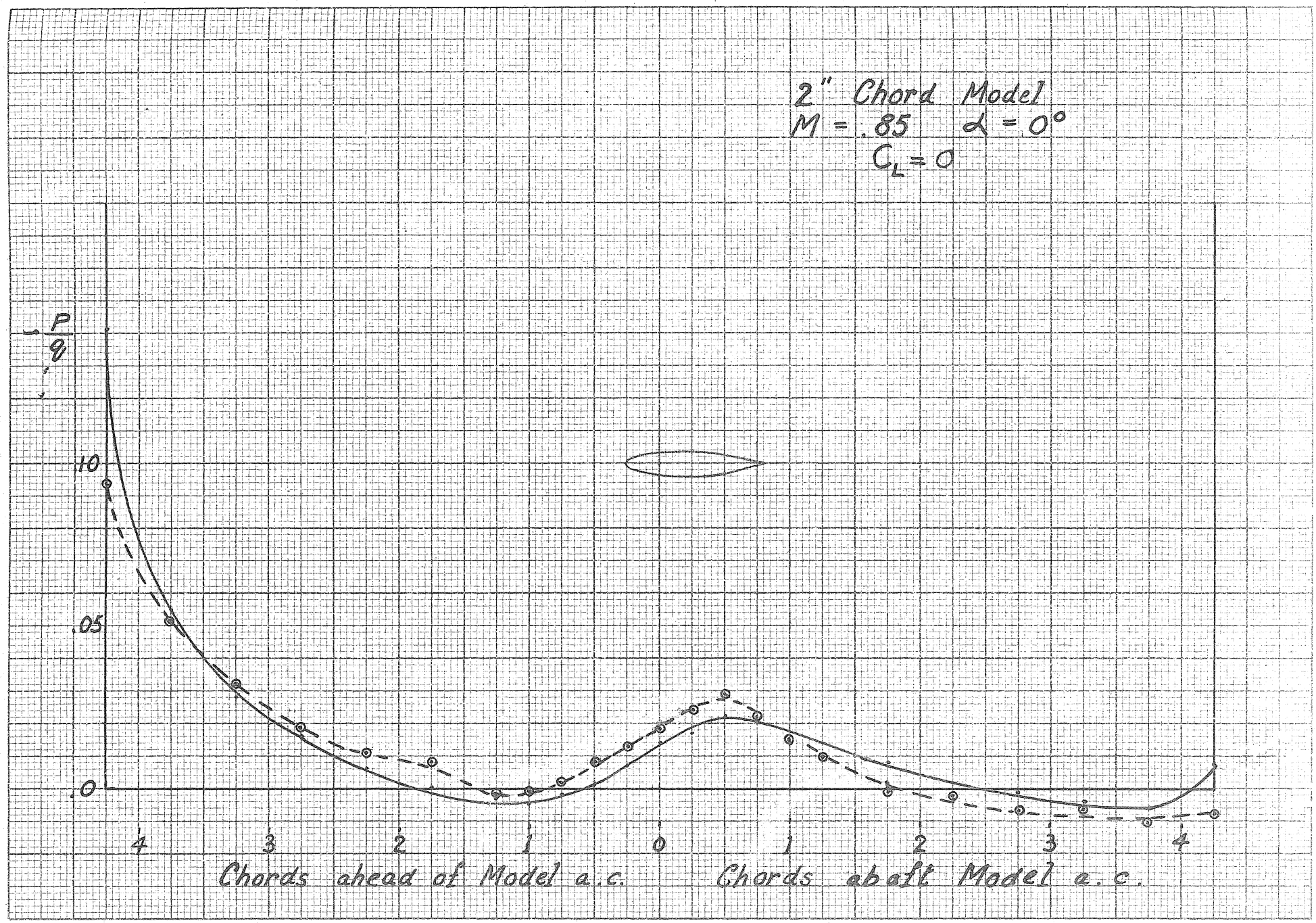
2" Chord Model
M = .85 α = 0°
$C_L = 0$
$-\frac{P}{q}$
.10
.05
0
4
3
2
1
0
1
2
3
4
Chords ahead of Model a.c.
Chords aft Model a.c.

FIG. 30

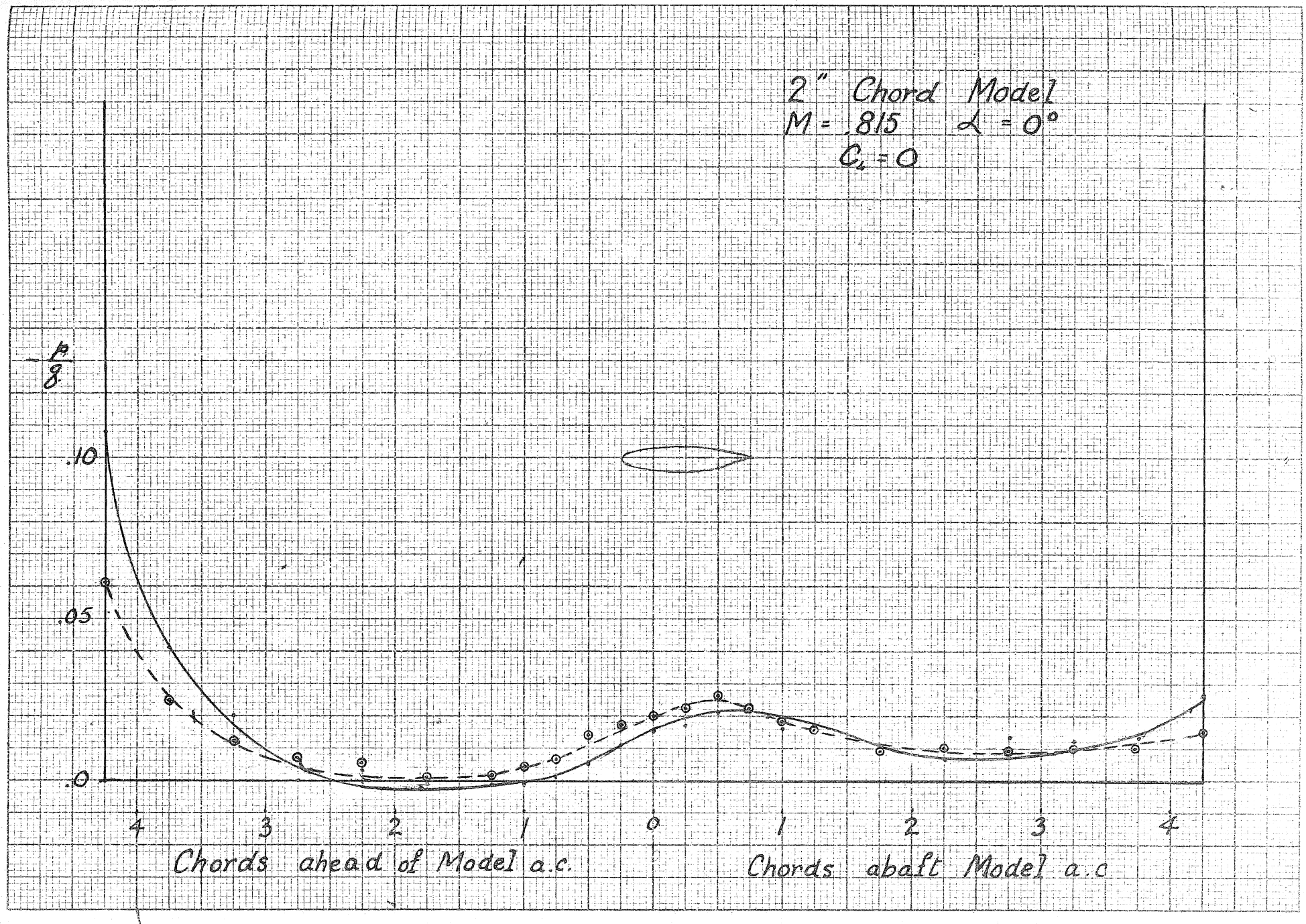
2" Chord Model
M = .815 α = 0°
C_L = 0
$-\frac{p}{q}$
.10
.05
.0
4
3
2
1
0
1
2
3
4
Chords ahead of Model a.c.
Chords abaft Model a.c.

Fig 31

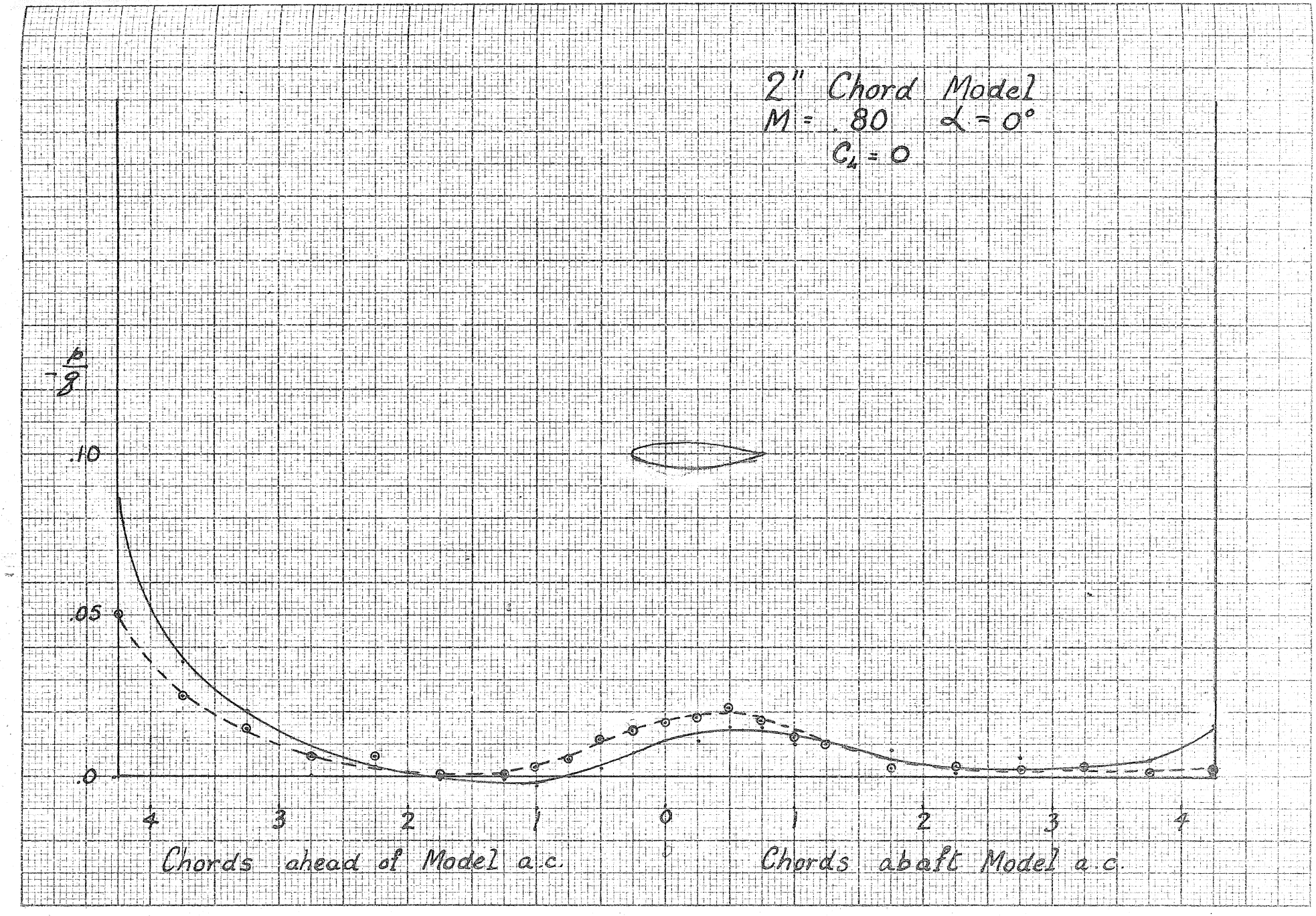
2" Chord Model
M = .80 α = 0°
$C_4 = 0$
$\frac{p}{q}$
.10
.05
.0
4
3
2
1
0
1
2
3
4
Chords ahead of Model a.c.
Chords abaft Model a.c.

Fig 32

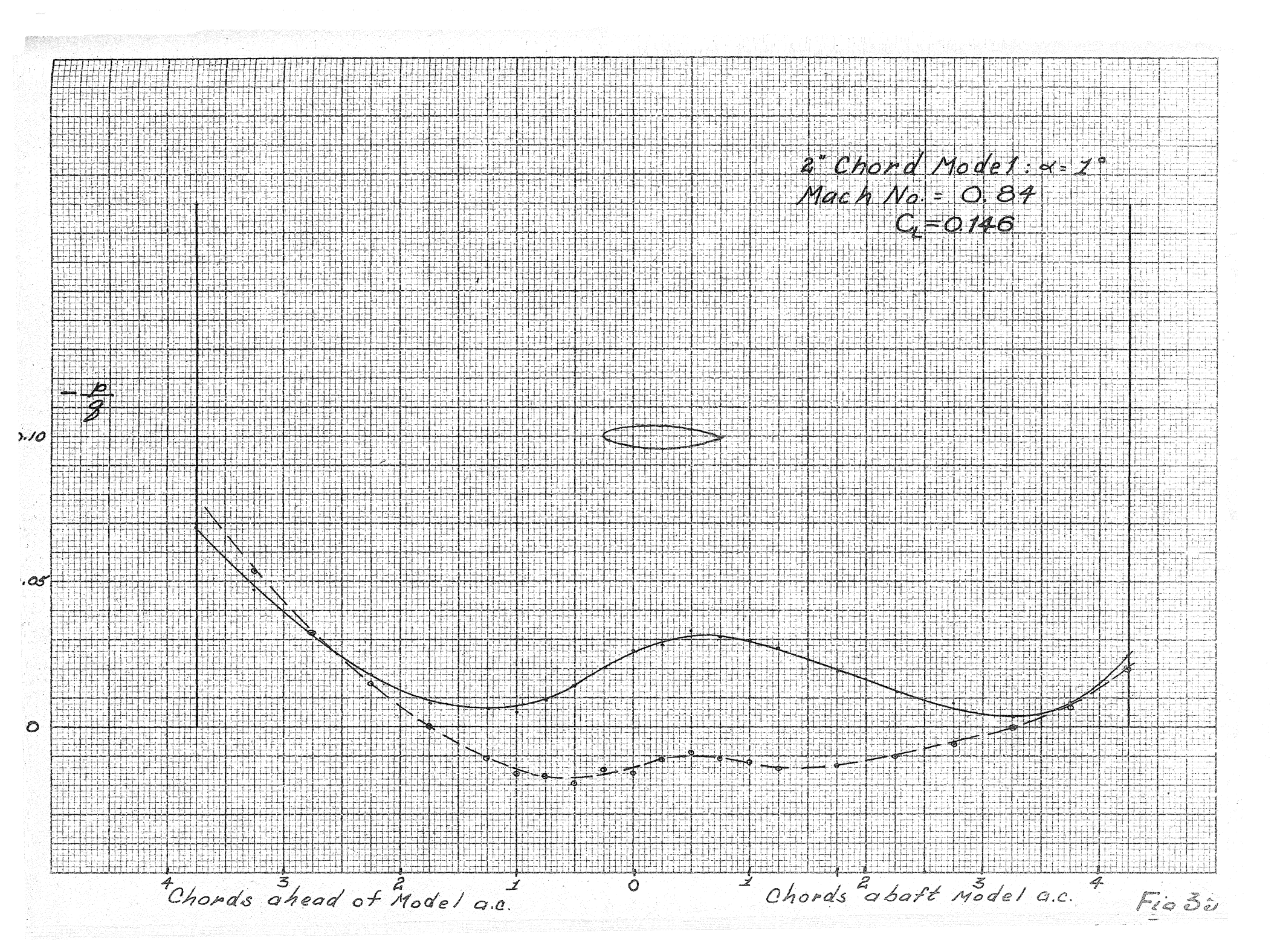
2" Chord Model : α = 1°
Mach No. = 0.84
C_L = 0.146
$-\frac{p}{q}$
.10
.05
0
4
3
2
1
0
1
2
3
4
Chords ahead of Model a.c.
Chords abaft Model a.c.

Fig 3a

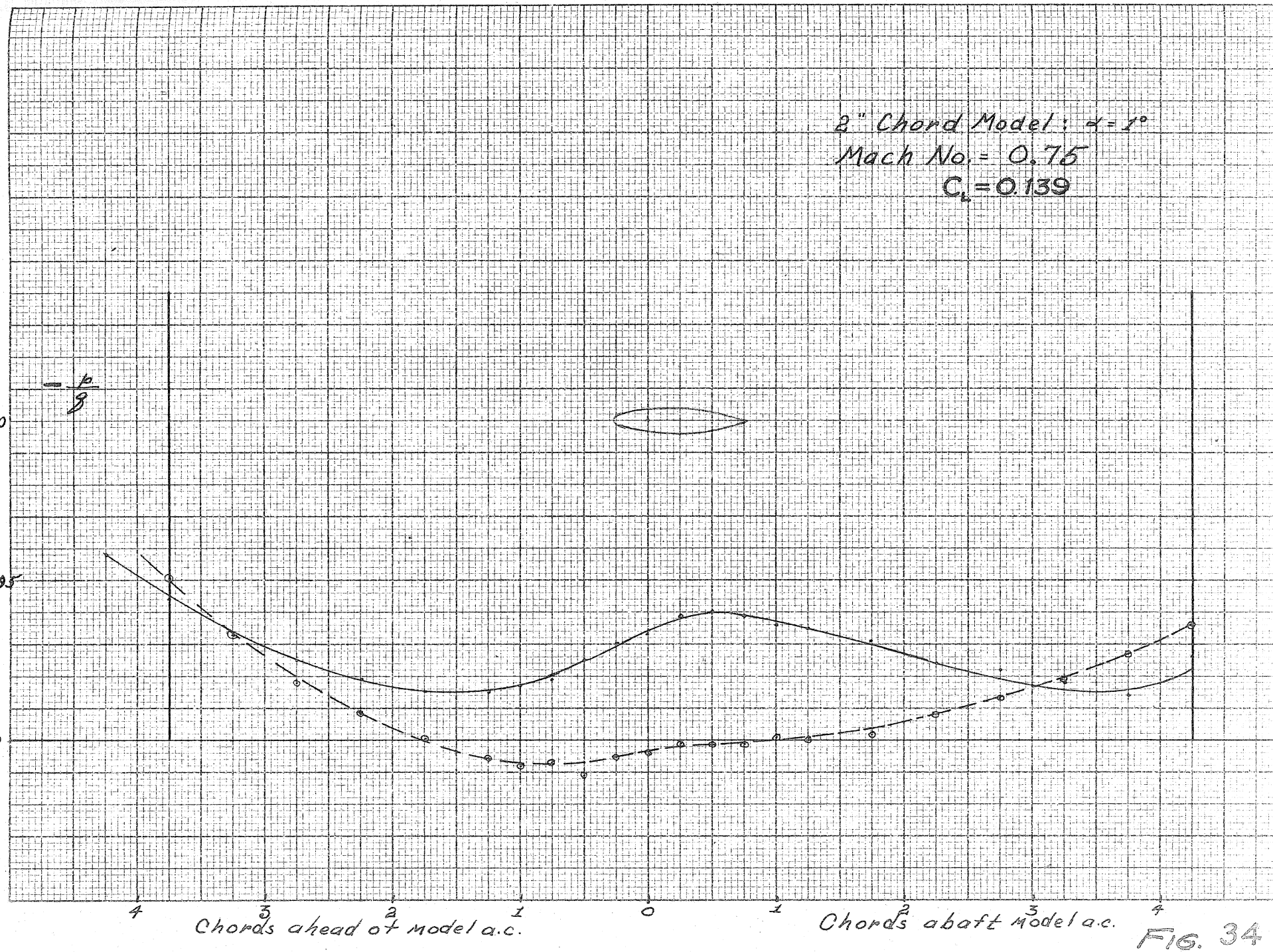
2" Chord Model : α = 1°
Mach No. = 0.75
C_L = 0.139
$-\frac{p}{q}$
0.10
0.05
0
4
3
2
1
0
1
2
3
4
Chords ahead of model a.c.
Chords abaft model a.c.

FIG. 34

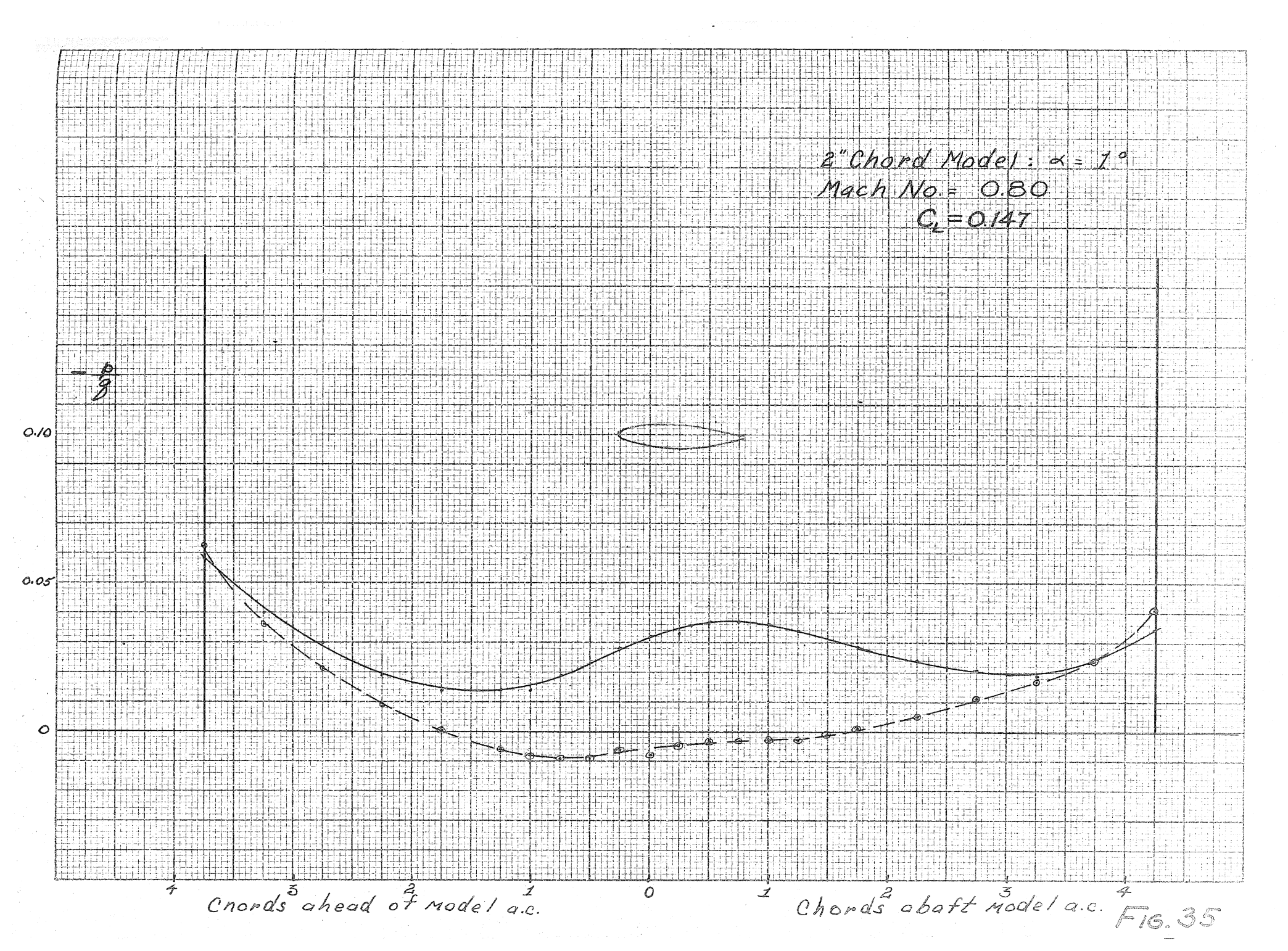
2" Chord Model : α = 1°
Mach No. = 0.80
C_L = 0.147
$-\frac{p}{q}$
0.10
0.05
0
4
3
2
1
0
1
2
3
4
Chords ahead of model a.c.
Chords abaft model a.c.

FIG. 35

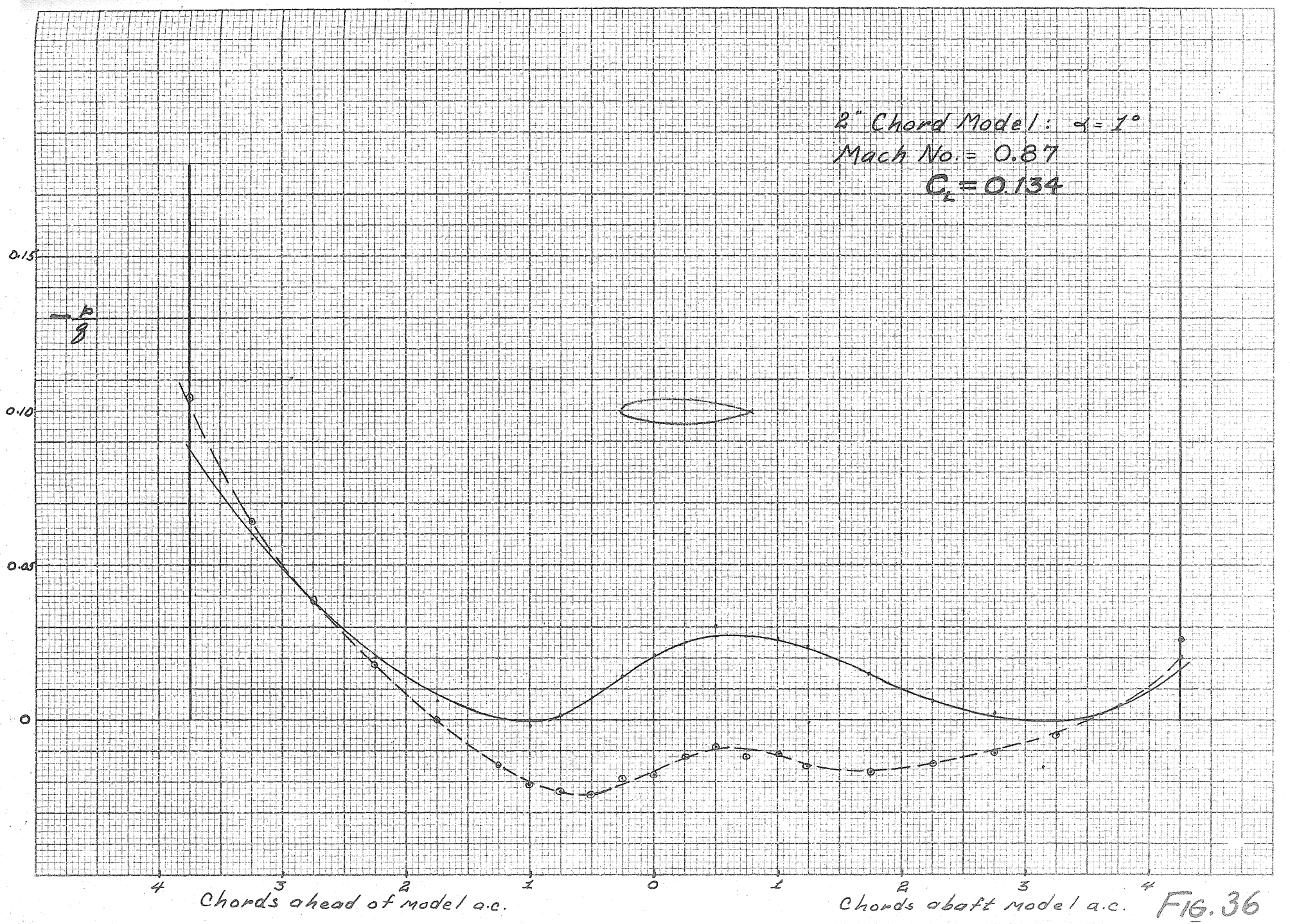
2" Chord Model : α = 1°
Mach No. = 0.87
C_L = 0.134
$-\frac{p}{q}$
0.15
0.10
0.05
0
4
3
2
1
0
1
2
3
4
Chords ahead of model a.c.
Chords abaft model a.c.

FIG. 36

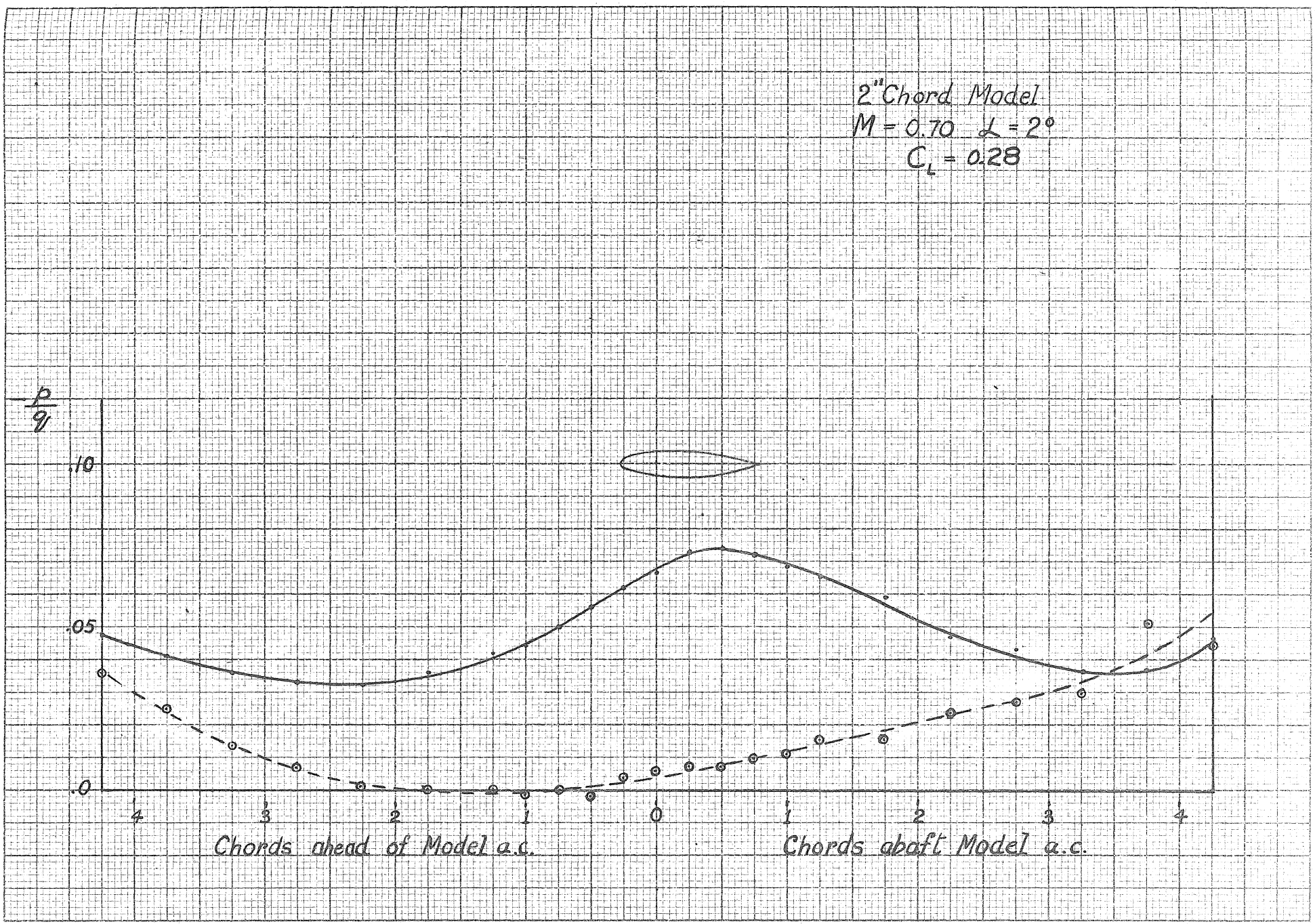
2" Chord Model
M = 0.70 α = 2°
C_L = 0.28
$-\frac{p}{q}$
.10
.05
.0
4
3
2
1
0
1
2
3
4
Chords ahead of Model a.c.
Chords abaft Model a.c.

FIG. 37

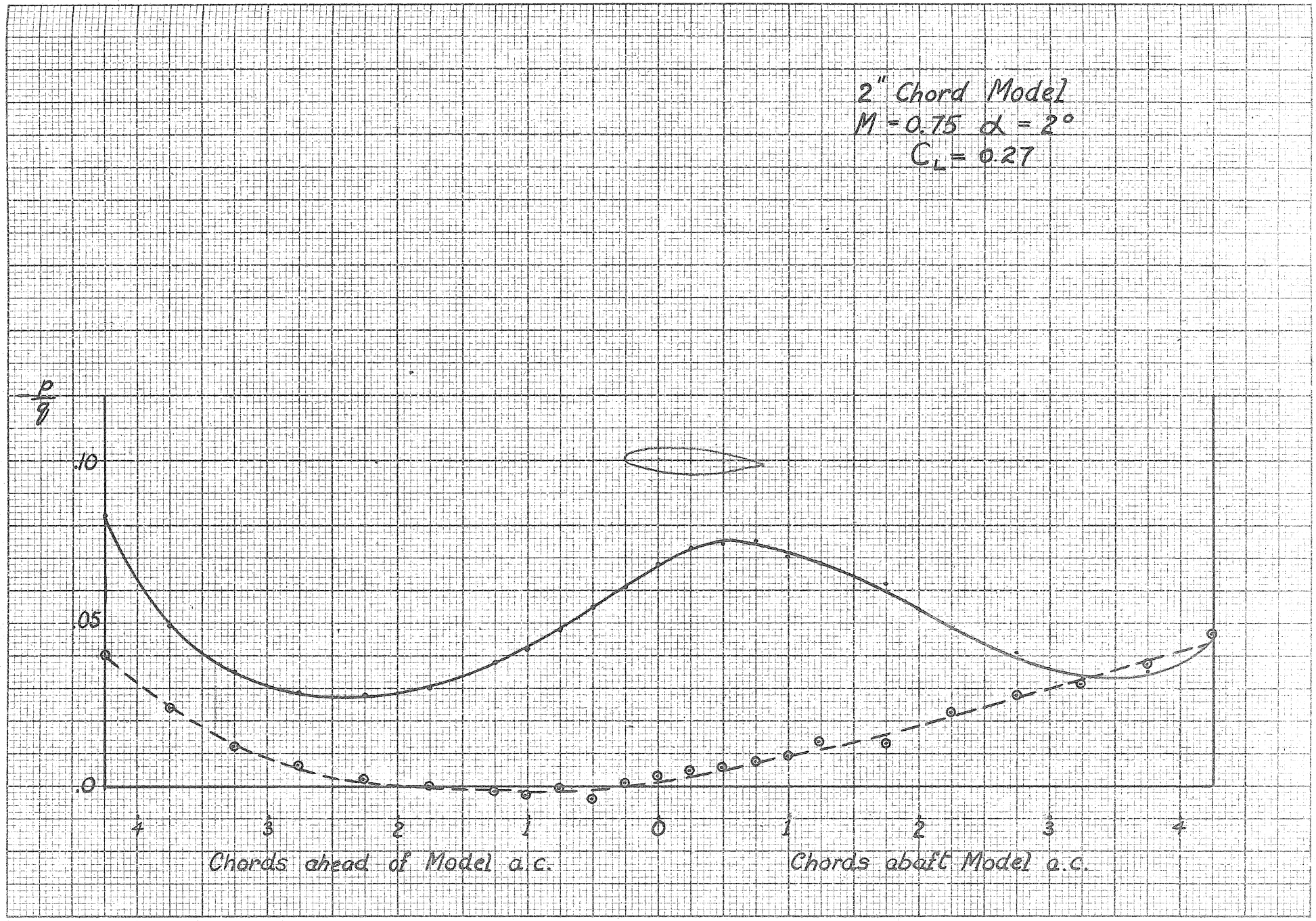
2" Chord Model
M = 0.75 α = 2°
C_L = 0.27
$-\frac{p}{q}$
.10
.05
.0
4
3
2
1
0
1
2
3
4
Chords ahead of Model a.c.
Chords abaft Model a.c.

FIG. 38

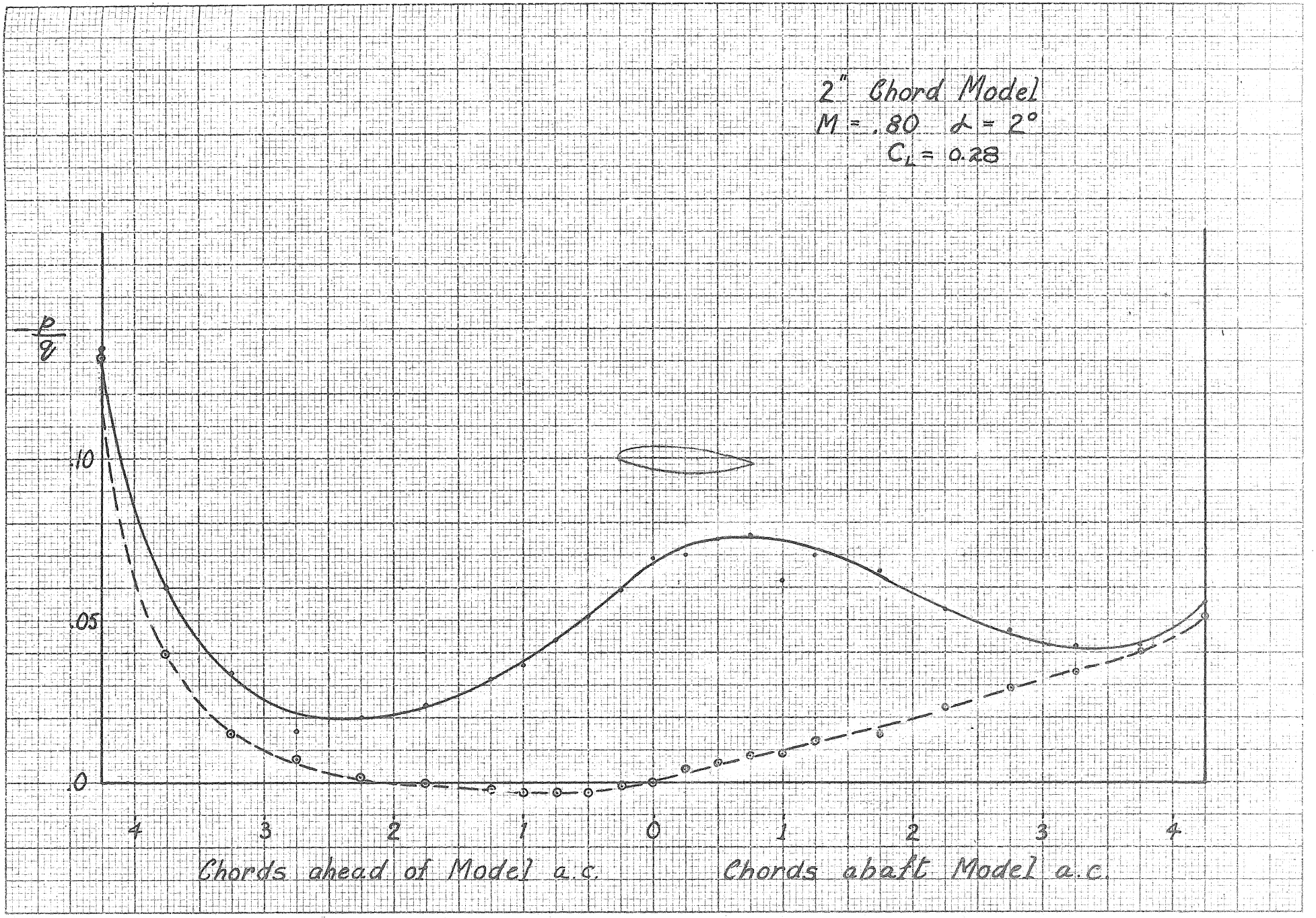
2" Chord Model
M = .80 α = 2°
C_L = 0.28
p/q
.10
.05
.0
4
3
2
1
0
1
2
3
4
Chords ahead of Model a.c.
Chords abaft Model a.c.

FIG. 39

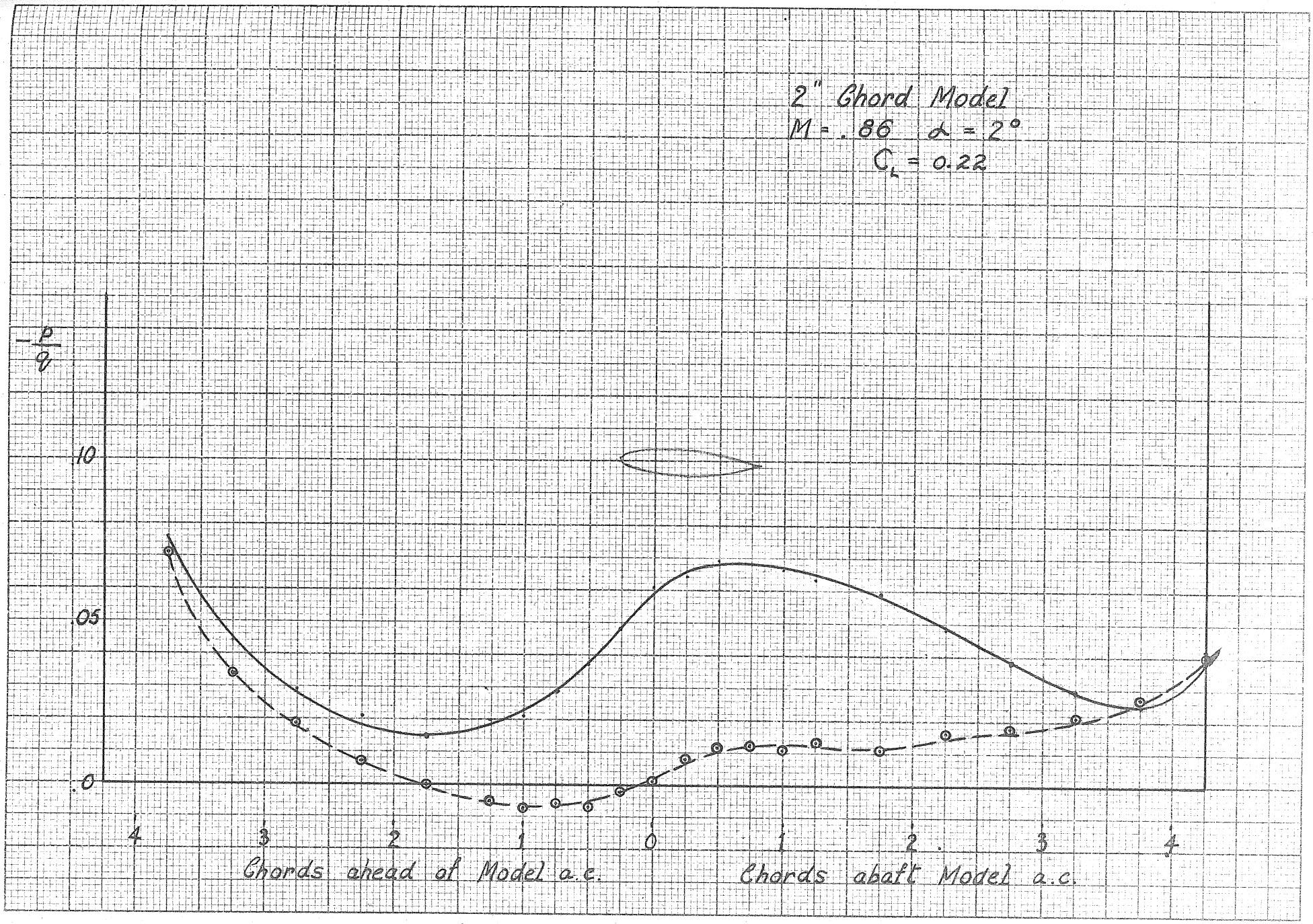
2" Chord Model
M = .86 α = 2°
C_L = 0.22
$-\frac{p}{q}$
.10
.05
0
4
3
2
1
0
1
2
3
4
Chords ahead of Model a.c.
Chords abaft Model a.c.

FIG. 40

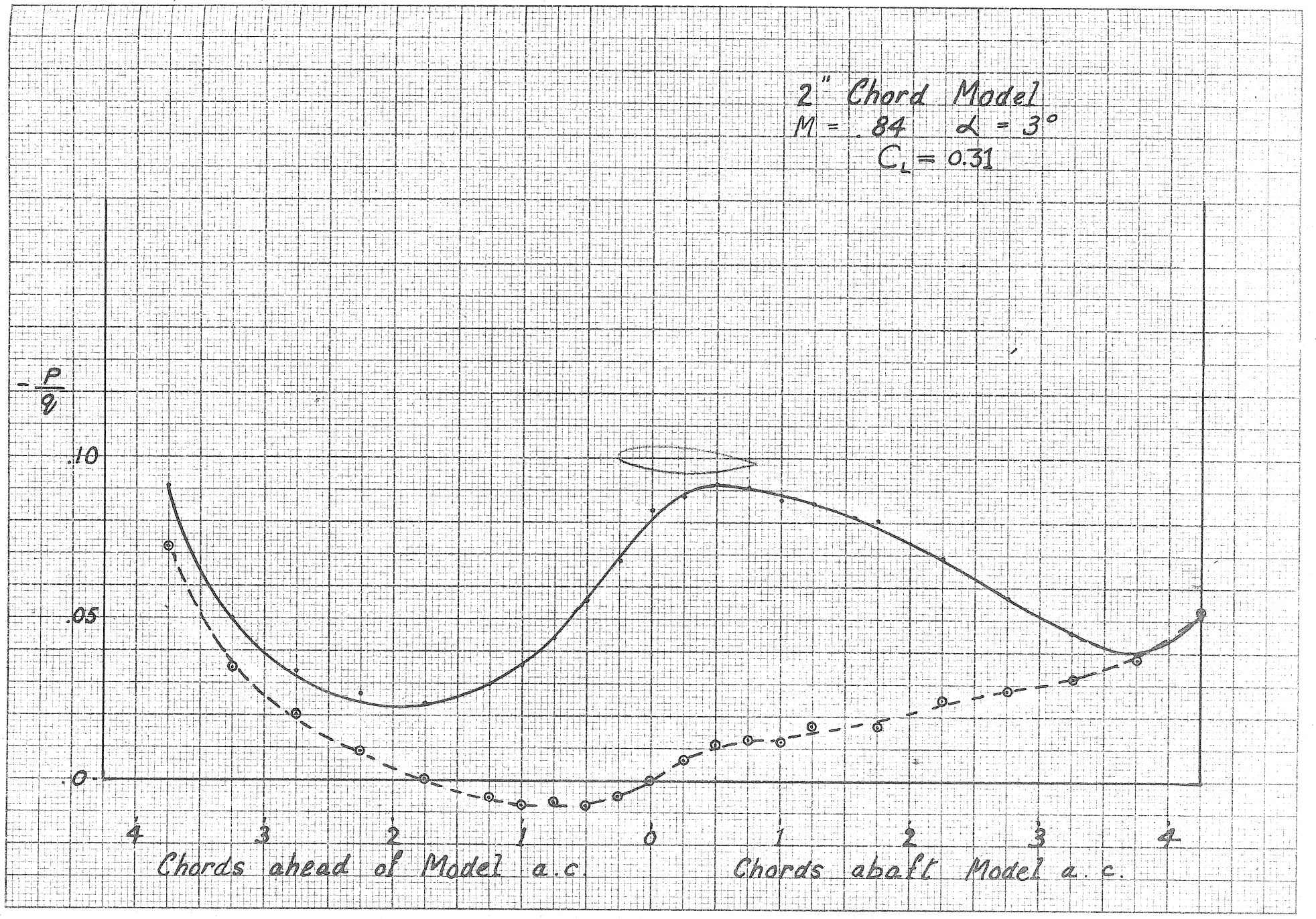
2" Chord Model
M = .84 α = 3°
C_L = 0.31
$-\frac{P}{q}$
.10
.05
0
4
3
2
1
0
1
2
3
4
Chords ahead of Model a.c.
Chords abaft Model a.c.

FIG. 41

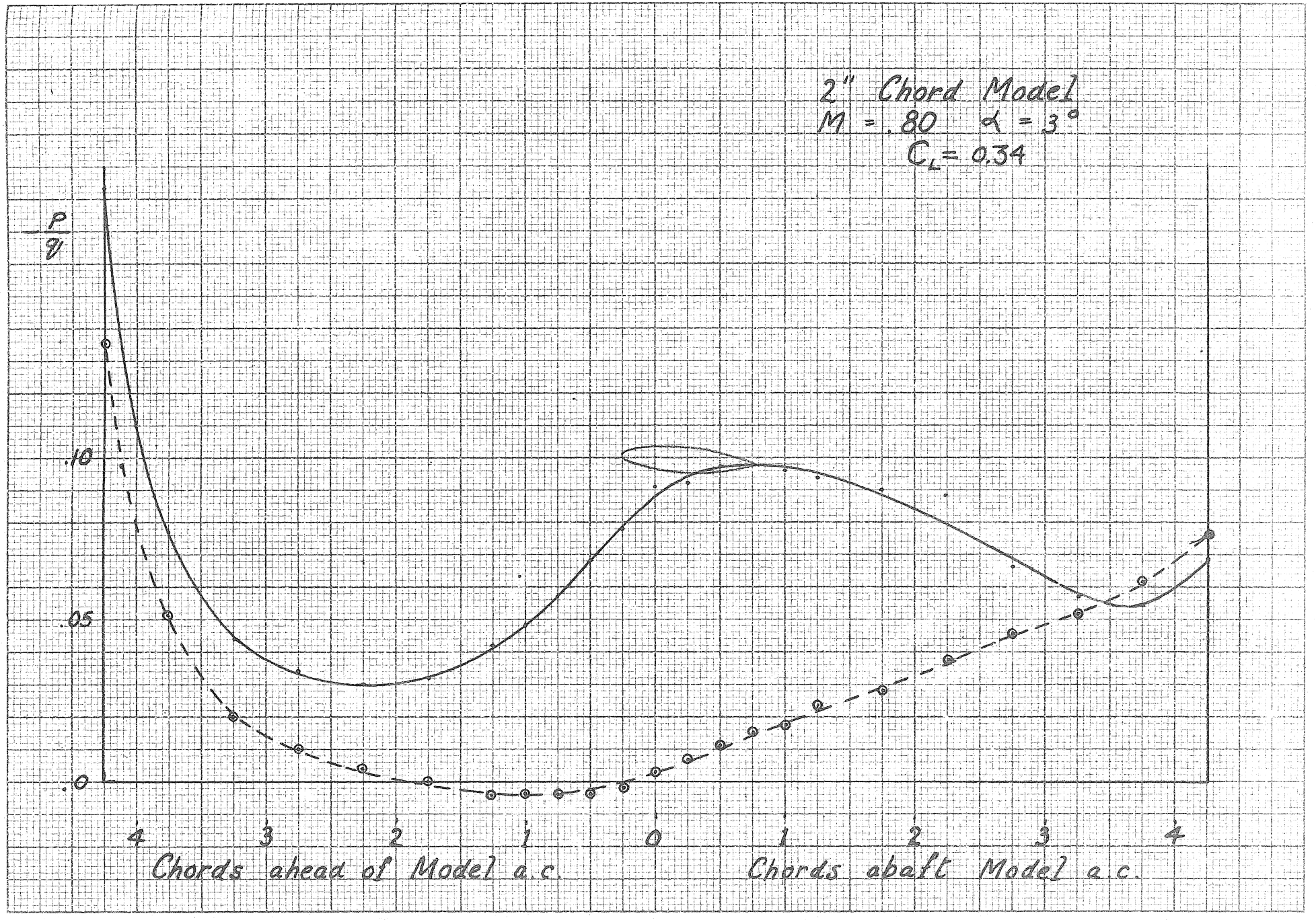
2" Chord Model
M = .80 α = 3°
C_L = 0.34
p/q
.10
.05
0
4
3
2
1
0
1
2
3
4
Chords ahead of Model a.c.
Chords abaft Model a.c.

Fig 4k

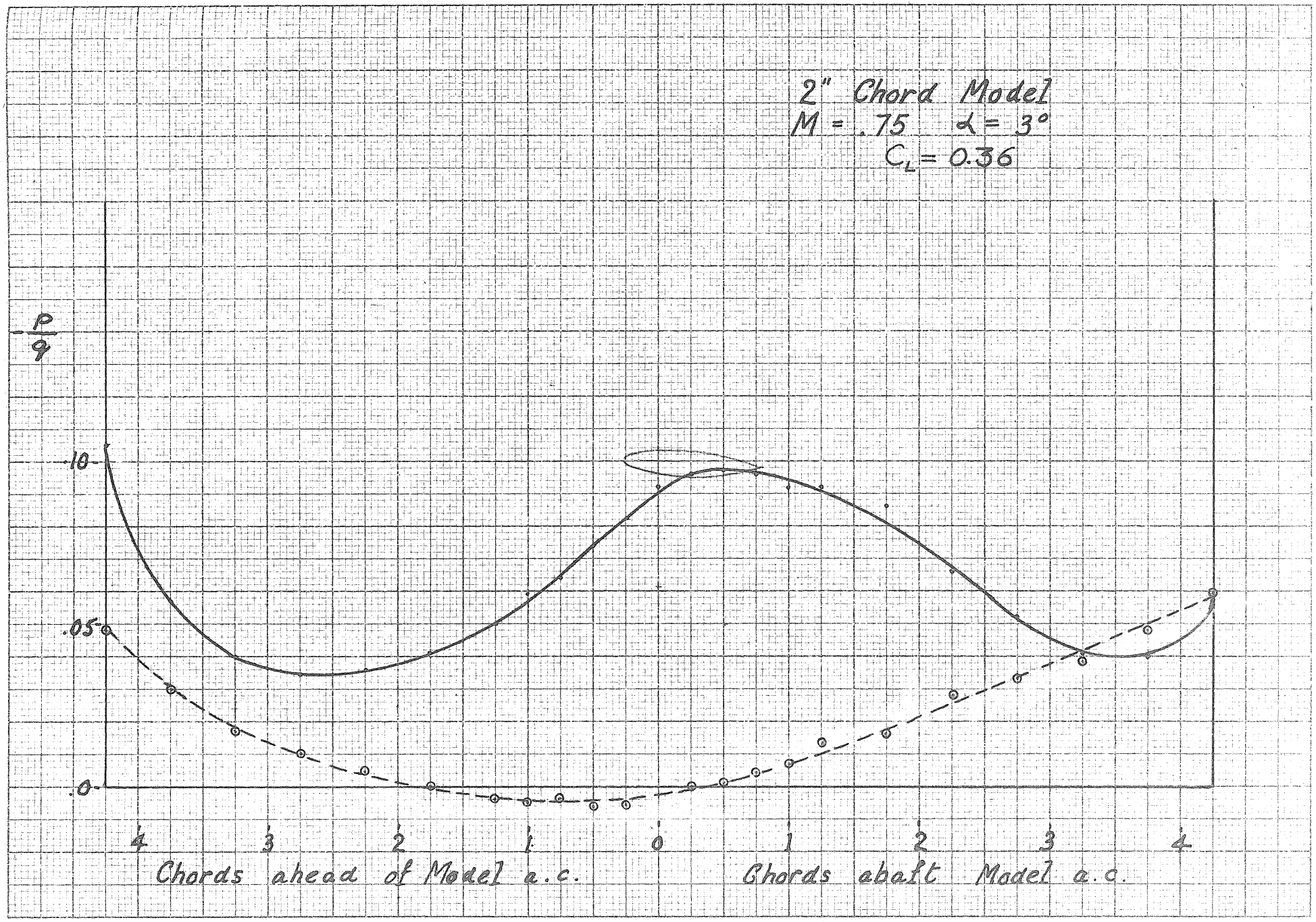
2" Chord Model
M = .75 α = 3°
C_L = 0.36
$-\frac{p}{q}$
.10
.05
.0
4
3
2
1
0
1
2
3
4
Chords ahead of Model a.c.
Chords abaft Model a.c.

FIG. 43

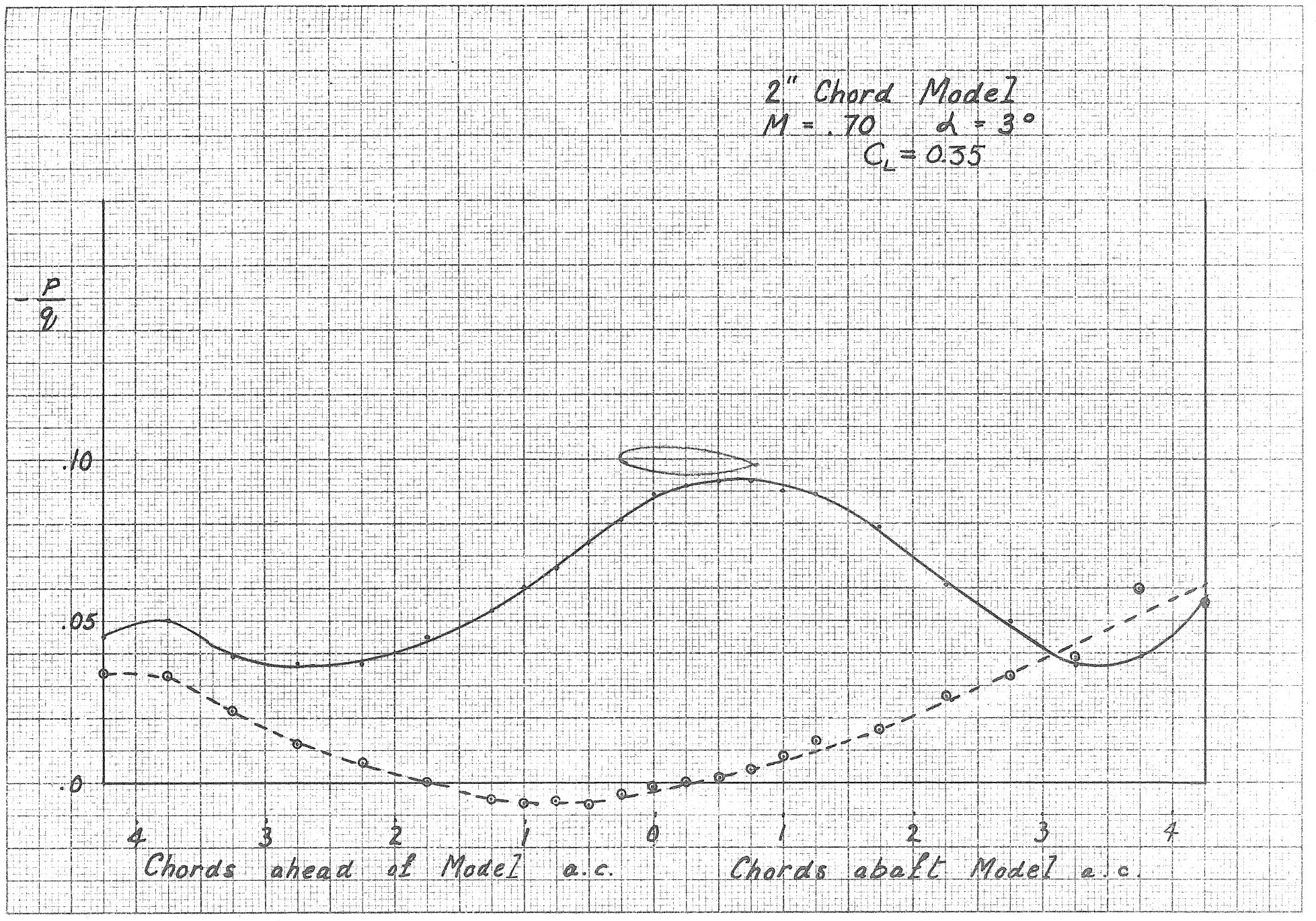
2" Chord Model
M = .70 α = 3°
C_L = 0.35
$-\frac{p}{q}$
.10
.05
.0
4
3
2
1
0
1
2
3
4
Chords ahead of Model a.c.
Chords abaft Model a.c.

FIG. 44

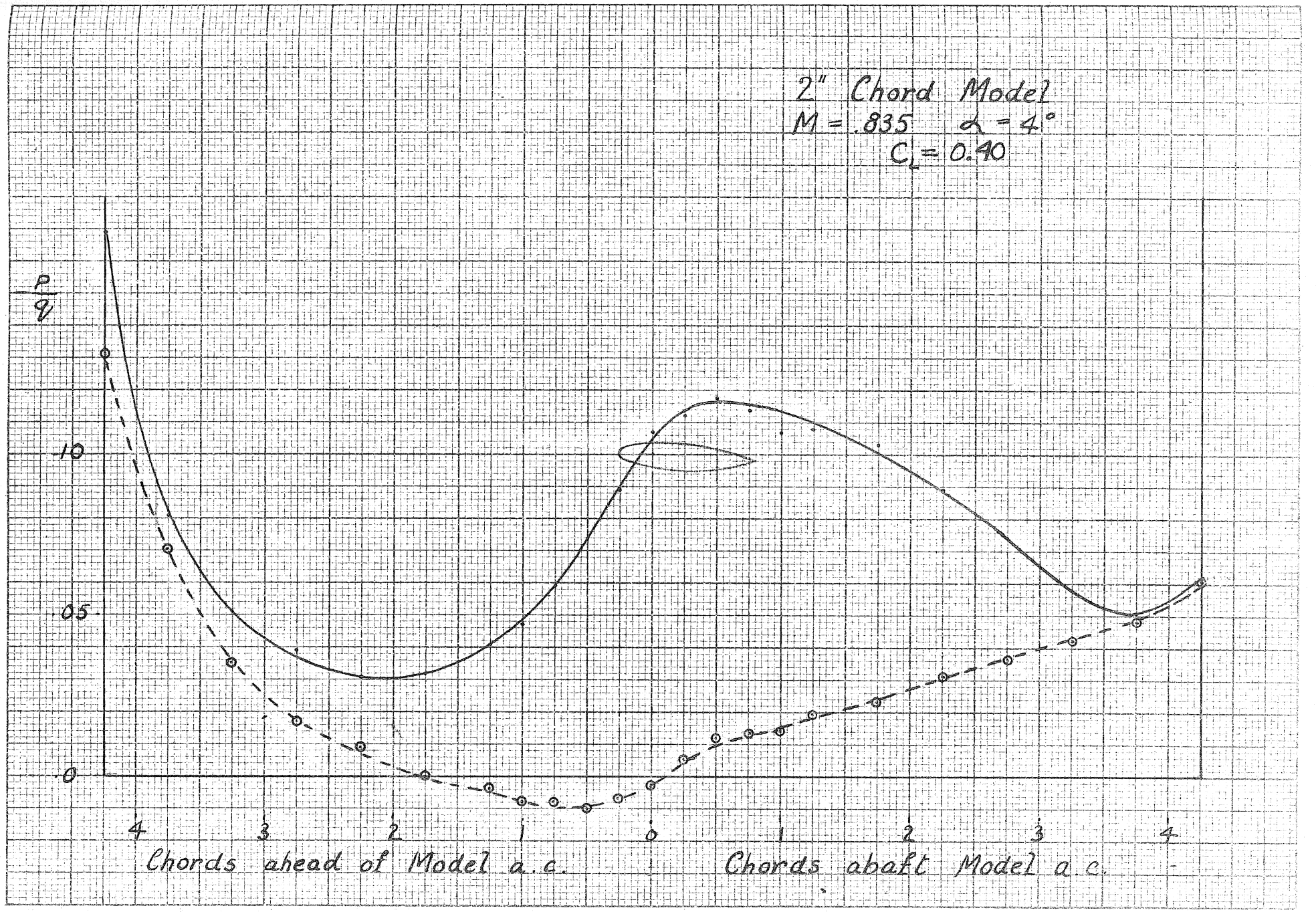
2" Chord Model
M = .835 α = 4°
C_L = 0.90
$\frac{P}{q}$
-.10
-.05
0
4
3
2
1
0
1
2
3
4
Chords ahead of Model a.c.
Chords abaft Model a.c.

FIG. 45

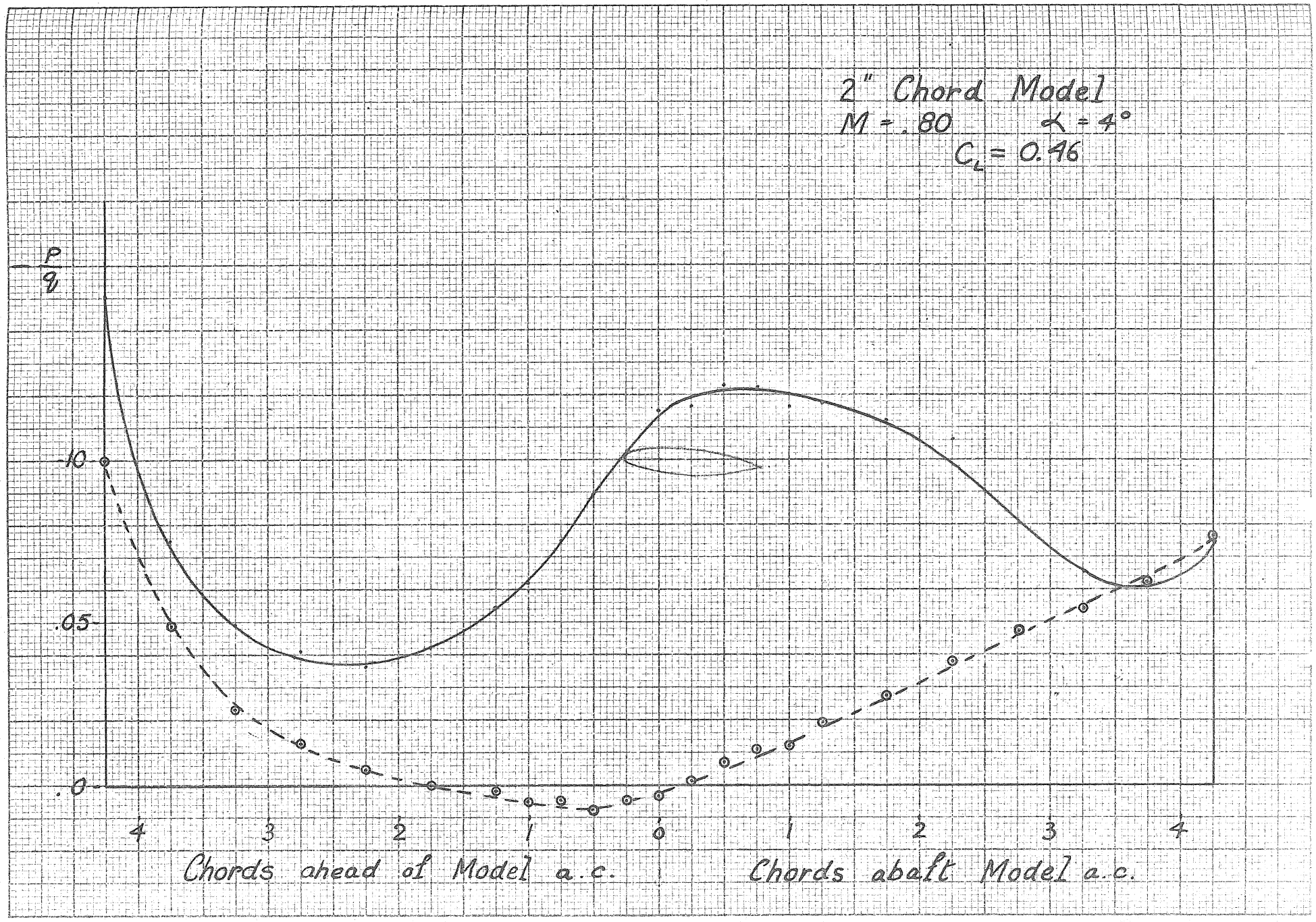
2" Chord Model
M = .80
α = 4°
C_L = 0.46
$\frac{p}{q}$
.10
.05
0
4
3
2
1
0
1
2
3
4
Chords ahead of Model a.c.
Chords abaft Model a.c.

FIG. 46

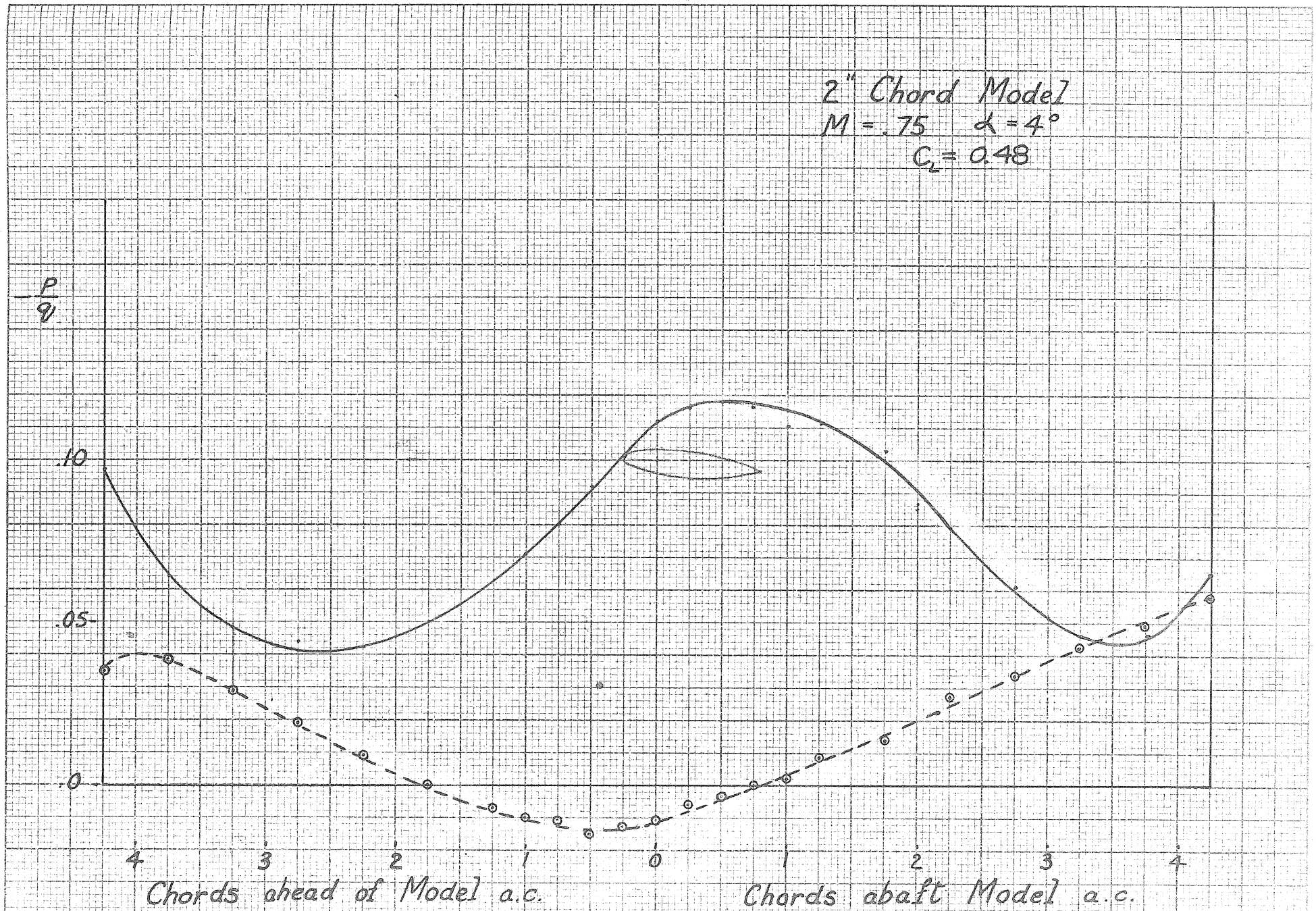
2" Chord Model
M = .75 α = 4°
C_L = 0.48
$\frac{p}{q}$
.10
.05
0
4
3
2
1
0
1
2
3
4
Chords ahead of Model a.c.
Chords abaft Model a.c.

FIG. 47

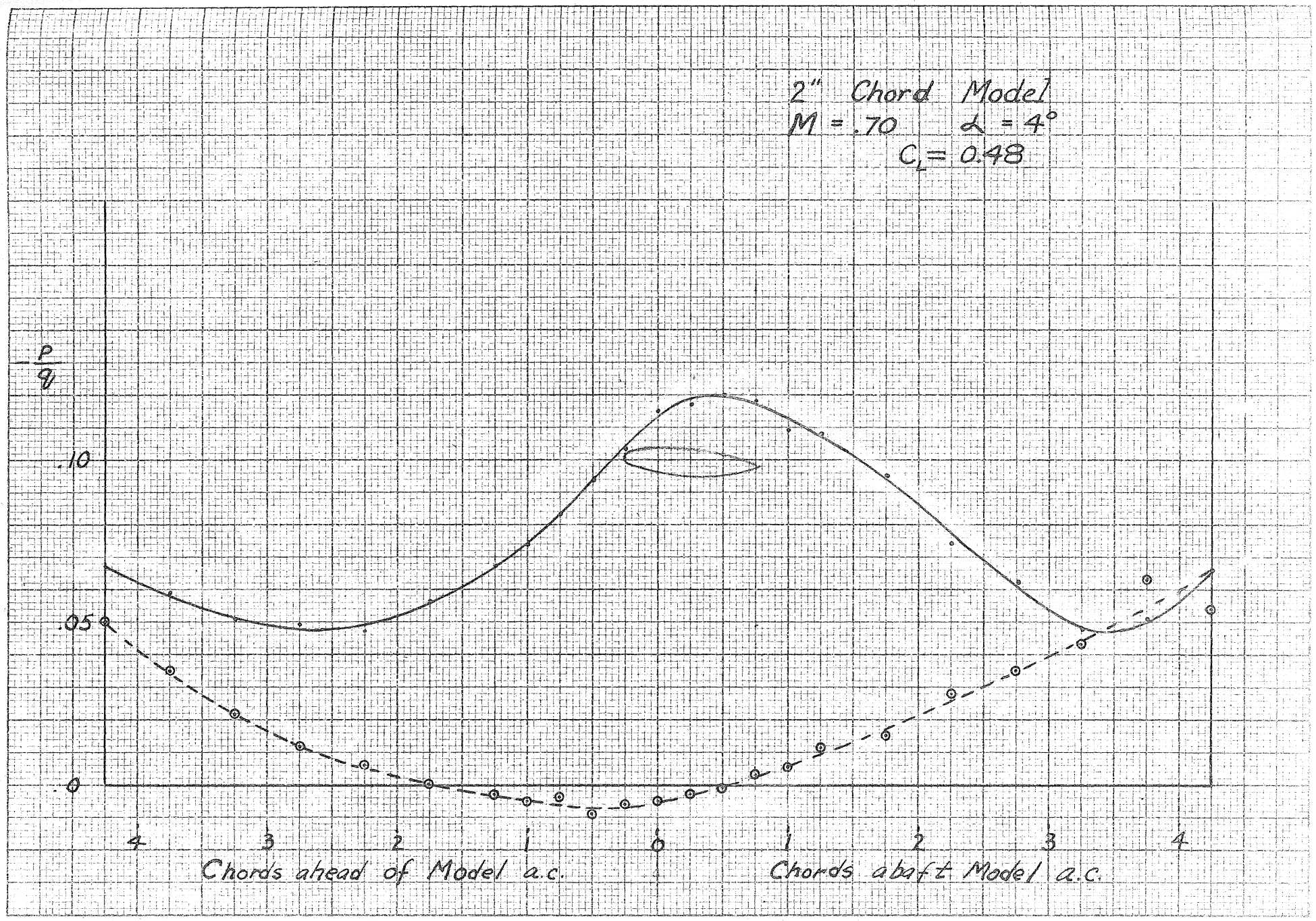
2" Chord Model
M = .70 α = 4°
C_L = 0.48
$-\frac{P}{q}$
.10
.05
0
4
3
2
1
0
1
2
3
4
Chords ahead of Model a.c.
Chords abaft Model a.c.

FIG. 48

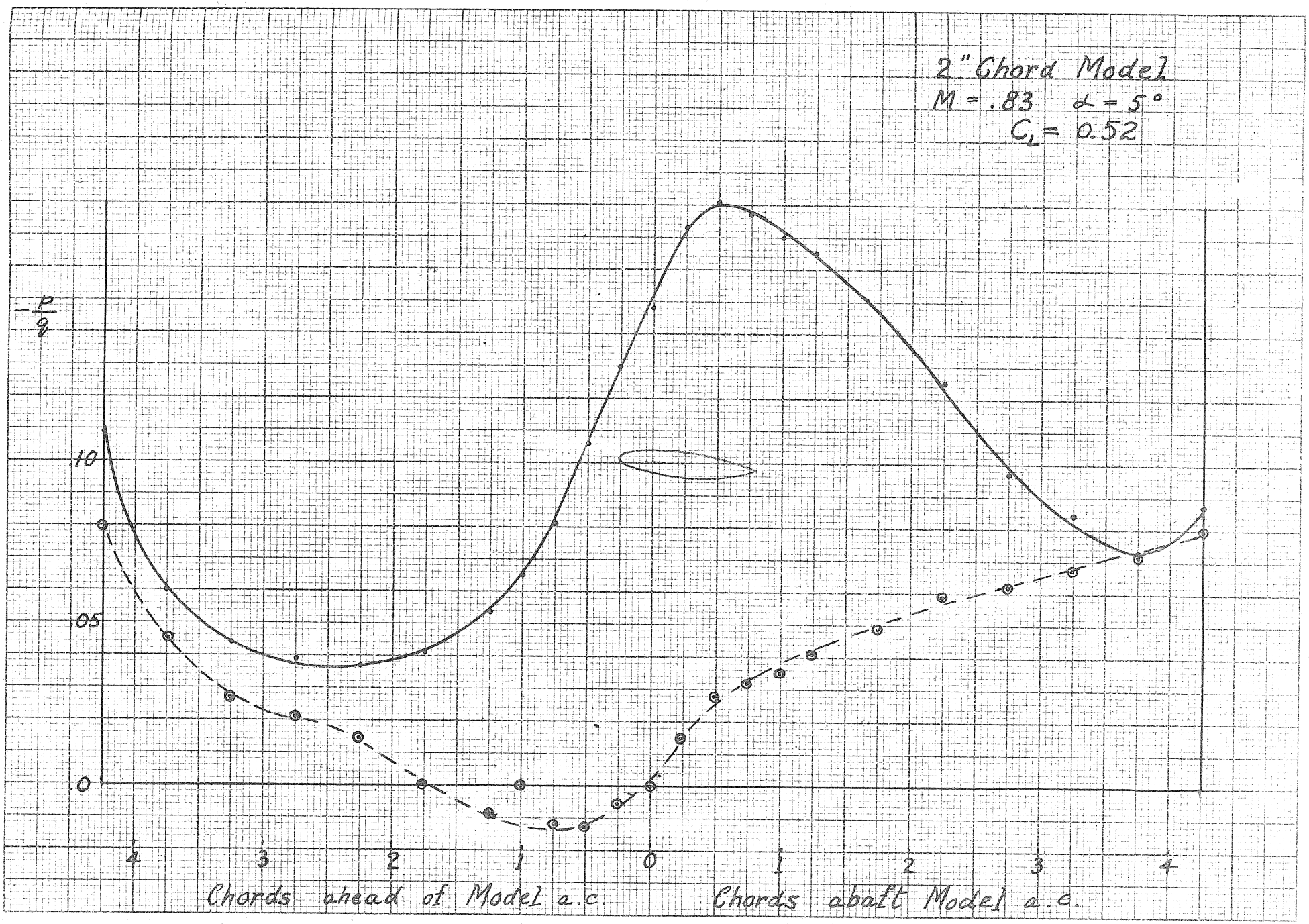
2" Chord Model
M = .83 α = 5°
C_L = 0.52
$-\frac{p}{q}$
.10
.05
0
4
3
2
1
0
1
2
3
4
Chords ahead of Model a.c.
Chords abaft Model a.c.

FIG. 49

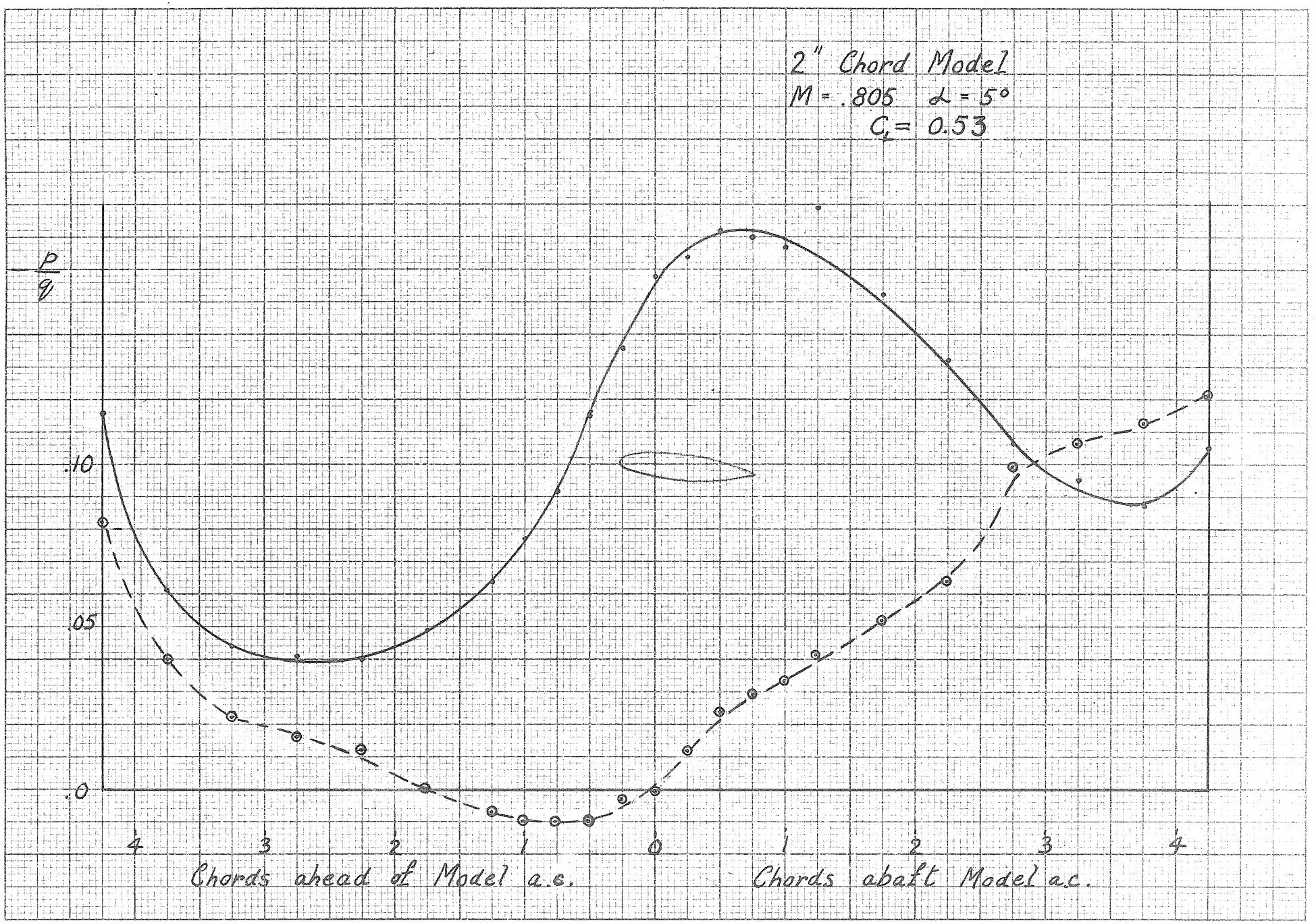
2" Chord Model
M = .805 α = 5°
C_L = 0.53
p/q
.10
.05
.0
4
3
2
1
0
1
2
3
4
Chords ahead of Model a.c.
Chords abaft Model a.c.

FIG. 50

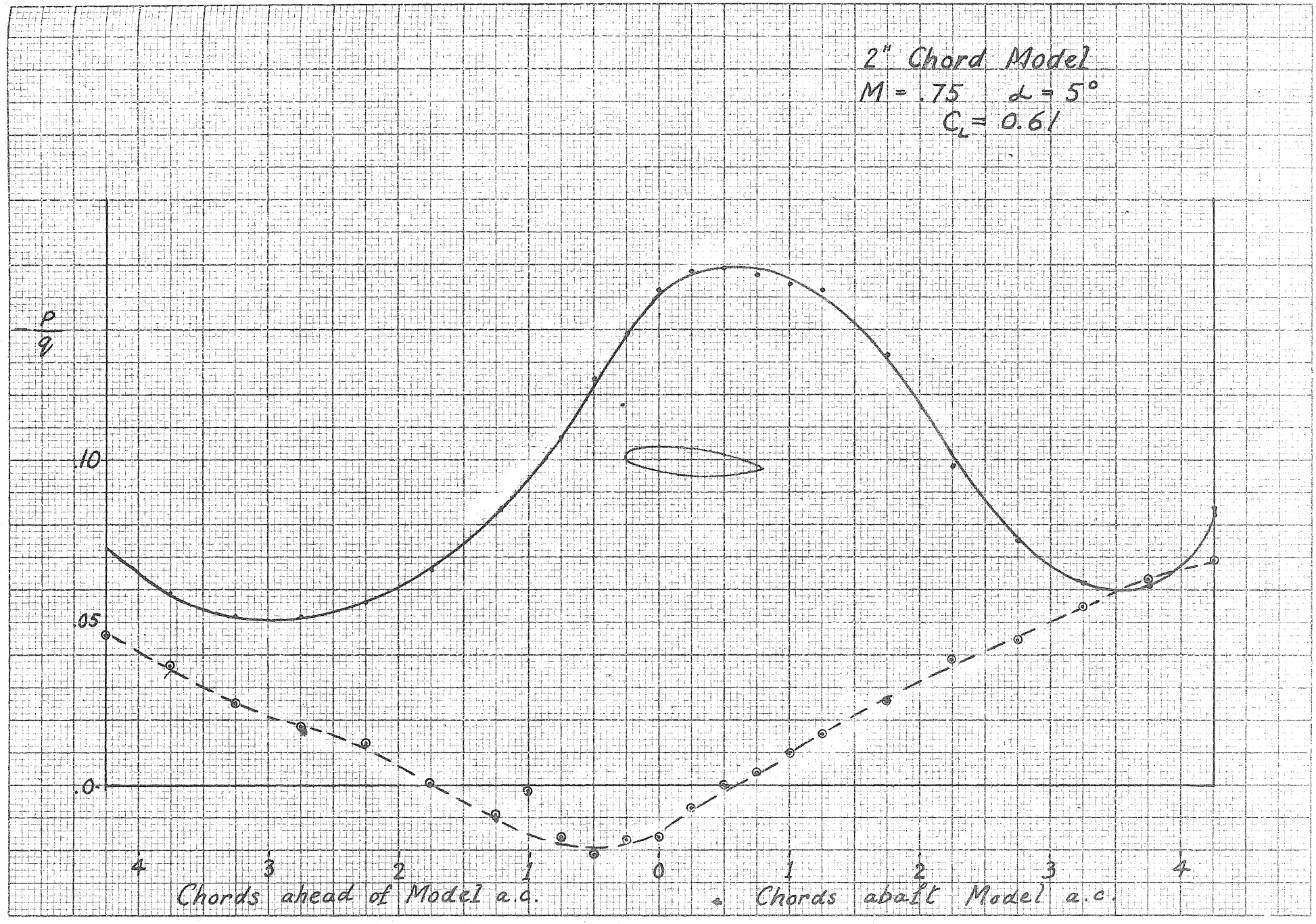
2" Chord Model
M = .75 α = 5°
C_L = 0.61
p/q
.10
.05
.0
4
3
2
1
0
1
2
3
4
Chords ahead of Model a.c.
Chords abaft Model a.c.

FIG. 51

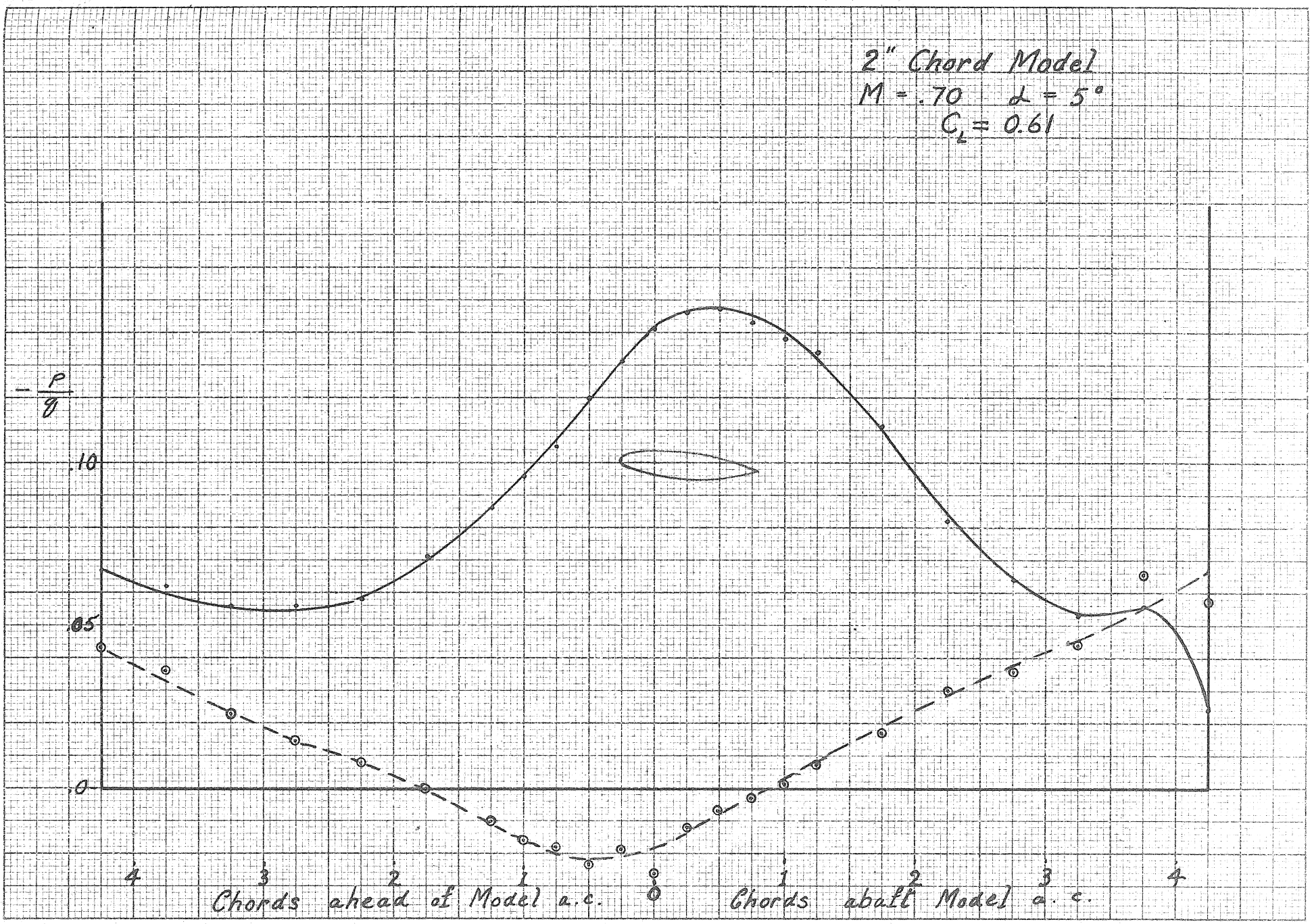
2" Chord Model
M = .70 α = 5°
C_L = 0.61
$-\frac{p}{q}$
.10
.05
0
4
3
2
1
0
1
2
3
4
Chords ahead of Model a.c.
Chords abaft Model a.c.

FIG. 52a

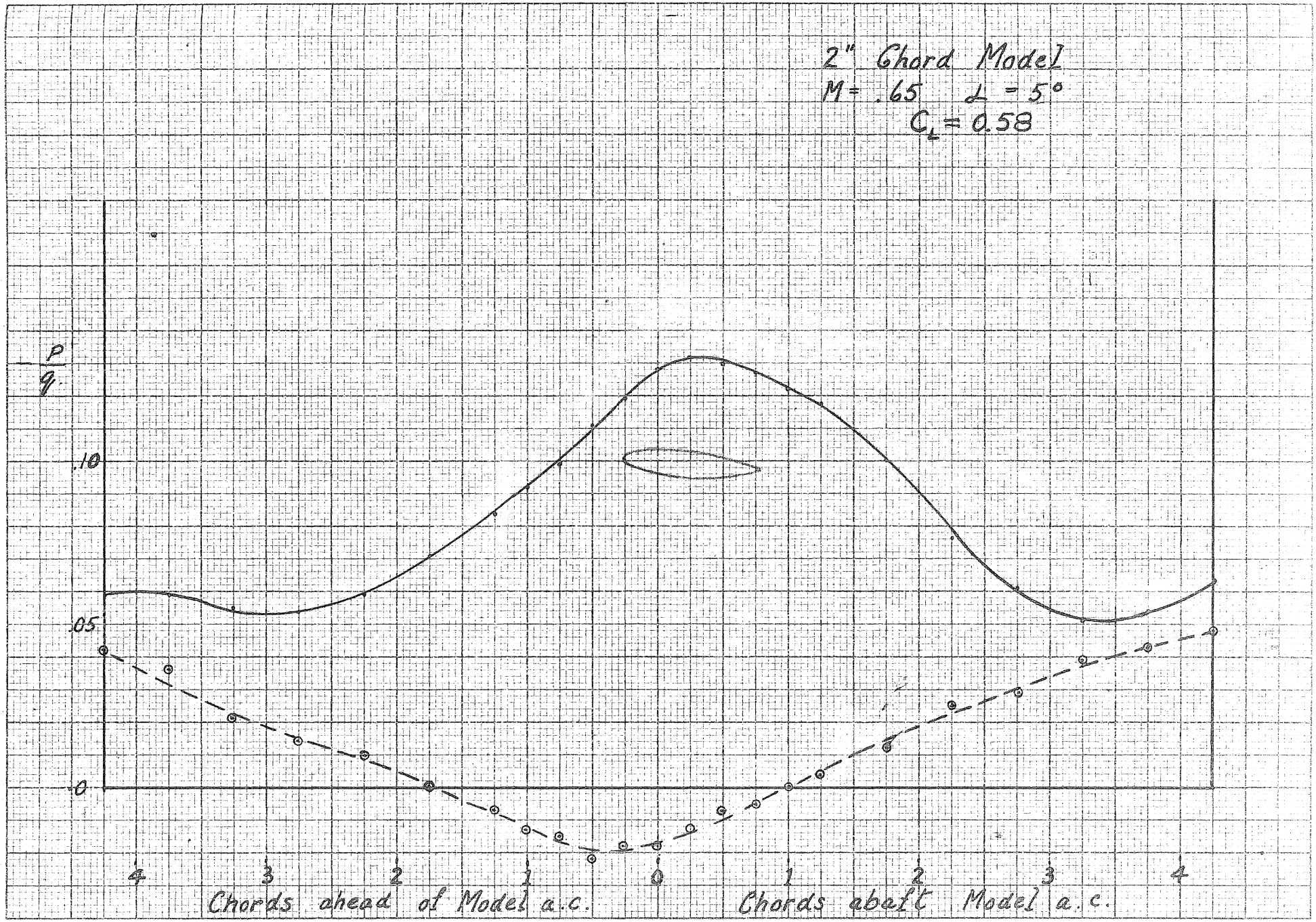
2" Chord Model
M = .65 α = 5°
C_L = 0.58
$\frac{p}{q}$
.10
.05
-0
4
3
2
1
0
1
2
3
4
Chords ahead of Model a.c.
Chords abaft Model a.c.

FIG. 52b

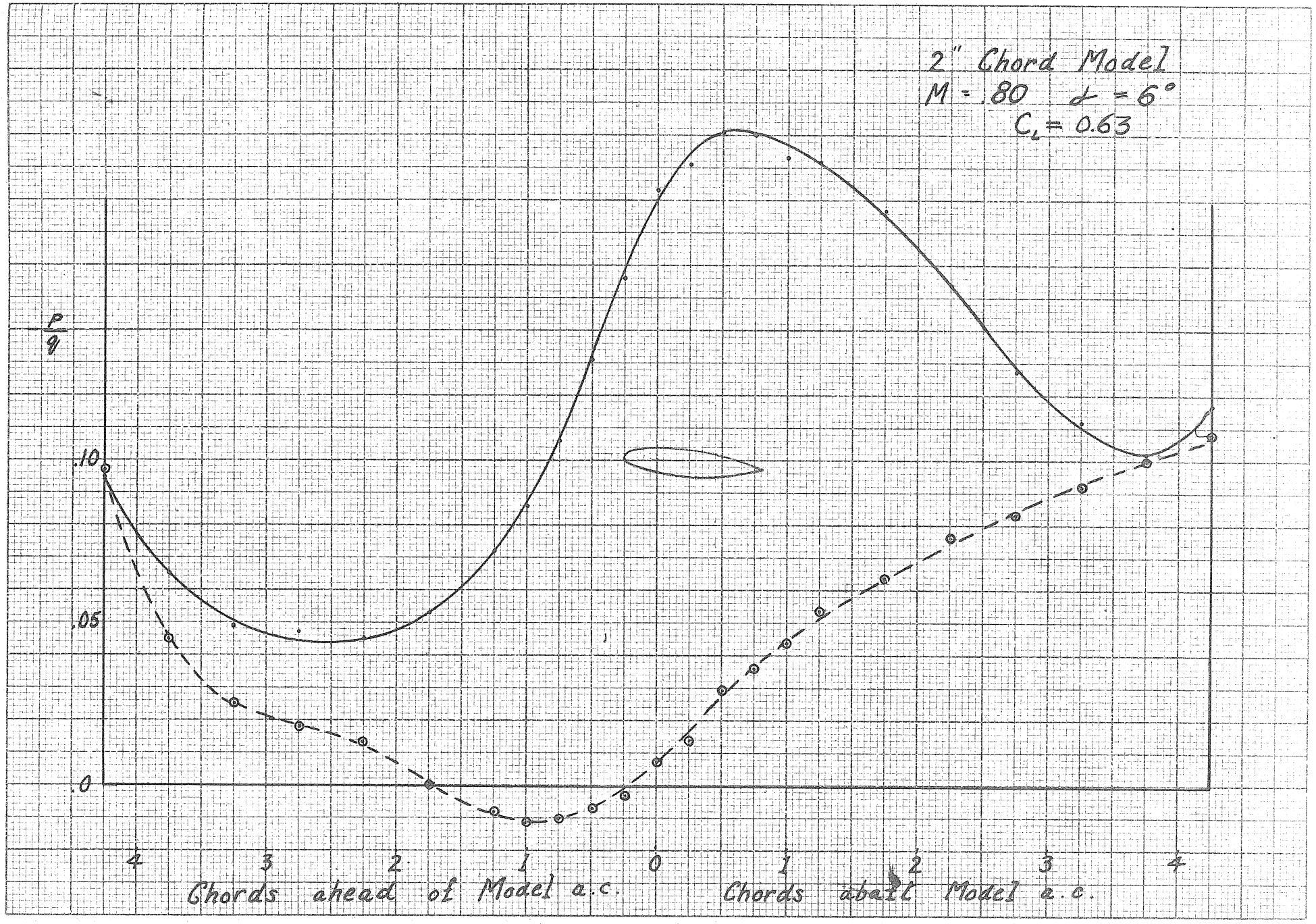
2" Chord Model
M = .80 α = 6°
C_L = 0.63
$\frac{P}{q}$
.10
.05
0
4
3
2
1
0
1
2
3
4
Chords ahead of Model a.c.
Chords abaft Model a.c.

FIG. 53

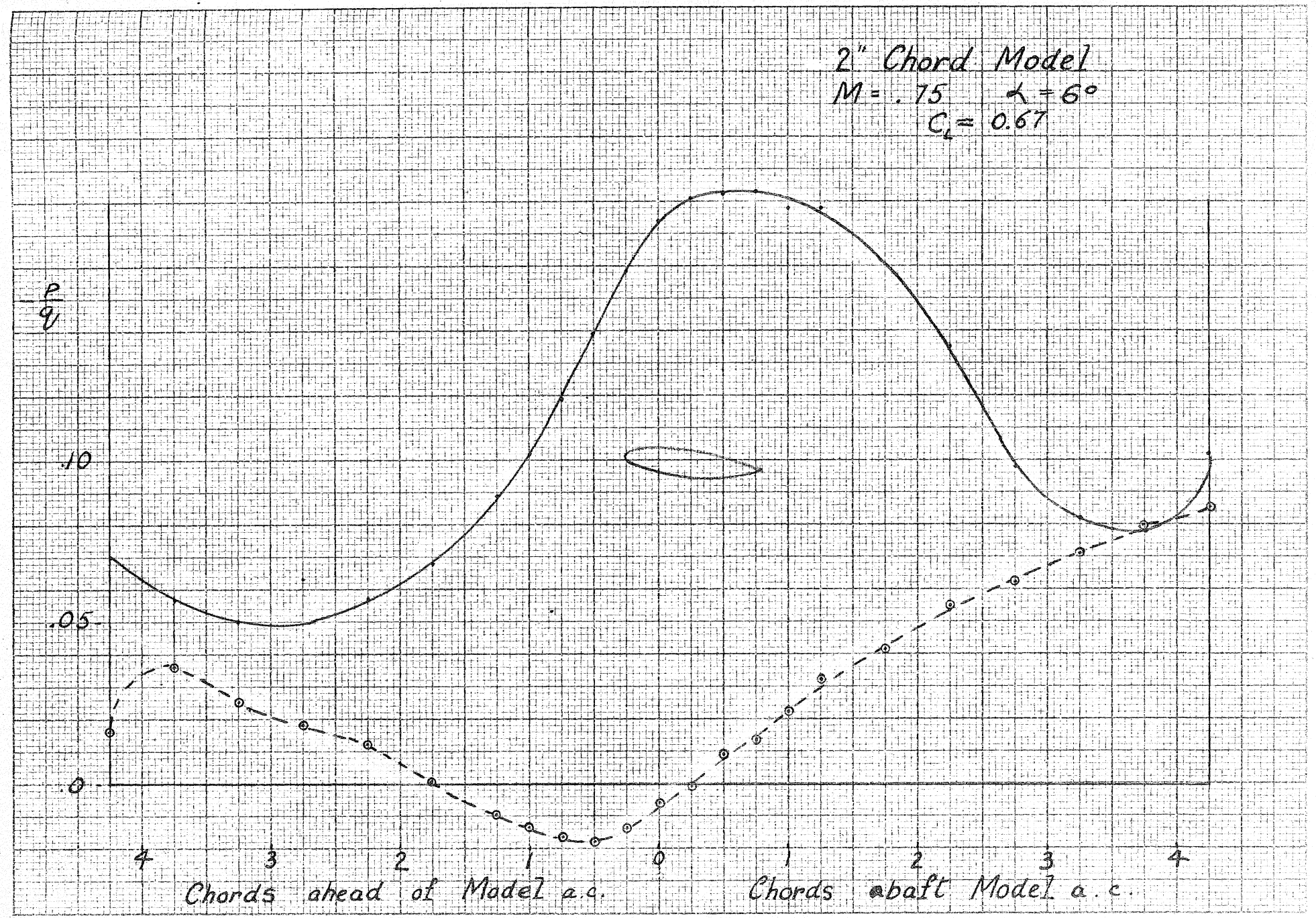
2" Chord Model
M = .75 α = 6°
C_L = 0.67
$-\frac{p}{q}$
.10
.05
0
4
3
2
1
0
1
2
3
4
Chords ahead of Model a.c.
Chords aft Model a.c.

FIG. 54

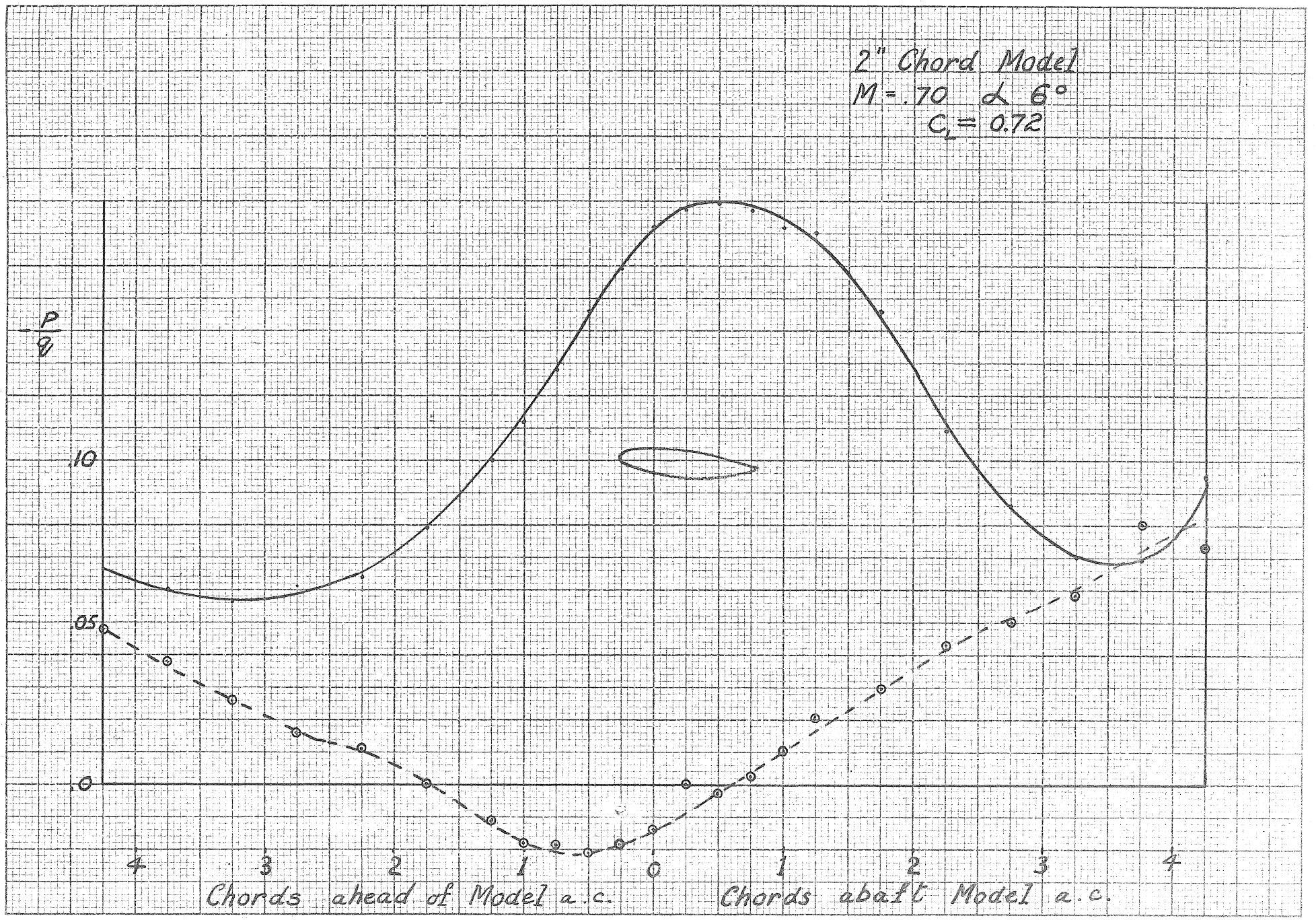
2" Chord Model
M = .70 α 6°
C_L = 0.72
$\frac{P}{q}$
.10
.05
0
4
3
2
1
0
1
2
3
4
Chords ahead of Model a.c.
Chords abaft Model a.c.

FIG. 55

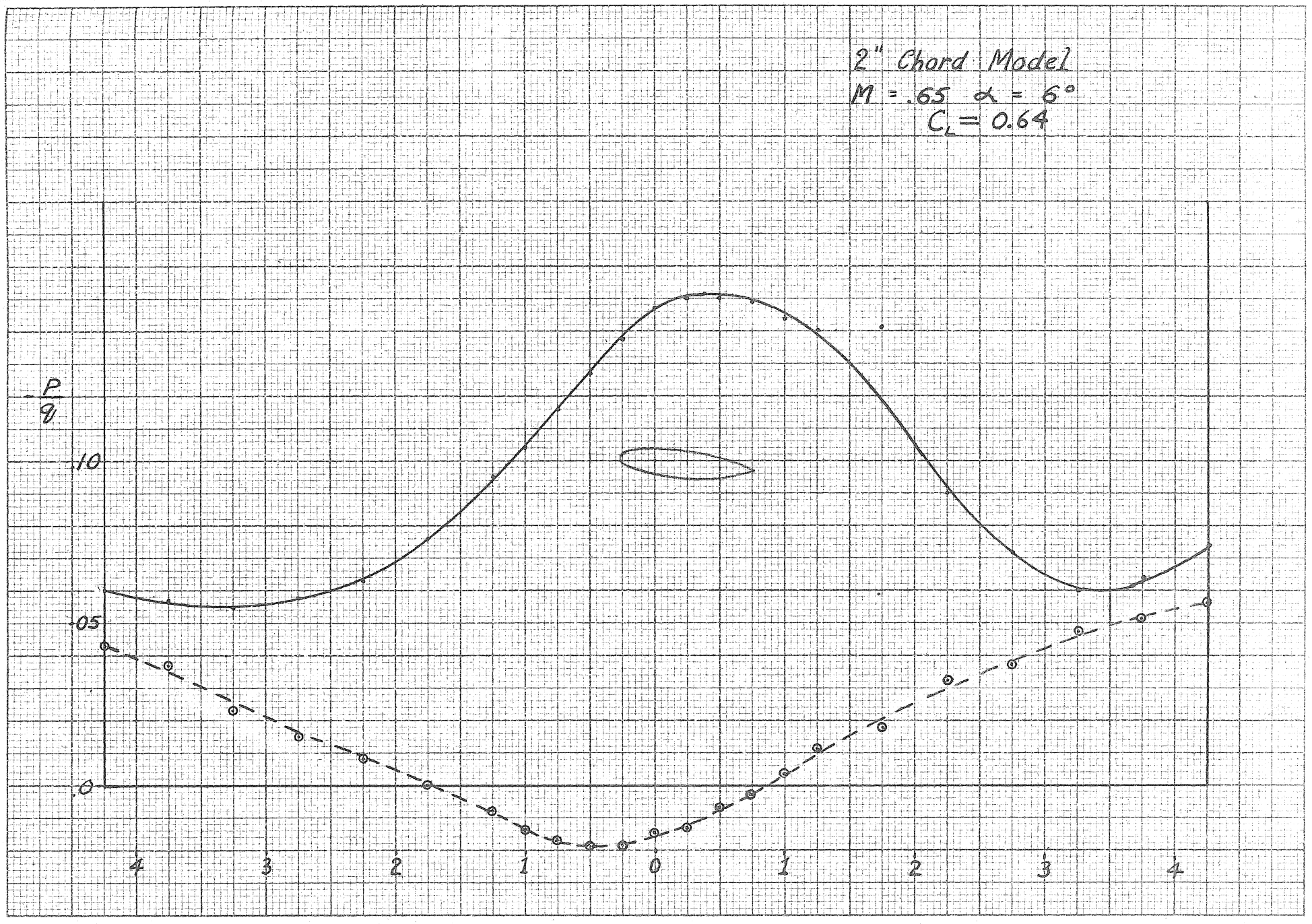

FIG. 56

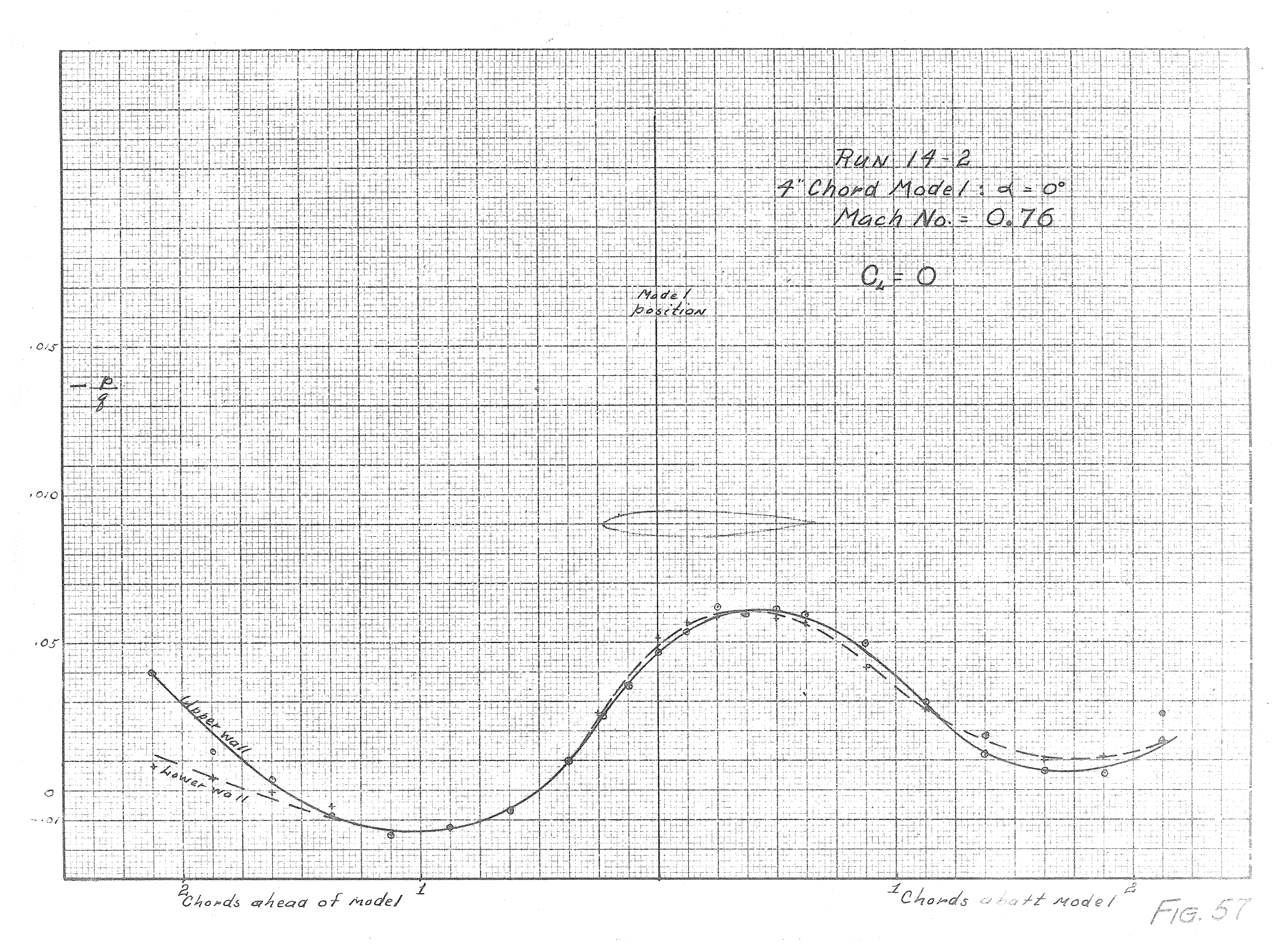
RUN 14-2
4" Chord Model : α = 0°
Mach No. = 0.76
$C_L = 0$
Model position
$-\frac{p}{q}$
.015
.010
.05
0
-.01
Upper wall
Lower wall
2 Chords ahead of model
1
1 Chords abatt model
2

FIG. 57

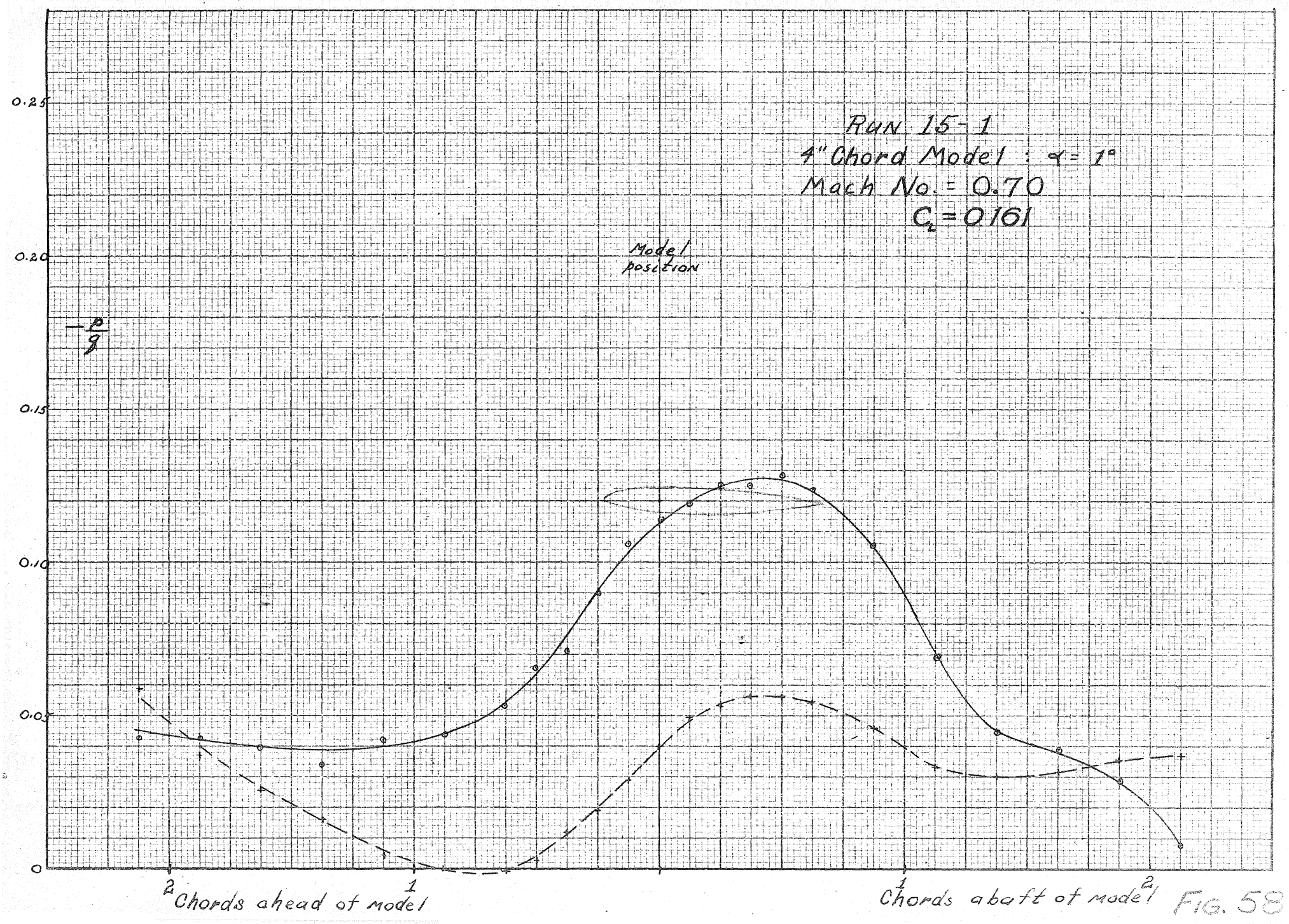
Run 15-1
4" Chord Model : α = 1°
Mach No. = 0.70
C_L = 0.161
Model position
$-\frac{p}{q}$
0.25
0.20
0.15
0.10
0.05
0
2 1
Chords ahead of model
1 2
Chords abaft of model

FIG. 58

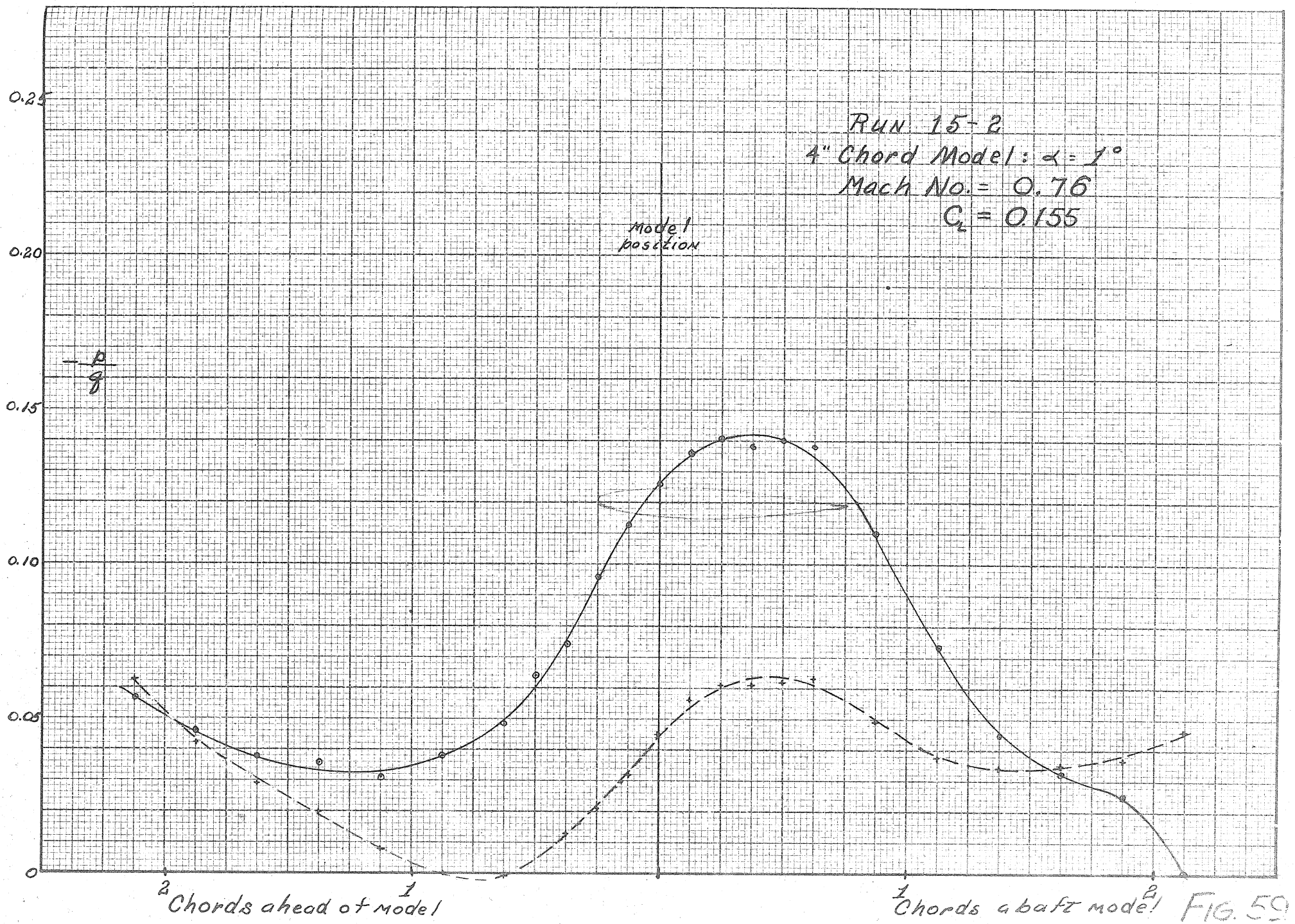
Run 15-2
4" Chord Model: α = 1°
Mach No. = 0.76
C_L = 0.155
model position
$-\frac{p}{q}$
0.25
0.20
0.15
0.10
0.05
0
2 Chords ahead of model
1
1
2 Chords abaft model

FIG. 59

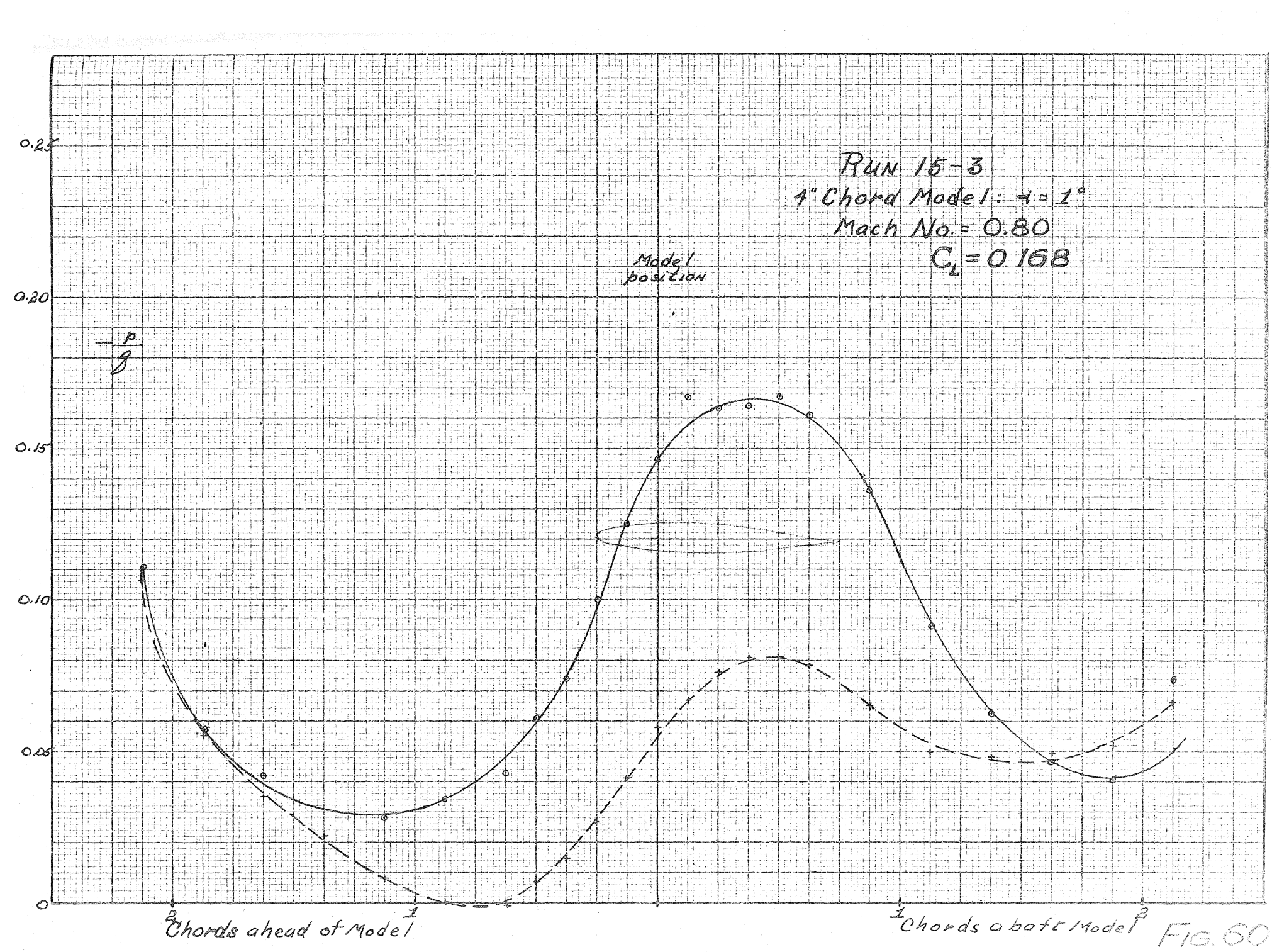
RUN 15-3
4" Chord Model : α = 1°
Mach No. = 0.80
C_L = 0.168
Model position
$-\frac{p}{q}$
0.25
0.20
0.15
0.10
0.05
0
2 Chords ahead of Model
1
1 Chords aboft Model
2

Fig. 60

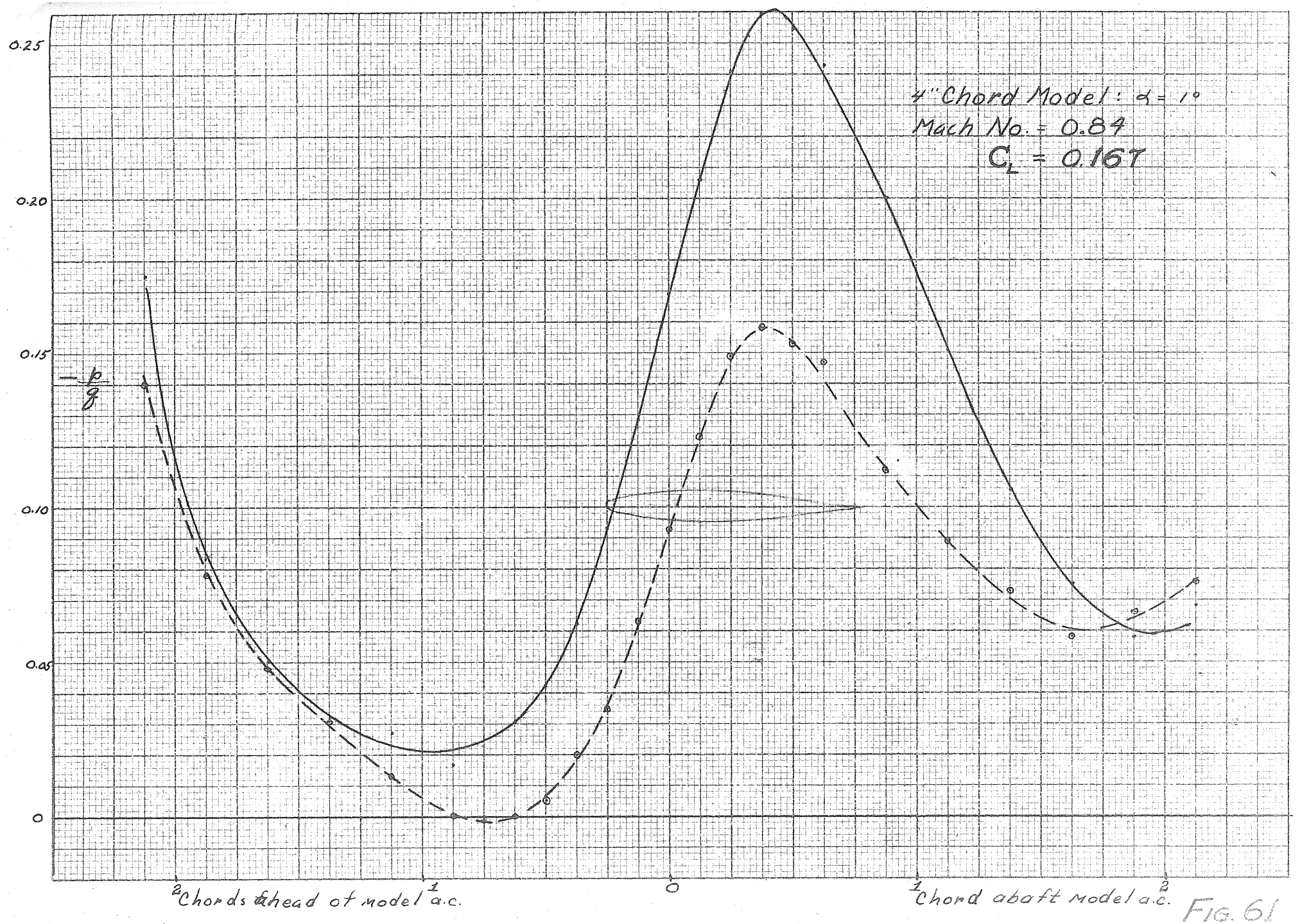
4" Chord Model : α = 1°
Mach No. = 0.84
C_L = 0.167
0.25
0.20
0.15
0.10
0.05
0
$-\frac{p}{q}$
2 Chords ahead of model a.c.
1
0
1 Chord abaft model a.c.
2

Fig. 61

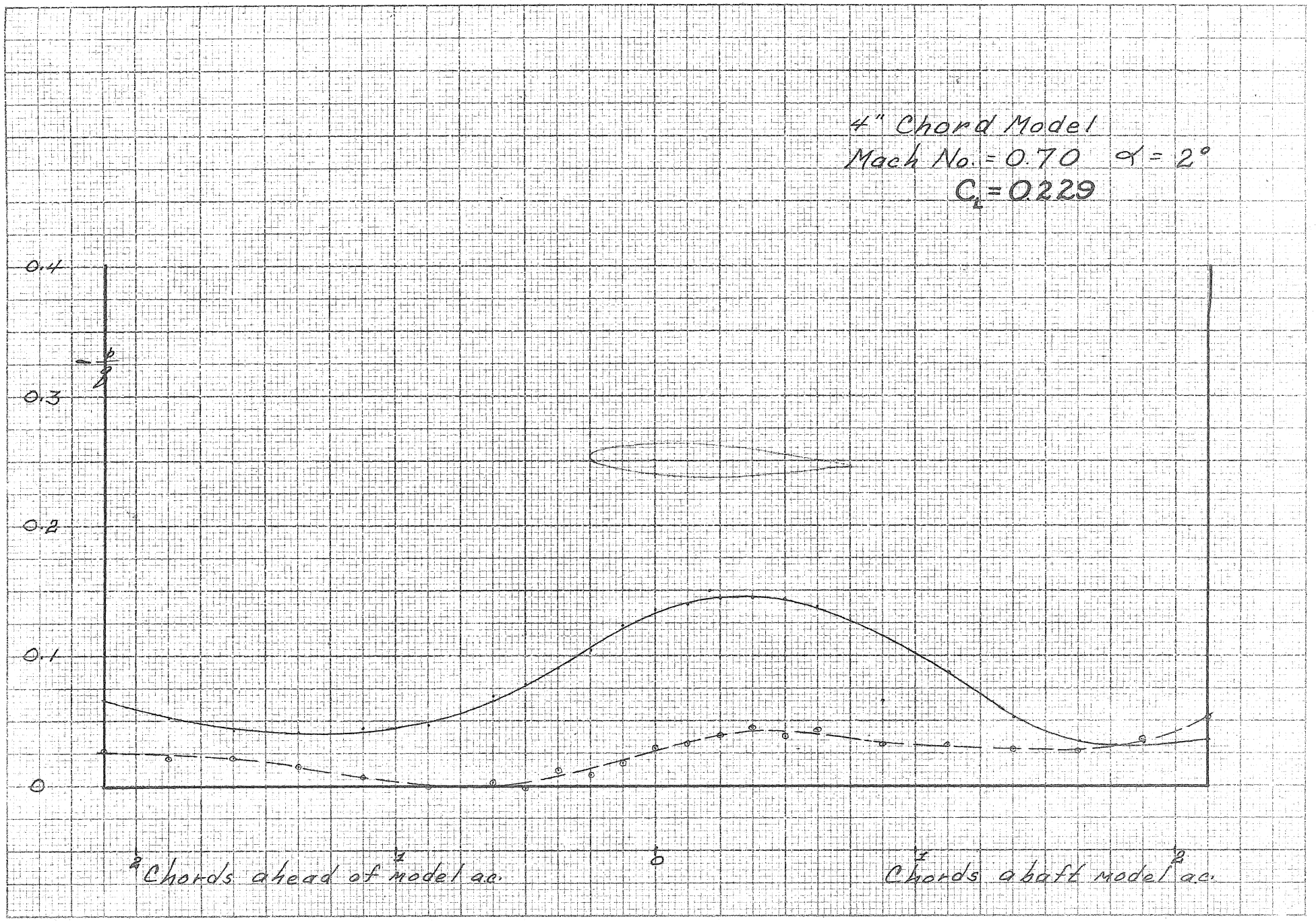
4" Chord Model
Mach No. = 0.70 α = 2°
C_L = 0.229
0.4
$-\frac{p}{q}$
0.3
0.2
0.1
0
2 Chords ahead of model a.c.
1
0
1
2 Chords aft of model a.c.

FIG. 62

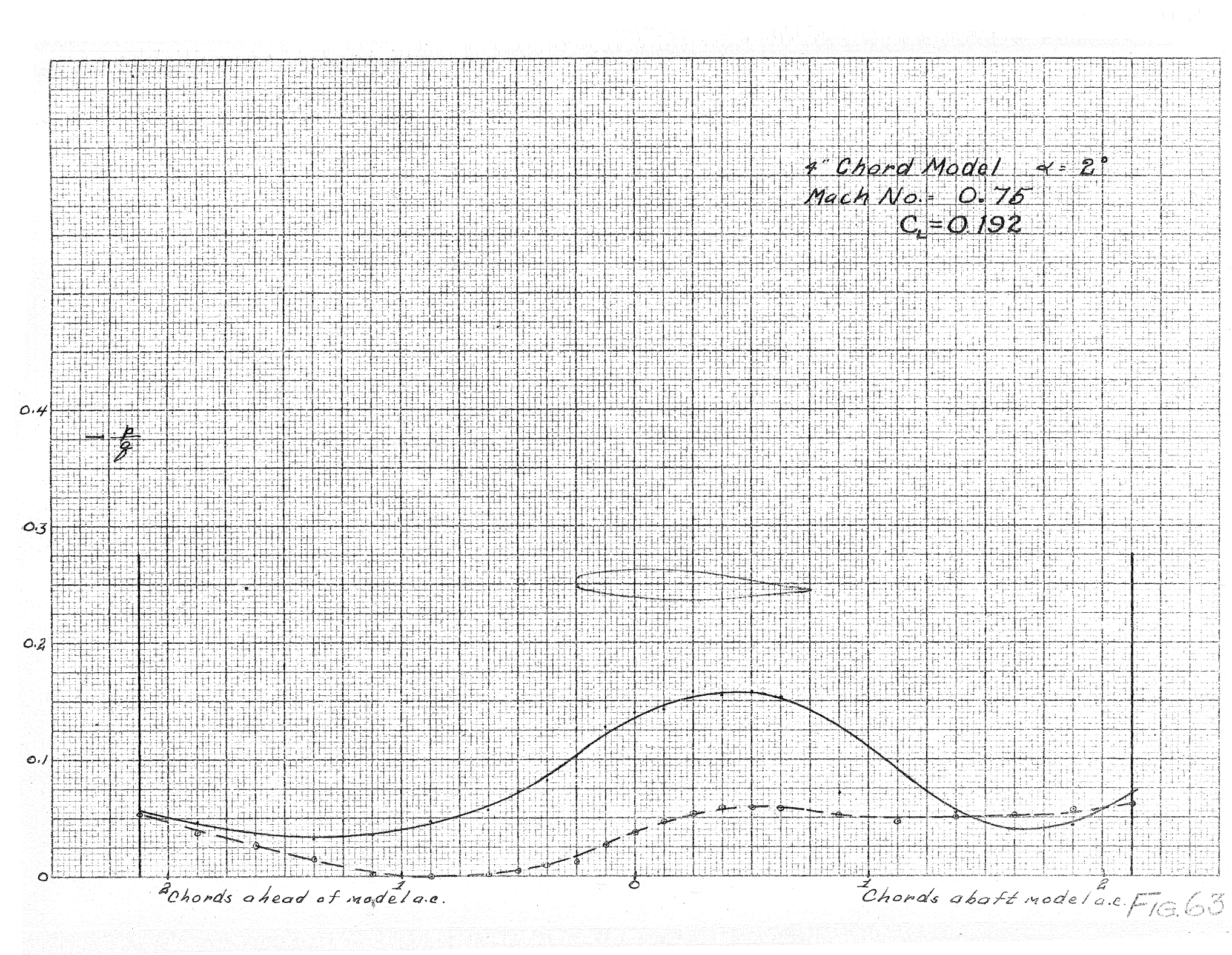
4" Chord Model α = 2°
Mach No. = 0.75
C_L = 0.192
$-\frac{p}{q}$
0.4
0.3
0.2
0.1
0
2 Chords ahead of model a.c.
1
0
1
2 Chords abaft model a.c.

FIG. 63

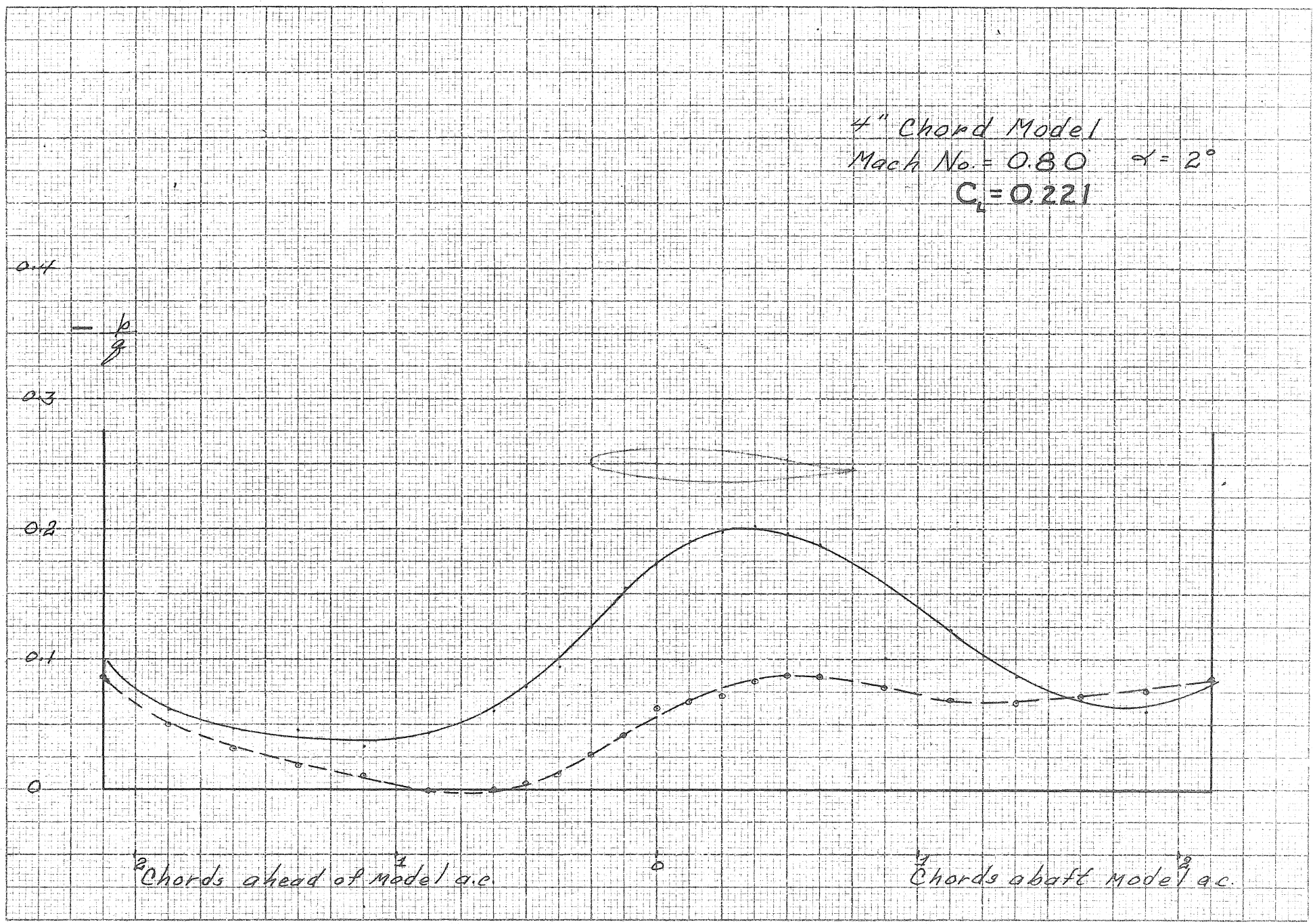
4" Chord Model
Mach No. = 0.80 α = 2°
C_L = 0.221
0.4
$-\frac{p}{q}$
0.3
0.2
0.1
0
$\frac{1}{2}$ Chords ahead of model a.c.
1
0
$\frac{1}{2}$
1
$\frac{1}{2}$ Chords abaft model a.c.

FIG. 64

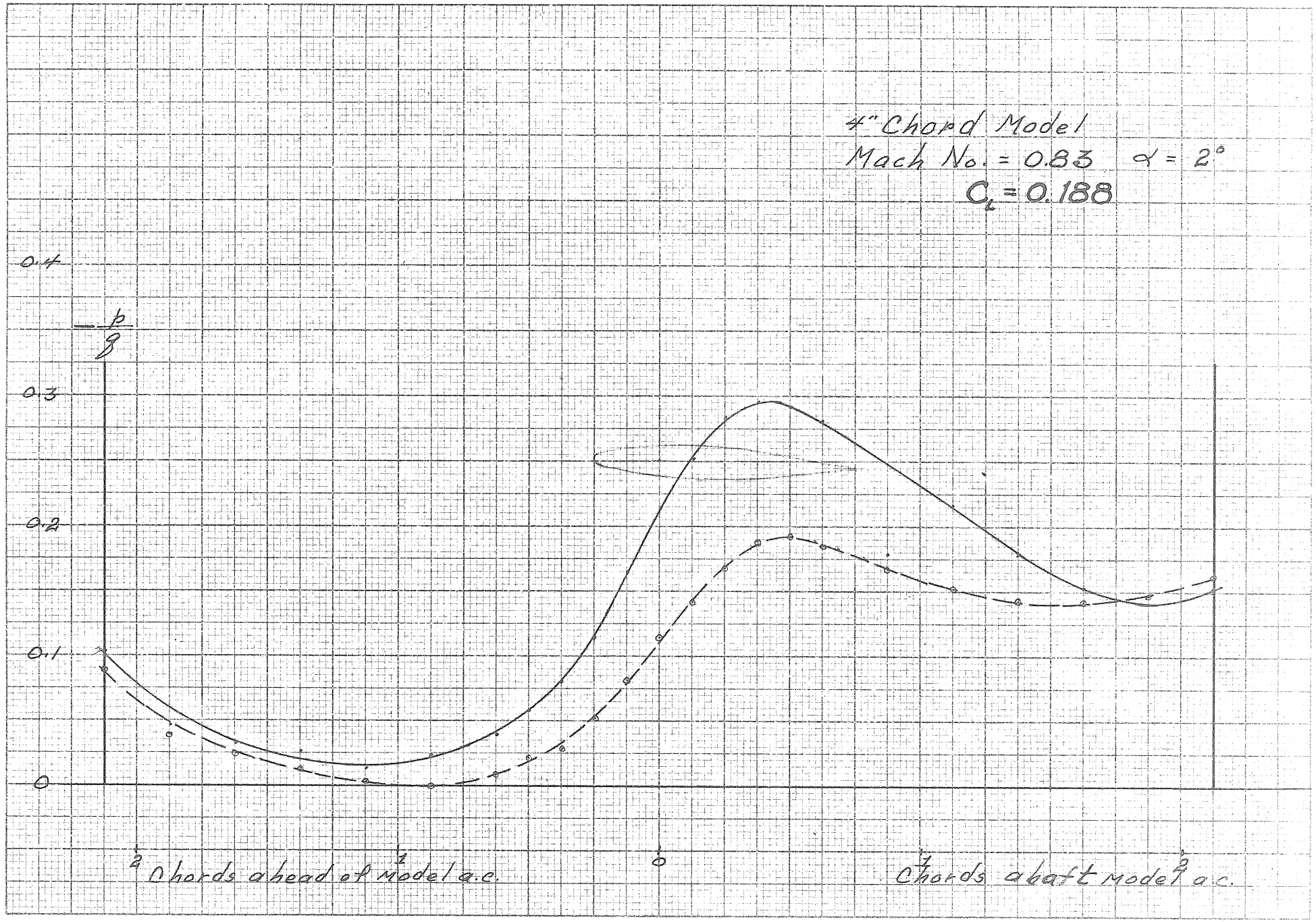
4" Chord Model
Mach No. = 0.83 α = 2°
C_L = 0.188
0.4
$\frac{p}{q}$
0.3
0.2
0.1
0
$\frac{1}{4}$ Chords ahead of model a.c.
$\frac{1}{4}$
0
$\frac{3}{4}$
$\frac{3}{4}$ Chords abaft model a.c.

FIG. 65

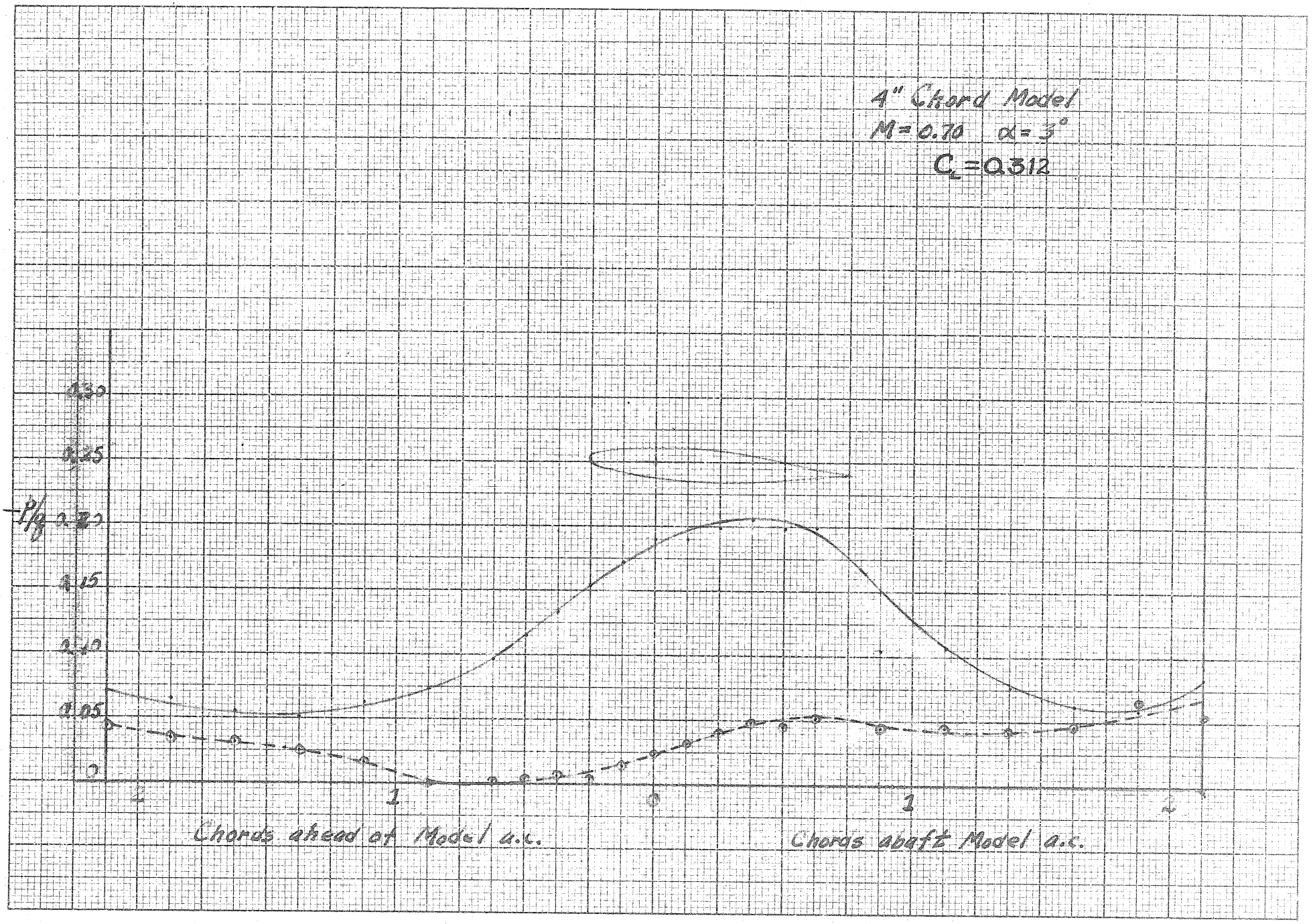
4" Chord Model
M = 0.70 α = 3°
C_L = 0.312
$-P/q_0$
0.30
0.25
0.20
0.15
0.10
0.05
0
2
1
0
1
2
Chords ahead of Model a.c.
Chords abaft Model a.c.

FIG. 66

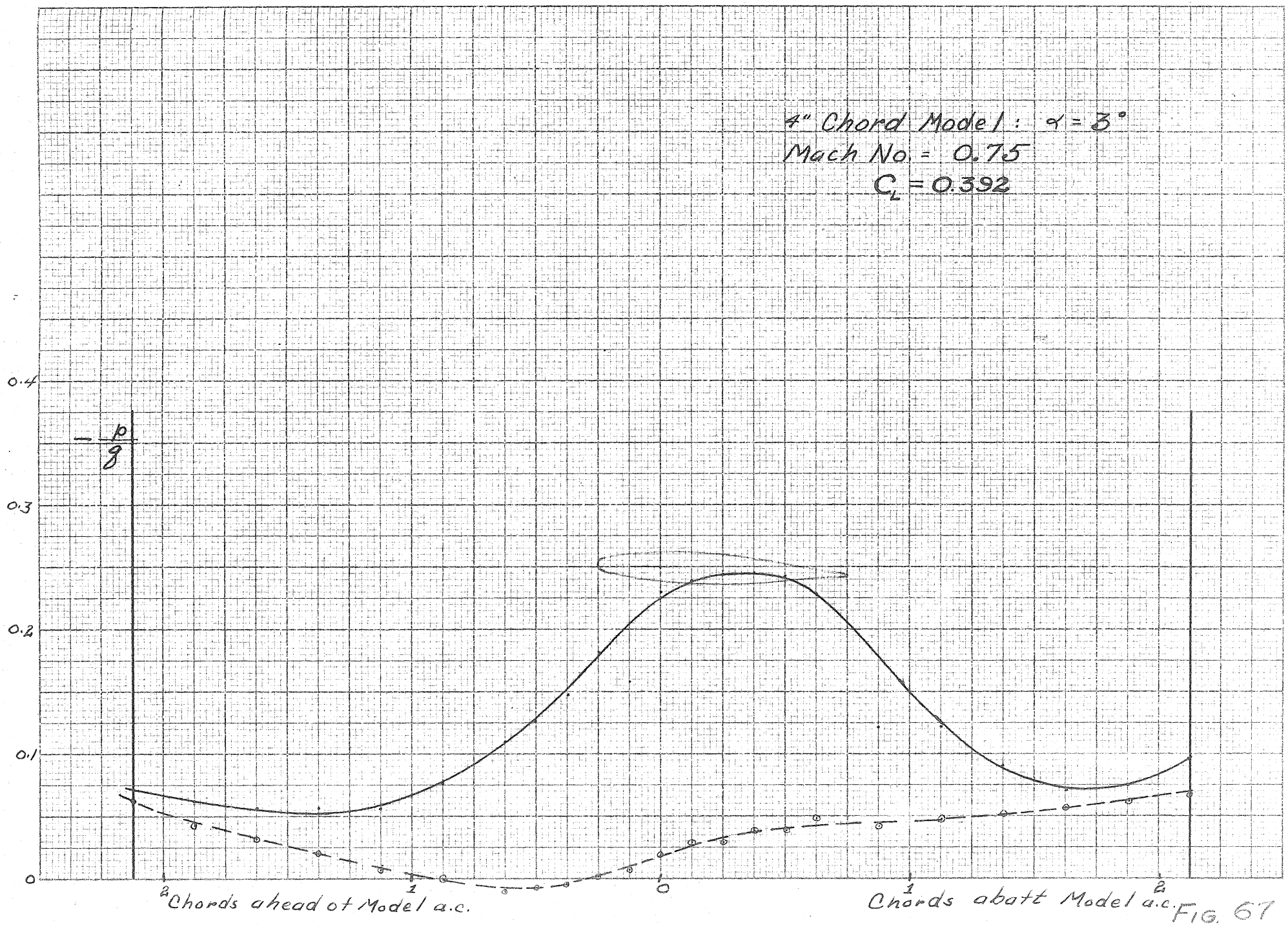
4" Chord Model : α = 3°
Mach No = 0.75
C_L = 0.392
$-\frac{p}{q}$
0.4
0.3
0.2
0.1
0
2 Chords ahead of Model a.c.
1
0
1
2 Chords abatt Model a.c.

FIG. 67

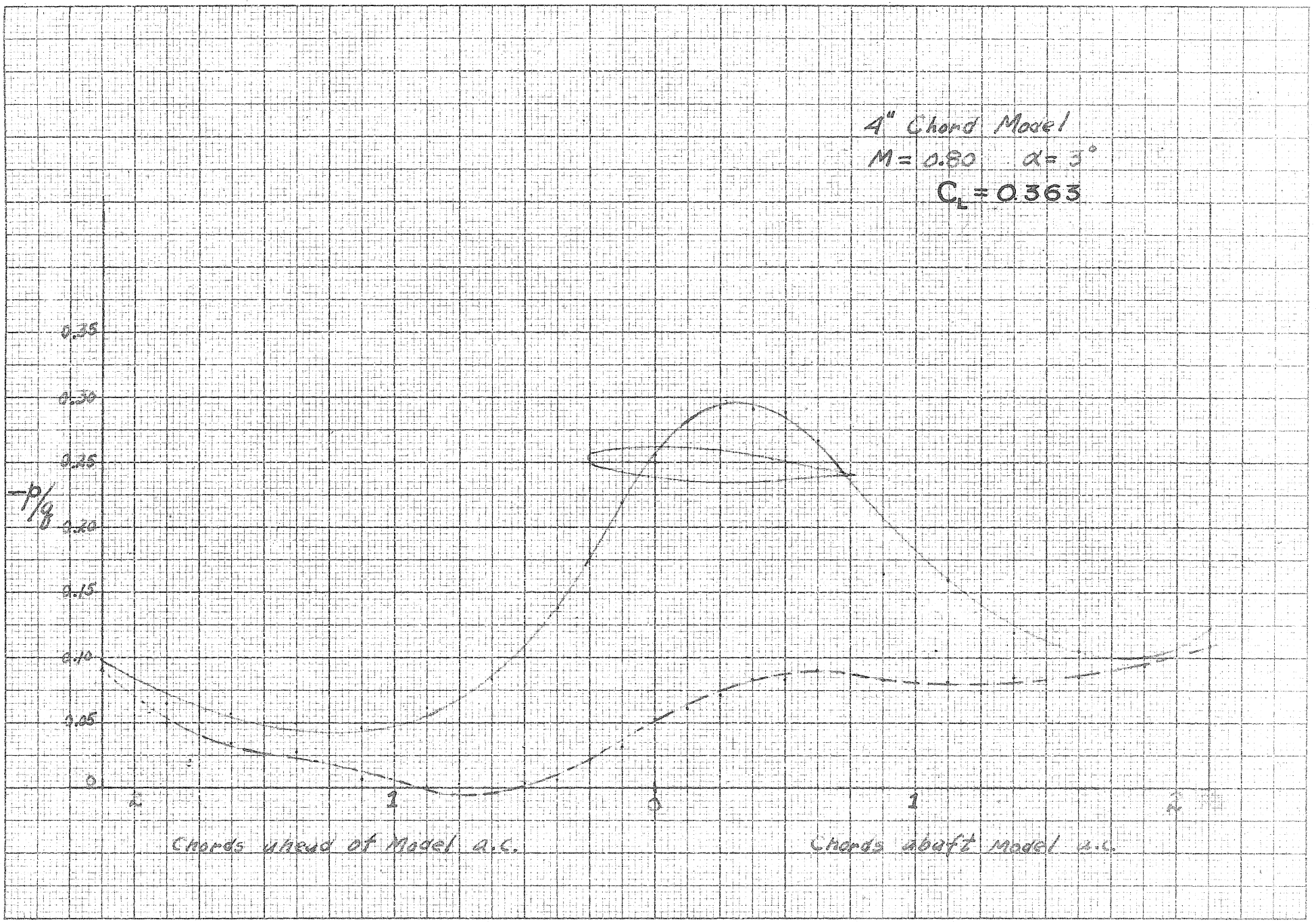
4" Chord Model
M = 0.80 α = 3°
C_L = 0.363
0.35
0.30
0.25
$-p/q$
0.20
0.15
0.10
0.05
0
2
1
0
1
2
Chords ahead of Model a.c.
Chords aboft Model a.c.

FIG. 68

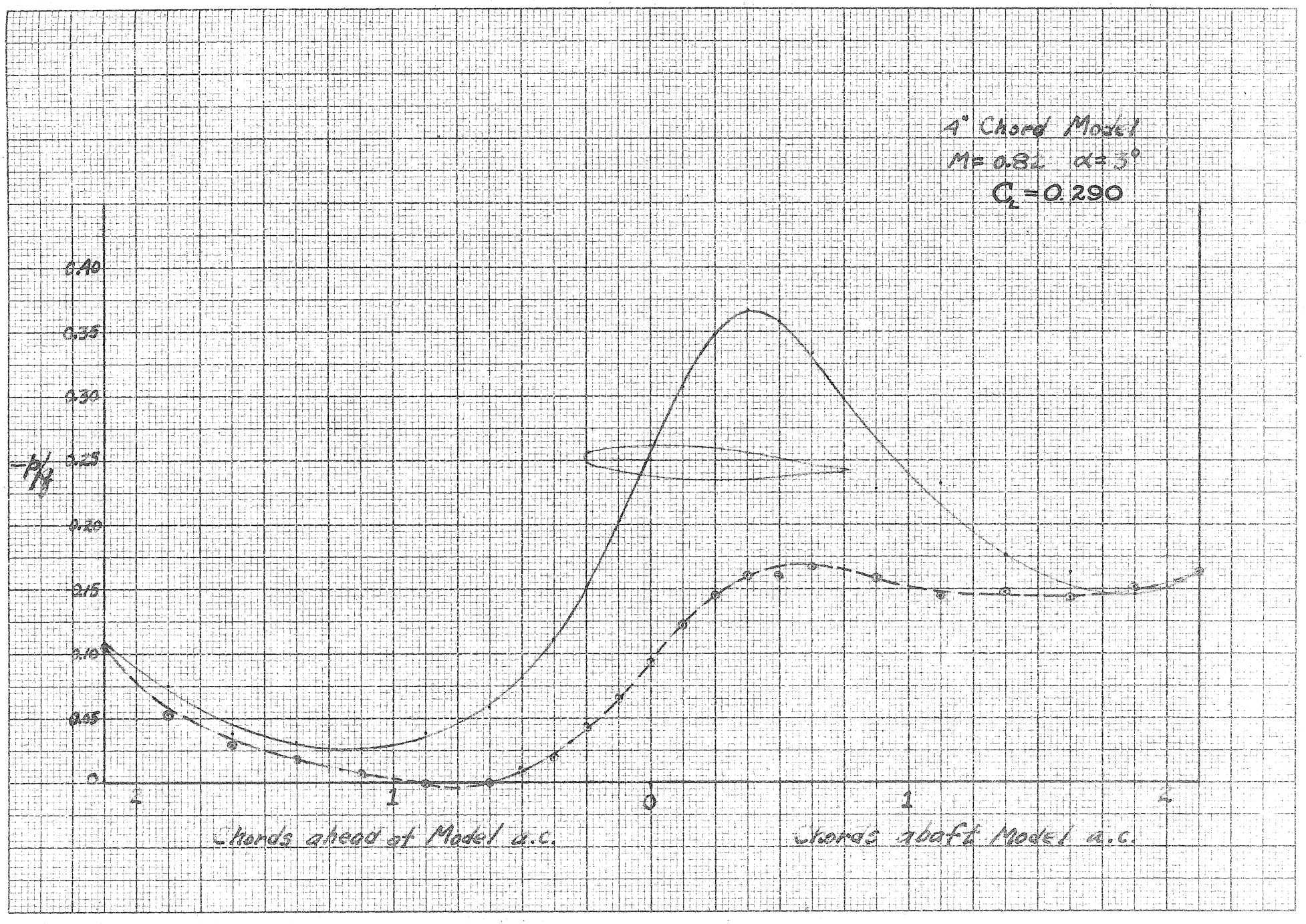
4" Chord Model
M = 0.82 α = 5°
C_L = 0.290
0.40
0.35
0.30
0.25
0.20
0.15
0.10
0.05
0
$-p'/q$
1
0
1
Chords ahead of Model a.c.
Chords aft of Model a.c.

Fig. 69

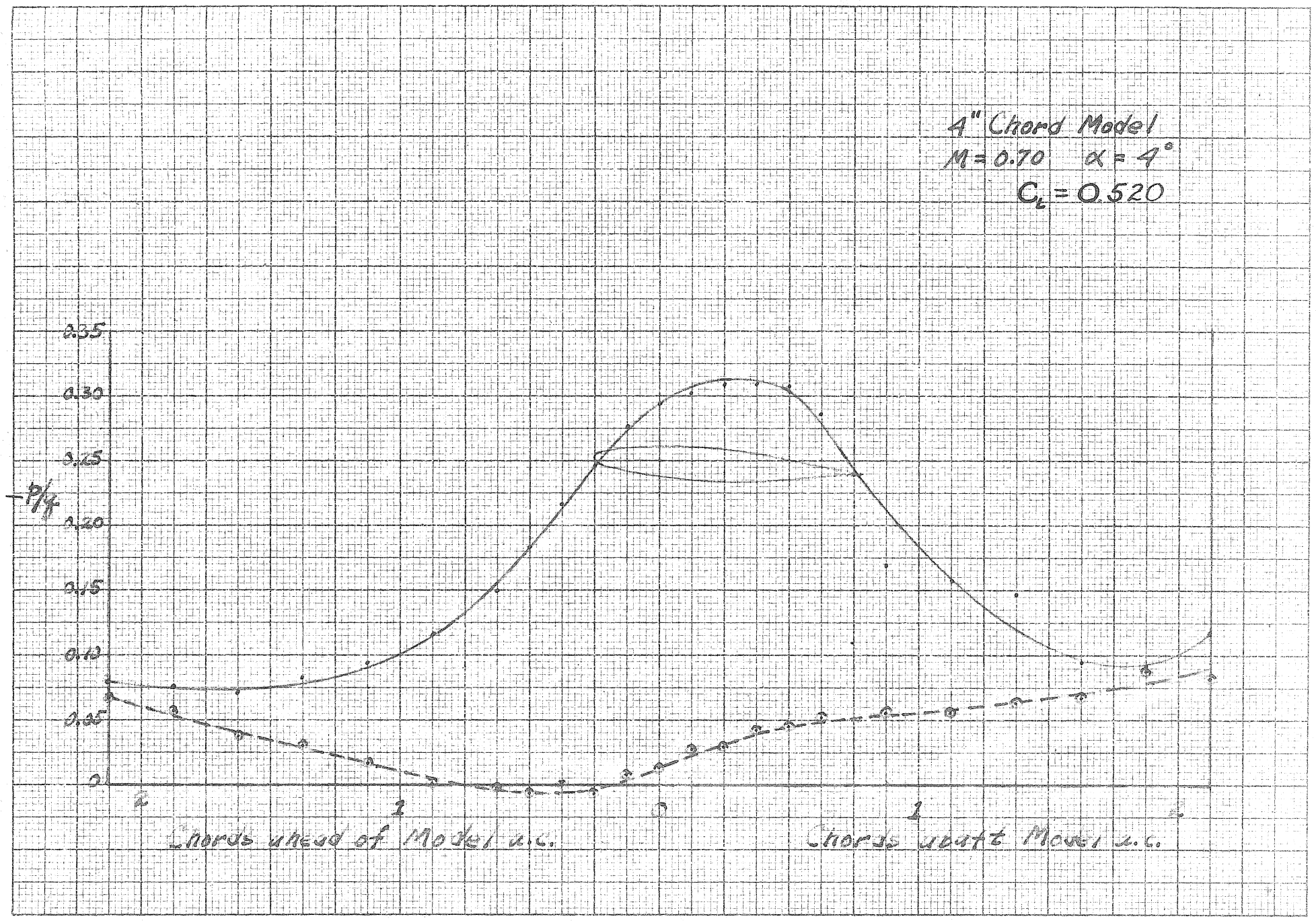
4" Chord Model
M = 0.70 α = 4°
C_L = 0.520
-p/q
0.35
0.30
0.25
0.20
0.15
0.10
0.05
0
2
1
0
1
2
Chords ahead of Model a.c.
Chords aft of Model a.c.

FIG. 10

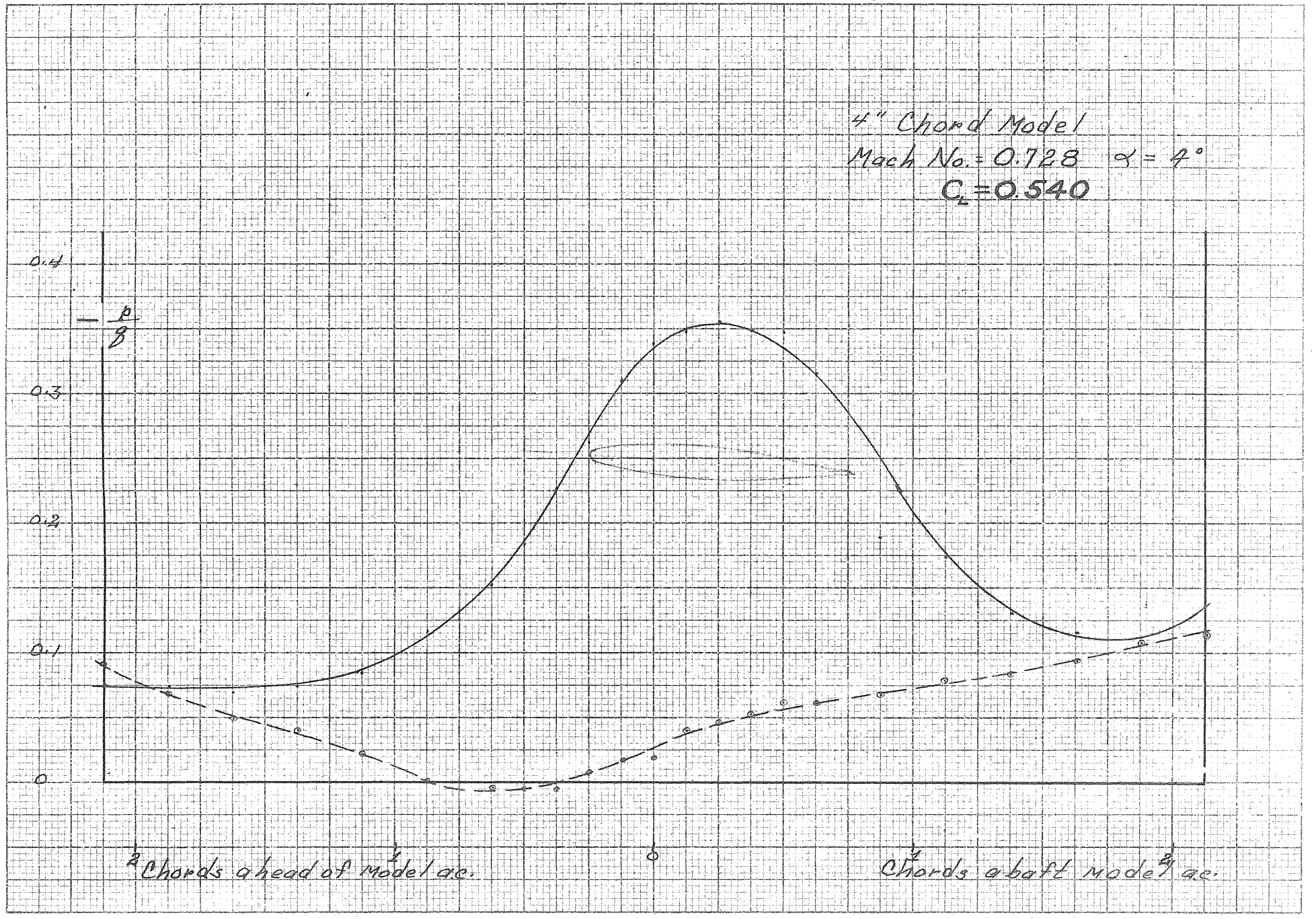
4" Chord Model
Mach No. = 0.728 α = 4°
C_L = 0.540
0.4
$-\frac{p}{q}$
0.3
0.2
0.1
0
½ Chords ahead of Model a.c.
½
Chords abaft Model a.c.

FIG. 71a.

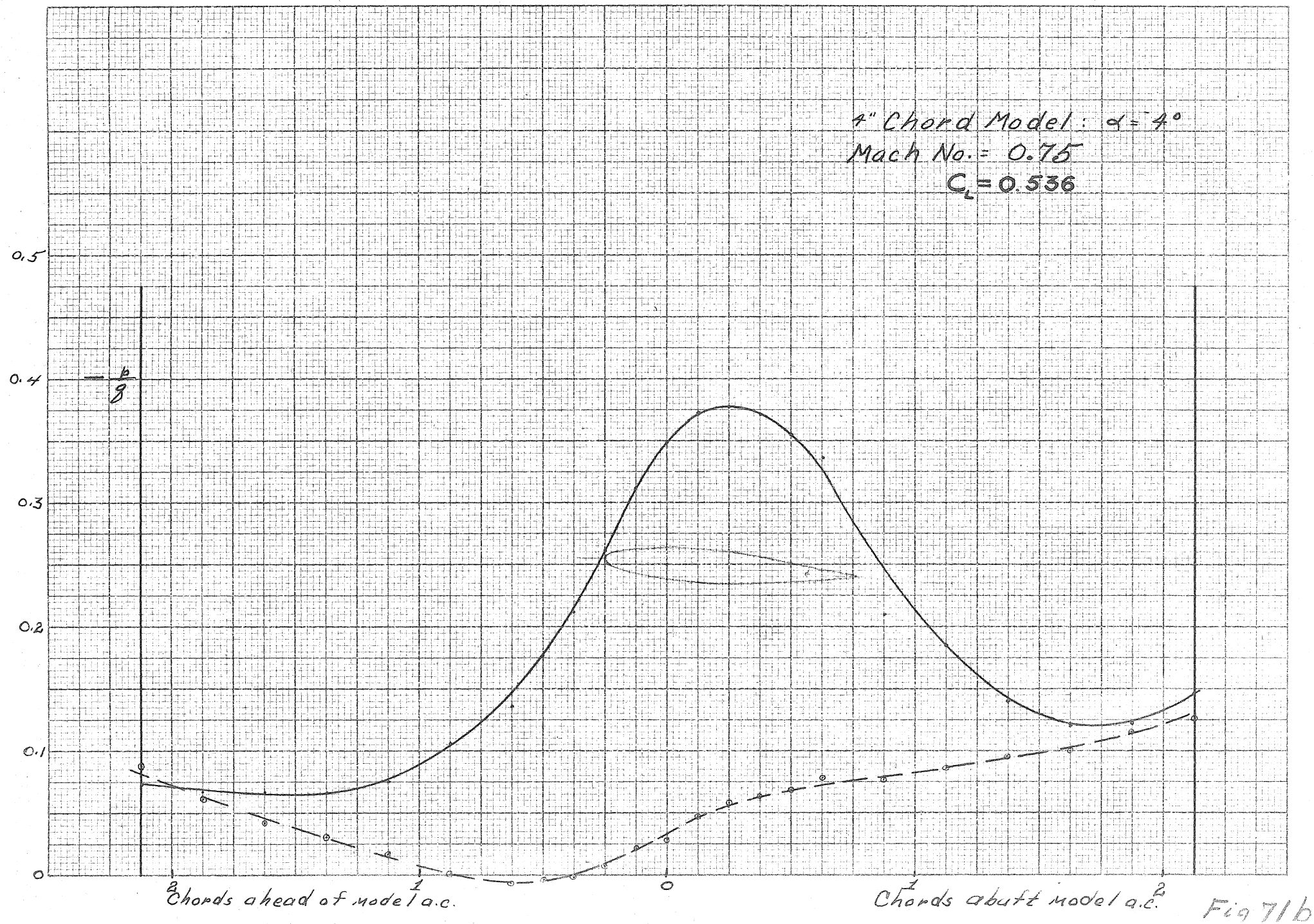
4" Chord Model : α = 4°
Mach No. = 0.75
C_L = 0.536
$-\frac{p}{q}$
0.5
0.4
0.3
0.2
0.1
0
2 Chords ahead of model a.c.
1
0
1
Chords abaft model a.c.
2

Fig 71b

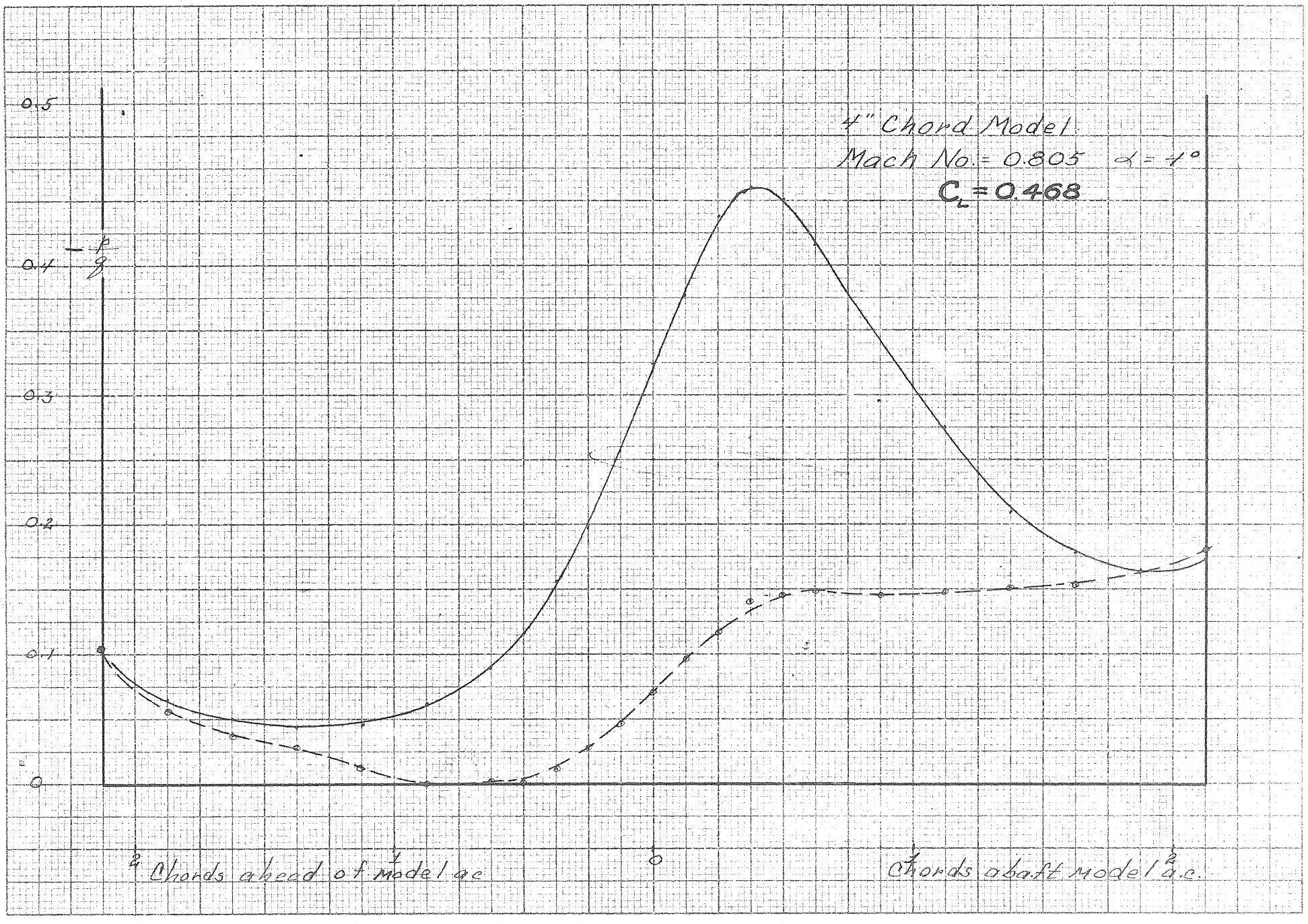
4" Chord Model
Mach No. = 0.805 α = 4°
$C_L = 0.468$
$-\frac{p}{q}$
0.5
0.4
0.3
0.2
0.1
0
½ Chords ahead of model a.c.
0
½ Chords abaft model a.c.

Fig 72

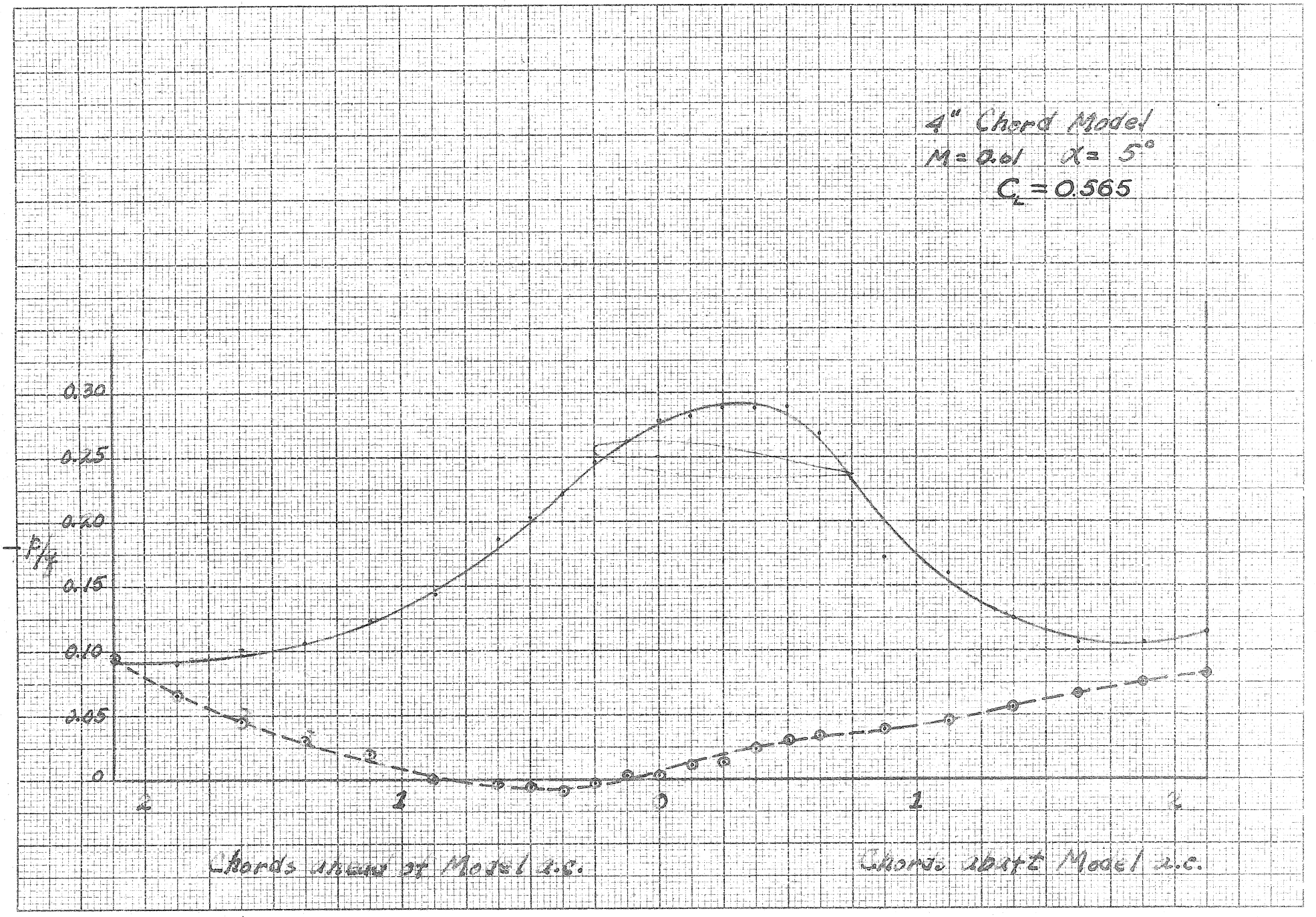
4" Chord Model
M = 0.61 α = 5°
C_L = 0.565
0.30
0.25
0.20
$-F/T$
0.15
0.10
0.05
0
2
1
0
1
2
Chords inside of Model L.E.
Chords about Model L.E.

Fig 7.7

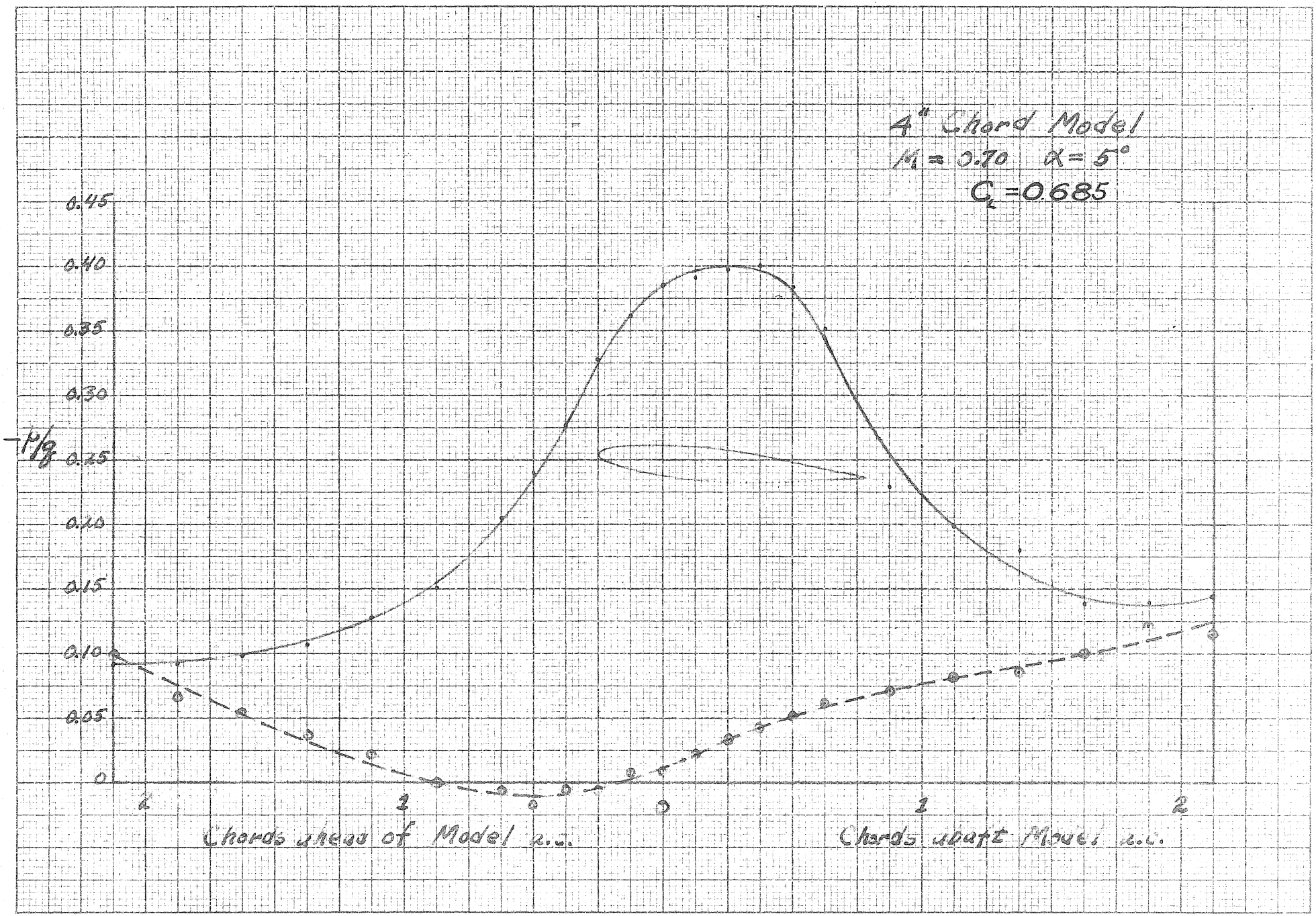
4" Chord Model
$M_1 = 0.70$ $\alpha = 5°$
$C_L = 0.685$
P/q
0.45
0.40
0.35
0.30
0.25
0.20
0.15
0.10
0.05
0
2
1
0
1
2
Chords ahead of Model L.E.
Chords aft of Model L.E.

Fig 74

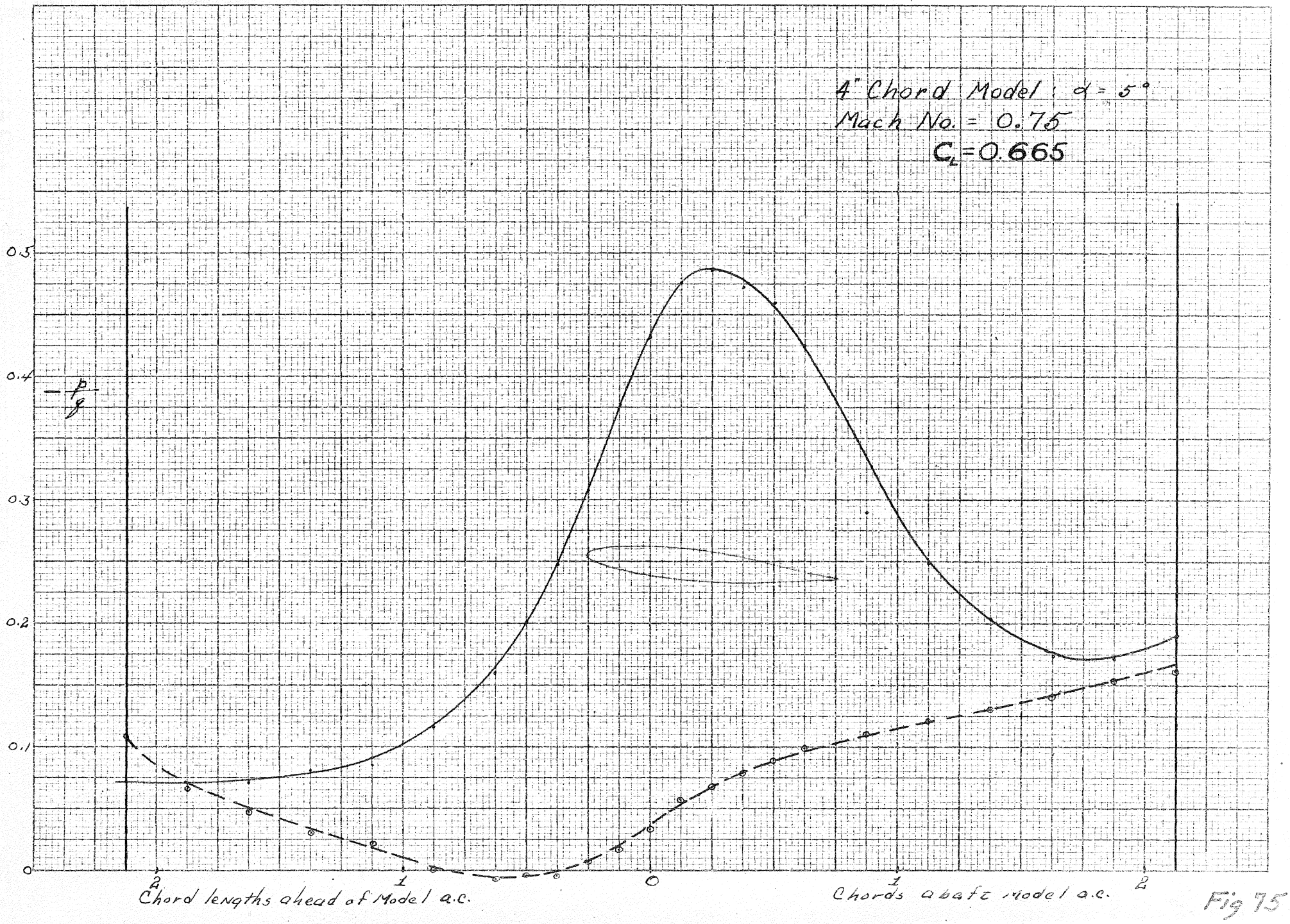
4" Chord Model : α = 5°
Mach No. = 0.75
C_L = 0.665
0.5
0.4
0.3
0.2
0.1
0
$-\frac{p}{q}$
2
1
0
1
2
Chord lengths ahead of Model a.c.
Chords abaft Model a.c.

Fig 75

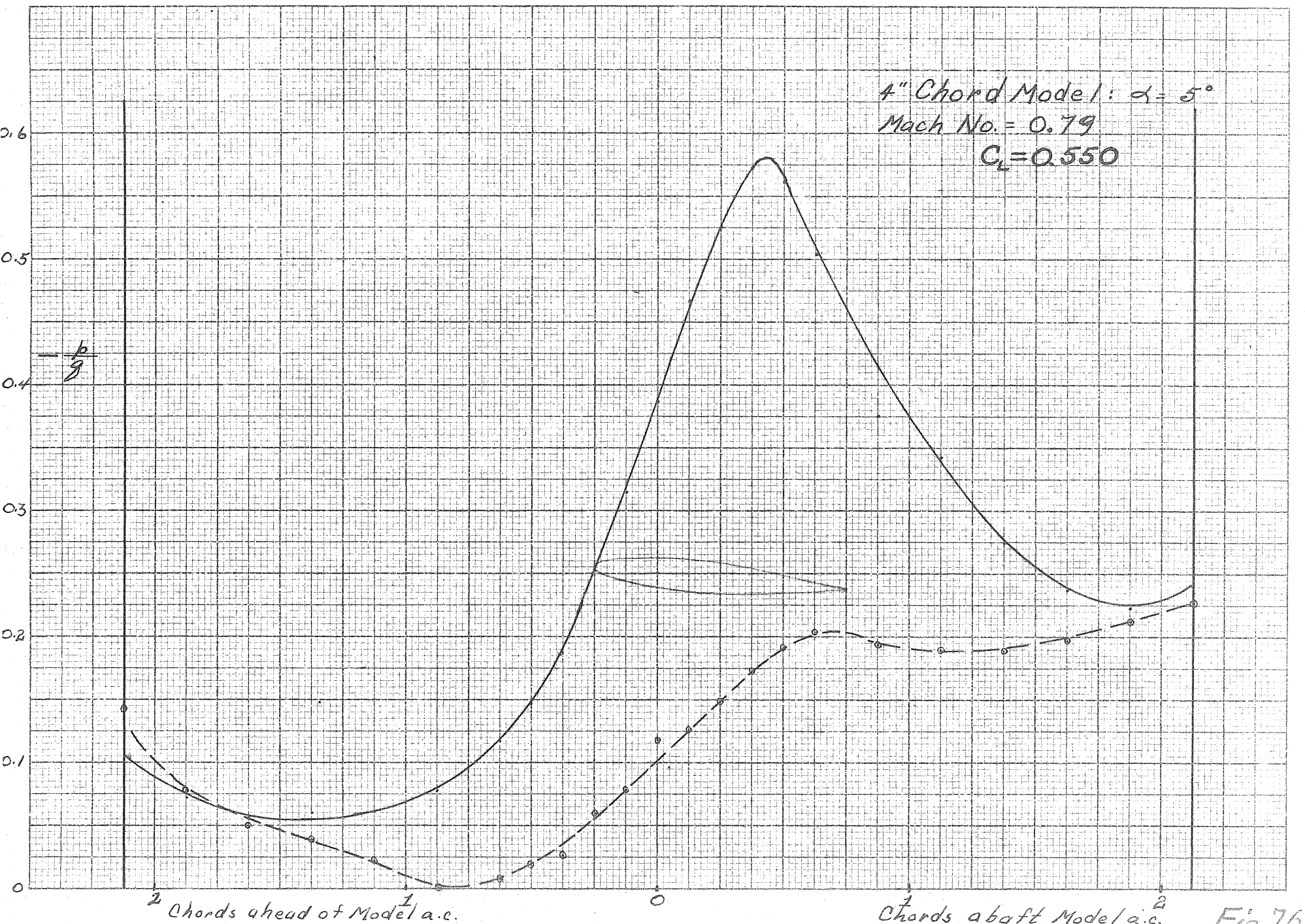
4" Chord Model : α = 5°
Mach No. = 0.79
C_L = 0.550
$-\frac{p}{q}$
0.6
0.5
0.4
0.3
0.2
0.1
0
2
1
0
1
2
Chords ahead of Model a.c.
Chords abaft Model a.c.

Fig 76

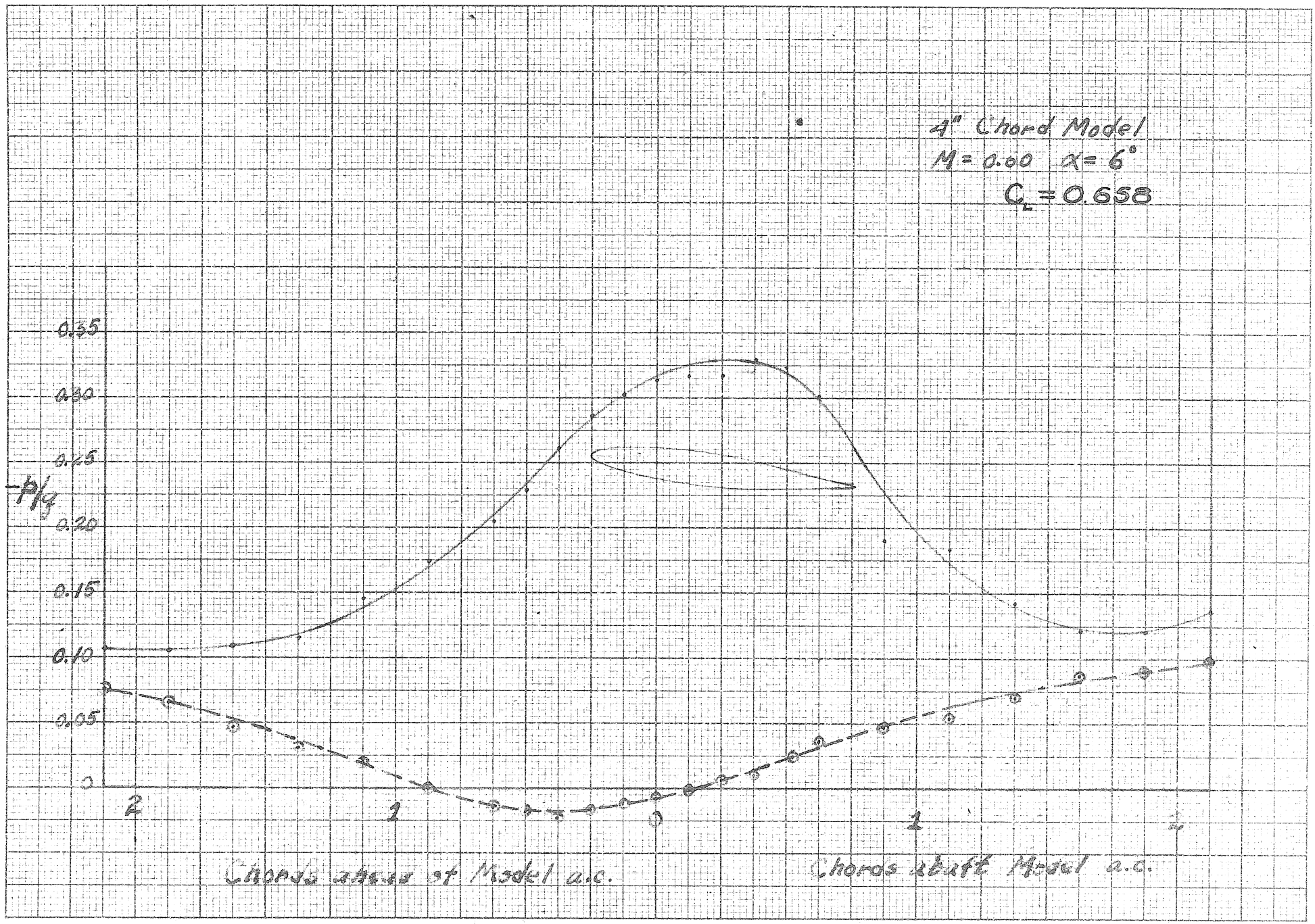
4" Chord Model
M = 0.00 α = 6°
C_L = 0.658
0.35
0.30
0.25
-p/q
0.20
0.15
0.10
0.05
0
2
1
0
1
2
Chords aft of Model a.c.
Chords abaft Model a.c.

Fig 77

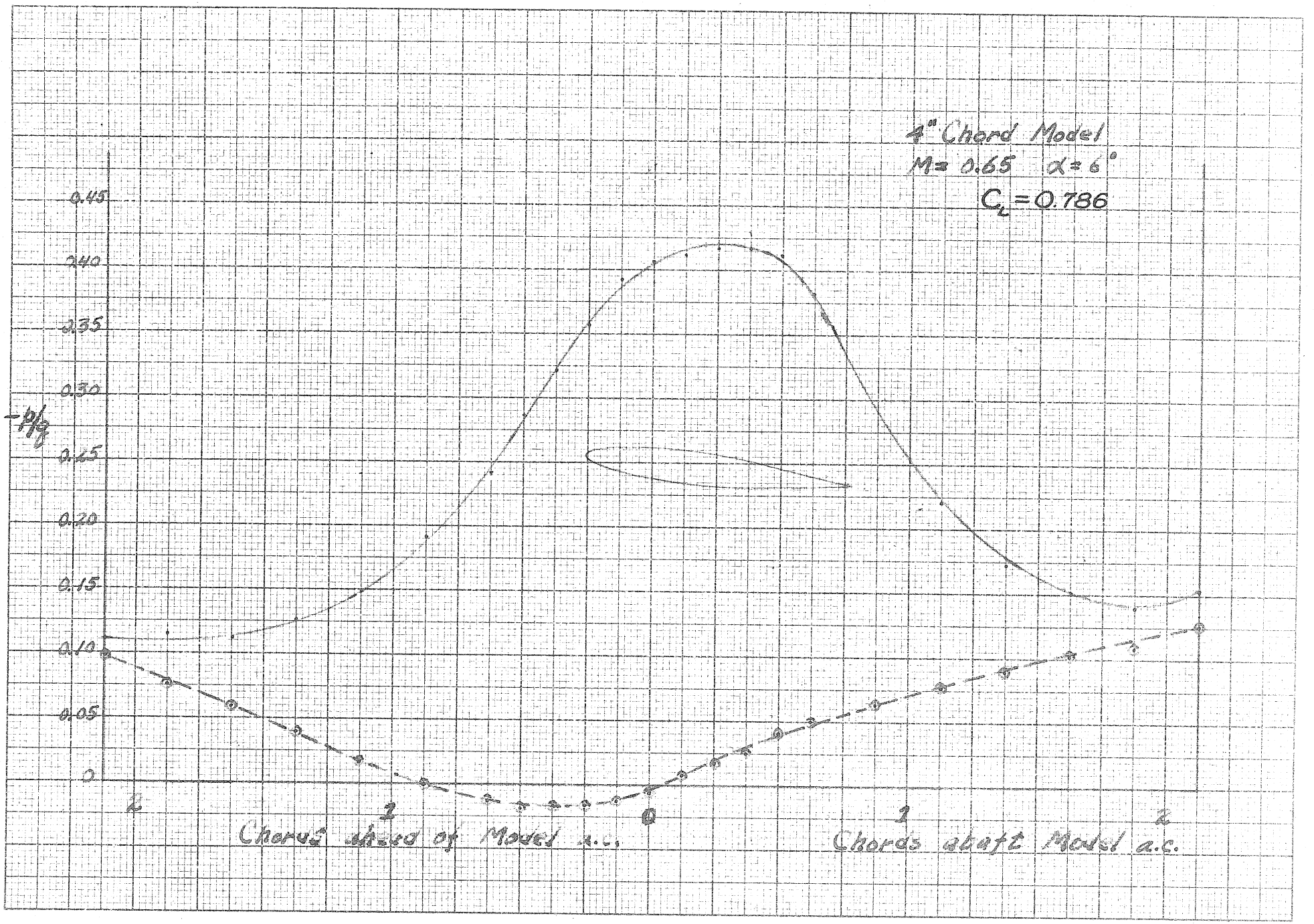
4" Chord Model
M = 0.65 α = 6°
C_L = 0.786
0.45
0.40
0.35
0.30
0.25
0.20
0.15
0.10
0.05
0
$-p/q$
2
1
0
1
2
Chords ahead of Model a.c.
Chords aft of Model a.c.

Fig 78

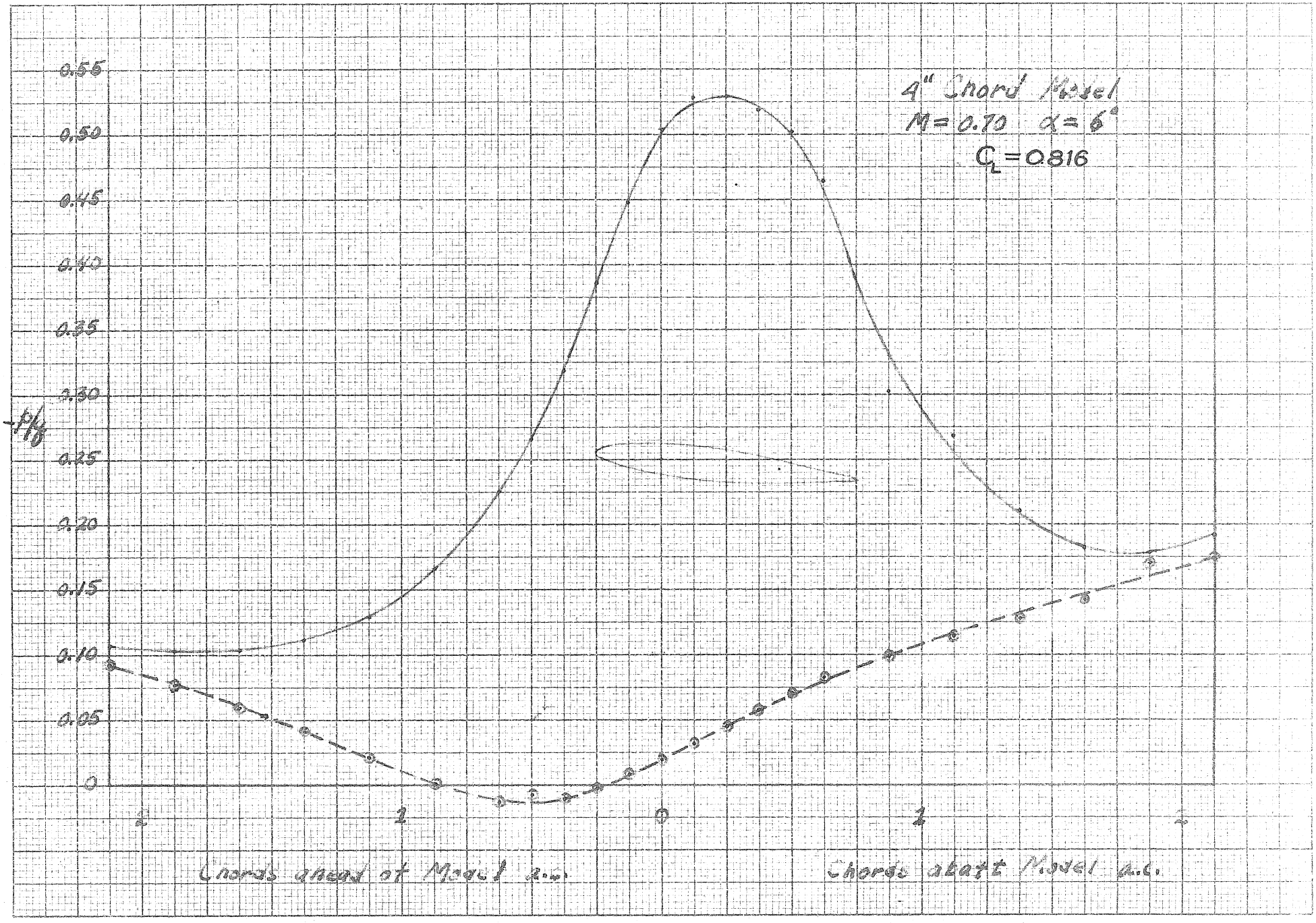
4" Chord Model
M = 0.70 α = 6°
C_L = 0.816
-p/q
0.55
0.50
0.45
0.40
0.35
0.30
0.25
0.20
0.15
0.10
0.05
0
2
1
0
1
2
Chords ahead of Model L.E.
Chords aft of Model L.E.

Fig 79

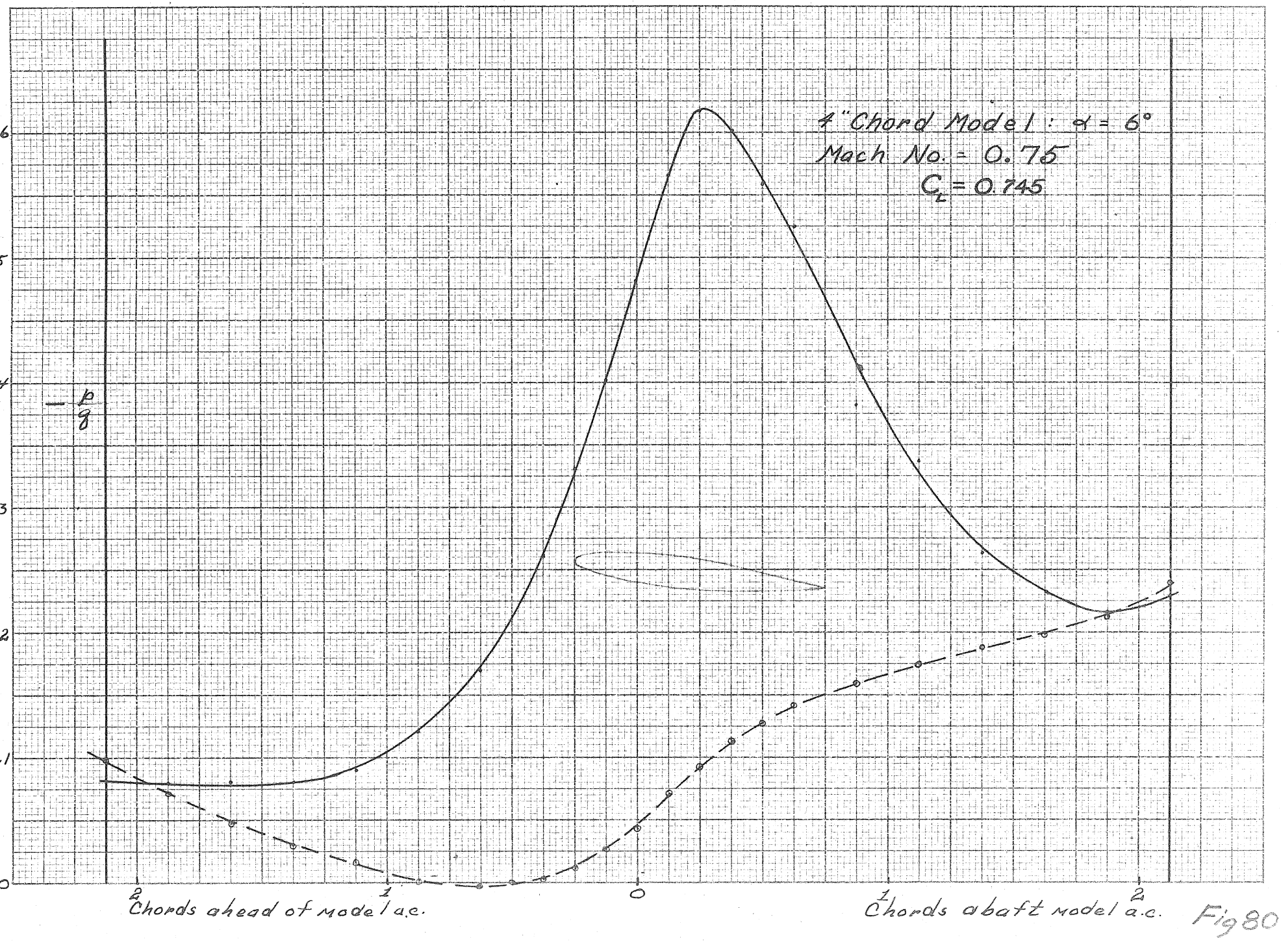
1" Chord Model : α = 6°
Mach No. = 0.75
C_L = 0.745
$-\frac{p}{q}$
6
5
4
3
2
1
0
2
1
0
1
2
Chords ahead of model a.c.
Chords abaft model a.c.

Fig 80

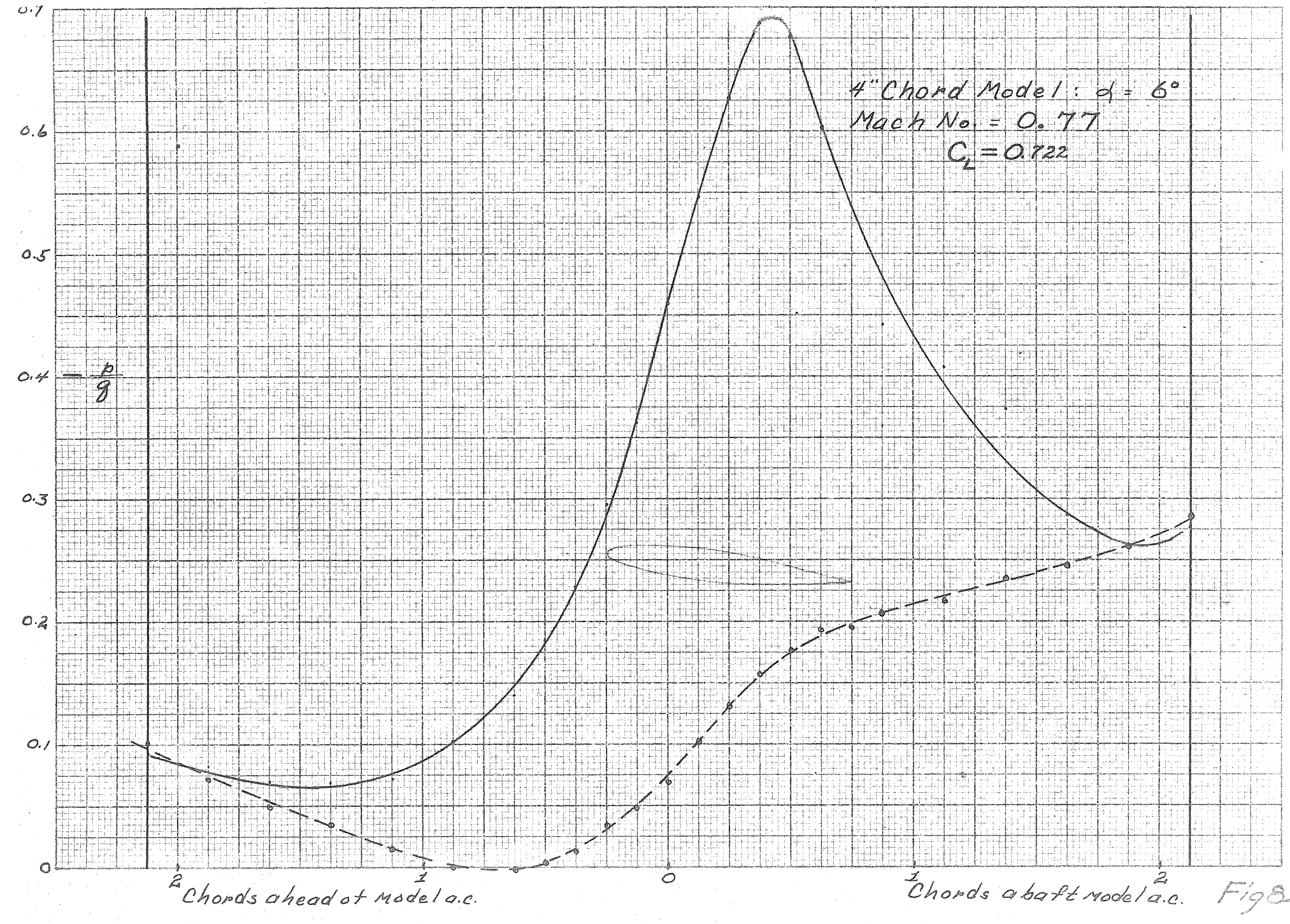
4" Chord Model : α = 6°
Mach No. = 0.77
C_L = 0.722
$-\frac{p}{q}$
0.7
0.6
0.5
0.4
0.3
0.2
0.1
0
2
1
0
1
2
Chords ahead of model a.c.
Chords abaft model a.c.

Fig 8x

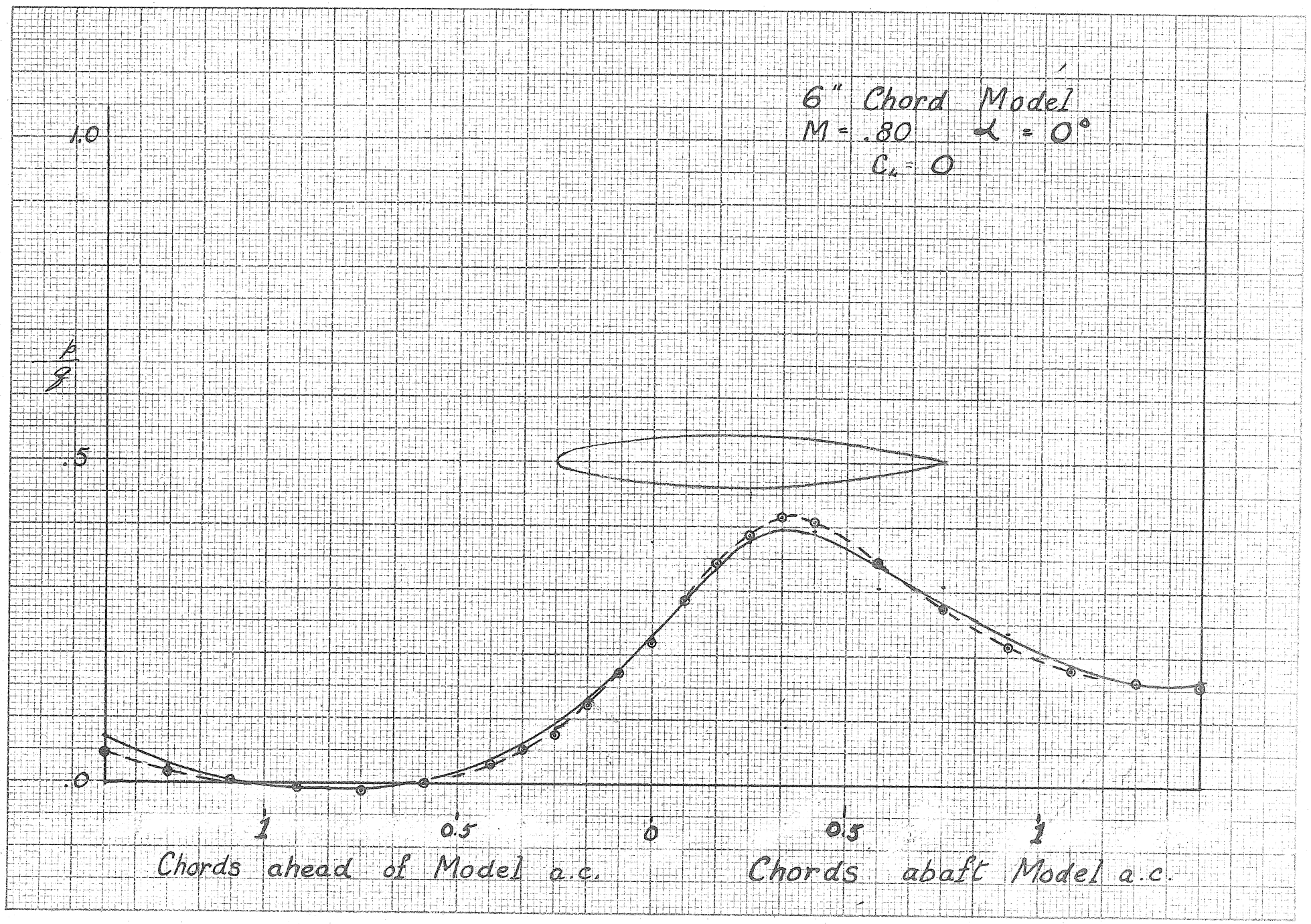
6" Chord Model
M = .80 α = 0°
C_L = 0
1.0
p/q
.5
.0
1
0.5
0
0.5
1
Chords ahead of Model a.c.
Chords abaft Model a.c.

Fig 82

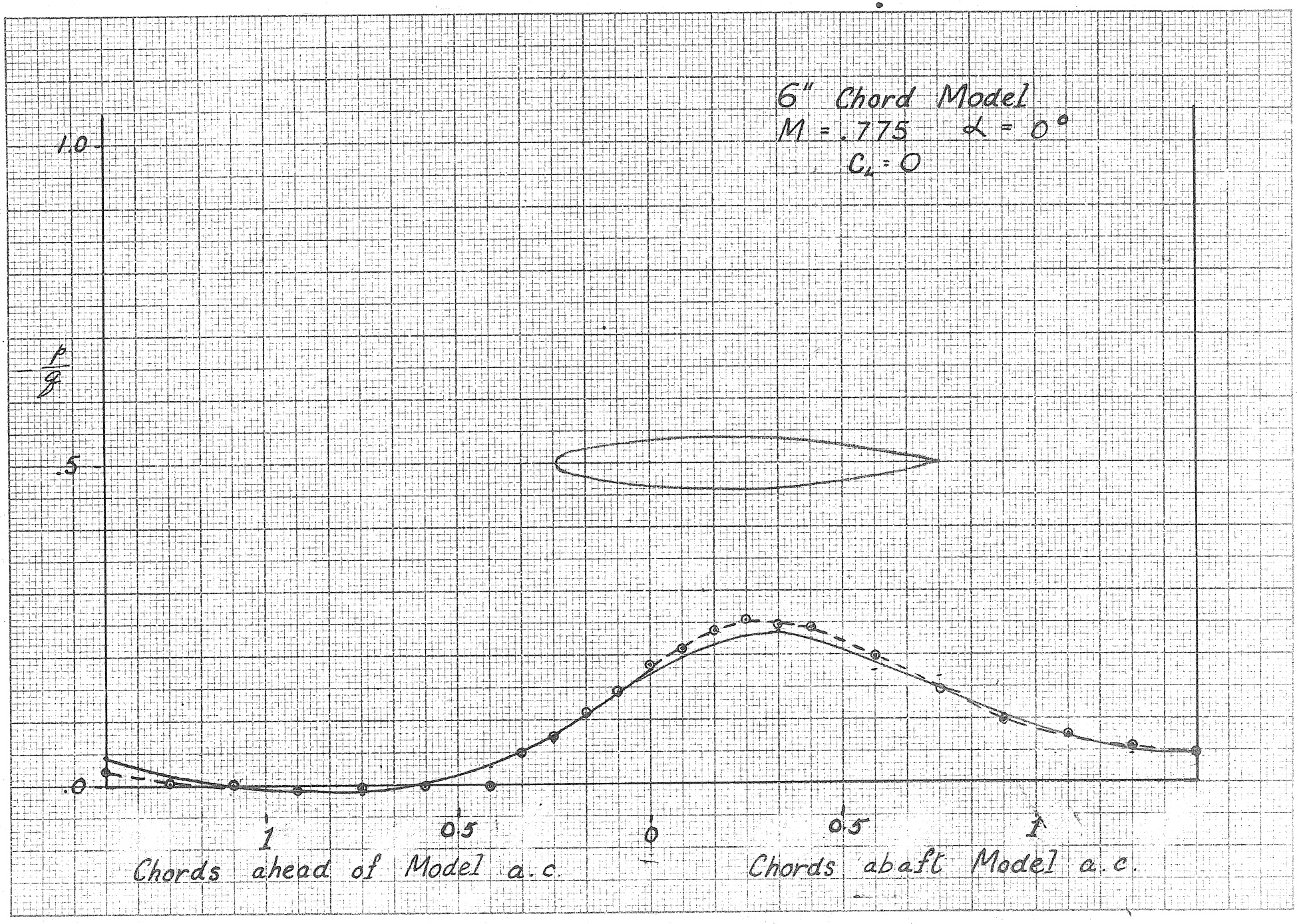
6" Chord Model
M = .775 α = 0°
C_L = 0
1.0
$\frac{p}{q}$
.5
.0
1
0.5
0
0.5
1
Chords ahead of Model a.c.
Chords abaft Model a.c.

Fig. 83

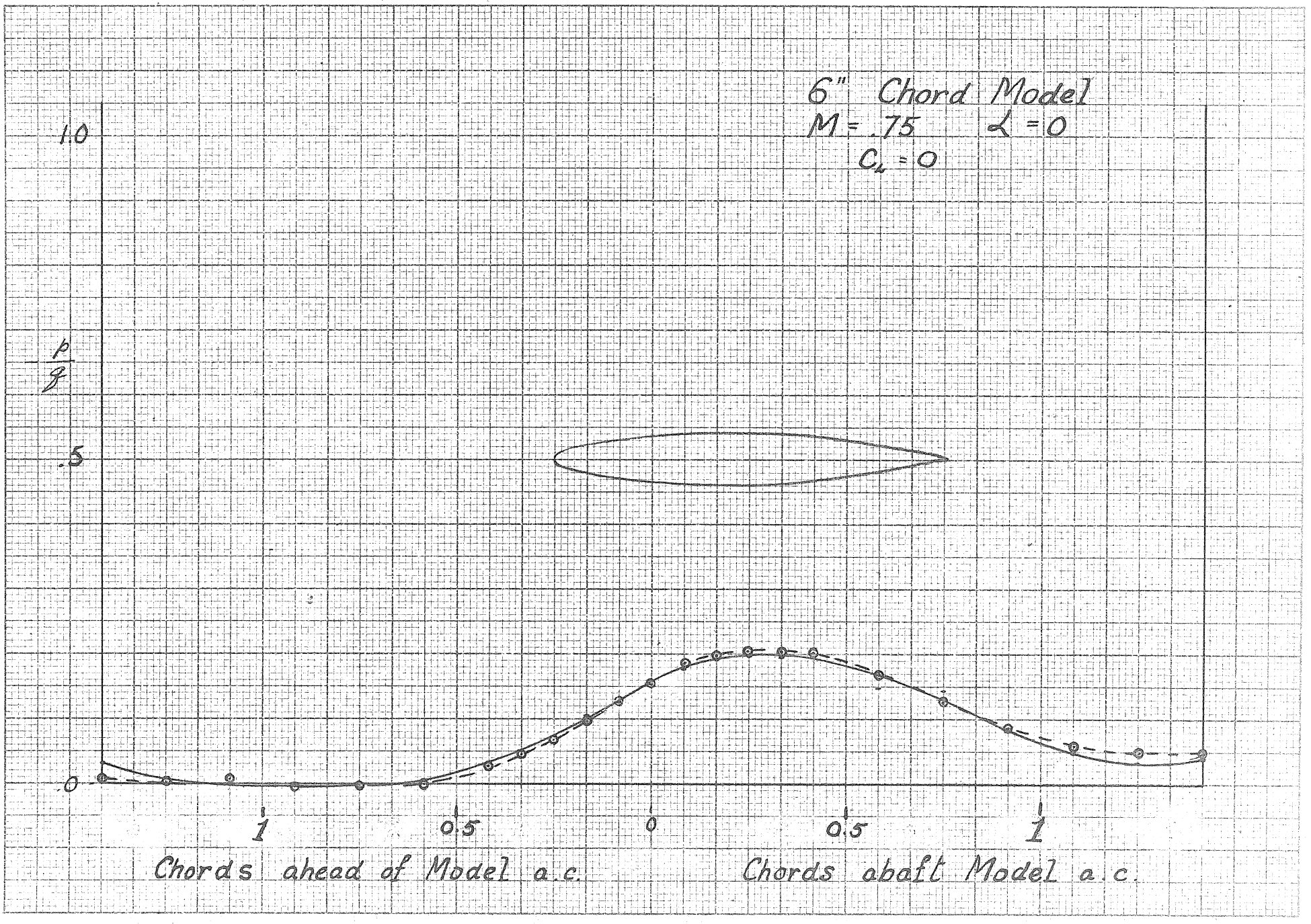
6" Chord Model
M = .75 α = 0
C_L = 0
1.0
$\frac{p}{q}$
.5
0
1
0.5
0
0.5
1
Chords ahead of Model a.c.
Chords abaft Model a.c.

Fig. 84

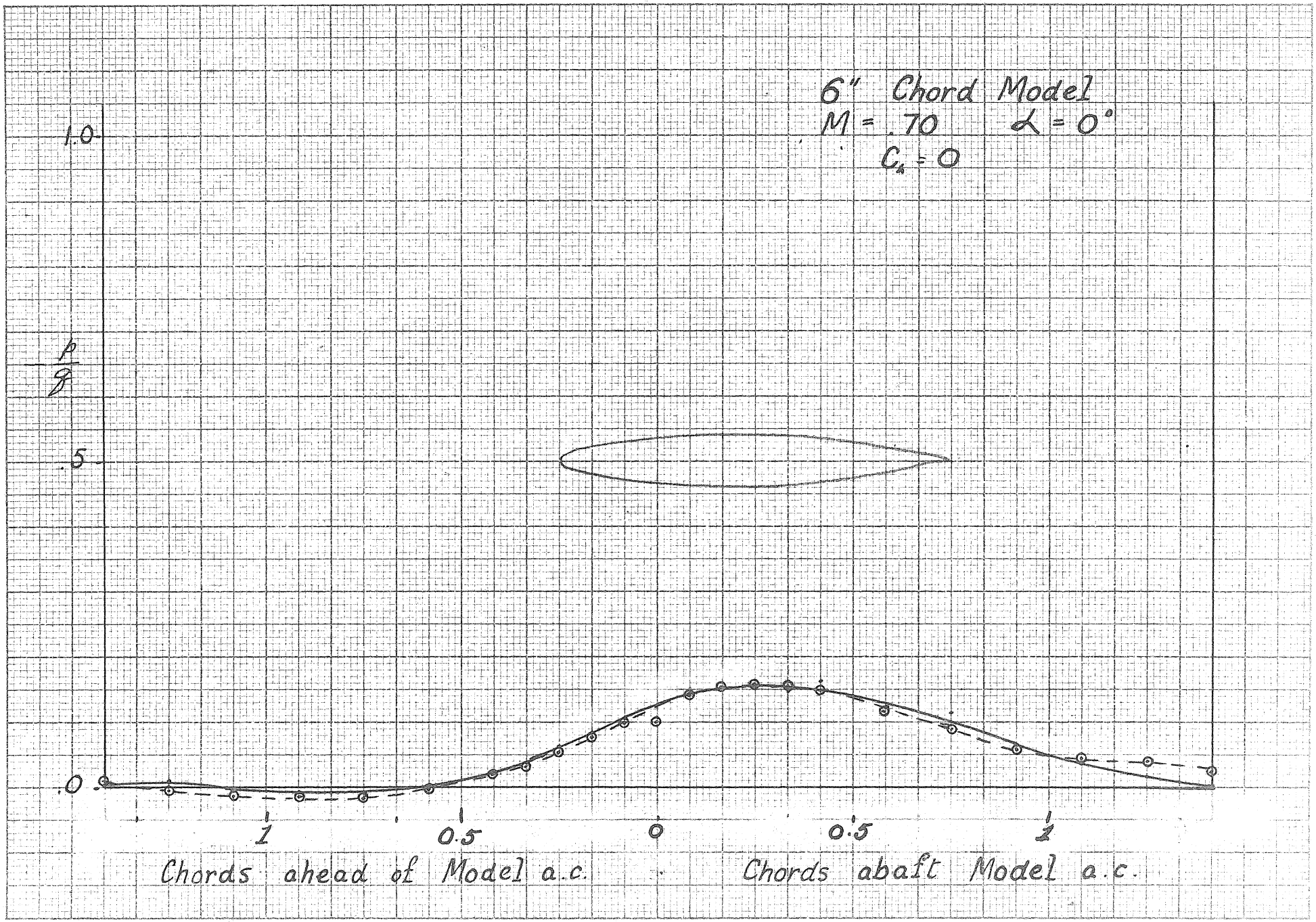
6" Chord Model
M = .70 α = 0°
C_L = 0
1.0
$\frac{p}{q}$
.5
.0
1
0.5
0
0.5
1
Chords ahead of Model a.c.
Chords abaft Model a.c.

Fig 85

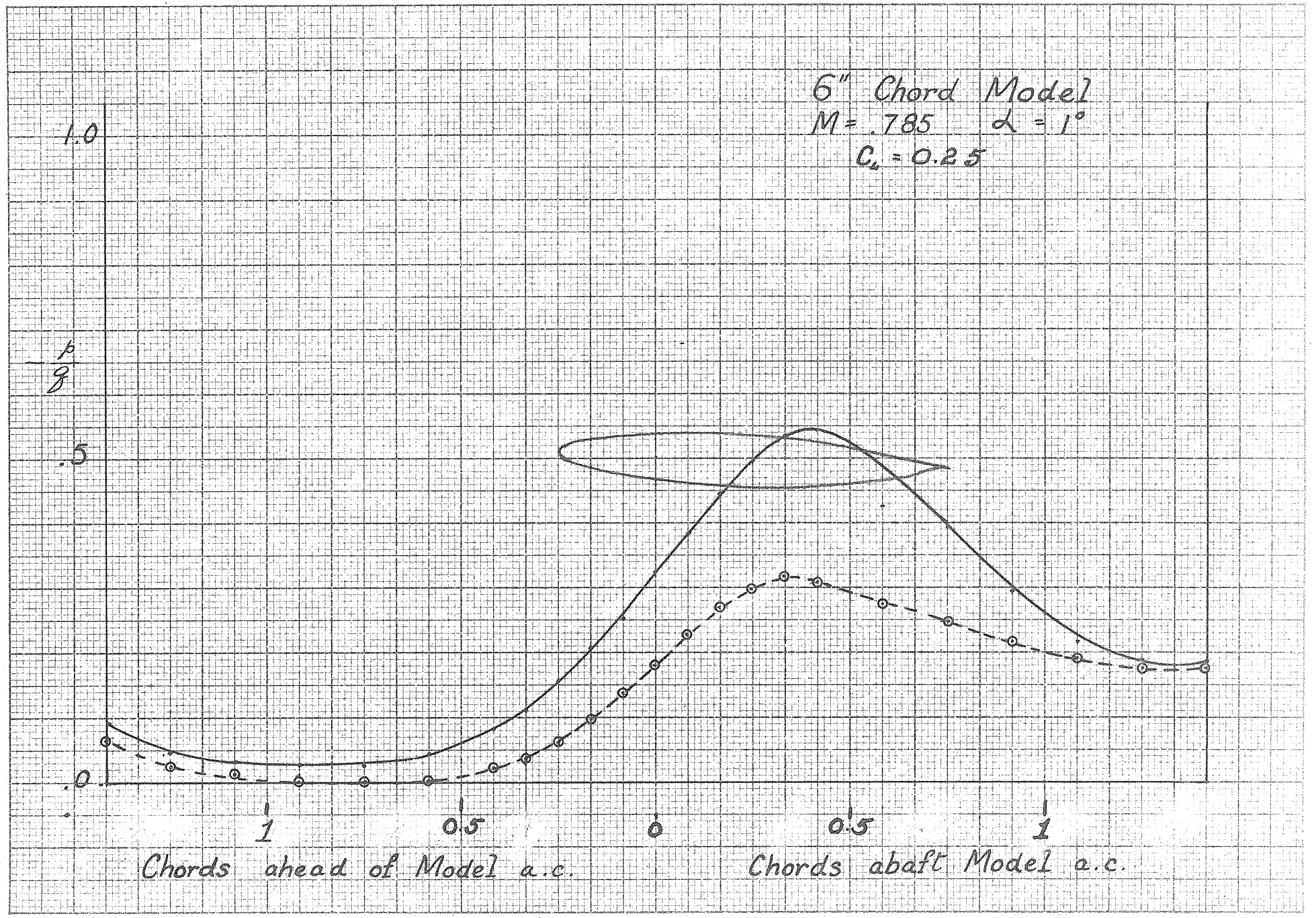
6" Chord Model
M = .785 α = 1°
C_{L_a} = 0.25
1.0
$\frac{p}{q}$
.5
0
1
0.5
0
0.5
1
Chords ahead of Model a.c.
Chords abaft Model a.c.

Fig. 86

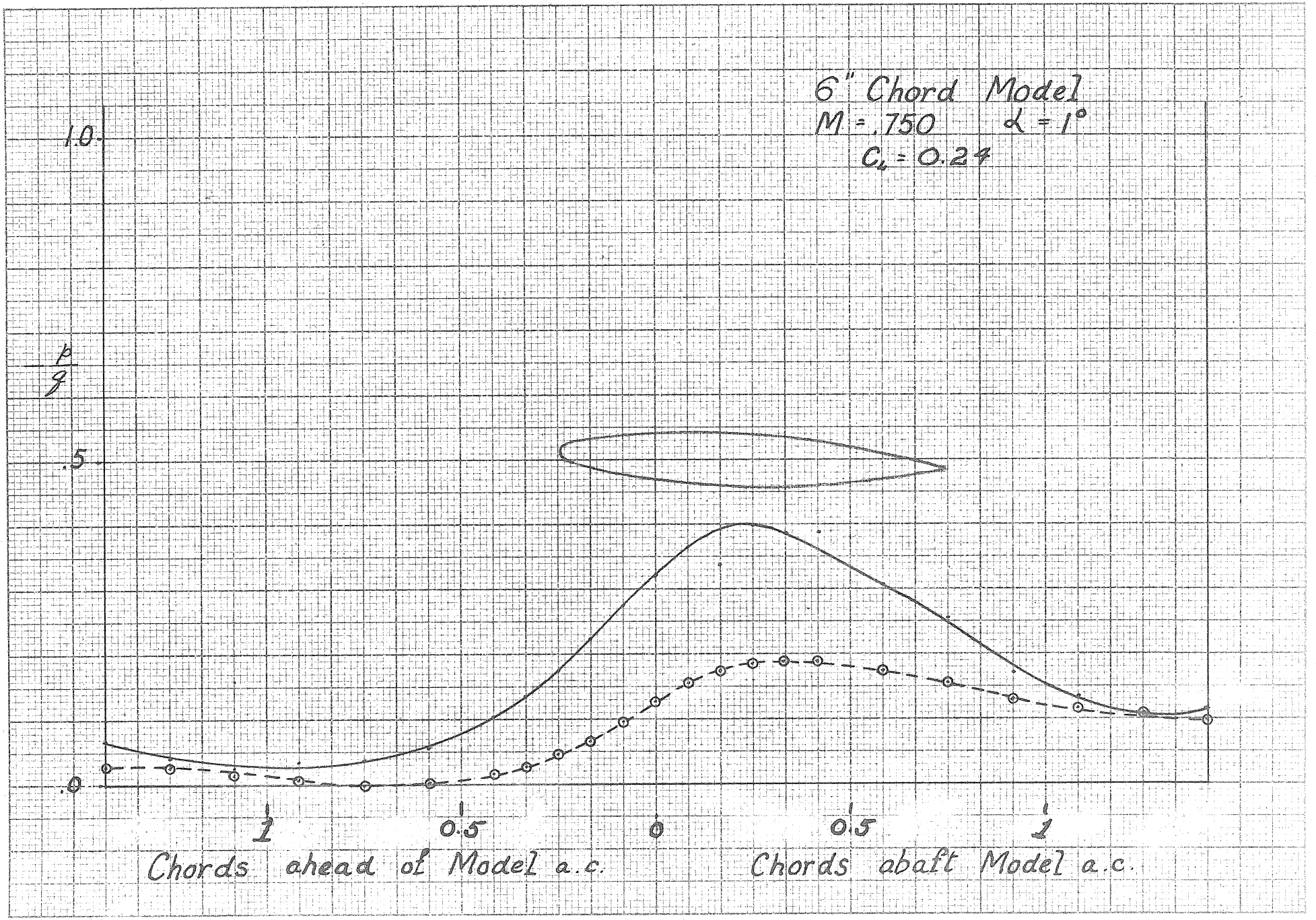
6" Chord Model
M = .750 α = 1°
C_L = 0.24
1.0
p/q
.5
.0
1
0.5
0
0.5
1
Chords ahead of Model a.c.
Chords abaft Model a.c.

Fig. 87

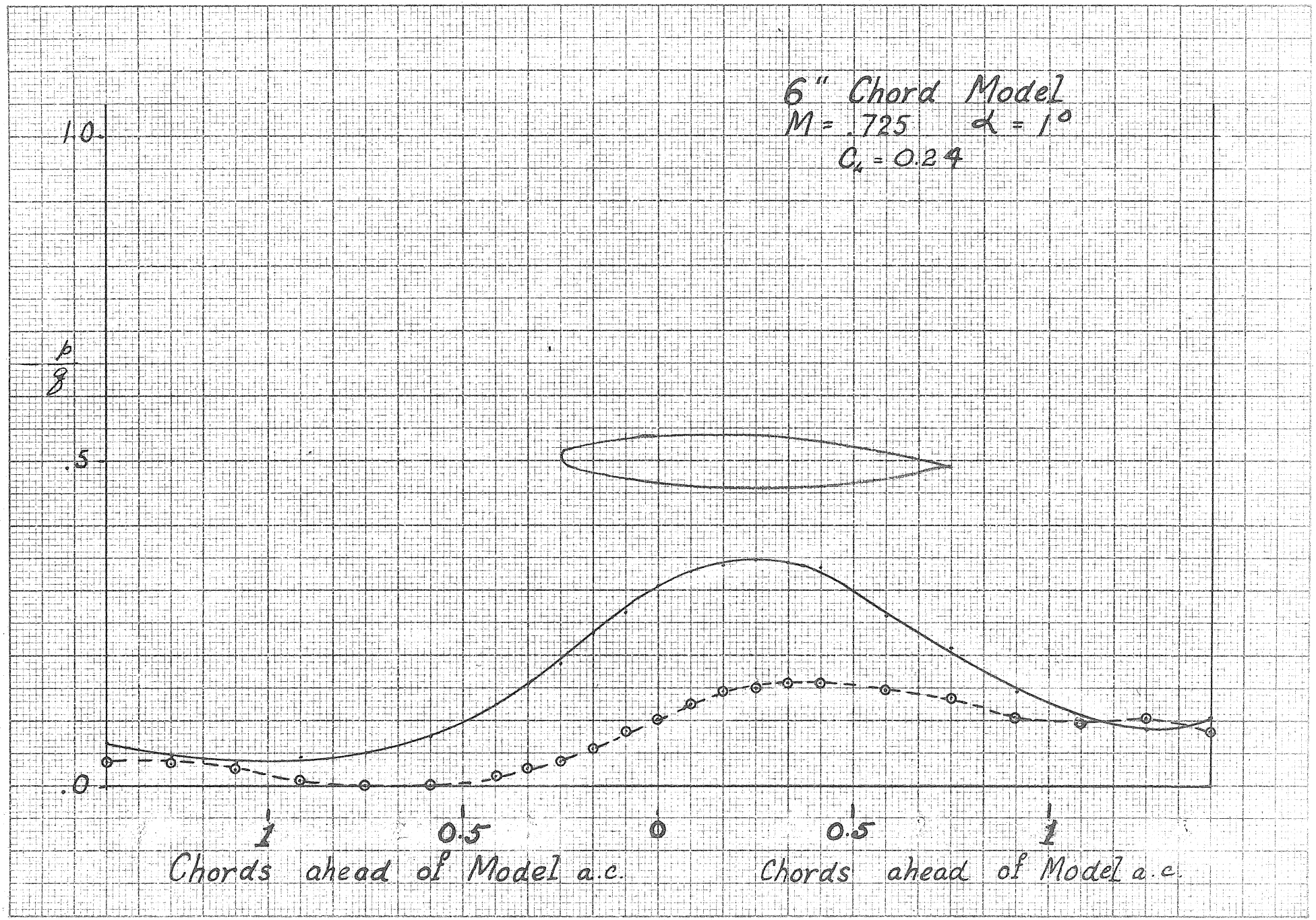
6" Chord Model
M = .725 α = 1°
C_L = 0.24
1.0
b/B
.5
.0
1
0.5
0
0.5
1
Chords ahead of Model a.c.
Chords ahead of Model a.c.

Fig. 88

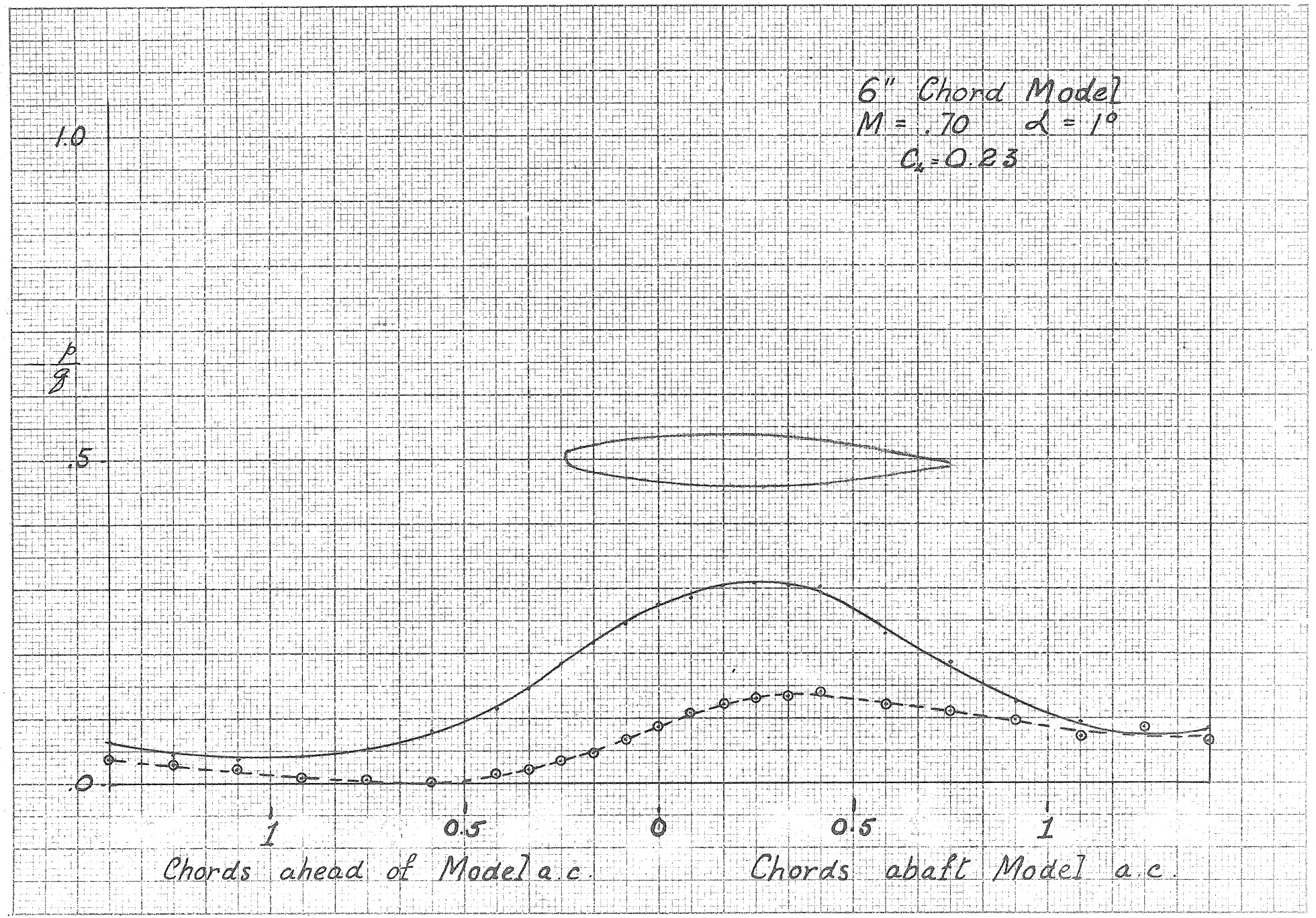
6" Chord Model
M = .70 α = 1°
C_L = 0.23
1.0
$\frac{p}{q}$
.5
0
1
0.5
0
0.5
1
Chords ahead of Model a.c.
Chords abaft Model a.c.

Fig. 89

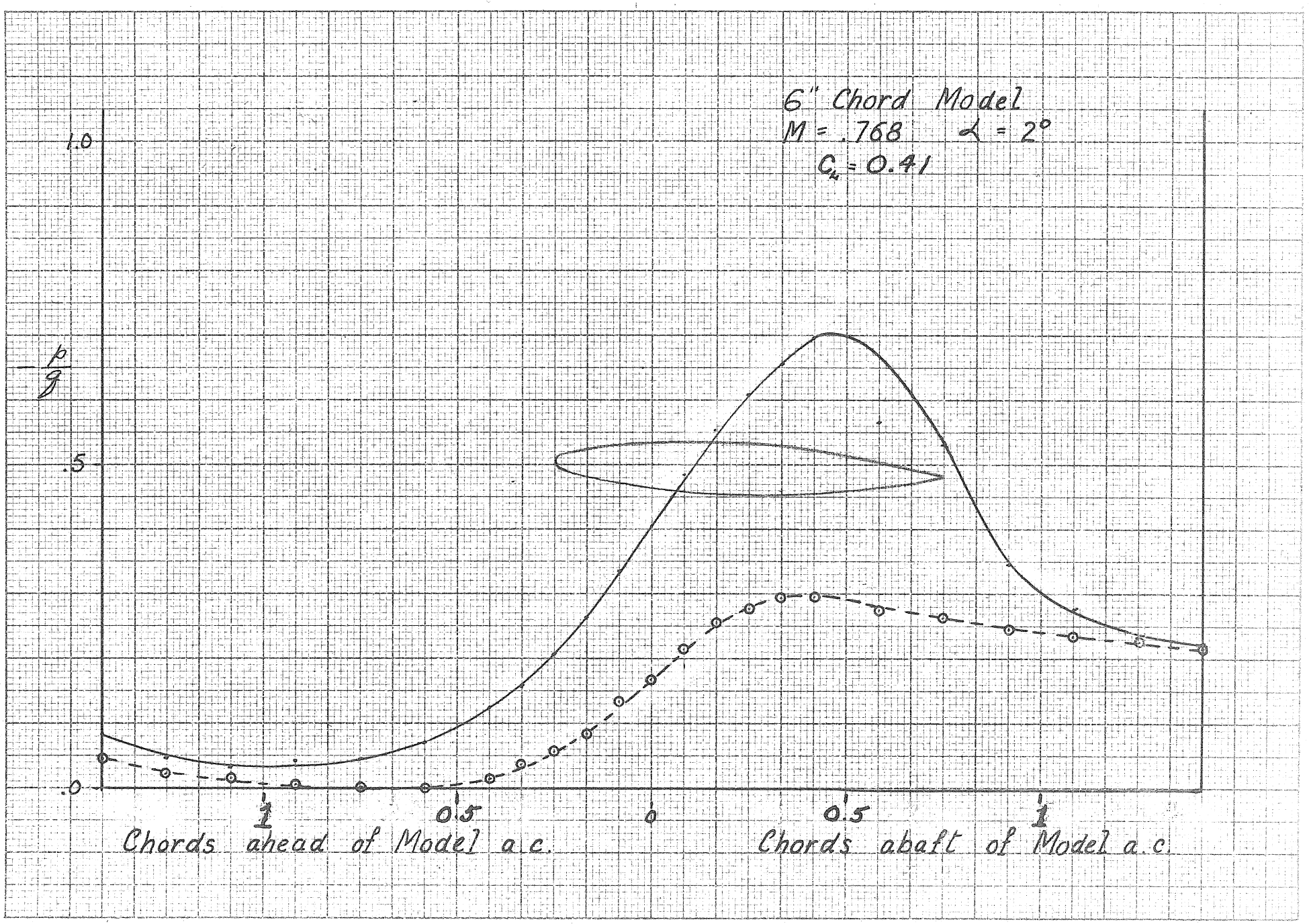
6" Chord Model
M = .768 α = 2°
C_L = 0.41
1.0
$-\frac{p}{q}$
.5
.0
1
0.5
0
0.5
1
Chords ahead of Model a.c.
Chords abaft of Model a.c.

Fig. 90

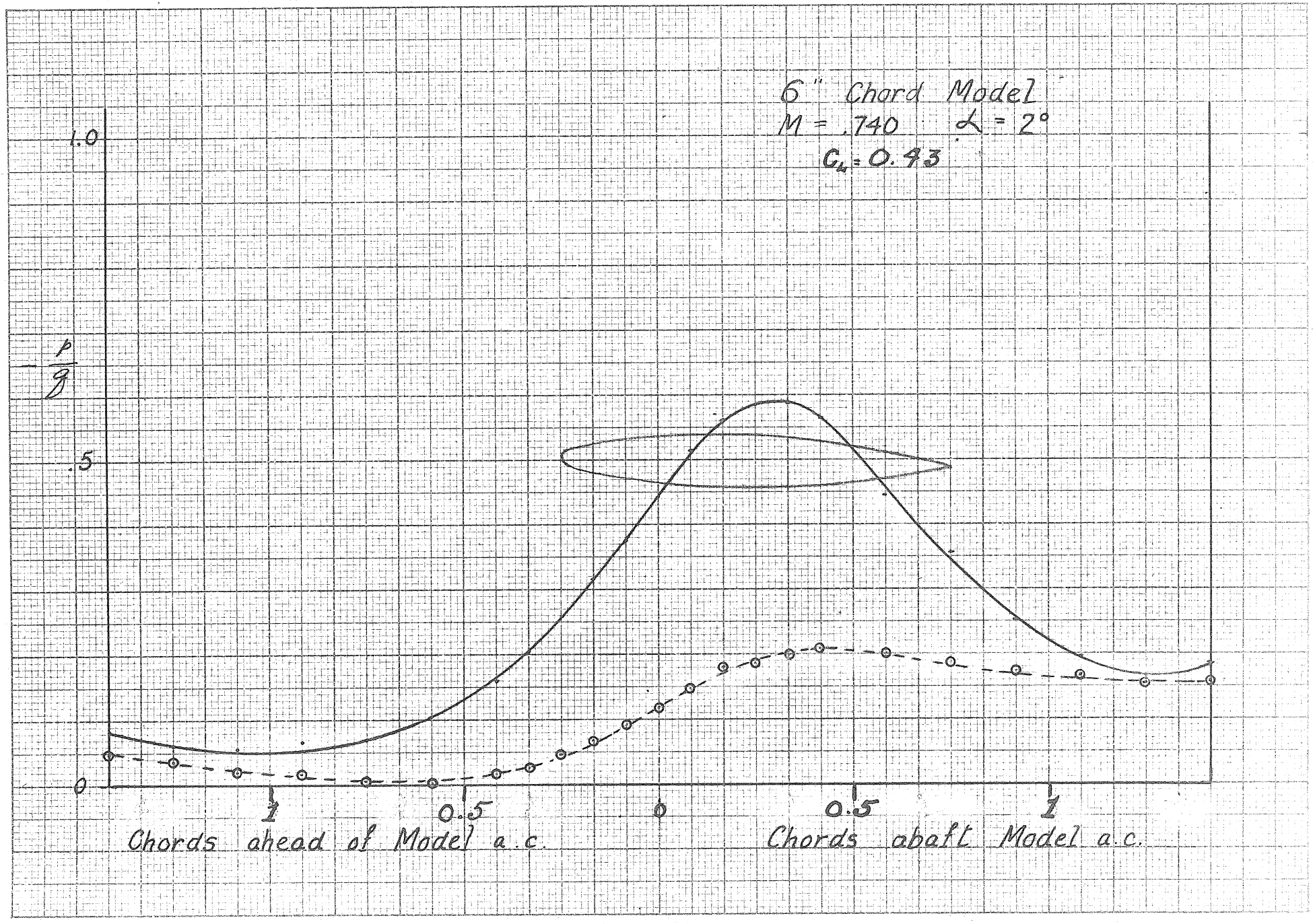
6" Chord Model
M = .740 α = 2°
C_L = 0.43
1.0
$-\frac{p}{q}$
.5
0
1
0.5
0
0.5
1
Chords ahead of Model a.c.
Chords abaft Model a.c.

Fig. 91

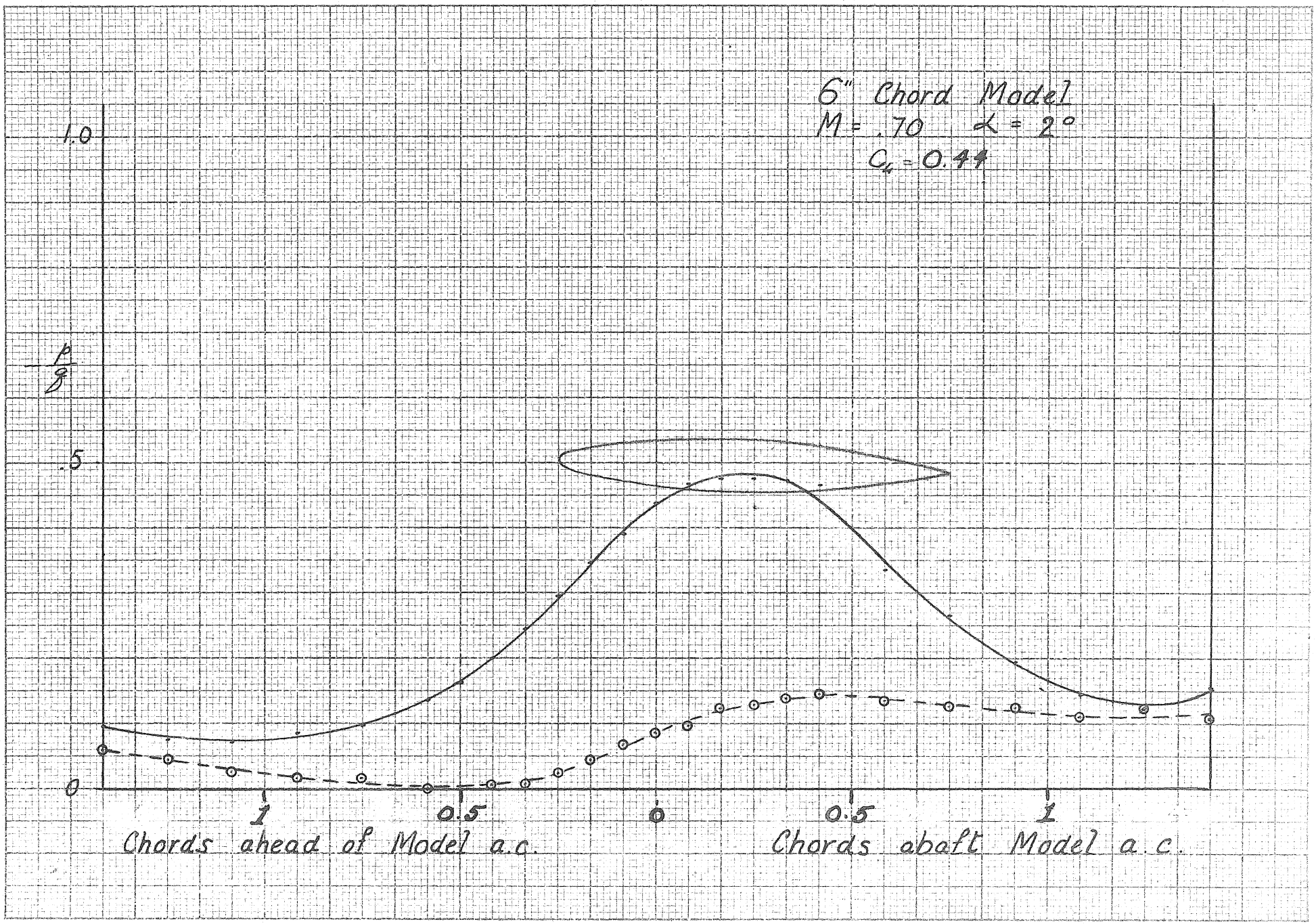
6" Chord Model
M = .70 α = 2°
C_L = 0.44
1.0
$-\frac{p}{q}$
.5
0
1
0.5
0
0.5
1
Chords ahead of Model a.c.
Chords abaft Model a.c.

Fig. 92

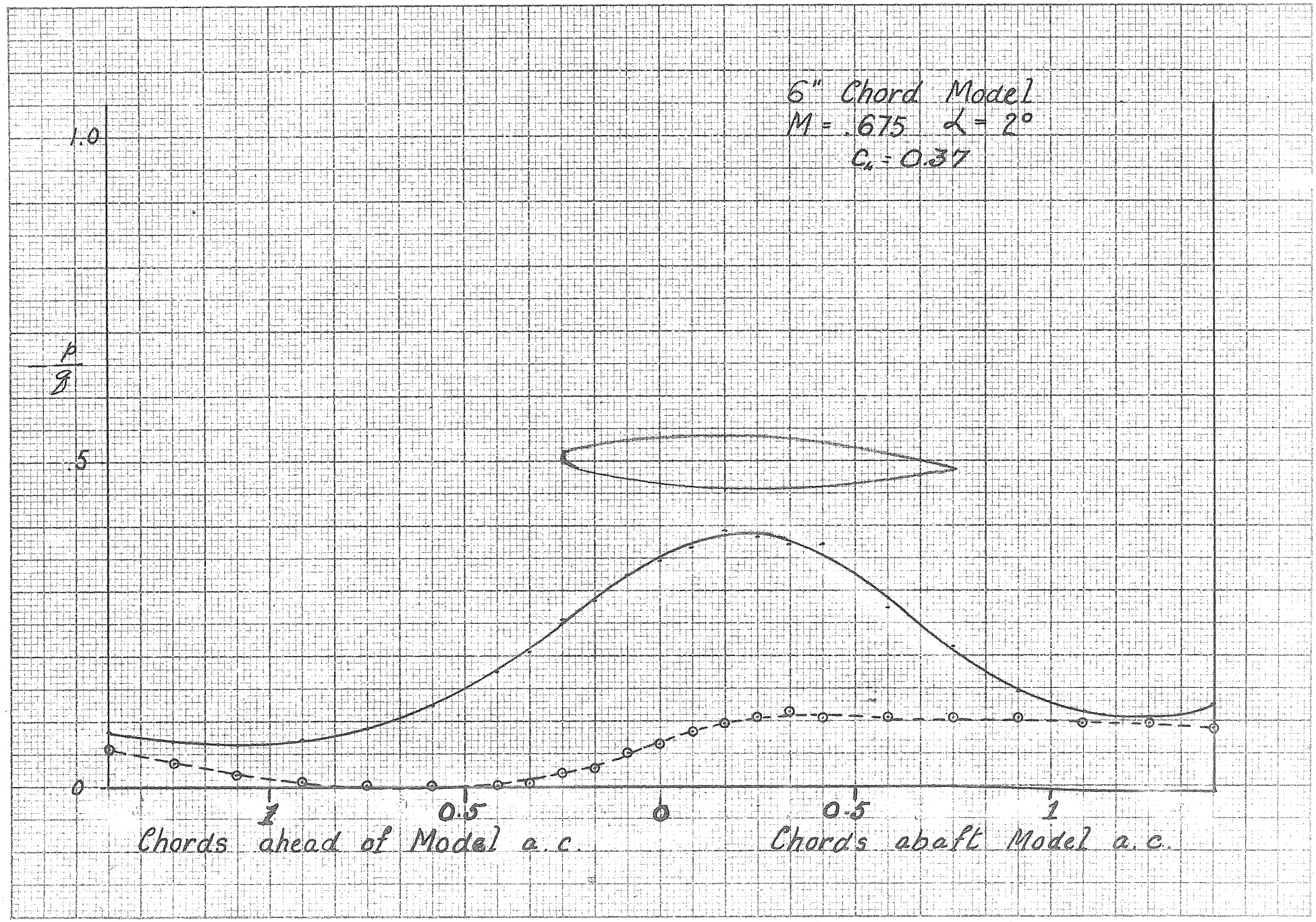
6" Chord Model
M = .675 α = 2°
C_L = 0.37
1.0
p/q
.5
0
1
0.5
0
0.5
1
Chords ahead of Model a.c.
Chords abaft Model a.c.

Fig. 93

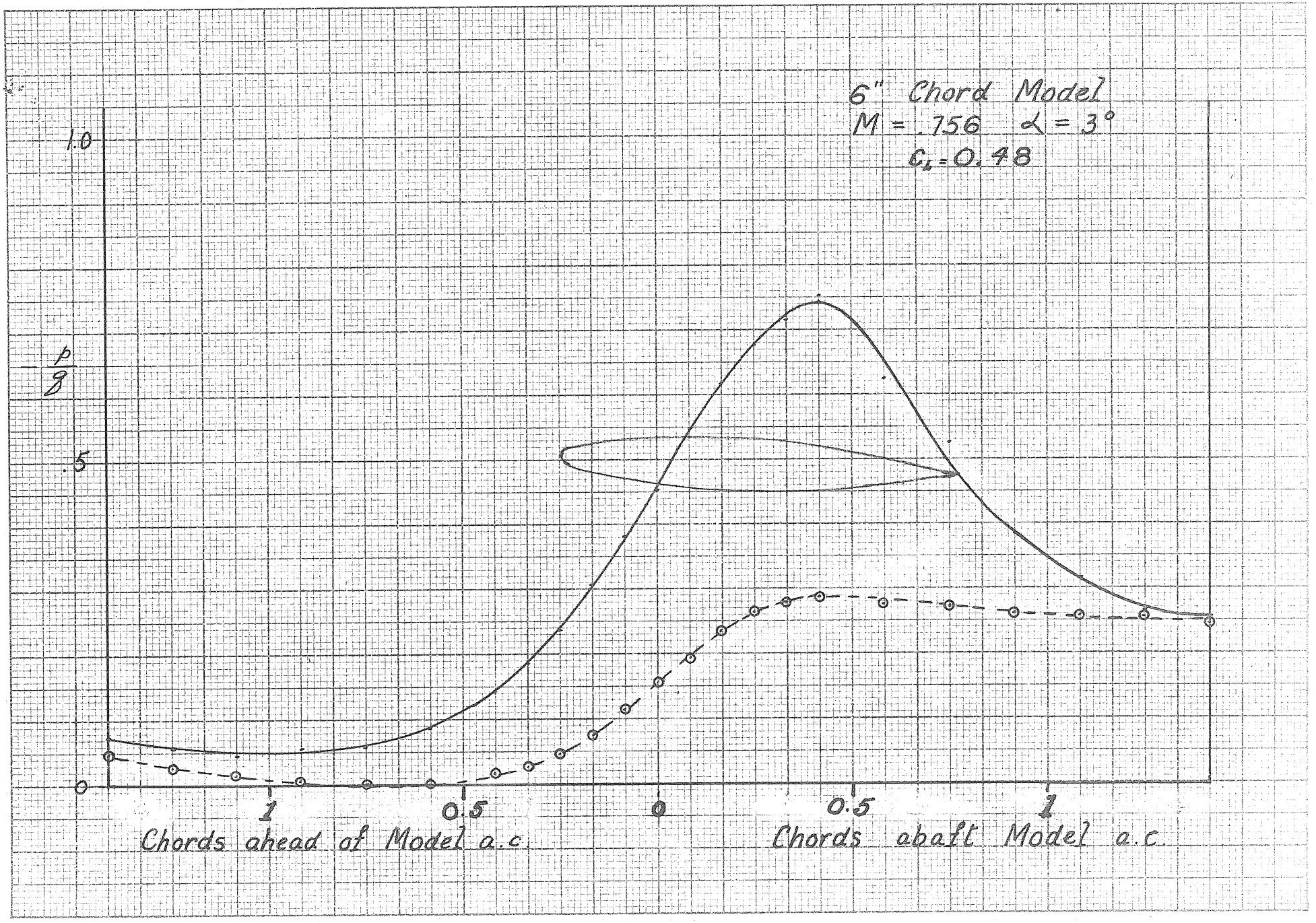
6" Chord Model
M = .756 α = 3°
c_l = 0.48
1.0
$-\frac{p}{q}$
.5
0
1
0.5
0
0.5
1
Chords ahead of Model a.c.
Chords abaft Model a.c.

Fig. 94

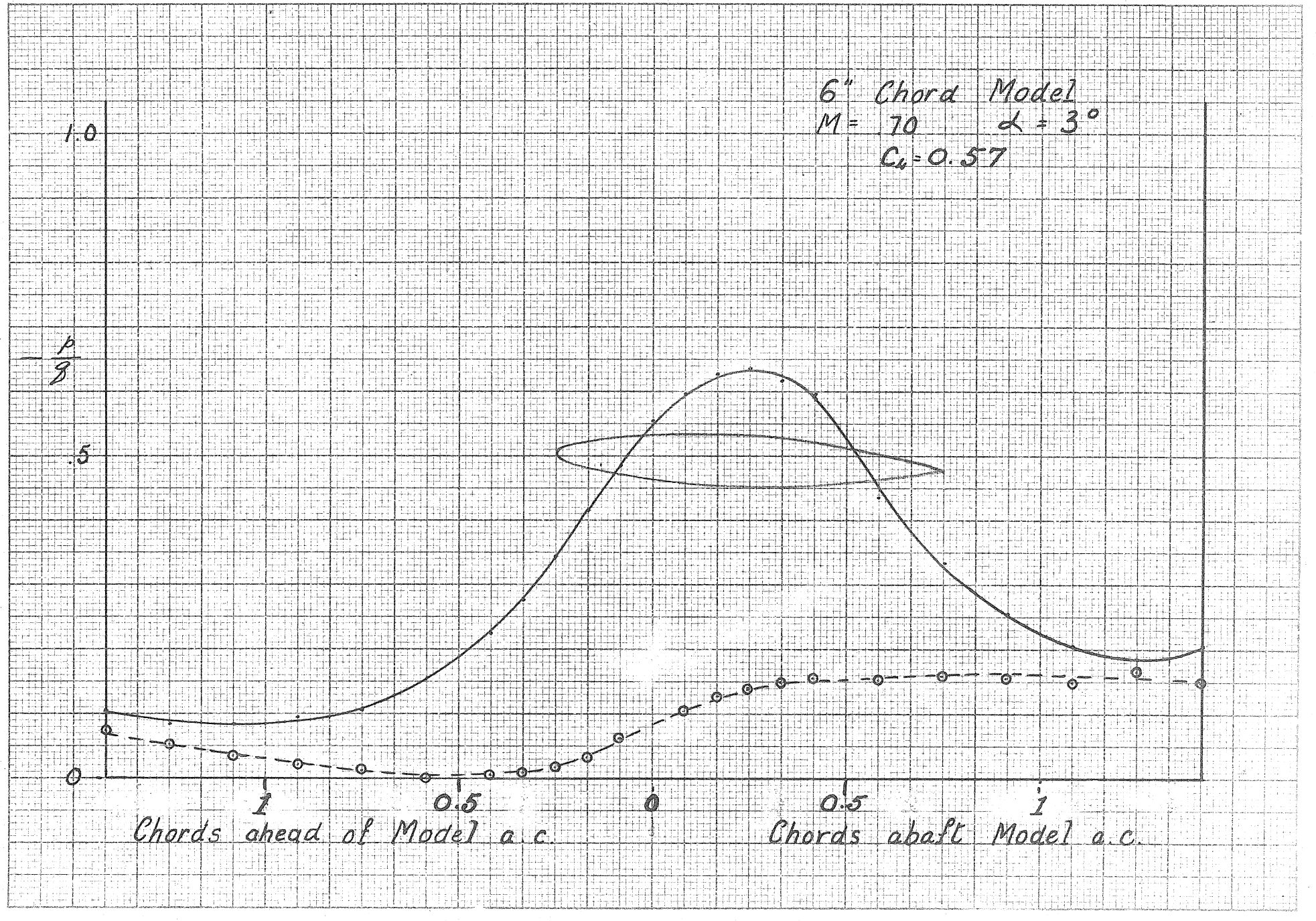
6" Chord Model
M = .70 α = 3°
C_L = 0.57
1.0
$-\frac{p}{q}$
.5
0
1
0.5
0
0.5
1
Chords ahead of Model a.c.
Chords abaft Model a.c.

Fig. 95

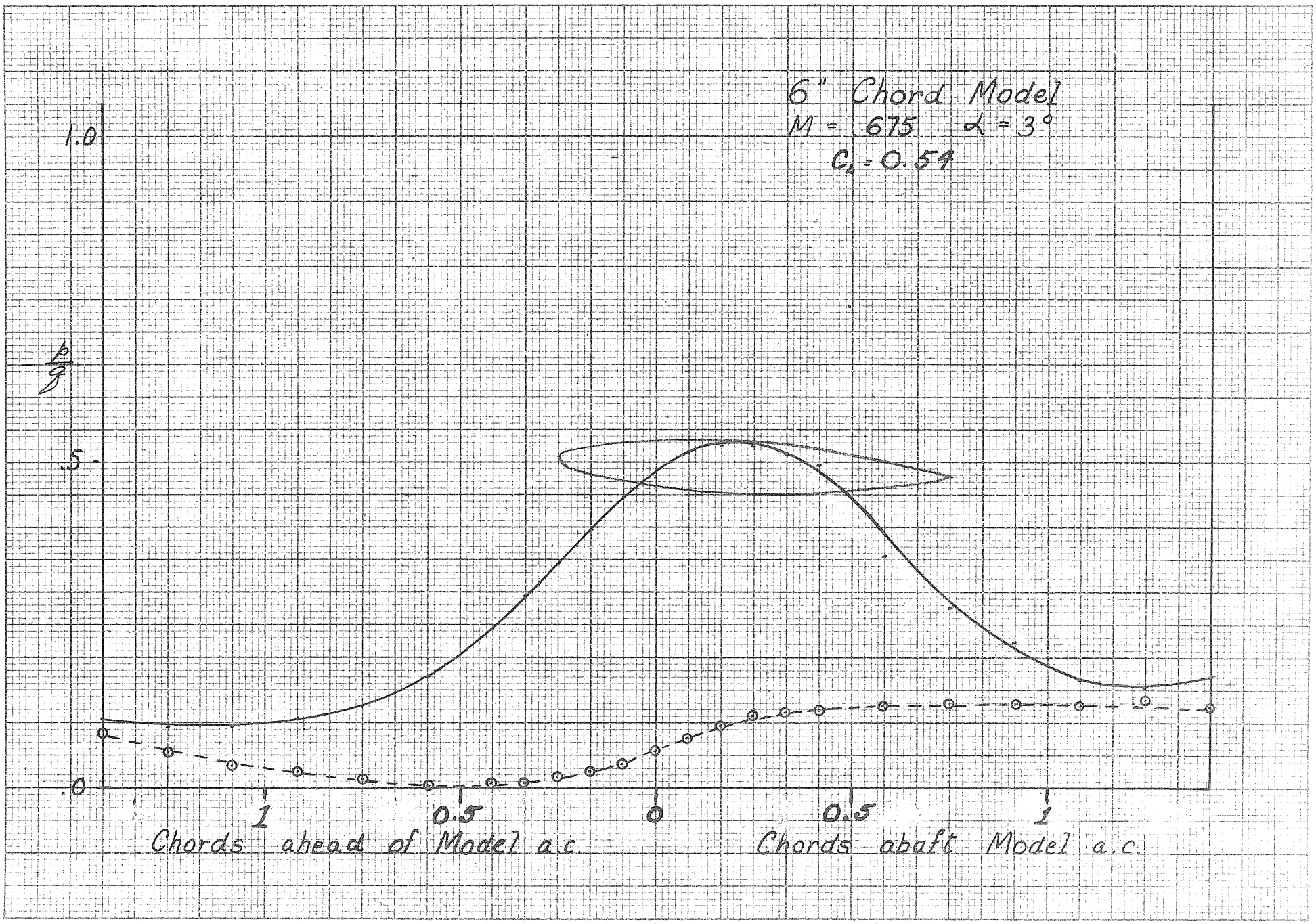
6" Chord Model
M = .675 α = 3°
C_L = 0.54
1.0
$\frac{p}{q}$
.5
0
1
0.5
0
0.5
1
Chords ahead of Model a.c.
Chords abaft Model a.c.

Fig. 96

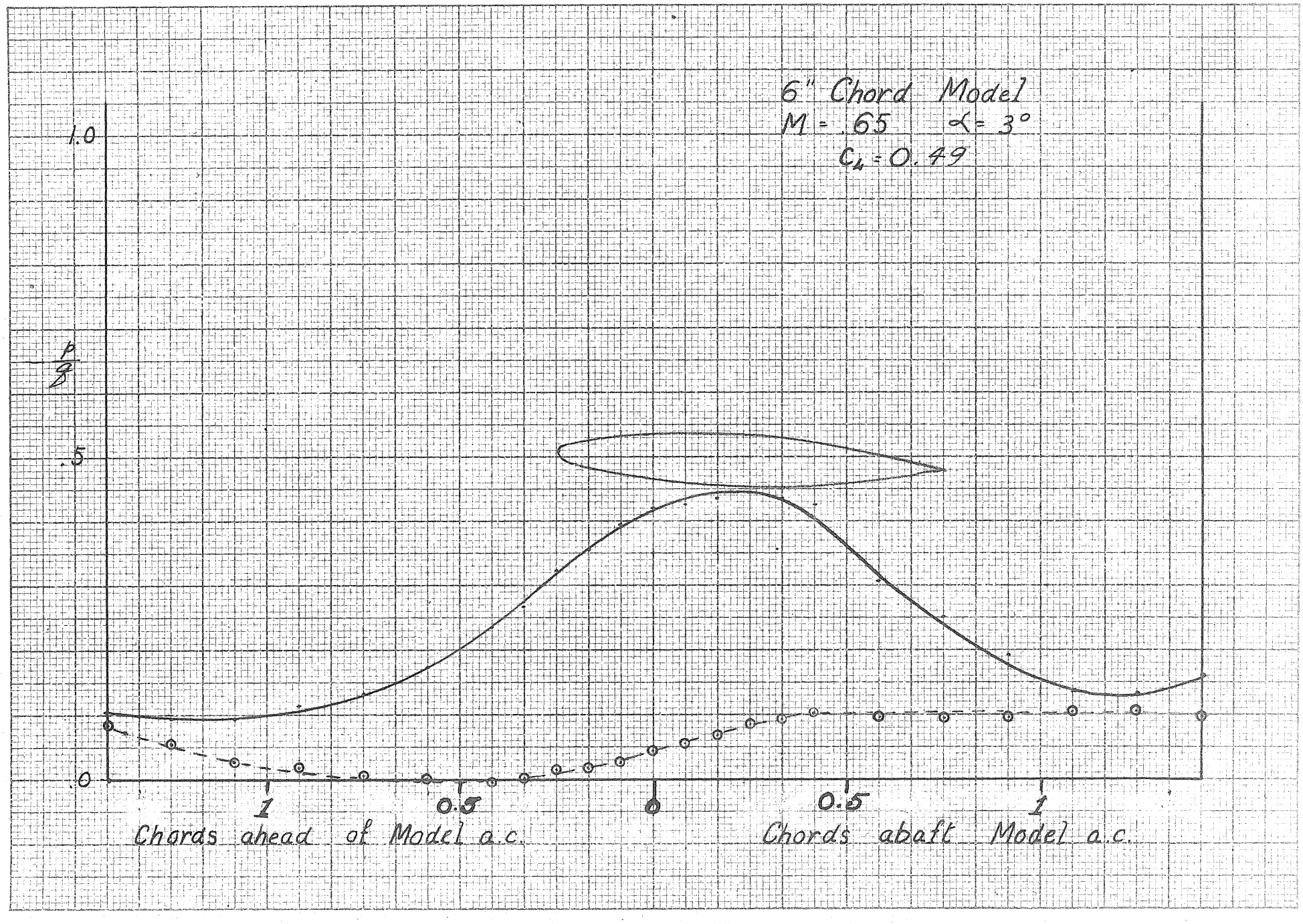
6" Chord Model
M = .65 α = 3°
C_L = 0.49
1.0
$\frac{p}{q}$
.5
0
1
0.5
0.5
1
Chords ahead of Model a.c.
Chords abaft Model a.c.

Fig. 97

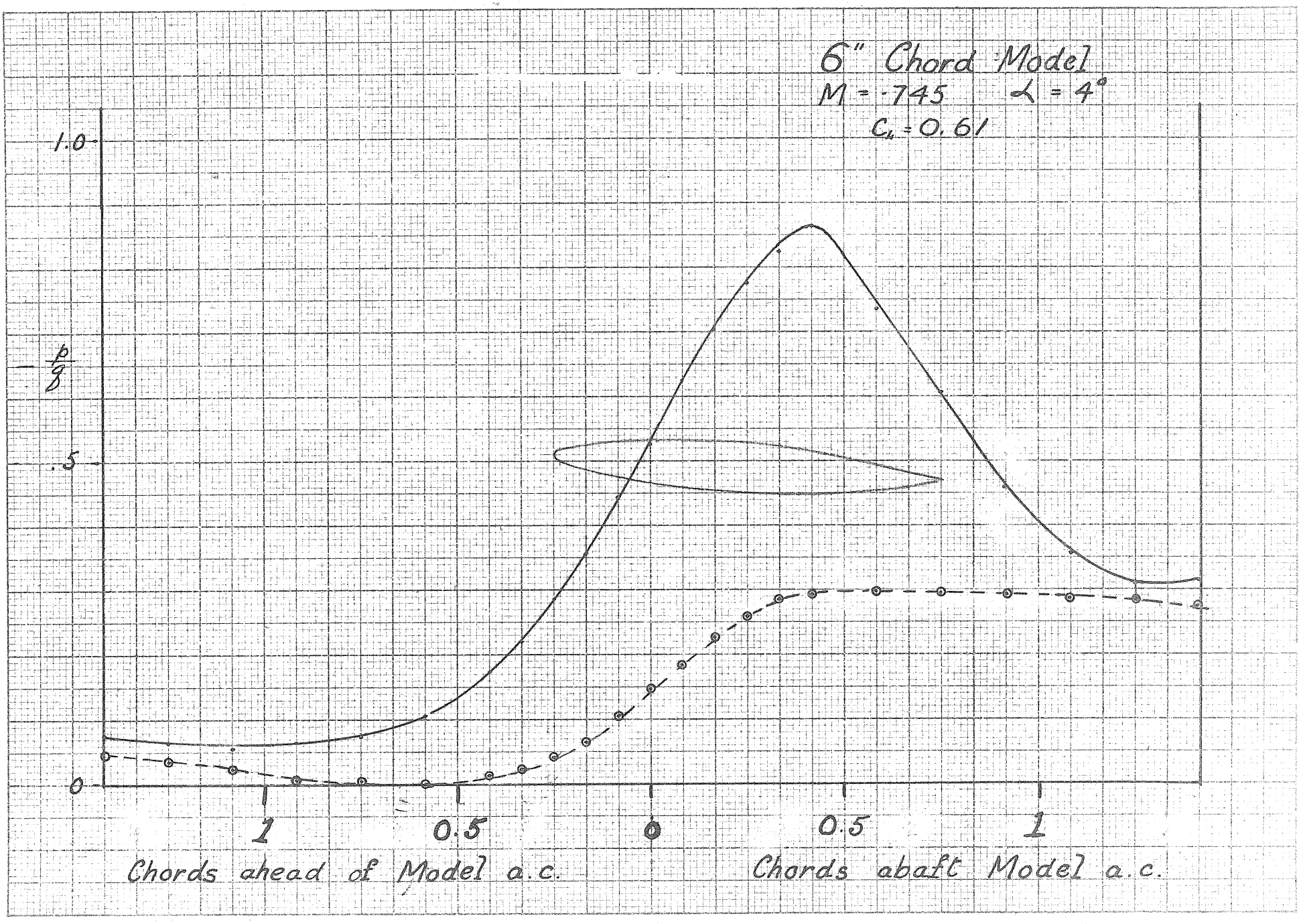
6" Chord Model
M = .745 α = 4°
C_L = 0.61
1.0
$\frac{p}{q}$
.5
0
1
0.5
0
0.5
1
Chords ahead of Model a.c.
Chords abaft Model a.c.

Fig. 98

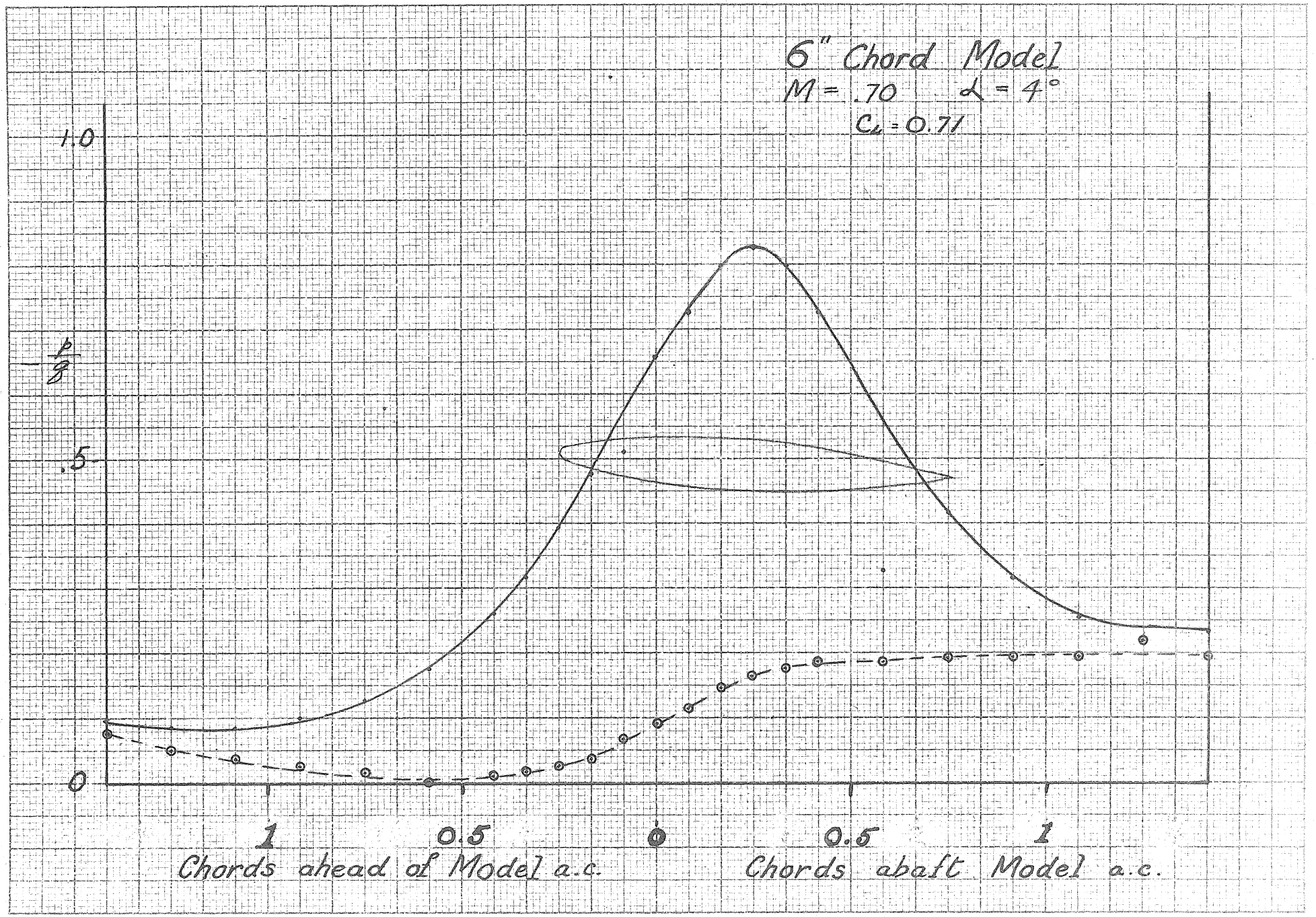
6" Chord Model
M = .70 α = 4°
C_L = 0.71
1.0
$-\frac{p}{q}$
.5
0
1
0.5
0
0.5
1
Chords ahead of Model a.c.
Chords abaft Model a.c.

Fig 99

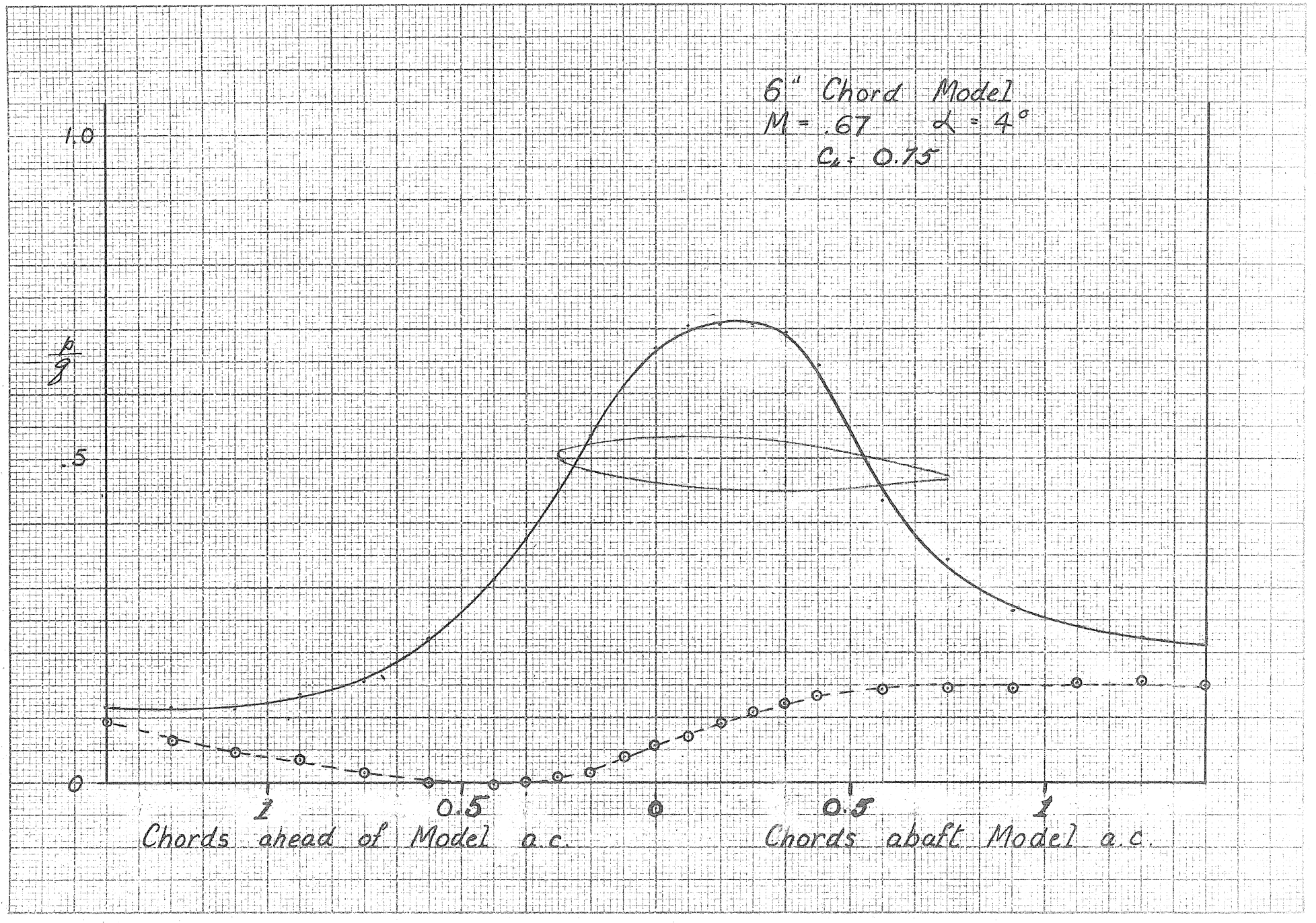
6" Chord Model
M = .67 α = 4°
C_L = 0.75
1.0
$\frac{p}{q}$
.5
0
1
0.5
0
0.5
1
Chords ahead of Model a.c.
Chords abaft Model a.c.

Fig 100

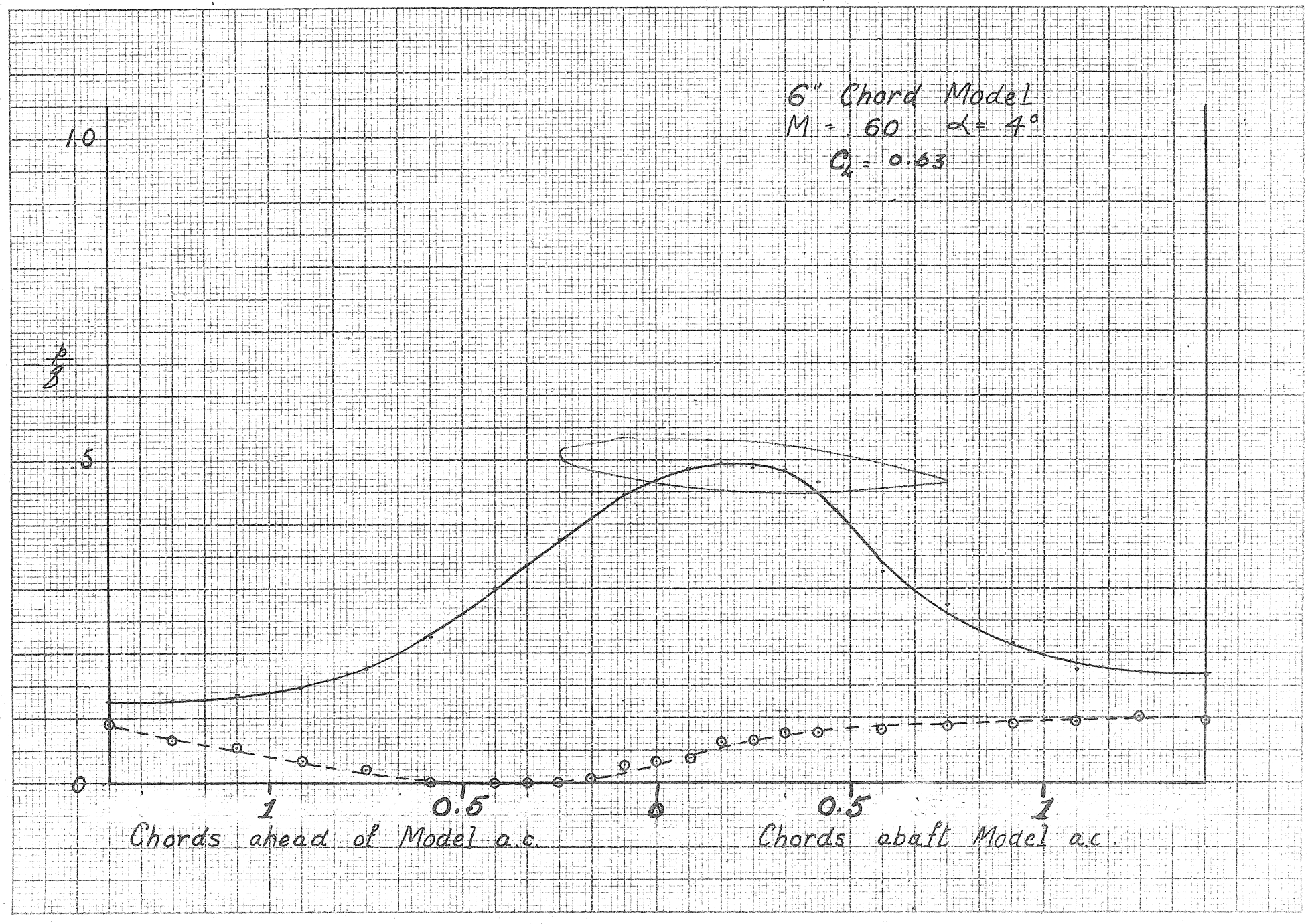
6" Chord Model
M = .60 α = 4°
C_L = 0.63
1.0
$-\frac{p}{q}$
.5
0
1
0.5
0
0.5
1
Chords ahead of Model a.c.
Chords abaft Model a.c.

Fig. 101